SUPERPLASTICITY AND ANELASTICITY IN FINE-GRAINED Sn-Pb ALLOYS

Joachim H. Schneibel

Linacre College, Oxford

A thesis submitted for the degree of Doctor of Philosophy in the University of Oxford

June, 1979

ABSTRACT

Superplasticity and anelasticity in fine-grained Sn-Pb alloys

Joachim H. Schneibel

Linacre College, Oxford

A thesis submitted for the degree of Doctor of Philosophy in the University of Oxford, June 1979

Mechanisms which may play a role in superplastic deformation (grain strain mechanisms, grain boundary sliding (GBS) mechanisms) are reviewed. Two well-known lattice dislocation mechanisms are re-evaluated for grain boundary dislocations (GBDs). The manner in which the deformation mechanisms interact, or are inhibited or obscured, is discussed.

Mechanisms of anelastic deformation are outlined, with particular reference to fine-grained materials. Expressions for anelastic recovery caused either by grain boundary (GB) tension or by the relaxation of GBD pile-ups are derived.

The plastic properties of Sn-38.1w/o Pb and Sn-2w/o Pb are measured. They are similar in both alloys. No threshold stress for plastic deformation is detected, for stresses and strain rates as low as 0.1MPa and $10^{-10}s^{-1}$, respectively. The presence of GB diffusion creep (Coble creep) is established experimentally in Sn-2w/o Pb with grain sizes $\geq$ 50μm. Coble creep is inhibited for small grain sizes (~10μm). The inhibition is explained by GBS caused by GBDs. In disagreement with the measurements, high threshold stresses are predicted for Sn-38.1w/o Pb. This implies that GBD line tensions are lower than those of lattice dislocations.

The anelastic properties of Sn-2w/o Pb and Sn-38.1w/o Pb are determined from the elastic after-effect (anelastic recovery after unloading). They are remarkable: anelastic contractions larger than 0.2% and relaxation strengths (= ratio of anelastically recovered to elastically recovered strain) in excess of 100 are found. The anelastic strains are approximately proportional to the stress and the inverse grain size. A wide range of relaxation times (~ 6 decades) is observed.

A mechanism based on the relaxation of GBD pile-ups is in qualitative agreement with the measured anelasticity. The high measured relaxation strengths, however, imply that the interaction between GBDs is much weaker (~ 2 orders of magnitude) than that between lattice dislocations. This could be due to a relatively low self-energy of GBDs and would be in qualitative agreement with the low GBD line tensions suggested above.

The influence of anelasticity on transients (e.g. stress relaxation, dip test) is investigated using a rheological model with three Voigt elements (anelasticity) and a non-linear dashpot (plasticity). Using independently determined plastic and anelastic parameters the 4-th order differential equation corresponding to the model is solved numerically for several examples. Measured transients are much more accurately predicted with the present model than with models neglecting anelasticity.

To my parents

PREFACE

This dissertation has been carried out by the author in the Department of Metallurgy and Science of Materials, of the University of Oxford, between October, 1975 and June, 1979. No part of it has been submitted previously at this, or any other university. Except where stated in the text the research described here is original.

I would like to thank the Florey Foundation (The Queen's College, Oxford), the Volkswagen Foundation and the German Academic Exchange Service for their financial support during the course of this research, and Professor Sir P.B. Hirsch, F. R. S., for the provision of laboratory facilities.

In particular I wish to thank Dr. P. M. Hazzledine for his helpful advise. The help provided by a number of people in the Department of Metallurgy and Science of Materials during this research is also gratefully acknowledged.

CONTENTS

CHAPTER 1

INTRODUCTION

At elevated homologous temperatures fine-grained metals and alloys are often superplastic. This means that they elongate in uniaxial tension often by more than 1000% without fracture (Edington, Melton and Cutler, 1976). Their industrial applications are based on this particular feature (see for example Balliett, Forster and Duncan, 1977; Coiley, 1974; Hestbech, Langer and Rosen, 1971; Pearce and Ganguli, 1972; and Saller and Duncan, 1971).

On a fundamental level superplastic materials have attracted attention because of the small size of their grains and because of their high volume fraction of grain boundaries (GBs) or phase boundaries. Certain deformation mechanisms, e.g., diffusion creep (see section 2.2.1), become dominant only for small grains. Dislocation creep mechanisms may change in fine-grained metals owing to the presence of GBs which act as barriers for dislocations (section 2.2.2). The GB properties, for example grain boundary sliding (GBS), become more and more important as the volume fractions of GBs (phase boundaries) associated with smaller grains increases. It may thus be possible to study the mechanical behaviour of GBs with no, or a negligable, interference from the bulk of the grains and to compare it with theoretical predictions. Indeed, as early as 1920, Rosenhain, Haughton and Bingham (1920) suggested that the pronounced anelastic behaviour of a fine-grained Zn-7%Al-4%Cu alloy was caused by the high percentage of amorphous GB material. Also, over the past few years increasing evidence has been found for

interface control in superplastic deformation (Ashby and Verrall, 1973; Burton, 1972; Newbury, 1972). Either the interface may be an imperfect source or sink for vacancies and thus inhibit diffusion creep, or the sliding of crystals along their mutual interfaces may be difficult.

In spite of considerable progress superplasticity is not well understood to date. After a careful examination of the superplastic Sn-Pb eutectic (Sn-38.1w/o Pb) which has been studied extensively(*) Mohamed and Langdon (1975) conceded that its mechanical properties are not in agreement with any of the existing models of superplasticity. In addition, there is also considerable disagreement between the mechanical data published for nominally identical materials. (see section 2.1).

The loss of superplasticity at high stresses and high strain rates is understandable: conventional lattice dislocation creep becomes dominant. At low stresses and strain rates, however, the situation is more complicated. The simplest concept explaining the occasionally observed loss of superplasticity at low strain rates is that of a threshold stress below which no deformation occurs. However, whereas Burton's (1971) results indicate a threshold stress in Sn-38.1w/o Pb, Geckinli and Barrett's (1974) stress relaxa-

(*) Superplastic Sn-Pb eutectic has been investigated by the following authors_ Aldrich and Avery (1970); Baudelet and Suery (1972); Burton (1971); Cline and Alden (1967); Cutler and Edington (1971); Dawson (1972); Dingley (1970); Geckinli and Barrett (1974);Geckinli and Barrett (1976); Homer and Baudelet (1977); Horiuchi, El-Sebai and Otsuka (1974); Humphries and Ridley (1977); Jones and Johnson (1966); Kutschej and Stüwe (1977); Martin and Backofen (1967); Melton, Cutler and Edington (1975); Murty (1972); Newbury (1972); Newbury (1973); Newbury and Joy (1970); Packer and Sherby (1967); Pearson (1934); Rawal and Murty (1972); Wray (1973); Zehr and Backofen (1968).

tion experiments demonstrate a threshold stress only over a certain range of strain rates; for strain rates below $\sim 10^{-9}$ s^{-1} the threshold disappears. Mohamed and Langdon (1975a), finally, did not find any evidence for a threshold stress.

At an early stage of this research the experiments indicated pronounced anelastic recovery after unloading (elastic after-effect). Anelasticity in small-grained materials has been found previously. Rosenhain, Haughton and Bingham (1920) studied the elastic after-effect in Al-7%Al-4%Cu qualitatively. Nuttall (1971), and Homer and Baudelet (1977) employed cyclic testing for the measurement of anelasticity in superplastic Zn-Al eutectoid and Sn-Pb eutectic, respectively. However, since superplastic materials deform plastically even at very low stresses the accurate interpretation of cyclic tests seems difficult since irreversible strains may be involved. Also a very wide range of frequencies would have to be employed in order to detect all the relaxation times contributing to the anelasticity. In measurements of the elastic after-effect, on the other hand, plastic deformation is ruled out completely (by definition, the plastic strain rate is 0 if the externally applied stress is 0) unless the sample weight itself causes plastic deformation. The results obtained from elastic after-effects are therefore more easily evaluated than those from cylic tests.

In order to gain a better understanding of the plastic and anelastic properties of superplastic materials, the microstructural mechanisms governing them have been reviewed

and new mechanisms suggested (chapters 2 and 3). In the discussion of the mechanisms of plastic deformation particular emphasis has been put on grain boundary sliding mechanisms and their significance for superplastic flow. The inconsistencies in the plastic data for Sn-Pb mentioned above required also a critical discussion of the mechanisms which have been suggested to explain the inhibition of superplasticity at low stresses which is sometimes found (e.g. Burton, 1971).

In chapter 3 the mechanisms responsible for anelasticity have been reviewed, with particular emphasis on the mechanisms operating in small grains and at high homologous temperatures. Two newly suggested processes which may be applicable to small grains have been derived and discussed.

The sparse and inconsistent data for Sn-Pb eutectic at strain rates below $\sim 10^{-7} s^{-1}$ (Burton, 1971; Geckinli and Barrett, 1974; Mohamed and Langdon, 1975a) demanded a repetition of these experiments using a creep rig with a high strain resolution (see chapter 5). The tests were done with the aim of verifying a threshold stress for plastic deformation. Another purpose was the identification of diffusion creep (Coble creep) in superplastic materials. Although the grain size dependence of the plastic strain rate often indicates diffusion creep, the strain rate sensitivity of the flow stress usually does not (Edington, Melton and Cutler, 1976). It was therefore decided to measure plastic strain rates in materials with a wide range of grain sizes and at a variety of strain rates with the

aim of possibly identifying diffusion creep. In order to do this, a Sn-2w/o Pb alloy rather than the Sn-Pb eutectic had to be used. The predictions of several theories are compared with the experimental data.

An extensive investigation of the small-grain anelasticity found in superplastic materials has been carried out in order to identify the mechanisms responsible for it and a tentative explanation is given in chapter 6. The anelasticity was measured from elastic after-effects, for the reasons discussed above.

Anelasticity can influence mechanical tests (e.g. stress relaxation tests (see for example Lubahn and Felgar, 1961). The strong anelasticity found in Sn-Pb makes it therefore necessary to explain the mechanical response of a material if plastic and anelastic deformation occur at the same time. Consequently, a rheological model capable of explaining, more accurately than has hitherto been done, the transient behaviour of superplastic alloys is developed in chapter 7.

CHAPTER 2

MECHANISMS OF SUPERPLASTIC DEFORMATION

2.1. Experimental background

Superplasticity has not yet been defined in terms of a generally accepted deformation mechanism. There is, however, wide-spread agreement about its definition in phenomenological terms. Thus, in a definition similar to the one employed by Newbury (1972), superplasticity can be characterized by the following three conditions:

(1) The strain rate sensitivity $m=\delta\log\sigma/\delta\log\dot{\varepsilon}$ is equal to or larger than 0.3 (Fig. 2.1). m is the exponent in the (locally defined) equation $\sigma\alpha\dot{\varepsilon}^m$ relating the flow stress σ and the plastic strain rate $\dot{\varepsilon}$.

(2) In uniaxial tension strains in excess of 100% may be achieved without failure of the material.

(3) Superplasticity occurs only in polycrystalline materials.

The third of these conditions explains the use of terms like "small-grain superplasticity" and "structural superplasticity" which are often used to describe this type of superplasticity. There is also an "environmental superplasticity" (Edington, Melton and Cutler, 1976) which is not treated here.

A few examples will illustrate the necessity of fulfilling all three conditions at the same time. For example, there are mechanisms of plastic deformation with $m \geq 0.3$ which may occur in single crystals. Harper-Dorn creep (Harper and Dorn, 1957) is such a mechanism ($m = 1$). Avery and Stuart (1967) have shown that any mechanism with $m \geq 0.3$ may fulfill condition (2) as long as it does not change during deformation and as long as microstructural instabilities,e.g. cavitation, do not occur. The large

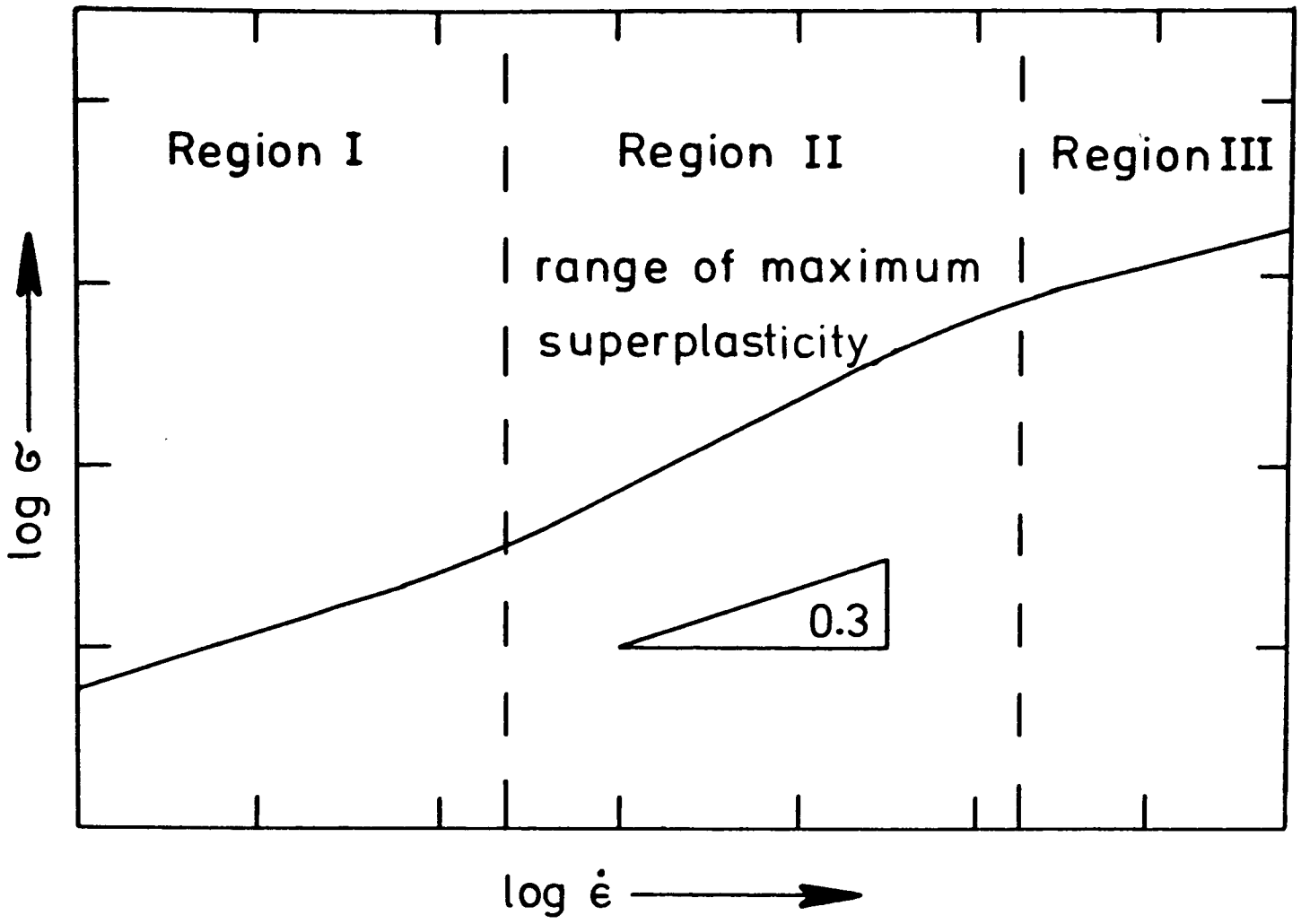

Fig. 2.1. Schematic relationship between the plastic strain rate, $\dot{\varepsilon}$, and the applied stress, σ, for a superplastic material. Superplasticity may not only occur in region II, but also in regions I and III, depending on the value of m.

elongations in tension which may thus in principle be achieved are in this case not caused by a superplastic mechanism since grain boundaries are not involved (condition (3)).

The large deformations required in condition (2) might also be achieved in easy glide in single crystals without conditions (1) and (3) being obeyed. The requirement "tension" is important since other modes of deformation, for example torsion, compression or rolling may suppress crack initiation or necking. Large deformations in themselves are therefore no proof of the presence of superplasticity.

The third requirement stresses the importance of grain or interphase boundaries. Superplasticity is usually observed for grain sizes in the range 1μm to 10μm, although this is not a strict requirement (Edington, Melton and Cutler, 1976, p.72). However, above a certain grain size (phase size), or for single crystals, conditions (1) and/or (2) should cease to be obeyed for a deformation mechanism which causes superplasticity below this grain size.

Detailed information on many aspects of superplasticity can be found in the recent review by Edington, Melton and Cutler (1976). It will therefore suffice to give only a very brief account of some characteristic features of superplastic materials and to give an idea about the variety in the mechanical behaviour which is evident from published data.

A plot of $\log\sigma$ vs. $\log\dot{\varepsilon}$ usually exhibits a region with a high slope (corresponding to a high strain rate sensitivity

$m = \delta \log \sigma / \delta \log \dot{\varepsilon}$) between two regions with a lower slope. This "S-shape" is represented schematically in Fig. 2.1. The region with the highest slope, region II, is usually associated with the largest elongation to fracture as demonstrated for example by Mohamed, Ahmed, and Langdon (1977) for Zn-22w/o Al. At fast strain rates (region III) m and the elongation to failure decrease: superplasticity ceases. The situation for low strain rates (region I) is less clear. Values for m between 0 and 1 have been reported and even results for nominally identical materials are often in conflict. This is illustrated by comparing the strain rate sensitivities obtained for Sn-Pb eutectic at low strain rates by Burton (1971) (m = 0), Geckinli and Barrett (1974) (m = 1) and Mohamed and Langdon (1975a) (m = 0.33). A similar discrepancy is found for Zn-22w/o Al for which m-values of 0.25, 0.55 and 1 have been obtained by Mohamed and Langdon (1975b), Eastgate (1978), and Misro and Mukherjee (1972), respectively.

Superplasticity occurs only at temperatures above approximately half the absolute melting point (Edington, Melton and Cutler, 1976, p.69). It is thermally activated with an activation energy often comparable to that for grain boundary or lattice self-diffusion (Alden, 1969b) which indicates the importance of diffusion for the deformation process.

An increase in the grain size usually leads to a strong decrease in the superplastic strain rate and often a

dependence

$$\dot{\varepsilon}\Big|_{\sigma=\text{const.}} \alpha\ L^{-p} \qquad (2.1)$$

on the grain size (phase size), L, has been found, with values of p often between 2 and 3 (Edington, Melton and Cutler, 1976, p.71).

Metallography shows that the grains remain essentially equiaxed during superplastic deformation. Extensive grain boundary sliding occurs and initially adjoining grains may end up many grain diameters apart (Geckinli and Barret,1976). Dislocation activity is generally low and textures present prior to testing disappear, at least partly (Edington, Melton and Cutler, 1976).

In the following sections of this chapter potential mechanisms of superplastic deformation will be discussed, i.e., mechanisms with m equal to or greater than 0.3 requiring the presence of grain boundaries. They will be superplastic mechanisms if they can operate sufficiently long without m falling below 0.3 and if microstructural instabilities are not introduced too soon during deformation.

At first bulk deformation mechanisms causing grain strains will be reviewed. The experimental findings discussed above make it necessary to discuss also the mechanisms which cause grain boundary sliding. Then the simultaneous occurrence of grain strain and grain boundary sliding will be examined. After a section on the importance of the vacancy - interface reaction for superplasticity, mechanisms obscuring or inhibiting superplasticity will be discussed.

2.2. Bulk deformation of the grains

2.2.1. Bulk deformation by vacancy transport

In diffusion creep deformation is caused by vacancy flow from and to differently stressed grain (phase) boundaries (or surfaces - but surfaces will not be considered here). In this paragraph the simplest kinds of diffusion creep will be discussed. The vacancy concentration, $c(\underline{r})$, at the grain boundaries is assumed to be determined by the stress, $\sigma(\underline{r})$, acting normal to them:

$$c(\underline{r}) = c_o \exp\left[\frac{\sigma(\underline{r})\ \Omega}{k\ T}\right] \sim c_o \left[1 + \frac{\sigma(\underline{r})\ \Omega}{k\ T}\right], \qquad (2.2)$$

where c_o is the equilibrium vacancy concentration in the unstressed state, $\underline{r}$ describes the location at the grain boundary, Ω is the atomic volume, k is Boltzmann's constant and T is the absolute temperature (Friedel, 1964, p.312). The rate of vacancy flow (corresponding to the flow of matter) is determined by the rate of diffusion through the lattice or the grain boundaries and not by the rate of creation or annihilation of vacancies at boundaries. Creation and annihilation of vacancies may occur anywhere at grain boundaries and does not require any work. Grains do not separate at boundaries and sliding along the boundaries is easy, i.e. the grain boundaries are fully relaxed. Surface tension effects due to finite grain boundary energies are neglected.

The shear strain rate caused by lattice diffusion under such conditions ("Nabarro-Herring creep") has been derived

for spherical grains by Herring (1950). Conversion of Herring's result into tensile stresses and strains (von Mises criterion, see for example Cottrell (1964)) gives immediately:

$$\dot{\varepsilon} = 13 \frac{\Omega \sigma D_L}{k T L^2} \sim \frac{13 b D_L G}{k T} \left(\frac{b}{L}\right)^2 \frac{\sigma}{G} , \qquad (2.3)$$

where $\dot{\varepsilon}$ is the tensile strain rate, σ is the flow stress, D_L is the lattice self-diffusion coefficient, L is the grain size, b is the lattice Burgers vector ($\Omega \sim b^3$) and G the lattice shear modulus.

The tensile strain rate caused by grain boundary diffusion ("Coble creep"), again for spherical grains, is after Coble (1963):

$$\dot{\varepsilon} = 47 \frac{\Omega D_B w \sigma}{k T L^3} \sim 47 \frac{D_B w G}{k T} \left(\frac{b}{L}\right)^3 \frac{\sigma}{G} , \qquad (2.4)$$

where D_B is the grain boundary self-diffusion coefficient and w the width of the grain boundaries.

Equations (2.3) and (2.4) may be combined, with slightly changed proportionality factors, to a more general equation for diffusion creep (Ashby and Verall, 1973):

$$\dot{\varepsilon} = 14 \frac{\Omega \sigma}{k T L^2} D_L \left(1 + \frac{\pi w}{L} \frac{D_B}{D_L}\right) . \qquad (2.5)$$

Diffusion creep has been evaluated for many grain shapes and the only effect of changing the grain shape while keeping the grains equiaxed is to alter slightly the numerical

factors on the right-hand sides of eqns. (2.3) and (2.4) (Burton, 1977a, p.5).

Spingarn and Nix (1978) have recently presented an exact two-dimensional treatment for the GB diffusion creep of hexagonal grains, with the tensile axis normal to one pair of the flat faces of the hexagons. The result is similar to equation (2.4) but is more satisfactory in that hexagonal grains may be close-packed and spherical ones may not. Different directions of the tensile axis with respect to the grains, however, may lead to changes in the strain rate (if the normal stresses at the GBs and therefore the concentration gradients across the grains become high, as for example for a tensile stress parallel to the flat faces of the hexagons in Fig. 2.2 (a)). Since this difficulty is not encountered with spherical grains they are preferred in this context.

If the grains in a polycrystalline aggregate rotate in an appropriate way it is possible that they remain almost eqiaxed even after large elongations of the aggregate. For example, if an individual grain in an aggregate elongates and is turned by 90^{o} its aspect ratio may decrease again until the grain becomes equiaxed once more. Under such circumstances eqns. (2.2) to (2.5) will always hold approximately for the individual grains.

On the other hand, if grains do not rotate during deformation they are expected to elongate. The resulting increase in the length of the diffusion paths causes the strain rate to decrease, for a constant applied stress. An

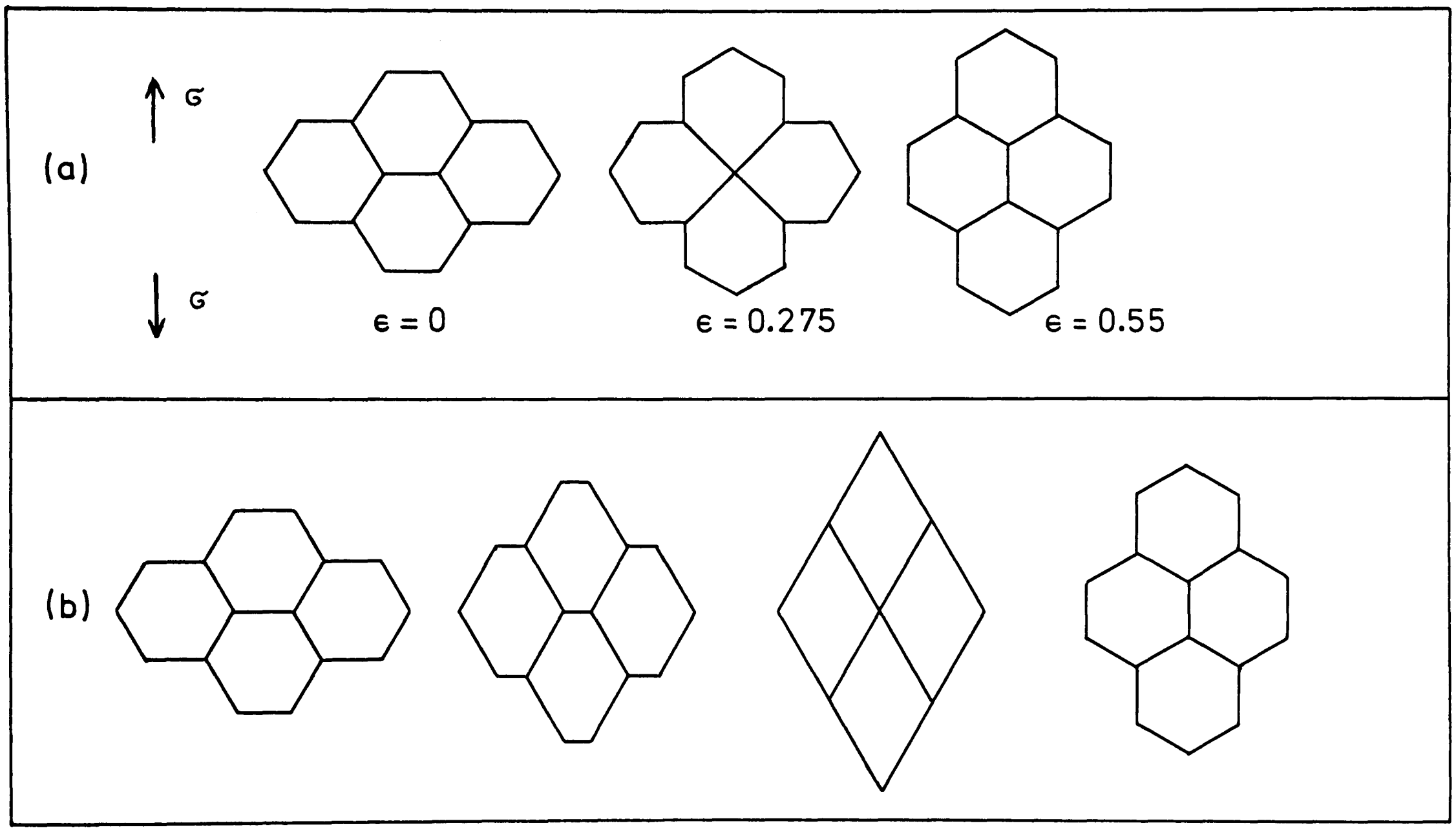

Fig. 2.2. Grain switching models
(a) Ashby-Verrall (1973)
(b) Lee (1969)

elongation by 100% results approximately in a halving of the strain rate (Green II, 1970).

It is, however, possible that non-rotating grains switch neighbours as suggested by Ashby and Verrall (1973) and Lee (1969) and depicted in Fig. 2.2. Such a mechanism can be extended to three dimensions (Hazzledine and Newbury, 1976) in order to ensure continuous operation of switching events. Grain switching leads to an acceleration of the strain rates as compared with those obtained from eqns. (2.3) and (2.4). Ashby and Verrall (1973) suggested a factor of 7; recently a more thorough analysis (Ashby, Edward, Davenport and Verrall, 1978) led to a value of the acceleration factor of between 1.7 and 5.5.

Diffusion creep may be obscured by other mechanisms acting at the same time, for example by other superplastic mechanisms which will be presented later. It is also possible for the strain rate sensitivity to be influenced by the vacancy-interface reaction at the GBs or by the GB tension. These effects will be discussed in later sections of this chapter.

With the exception of very simple grain geometries (e.g. bamboo structure) grain boundary sliding will always accompany diffusion creep. This has been pointed out by Lifshitz (1963) and has been further discussed by others (Stevens, 1971; Cannon and Nix, 1973; Cannon, 1971). The amount of GBS necessary for diffusion creep corresponds to about 50% of the total deformation. Any of the GBS mechanisms discussed in a later paragraph may therefore

determine the strain rate provided that the sliding rate which it predicts is smaller than the one needed for diffusion creep with freely sliding GBs.

In summary, diffusion creep is a superplastic mechanism. Its role after large deformations ($\varepsilon \gtrsim 1$) is somewhat uncertain since the influence of grain switching and grain rotation is not easy to find out. Characteristic features of diffusion creep are its strain rate sensitivity of 1, its dependence of the strain rate on the inverse square or cube of the grain size and an activation energy corresponding to that for lattice or grain boundary self-diffusion.

2.2.2. Bulk deformation by lattice dislocations

In a mechanism suggested by Friedel (1964) lattice dislocations pile up against grain boundaries and escape by climbing up the GBs. The climbing is the rate-controlling process. Such a model was developed in more detail by Ball and Hutchison (1969). It may be regarded as a bulk mechanism since dislocations traverse the whole of the grains in order to form pile-ups and thus do deform the interior of the grains. Additional support for this view is that the mechanism operates with freely sliding GBs, i.e., not GBS but bulk deformation must be rate-controlling.

In the simplest case the sliding of two grains along their common boundary is impeded by a third, blocking grain which is then deformed. In more complicated cases rows of grains sliding along a common boundary may cause

stress concentrations at an obstructing grain and thus an increase in the strain rate may result. In the simplest case Ball and Hutchison's equation for the strain rate reduces to:

$$\dot{\varepsilon} = \frac{8\ G\ b\ D_B}{k\ T}\ (\frac{b}{L})^2\ (\frac{\sigma}{G})^2\ , \qquad (2.6)$$

where all symbols have their previous meaning. This result was obtained by setting Ball and Hutchison's ratio R (number of easy sliding grains/number of obstructing grains) equal to 1; the unit of sliding was set equal to the Burgers vector b, the climb distance of the dislocations was assumed to be one half of the grain size and the atomic volume was set equal to b^3.

For large grain sizes and/or high stresses eqn. (2.6) is expected to break down. Intercrystalline barriers (sessile dislocations, dislocation tangles, cell boundaries) will become more important than the grain boundaries. The parameter L can no longer be identified with the grain size; it becomes smaller than the grain size and stress dependent. Conventional power-law creep, with a stress exponent $n = \delta\log\dot{\varepsilon}/\delta\log\sigma$ between 4 and 5 (corresponding to a strain rate sensitivity m between 0.2 and 0.25) will become predominant and superplasticity will cease.

Below a stress $\sigma_o \sim (G\ b)/L$ lattice dislocations will probably not be generated in the grains since the GBs are considered to be effective barriers for lattice dislocations. Similarly, the equilibrium distance between two identical

dislocations for a stress $\sigma_o \sim (G\ b)/L$ is of the order of the grain size. Pile-ups are therefore not thought to form below this stress. The main assumptions for the derivation of equation (2.6) thus break down; the Ball and Hutchison mechanism ceases below $\sigma_o = (G\ b)/L$.

A lattice dislocation model based on slip bands (where slip bands are sliding GBs as well as actual dislocation slip bands) has been recently advanced by Spingarn and Nix (1979). It predicts a continuous variation of the strain rate sensitivity as a function of the stress, as might be expected from the discussion above. Over a range of stresses, the model predicts strain rates similar to those predicted by the Ball and Hutchison model, although the analysis of the stresses causing diffusion is different. At high stress levels, conventional dislocation creep is predominant, whereas at low stresses the strain rate is virtually identical to the Coble creep rate.

If the grains in a superplastic polycrystal do not rotate Ball and Hutchison's mechanism leads to elongation of the individual grains because the slip planes are not likely to change. As pointed out by Mukherjee (1971), however, grain rotation may cause the progressive activation of different slip planes, in accordance with the maximum shear stress criterion for plastic flow. This could account for the experimentally found absence of appreciable grain elongation during superplastic flow.

Hayden, Gibson, Merrick and Brophy (1967) suggested a lattice dislocation mechanism which differs from the

Ball and Hutchison model in the grain size dependence of the creep rate. Without detailed derivation they proposed:

$$\dot{\varepsilon} = A\, D_B \frac{\sigma^2}{L} , \qquad (2.8)$$

where A is a constant. This result can be obtained along similar lines to Ball and Hutchison's (1969) derivation. Instead of only one pile-up per grain, however, one has to permit several parallel pile-ups in each grain and, in addition, that their spacings do not depend on the grain size or the applied stress. The climb distance is again assumed to be of the order of the grain size.

In general, some GBS will be associated with the operation of the mechanisms outlined above since dislocations climbing near boundaries will usually have a component of their Burgers vector parallel to the boundary and thus cause sliding. It is on the other hand not certain how much sliding is required for continuous deformation. This difficulty will again appear in the discussion of simultaneous grain deformation and GBS in section 5 of this chapter.

So far only bulk mechanisms have been discussed. They are mechanisms which can in principle operate anywhere in the grains of a polycrystal. Attention will now be turned to deformation mechanisms either in the GBs (intrinsic GBS) or close to them (accommodated GBS). The special role of intersecting GBs will also be considered since intersections may change the grain size dependence of the strain rate. In terms of Gifkin's (1976) "core and

mantle" analogy the "mantle" of the grains (GBs or regions close to them) is now discussed whereas previously the "core" (bulk) has been examined. Clearly, this distinction is not an exclusive one. For, if the mantle is wider than the GB-thickness there will always be a grain size below which the core disappears. Then the distinction between core and mantle becomes meaningless. Diffusion creep provides an example of a process which, equally correctly, can be called bulk deformation or accommodated GBS, no matter what the grain size is. Thus in Raj and Ashby's (1971) treatment diffusion creep is regarded as diffusional accommodated sliding of GBs which are undulating with an amplitude and wavelength of the order of the grain size. The zone perpendicular to the GBs corresponding to the mantle has a width similar to the grain size. In this description the grains do not have a core. In section 2.1 above, however, diffusion creep is regarded as a bulk mechanism. The width of the mantle coincides with the width of the GBs and the only function of the mantle is to provide easy GBs - it is not rate-controlling.

2.3. Grain boundary sliding

The discussion of the mechanisms of grain deformation showed that grain boundary sliding may be of importance. In particular GBS may be rate determining if diffusion creep is the only other deformation mechanism operating. In this paragraph GBS will be discussed with the stipulation that it is necessary for the deformation of a polycrystal

and that it is rate-controlling. The more complicated situation of simultaneous GBS and grain deformation and the interaction of the respective mechanisms will be commented upon in a later paragraph.

2.3.1. Intrinsic grain boundary sliding (sliding within the thickness of the grain boundaries)

(a) Influence of grain boundary intersections neglected

The displacement rate of two crystals parallel to their common boundary, $\dot{u}$, is determined by the shear stress, τ, acting parallel to the boundary, the test temperature, T, and the structure, S, of the boundary (e.g. dislocation content, misorientation of the two crystals):

$$\dot{u} = \dot{u}(\tau, T, S) \quad . \tag{2.9}$$

The GB area per unit volume depends on the grain size, L, as $L^2/L^3 = 1/L$. The strain rate of a polycrystal of grain size L is then approximately given by:

$$\dot{\varepsilon} \sim \frac{\dot{u}(\tau, T, S)}{L} \sim \frac{\dot{u}(\sigma, T, S)}{L} \quad , \tag{2.10}$$

where σ is the tensile stress acting on the polycrystal. The strain rate in eqn. (2.10) is determined only by GBS. Equation (2.10) will be used to convert the GBS rates derived by various authors into polycrystalline strain rates.

Intrinsic GBS by diffusion

The (intrinsic) diffusional sliding rate of a GB is,

after Friedel (1964, p.318), determined by the Einstein equation relating the diffusion velocity of vacancies to the force acting on them. The displacement of an atom by a distance b, where b is the Burgers vector, causes a displacement by b of a GB region of an area b^2. With equation (2.10), the strain rate of a polycrystal with a grain size L is found to be:

$$\dot{\varepsilon} = \frac{D_B \, G \, b}{k \, T} \frac{b}{L} \frac{\sigma}{G} \, . \qquad (2.11)$$

As will be seen in the paragraph on accommodated GBS, eqn. (2.11) corresponds to diffusional accommodation of a freely sliding GB which is not smooth on the atomic level.

A comparison with equation (2.4) (assuming w = 2b) shows that Coble creep is slower than the strain rate above by a factor of about $100b^2/L^2$. This is explained by the larger volume which has to be transported as well as by the relatively long diffusion paths in Coble creep.

Intrinsic GBS by means of GBDs

Gates (1973) developed a model for intrinsic GBS based on the diffusion controlled movement of GBDs. Similar to the numerical values suggested by him, the diffusion distance between a climbing GBD and a vacancy source or sink in the GB is assumed to be of the order of 10b (b = lattice Burgers vector). The atomic volume is approximated by b^3 and the GB width by 2b. A stress independent density of moving structural GBDs of approximately 1/(100b)

is assumed (in analogy to the dislocation density in 3 dimensions the density in 2 dimensions is a reciprocal length: length of dislocation line per unit area of GB). With these simplifying assumptions and after setting geometrical factors equal to 1, Gates' equation 28 leads to

$$\dot{\varepsilon} = \frac{D_B \; G \; b}{500 \; k \; T} \frac{b}{L} \frac{\sigma}{G} \; . \qquad (2.12)$$

The strain rate given by eqn. (2.12) is significantly lower than that given by equation (2.11). This is due to the fact that the diffusion paths are longer than those associated with intrinsic diffusional GBS and that the dislocation density is relatively low. More generally, Ashby (1972) has shown that the GBS rate based on GBD movement will usually be smaller than the intrinsic diffusional sliding rate by a factor of $1/(\rho \; \lambda)$ where λ is the translational periodicity in the boundary and ρ the GBD density.

GBD mechanisms may also lead to strain rate sensitivities smaller than 1. Ashby and Verrall (1973) suggested a linear increase of the GBD density with the stress and obtain for viscously dragged dislocations:

$$\dot{\varepsilon} = M \; G \; \frac{b}{L} \; \left(\frac{\sigma}{G}\right)^2 \; , \qquad (2.13)$$

where M is the mobility of the GBDs, defined by $v = M \; F$ (v = dislocation velocity, F = force per unit length acting on the dislocation considered).

Equation (2.13) corresponds to a strain rate sensitivity

of 0.5. It is also conceivable that GBS has a strain rate sensitivity of 0.33 as can be seen by applying Nabarro's dislocation climb mechanism (1967) to GBDs in GBs. The corresponding strain rate has been derived along similar lines to Nabarro's original mechanism (appendix A1). For GBD Burgers vectors similar to lattice dislocation Burgers vectors, and for similar glide and climb components of the Burgers vectors of climbing GBDs, the result is:

$$\dot{\varepsilon} = 4 \frac{D_B G b}{k T} \frac{b}{L} \left(\frac{\sigma}{G}\right)^3 . \qquad (2.14)$$

Strain rates substantially lower than those given by equation (2.12) are expected from eqn. (2.14) for stresses lower than $2.2 \cdot 10^{-2} G$. Below a critical stress which depends on the GBD mobility the mechanism suggested above should also be slower than the one proposed by Ashby and Verrall (equation (2.13)).

So far intrinsic GBS mechanisms for planar GBs have been dealt with. In polycrystals, intersecting GBs were assumed to slide independently from each other. Strain rates varying as σ^n/L have been found, with n between 1 and 3. In the following section the influence of triple edges, i.e., intersecting GBs, will be examined.

(b) Intersecting grain boundaries

The Ball and Hutchison model for lattice dislocations (equation (2.6)) can also be applied to GBDs. One assumes that GBDs pile up against triple edges and climb, under

the action of the stresses at the heads of the pile-ups, a distance of the order of the grain size until they are annihilated. The straightforward derivation which is presented in appendix A2, leads to:

$$\dot{\varepsilon} = \frac{8\ G\ b_L^2\ D_B}{k\ T\ b_B} \left(\frac{b_L}{L}\right)^2 \left(\frac{\sigma}{G}\right)^2 , \qquad (2.15)$$

where b_L and b_B are the lattice and GB dislocation Burgers vectors, respectively. The strain rate obtained is faster than that for equation (2.6) by a factor (b_L/b_B). The critical stress below which the mechanism is not likely to operate is however only $(G\ b_B)/L$ as compared to $(G\ b_L)/L$ for the Ball and Hutchison mechanism (usually b_B will be smaller than b_L, see sor example Ishida and MeLean (1973)).

Another model based on GBDs which takes also account of GB intersections was suggested by Gifkins (1976). Here the GBS rate is inversely proportional to the length of the sliding GBs(~ grain size). This result is obtained by assuming that GBS occurs by the sequential and dependent movement of the GBDs in the boundary. For low stresses ($\sigma < (2\ k\ T)/(A\ b_L)$, where A is an activation area which is approximately 1000 b_L^2) an equation

$$\dot{\varepsilon} = \frac{Z\ A}{2\ k\ T\ b_L} \left(\frac{b_L}{L}\right)^2 \frac{\sigma}{G} \exp\left(-\frac{Q}{k\ T}\right) \qquad (2.16)$$

is obtained, where Z is a parameter containing the frequency with which dislocations move across barriers in the GBs and Q is an activation energy. GB and lattice dislocation

Burgers vectors have been assumed to be similar in Gifkin's derivation.

2.3.2. Accommodated grain boundary sliding

(a) Influence of grain boundary intersections neglected

Diffusional accommodation

Diffusional accommodation of the sliding of non-planar GBs has been treated by Raj and Ashby (1971). Sliding within the width of the GBs is assumed to be very easy. Its rate is, for example, determined by GB diffusion (see equation (2.11). Then the GBs can be regarded as sliding freely within their thickness. Since they are corrugated, stresses are set up during sliding which cause rate-controlling diffusive fluxes between compressed and dilatated regions adjacent to the GBs. The GBs can be described by a sine function and the sliding rate, $\dot{u}$, depends on the amplitude, h, and the periodicity, λ , of this function. Raj and Ashby's equation 11 can then be written approximately as

$$\dot{\varepsilon} = \frac{\dot{u}}{L} = \frac{8\ \lambda\ b^2\ G}{\pi\ h^2\ k\ T} \left(1 + \frac{\pi\ w}{\lambda} \frac{D_B}{D_L}\right) D_L \frac{b}{L} \frac{\sigma}{G} \qquad (2.17)$$

for a polycrystal of grain size L.

As Raj and Ashby have pointed out that a polycrystal will approximately have $\lambda = 2L$ and $h = L$ equation (2.17) reduces immediately to the diffusion creep equation (eqn. (2.5), with slightly different numerical factors).

If the GBs are smooth above the atomic level wavelength

and periodicity are $\lambda \sim 2b$ and $h \sim b$. Under these circumstances the strain rate in equation (2.17) is given by the intrinsic diffusional sliding rate of the GBs (compare with equation (2.11)). The accommodated GBS has become intrinsic GBS.

Lattice dislocation accommodation

Langdon (1970) suggested GBS by glide and climb of lattice dislocations, climb being the rate limiting process. If GBS is rate controlling the strain rate of a polycrystal is then approximately given by:

$$\dot{\varepsilon} = \frac{b\ D_L\ G}{k\ T}\ \frac{b}{L}\ \left(\frac{\sigma}{G}\right)^2 \quad . \tag{2.18}$$

It is worth noting that the diffusion coefficient in equation (2.18) is that for lattice self-diffusion. This confirms that this kind of GBS is indeed a lattice mechanism. The GBS occurs essentially in the lattice and does hence not require any intrinsic GBS.

(b) Intersecting grain boundaries

GBDs may pile up against triple edges, dissociate into lattice dislocations which glide and climb through the lattice and react again with the GBs and so on. The lattice dislocations are thus responsible for the deformation of the mantle near the GBs. The strain rate for such a model was derived by Gifkins (1976):

$$\dot{\varepsilon} = \frac{64\ G\ b\ D_L}{k\ T}\ \left(\frac{b}{L}\right)^2\ \left(\frac{\sigma}{G}\right)^2 \quad . \tag{2.19}$$

This result differs from the Ball and Hutchison equation

(eqn. (2.6)) mainly in the choice of the diffusion coefficient.

2.4. Representation of the superplastic mechanisms by means of deformation maps

A few of the mechanisms of superplasticity will now be depicted in deformation maps in order to illustrate their relative importance at various stresses. In the particular type of deformation map chosen the normalized grain size is shown as a function of the normalized stress in a double-logarithmic plot (Mohamed and Langdon, 1974). As will be seen below various areas of the map correspond to various mechanisms.

The following mechanisms were considered:

Nabarro-Herring creep (NH), eqn.(2.3),

Coble creep (C), eqn.(2.4),

Ball and Hutchison creep (BH), eqn.(2.6),

2-dimensional Nabarro climb creep (N), eqn.(2.14).

The following data was used for the construction of the plots:

$T = 400K$,

D_B (Sn, 400K) = $3.83 \cdot 10^{-11}$ m^2/s (Lange and Bergner, 1962),

D_L (Sn, 400K) = $2.60 \cdot 10^{-17}$ m^2/s (Lange, Hassner and Berthold, 1961),

G (Sn) = 20GPa (Cottrell, 1968, p.308),

$b = b_L = b_B = 0.3nm$,

$w = 2b$.

Equating the strain rates corresponding to the various mechanisms considered, leads to equations for boundaries in

the deformation maps. Any of these boundaries marks a reversal in the relative importance of two deformation mechanisms. The following equations were obtained:

NH - C: $L/b = (94\ D_B)/(13\ D_L) \Rightarrow \log(L/b) = 7.03$,

NH - BH: $\sigma/G = (13\ D_L)/(8\ D_B) \Rightarrow \log(\sigma/G) = -5.96$,

NH - N: $L/b = ((26\ \pi\ D_L)/D_B)\ (\sigma/G)^{-2} \Rightarrow \log(L/b) = -4.26 - 2\ \log(\sigma/G)$,

C - BH: $L/b = (94/8)\ (\sigma/G)^{-1} \Rightarrow \log(L/b) = 1.07 - \log(\sigma/G)$,

C - N: $L/b = (188\ \pi)^{1/2}\ (\sigma/G)^{-1} \Rightarrow \log(L/b) = 1.38 - \log(\sigma/G)$,

BH - N: $L/b = 16\ \pi\ (\sigma/G)^{-1} \Rightarrow \log(L/b) = 1.70 - \log(\sigma/G)$.

There is a minimum stress below which the Ball and Hutchison mechanism cannot operate. It is the stress for which two identical lattice dislocations have an equilibrium distance of the order of the grain size. The corresponding line (called BHM) in the deformation map is given by:

BHM: $\sigma/G = (1/\pi)\ (L/b)^{-1} \Rightarrow \log(L/b) = -0.50 - \log(\sigma/G)$.

Fig. 2.3 shows a particularly simple example of a deformation map. Only Nabarro-Herring creep, Coble creep, and Ball and Hutchison creep are present. Three fields separated by thick lines are obtained and each is named after the fastest of the three mechanisms (the rate-controlling one) in it. It is easily realized that, in general, if two mechanisms have the same stress dependence of the strain rate then they are separated by horizontal lines in such a map, whereas mechanisms with the same grain size dependence are separated by vertical lines. Similarly, mechanisms with the same temperature dependence

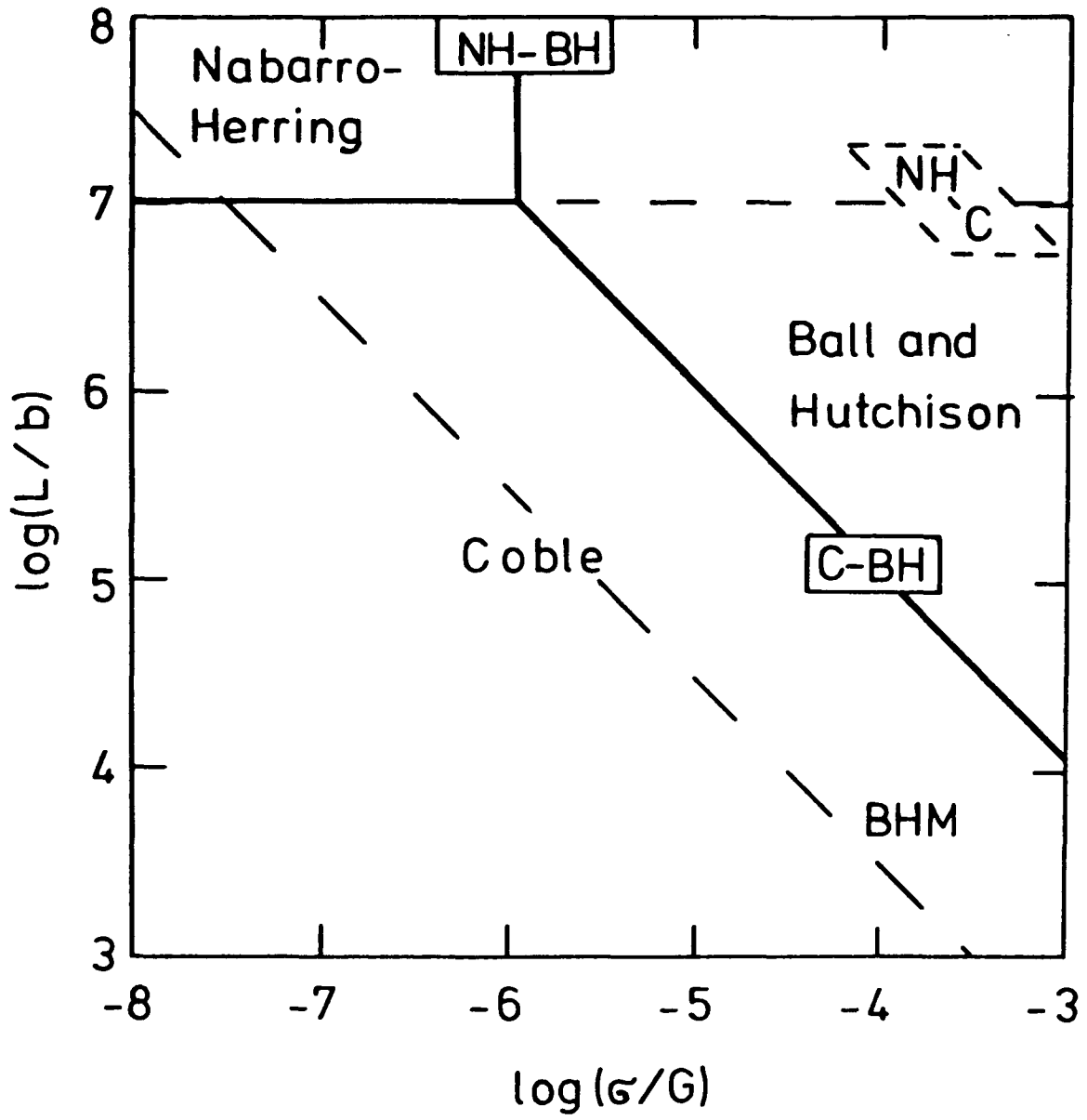

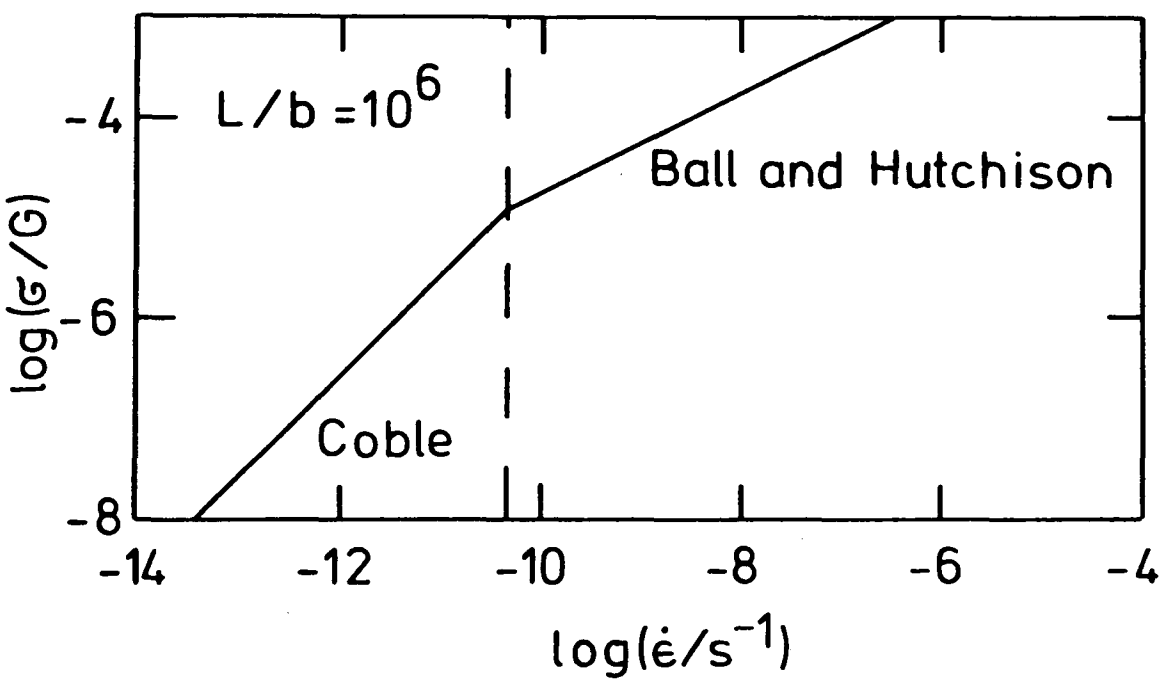

Fig. 2.3. Deformation map for Nabarro-Herring creep, Ball and Hutchison creep, and Coble creep; and the corresponding stress-strain rate relationship for $L/b = 10^6$.

of the strain rate (identical activation energies) will be separated by temperature-independent lines (e.g. Coble creep and Ball and Hutchison creep in Fig. 2.3). Since activation energies for GB self-diffusion are generally smaller than those for lattice self-diffusion an increase in the temperature in Fig. 2.3 will increase the Nabarro-Herring field at the expense of the Ball and Hutchison field and the Coble field.

A horizontal section through the deformation map in Fig. 2.3 shows, for a particular grain size, which mechanism is prevalent at which stress. Using the corresponding strain rate sensitivities it is then easy to construct the relationship between stress and strain rate. A half-schematic example is shown in Fig. 2.3 (Half-schematic because Coble creep is not assumed to occur in the Ball and Hutchison field and vice versa: this is not entirely true). Stess-strain rate relationships for different grain sizes are readily constructed, as well as dependencies of the strain rate on the grain size (vertical sections through the deformation map).

In another example, 2-dimensional Nabarro climb creep is taken into account (Fig. 2.4). With the approximations used the minimum stress required for its operation corresponds approximately to that required for the operation of the Ball and Hutchison mechanism. 2-dimensional Nabarro climb creep (i.e. GBS) is assumed to be rate controlling if it is slower than Coble creep, Nabarro-Herring creep, or

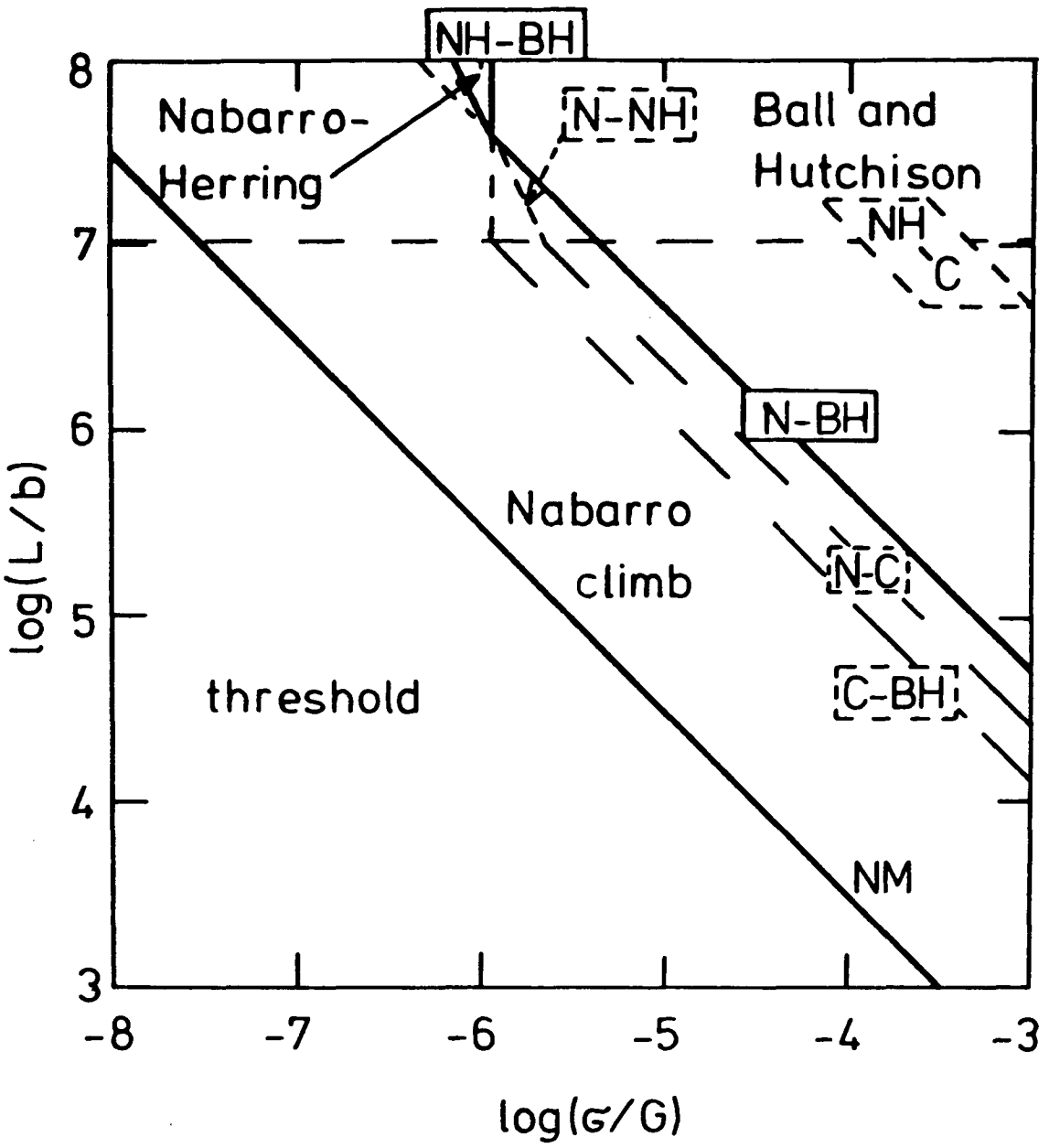

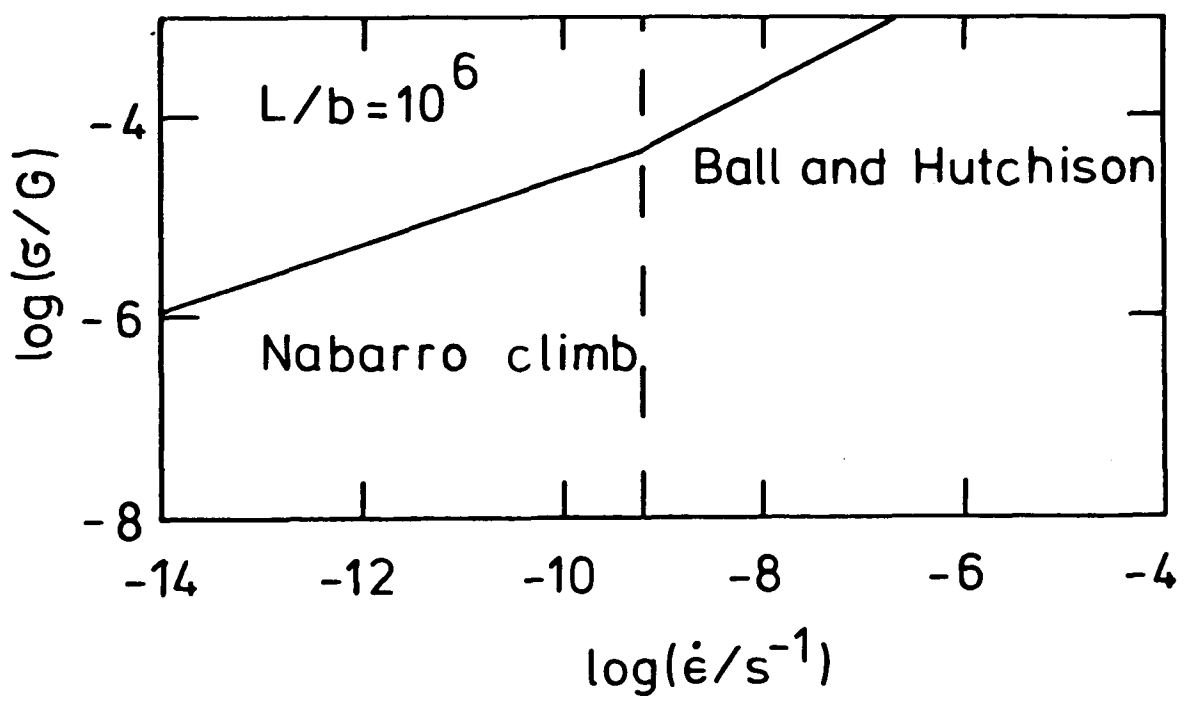

Fig. 2.4. Deformation map for Nabarro-Herring creep, Coble creep, Ball and Hutchison creep, and 2-dimensional Nabarro climb creep; also the corresponding stress-strain rate relationship for $L/b = 10^6$.

Ball and Hutchison creep. Below the minimum stress required for the operation of 2-dimensional Nabarro-Herring creep (annotated NM in Fig. 2.4) no deformation will therefore occur. In other words, there is a threshold stress below which no deformation takes place. The corresponding deformation map in Fig. 2.4 demonstrates the marked change caused by the introduction of an additional mechanism. The Ball and Hutchison field and in particular the Nabarro-Herring field have become much smaller than in Fig. 2.3. Coble creep is suppressed completely and a threshold stress region appears. The relationship between strain rate and stress changes as well (compare Figs. 2.3 and 2.4).

In principle all the mechanisms discussed in previous sections of this chapter could be represented in one deformation map. The number of boundaries separating individual mechanisms, however, would become very large and the map would lose its simplicity. Therefore such a map is not represented here.

2.5 Relationship between grain strain and grain boundary sliding

So far grain strain and GBS have been treated separately as far as possible. In practice, however, the two deformation modes will occur simultaneously. It is, in general, a difficult task to decide how much of the total strain of a polycrystalline aggregate is caused by GBS and to determine whether GBS or grain strain is rate-determining under particular experimental conditions.

The contribution of GBS to the total strain of a polycrystal was first realized by Rachinger (1952-3). However, only for very special grain geometries (diamond shaped grains) is it conceivable that virtually the whole deformation is caused by GBS alone (Cannon, 1971). Therefore the view is adopted that the grain strains and the strains due to GBS are of comparable magnitude for a realistic aggregate of grains (Hazzledine and Newbury, 1976). For this reason the question about the relative contributions of GBS and grain strain seems to be less important than the question which of the two modes of deformation, GBS or grain strain, is rate determining.

2.5.1. Grain strain and intrinsic grain boundary sliding

(a) Grains with homogeneous deformation properties

Crossman and Ashby (1975) used a finite element analysis to calculate the total strain rate of a polycrystalline aggregate. In their model, hexagonal grains form a regular array (in two dimensions) and any volume element within the grains deforms by power-law creep, whereas the GBs slide with a strain rate proportional to the applied stress. The stress exponent, n, of the power-law creep determines almost exclusively the stress exponent of the polycrystalline aggregate regardless of whether the GBs slide freely or whether they do not slide at all. There is only a small transition region (approximately half a decade in the strain rate) in which the stress exponent of the aggregate is smaller than n. The strain rate of a polycrystal with freely

sliding GBs is faster, by a factor of about $(1.2)^n$, than the corresponding strain rate with non-sliding GBs, for identical stresses. This difference is surprisingly small if one considers the highly localized flow field for freely sliding GBs.

For the bulk mechanisms of superplasticity outlined above, Crossman and Ashby's model does not seem to be applicable. The derivation of the stress exponents of these mechanisms requires the consideration of whole grains and cannot be applied to small volume elements within these grains. It seems therefore unlikely that a small volume element of these grians would behave in the same way as individual grains as a whole. A main assumption required for the application of the Crossman and Ashby theory is thus not fulfilled.

(b) Grains with inhomogeneous deformation properties

Grain deformation by diffusion creep is inhomogeneous since, for small strains, the major parts of the grains remain unchanged during deformation and only near the GBs is material inserted or removed. Depending on their respective rates, either diffusion creep or intrinsic GBS may be rate determining (see section 2.2.1).

The Ball and Hutchison mechanism (section 2.2.2) is also an inhomogeneous deformation mechanism. In the original form its derivation assumes easily sliding GBs. If, however, intrinsic GBs is slow or inhibited, some accommodated GBS (for example by lattice dislocations close to the GBs) is probably necessary for the continuous operation of the mechanism.

2.5.2. Grain strain and accommodated grain boundary sliding

(a) Grains with homogeneous deformation properties

Assume a core in the interior of the grains which deforms without any influence from the GBs. The core is surrounded by a mantle adjacent to the GBs the deformation behaviour of which is in some way linked to the presence of GBs (accommodated GBS). In limiting cases, the core may be regarded either as a hard inclusion or as a void of constant volume.

Based on this concept Gifkins (1976) has derived a stress-strain rate relationship (eqn. (2.19)) which has the same stress and grain size dependence of the strain rate as Ball and Hutchison creep (eqn. (2.6)) but is faster by a factor of approximately 10. This is not surprising since Gifkins deformation rate is determined only by deformation of the mantle.

(b) Grains with inhomogeneous deformation properties

As has been suggested above, an inhomogeneous deformation mechanism like the Ball and Hutchison mechanism may require accommodated GBS, for example by lattice dislocations, in order to operate continuously. However, the dislocations in the cores of the grains (in particular the pile-ups associated with the Ball and Hutchison mechanism) and the dislocations in the mantle (accommodated GBS) are expected to interact. A theoretical treatment of such a situation seems difficult.

2.6. Vacancy-interface reaction control

In all the mechanisms treated so far it has been

assumed that GBs and dislocations are good sources and sinks for vacancies. If this is not the case superplasticity may be completely inhibited (this will be discussed in section 2.7) or the strain rate sensitivity of a particular mechanism may be reduced. Burton (1972) suggested that Nabarro-Herring creep may be modified by the vacancy-interface reaction. In his model vacancies are generated or annihilated by GBD spiral climb sources. Nabarro-Herring creep is slowed down and its rate is governed by the absorption and emission of vacancies at the interface. Burton suggests a value of 1/10 for the average jog concentration at GBDs. With a co-ordination number of 2, his equation 15 may be approximately written as:

$$\dot{\varepsilon} = \frac{G\ b\ D_L}{100\ k\ T}\ \frac{b}{L}\ \left(\frac{\sigma}{G}\right)^2 . \qquad (2.20)$$

The stress below which the interface-reaction controls the deformation rate can be obtained by equating the strain rate given by eqn.(2.20) and the strain rate for Nabarro-Herring creep (eqn. (2.3)) and is given by:

$$\frac{\sigma}{G} = 1300\ \left(\frac{b}{L}\right). \qquad (2.21)$$

Below a grain size dependent stress the creep rate is expected to be controlled by the interface reaction. The resulting mechanism, however, can still be called superplastic owing to the high strain rate sensitivity in eqn. (2.20).

2.7. Mechanisms preventing superplasticity

2.7.1. High stresses/high strain rates

Above a certain stress (or strain rate) the strain rate sensitivity of a superplastic material becomes smaller than 0.3 and superplasticity ceases (Fig. 2.1). Above this stress, the lattice dislocation structure is expected to be much finer than the grain size. Conventional dislocation creep (see for example Takeuchi and Argon, 1976) should be prevalent. In the presence of GBS the Crossman and Ashby analysis sould be applicable (see section 2.5.1 (a)) since the grains may now probably be regarded as a continuum with homogeneous deformation properties.

A model which, for small grain sizes, describes the measured grain size dependence of the strain rate for dislocation creep better than the Crossman and Ashby analysis has been proposed by Gifkins (1973). He obtained:

$$\dot{\varepsilon} = (1 + (2\ A\ y\ a)/L^2)\ \dot{\varepsilon}_o\ , \qquad (2.22)$$

where A is a factor describing the stress concentration at triple points, y is the width of triple point folds, a is the subgrain size and $\dot{\varepsilon}_o$ is the dislocation creep rate for a single crystal (Weertman, 1968):

$$\dot{\varepsilon}_o = B\ \frac{D_L\ G\ b}{k\ T}\ \left(\frac{\sigma}{G}\right)^{4.5}\ , \qquad (2.23)$$

where B is a constant.

2.7.2. Low stresses/low strain rates

Whereas the mechanisms governing the plastic deformation at high stresses are fairly well understood, there is considerable disagreement about the mechanisms inhibiting superplasticity at low stresses. The most common mechanism is that of a threshold stress for which many reasons have been advanced. The processes which may inhibit superplasticity are conveniently divided into vacancy-interface reactions, GBS mechanisms and GB tension mechanisms.

(a) Vacancy-interface reaction

Work may have to be done in order to create or annihilate a vacancy at a GB (Ashby and Verrall, 1973). This work may be described by an interface potential, $\Delta\mu_i$. The stress σ in the diffusion creep equation (2.5) has then to be replaced by $(\sigma-\Delta\mu_i/\Omega)$, where $\Delta\mu_i/\Omega$ is a grain size independent threshold stress below which no deformation occurs. An interface potential could also cause a threshold stress for the dislocation mechanisms of superplasticity described previously.

If the volume of vacancies emitted or absorbed at the GBs is some function, f, of the applied stress, Greenwood (1970) has shown that an equation of the type

$$\dot{\varepsilon} \alpha f(\sigma)/L \qquad (2.24)$$

holds for the diffusion creep rate. Equation (2.24) expresses the inverse grain size dependence which interface processes may cause. If $f(\sigma)$ is 0 below a grain size-independent stress a threshold stress results as above.

(b) Grain boundary sliding mechanisms

GBDs moving along a GB containing a dispersion of particles will have to bow out in order to by-pass the particles (Ashby, 1969). Due to the self-energy of the dislocations this bowing-out will not occur below a certain threshold stress which is defined by $2E/(b_B \lambda) \sim (G b_B)/\lambda$, where E is the dislocation line energy and λ the particle spacing. It is reasonable to assume that λ is of the order of the grain size for a dispersion free GB in which case the threshold stress is $(G b_B)/L$. Of course a GBS threshold stress becomes effective only if GBS is rate-limiting as may be the case in diffusion creep.

(c) Grain boundary tension effects

Ashby and Verrall (1973), for the switching event proposed by them (Fig. 2.2(a)), calculated the increase of the GB area of a group of four grains in the intermediate position of the switching event, with respect to the initial position. This area increase corresponds to an energy increase which must be supplied by the applied stress. The switching event employed by Ashby andVerrall leads to a threshold stress of $0.72\ (\gamma/L)$ where γ is the specific GB energy (GB energy per unit area). It should be noted that switching events during deformation of a previously annealed sample with an equilibrium grain structure occur possibly only after strains of the order of 0.25. Therefore, for strains smaller than ~ 0.25 there may be no or only a low threshold stress.

An assumption in Ashby and Verrall's derivation is that the energy required to pass from the initial to the intermediate state of the switching event is irreversibly lost.

The transition from the intermediate to the final state in Fig. 2.2(a), however, is accompanied by a reduction of the GB area. The GB tension may thus generate mechanical work. A similar effect has been demonstrated experimentally by Heumann and Wulff (1976) with bamboo-structured wires (not only GB tension but also surface tension operates in this case). If many switching events are in different stages at the same time the total energy input may be zero and no threshold stress may arise. An incomplete energy release in passing from the intermediate to the final state would cause the threshold stress to be smaller than 0.72 (γ/L).

2.8. Summary

The strain rates predicted by bulk mechanisms of superplasticity depend on the stress, σ, and the grain size, L, like σ/L^2, σ/L^3, σ^2/L, or σ^2/L^2.

If GBS controls the total strain rate, dependencies like σ/L, σ/L^2, σ/L^3 or σ^2/L^2 are possible. Grain size dependencies different from 1/L arise because of the interaction of GBDs in intersecting GBs.

The mechanisms for GBS and grain deformation will in general operate simultaneously. With the exception of diffusion creep, none of these mechanisms is well known. Mechanisms involving both GBS and grain deformation are therefore in most cases only amenable to a qualitative discussion.

Superplasticity may be obscured by conventional dislocation creep (at high stresses) and be inhibited by a

variety of mostly interface mechanisms (at low stresses). The inhibition can be caused by dislocation line tension, insufficient sink-source ability of the GBs or GB tension. The threshold stresses are often proportional to the inverse grain size.

CHAPTER 3

MECHANISMS OF ANELASTICITY

3.1. Introduction

Anelasticity (Nowick and Berry, 1972) describes time-dependent, recoverable deformation of a material. Whereas elastic deformation occurs usually quickly (the delay time after application of a stress is determined by the small inertia of the tested sample), anelastic deformation is relatively slow. Under many experimental conditions, elastic deformation is therefore said to be time-independent, whereas anelastic deformation depends on the time.

A schematic plot of the total deformation, ε , as a function of the time, t, if only elastic and anelastic deformation are present is shown in Fig. 3.1. The anelastic deformation, ε_a, at any time is given by:

$$\varepsilon_a(\sigma,t) = \varepsilon(\sigma,t) - \varepsilon_e(\sigma), \qquad (3.1)$$

where ε_e is the elastic deformation which is uniquely determined by the applied stress, σ. The process of anelastic deformation due to loading ($\sigma \neq 0$) is sometimes called strain relaxation and the anelastic strain following unloading ($\sigma = 0$) is also referred to as the elastic after-effect.

Anelasticity is often assumed to be linear in stress. This means that, for an initially relaxed sample ($\varepsilon_a = 0$) the relation $\varepsilon_a(t_o) \alpha \sigma$ holds, where σ is the stress applied at $t = 0$ and t_o is a specified time greater than 0. Also, the Boltzmann superposition principle is usually supposed to hold. If a material is subjected to different stress

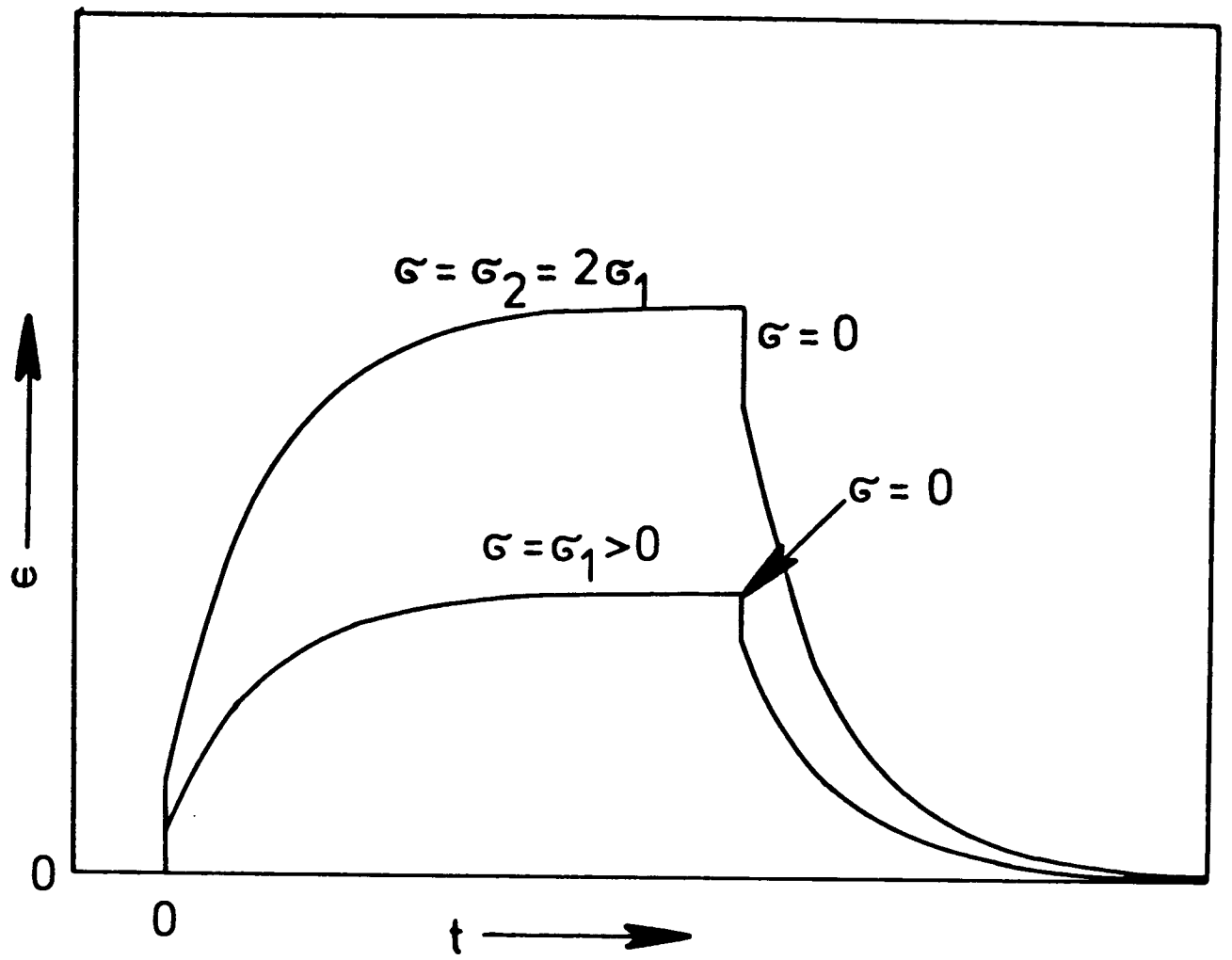

Fig. 3.1. Total deformation, ε (elastic and anelastic) for different applied stresses, σ, as a function of the time, t (schematic). $\sigma = 0$ for $t < 0$.

increments at different times this principle states that each of the stress increments contributes to the deformation as if it were acting alone. Both linearity and superposition principle facilitate the theoretical treatment of anelasticity and are also often borne out in experiments (Nowick and Berry, 1972).

In the case of linear anelasticity it is often convenient to define an anelastic compliance, J_a, by:

$$J_a(t) = \varepsilon_a(t,\sigma)/\sigma. \qquad (3.2)$$

In order to insure a consistent value of J_a for an experiment of the type syown in Fig. 3.1 it is convenient to set ε_a to 0 at the moments of loading and unloading. Unloading from a stress σ_o is formally represented by superimposing a stress $-\sigma_o$ at the moment of unloading.

A useful parameter to describe linear anelasticity is the relaxation strength, Δ_r:

$$\Delta_r = \varepsilon_a(t = \infty)/\varepsilon_e, \qquad (3.3)$$

where the investigated sample should be completely equilibrated at $t=t_o$, when the loading or unloading takes place.

Another important parameter is the relaxation time, τ, which in terms of Fig. 3.2(a) is given by:

$$\tau = E_o/\eta, \qquad (3.4)$$

where E_o is the modulus and η the viscosity of a Voigt element. The time-dependence of anelastic deformation may now be expressed as:

$$J_a(t) = J_o\ (1 - \exp(-t/\tau))\ , \qquad (3.5)$$

where $J_o = 1/E_o$.

Real materials will usually deform plastically, as well as elastically and anelastically. Plastic deformation does not influence the elastic after-effect since, by definition, an external stress equal to 0 does not cause any plastic strain. For $\sigma \neq 0$, however, the situation is less clear. In the simplest approximation elastic, anelastic and plastic strains are additive. More generally, plastic and anelastic deformation interact and can therefore not be added up in a simple manner. That this may be so can be seen from the simplest rheological representation of anelasticity (see the Voigt element in Fig. 3.2(a)): Anelasticity involves "plastic deformation" which is however not driven by an external stress (which would cause conventional plasticity) but by an internal stress. Since the two kinds of plasticity, the one caused by external and the one caused by internal stresses may be interlinked or be identical, simple addition of anelasticity and plasticity will not always be satisfactory.

There is an extensive literature on anelasticity, which is reviewed and discussed in Nowick and Berry's (1972) monograph. However, a short account of the mechanisms

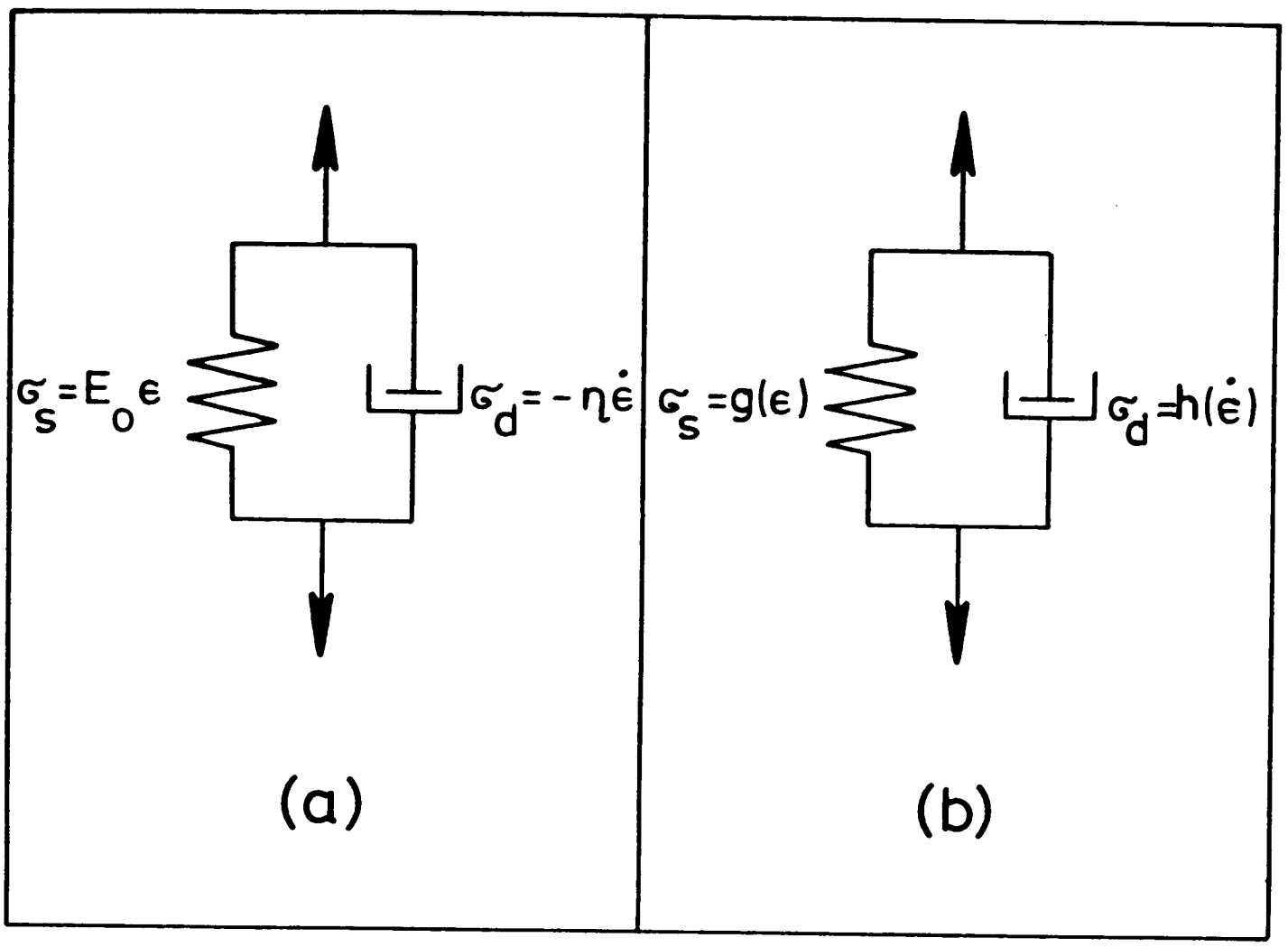

Fig. 3.2. Two examples for rheological models of anelasticity:

(a) Voigt element: linear spring with Young's modulus E_o and Newtonian-viscous dashpot with a viscosity of η.

(b) general element: the stresses are general functions g and h of the strain and the strain rate, respectively.

known to date and of other mechanisms which may be of importance will be given in order to facilitate the discussion of the experiments in chapter 6. Since the experimental results will be seen to indicate a "high-temperature" and "small grain" mechanism(s) mainly such processes have been reviewed. In particular low-temperature mechanisms such as those which cause the Bordoni-peak (Nowick and Berry, 1972) have been omitted.

3.2. Driving force for anelasticity caused by point defects

3.2.1. Elastic interaction between point defects and crystal

Point defects may produce anelastic deformation by stress-induced site change. The relaxation strength, Δ_r, for cubic crystals is approximately given by (Nowick and Berry, 1972, p.194):

$$\Delta_r = \frac{\nu \Omega E_u}{k T} (\delta\lambda)^2, \qquad (3.6)$$

where ν is the mole fraction of the defects in consideration, E_u is the elastic ("unrelaxed") modulus, and $\delta\lambda$ is the difference in the principal values of the strain tensor of the defects in their different sites.

The relaxation strength given by equation (3.6) is usually much smaller than 1. For typical values $\nu = 10^{-2}$, $\Omega = 10^{-29} m^3$, $E_u = 100GPa$, $T = 300K$, and $\delta\lambda = 0.1$, a value of only 0.02 is obtained.

The relaxation time for the process above is linked to the rate with which defects change sites (i.e. to their

diffusion properties) and is therefore strongly temperature-dependent.

A well known example of anelasticity caused by elastic interaction between point defects and the lattice is the Snoek-effect (see Nowick and Berry, 1972). Interstitial carbon atoms in iron change their sites in response to an applied stress and anelasticity results.

3.2.2. Composition changes in two-component, two-phase systems

Application of a hydrostatic stress changes the equilibrium concentrations in a two-phase, two-component system. The resulting diffusional transport can cause anelastic deformation. Krivoglaz (1960) has treated this problem for small spherical particles of one phase in a matrix of another phase. The relaxation time, τ, is given by:

$$\tau = \frac{r_o^2}{3\ D\ \nu_p}, \tag{3.7}$$

where r_o is the radius of the spherical particles, D is the coefficient of interdiffusion in the matrix phase, and ν_p is the volume fraction of the particles.

The relaxation strength qualitatively depends on the influence of hydrostatic stresses on the phase diagram. This influence is only important near the phase-transformation temperature of the investigated system, where Krivoglaz's mechanism may become important. However, no

quantitative estimate for the relaxation strength has been given.

3.3. Driving force for anelasticity caused by elastic grain deformation

Zener (1941) has presented a model based on viscous GBS and elastic grain strains. The loading of a (previously relaxed) polycrystalline sample leads initially to a homogeneous elastic strain. Subsequently the shear stresses along the GBs are relaxed by viscous GBS. This relaxation is time-dependent and recoverable and is therefore an anelastic process. For spherical grains Zener found an expression for the relaxed Young's modulus corresponding to a relaxation strength

$$\Delta_r = \frac{7 - 3\nu - 10\nu^2}{7 + 5\nu}, \qquad (3.8)$$

where ν is Poisson's ratio. For typical values of ν, eqn. (3.8) leads to (grain size independent) relaxation strengths of approximately 0.6. Elastic grain strains cannot be stored if GBS is difficult: then the Zener mechanism does not operate. For viscous GBS, a regular array of equiaxed grains is characterized by a single relaxation time (Nowick and Berry, 1972, p.437), τ,

$$\tau = \frac{\eta_B L}{w\, G_u}, \qquad (3.9)$$

where w is the GB width, G_u the lattice shear modulus, and η_B the viscosity of the GBs (defined by $v = (\sigma\, w)/\eta_B$,

for an applied shear stress σ and a GBS rate v).

τ in eqn. (3.9) is proportional to the grain size. A distribution of grain sizes should therefore lead to a spectrum of relaxation times. If the grains are not equiaxed relaxation strengths much higher than 0.6 may also be possible as have been pointed out by Zener (1948, p.158). An example is a polycrystal with elongated, aligned grains stressed in shear parallel to the long axes of the grains.

A numerical treatment of Zener's model which is applicable to non-spherical, close-packed grains has been given by Raj and Ashby (1971).

There is substantial evidence that Zener's process occurs in real materials (see Nowick and Berry, 1972, chapter 15), although there are clearly anelastic data for polycrystals which need further explanation. It is for example conceivable that the rate of GBS obeys a non-linear law such as

$$v \alpha \sigma^n, \qquad (3.10)$$

with n = 2 or 3. Mechanisms predicting such a relationship have been discussed in chapter 2. There is also experimental evidence, derived from GBS tests, for eqn. (3.10) (see Gleiter and Chalmers, 1972).

A relationship like eqn. (3.10) does not change the relaxation strength given by eqn. (3.8) but only the kinetics. Consideration of a suitable rheological model (linear spring and non-linear dashpot in parallel, compare

Fig. 3.2(b)) leads immediately to a relation between anelastic strain and strain rate for the elastic after-effect,

$$\dot{\varepsilon}_a \alpha -\varepsilon_a^n, \qquad (3.11)$$

where the anelastic strain in this case is defined to be 0 in the completely relaxed and stress-free state. It can be seen that, in contrary to the behaviour of a Voigt element, the relaxation times now depend on the strain stored in the non-linear spring of the rheological element. Elastic after-effects cannot be described by a single relaxation time any ore, even in a material with a uniform grain size, and a relaxation time spectrum has to be employed.

3.4. Driving force for anelasticity caused by grain boundary tension

The GB area of initially eqiaxed grains increases during deformation if the grain deformation is geometrically similar to the macroscopic deformation of the polycrystalline aggregate considered. For an array of cubic grains the following expression can be found for the GB area, A, delimiting each grain, as a function of the strain (see Fig. 3.3):

$$A = 2\ L^2\ (2\ e^{\varepsilon/2} + e^{-\varepsilon}) \sim 6\ L^2\ (1 + \varepsilon^2/4), \qquad (3.12)$$

for $\varepsilon \lesssim 1$. The edge-length, L, of the cubic grains is here identified with the grain size.

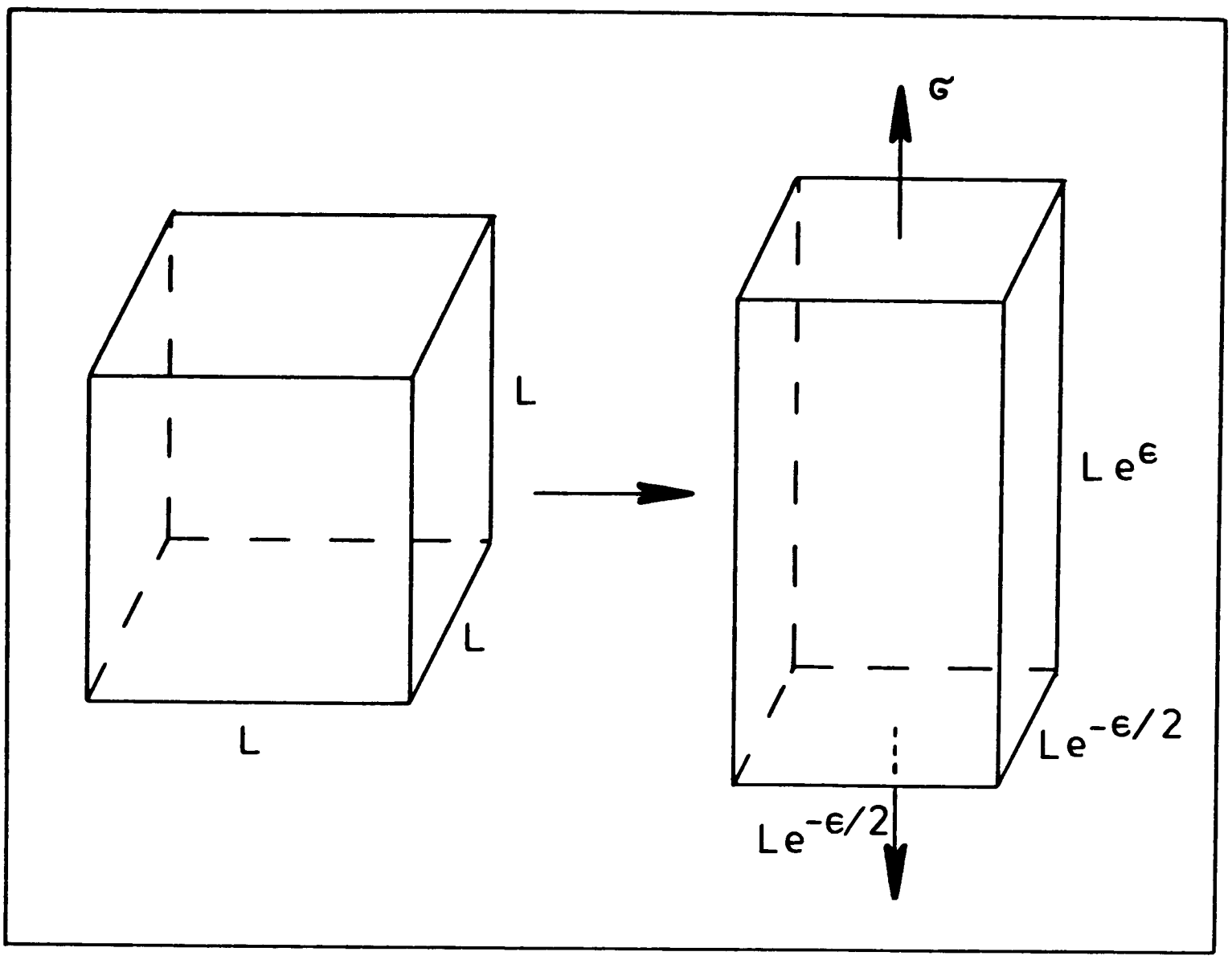

Fig. 3.3. The change in the edge lengths of an initially cube-shaped grain deformed by ε.

The work needed in order to increase the GB area is supplied by the applied stress, σ , according to

$$\sigma L^3 \, d\varepsilon = \frac{\Gamma}{2} \, dA, \tag{3.13}$$

where Γ is the GB energy per unit area (a factor 1/2 has been introduced since each GB is shared by two grains). With eqn. (3.12), one obtains immediately for the driving force, σ_s, for an elastic after-effect (if the process described by eqn. (3.13) is reversible):

$$\sigma_s = B \, \varepsilon, \tag{3.14}$$

where $B = (3\,\Gamma)/(2\,L)$. The stress given by eqn. (3.14) is linear in the strain. It is caused by the energy release during contraction of an initially elongated grain.

Together with a suitable deformation mechanism for the grains, anelastic behaviour corresponding to a Voigt element can now be obtained. With

$$\sigma_d = \eta \, d\varepsilon/dt, \tag{3.15}$$

where η is the viscosity of the plastic process, a short calculation leads to expressions for the relaxation time and the relaxation strength:

$$\tau = \frac{\eta}{B} = \frac{2\,L\,\eta}{3\,\Gamma}, \tag{3.16}$$

and

$$\Delta_r = \frac{E_u}{B} = \frac{2\ L\ E_u}{3\ \Gamma}, \qquad (3.17)$$

where E_u is the Young's modulus of the grains.

The relaxation strength depends on Young's modulus, the GB energy, and the grain size of the material and does not depend on the plastic component of the anelastic mechanism. Realistic values of E_u = 100GPa, L = 1μm, τ = 0.3J/m^2 (see Murr, 1974,p.131) lead to a value of $\Delta_r = 2.2 \cdot 10^4$ (provided that the anelastic strains are smaller than 1, see also eqn. (3.12)), which is much higher than the relaxation strengths of the previously discussed mechanisms.

If the plastic component of the anelasticity is Coble creep (eqn. (2.4)), one obtains for the relaxation time:

$$\tau = \frac{k\ T\ L^4}{70\ \Gamma\ \Omega\ D_B\ w}\ . \qquad (3.18)$$

The strong grain size dependence of τ should be noted.

Similarly, Nabarro-Herring creep (eqn. (2.3)) leads to:

$$\tau = \frac{k\ T\ L^3}{2o\ \Omega\ \Gamma\ D_L}\ . \qquad (3.19)$$

The deformation may also be determined by GBS if GBS is slower than diffusion creep (see section 2.2.1). The viscosity in eqn. (3.15) is then $\eta = (\eta_B\ L)/w$, where η_B is the GB viscosity, and the relaxation time is:

$$\tau = \frac{2\,\eta_B\,L^2}{3\,\Gamma\,w} \quad . \tag{3.20}$$

The situation becomes more complicated if instead of eqn. (3.15) a non-linear law relates stress and strain rate. This case has been briefly discussed in section 3.3.

Another complicating factor is the grain size distribution which a real solid usually has. A spread in the observed relaxation times is caused which, for a given grain size distribution, will be most pronounced for Coble creep (see eqn. (3.18). The correct prediction of the relaxation spectrum seems difficult since the deformation of an individual grain depends on the deformation of many other surrounding grains.

A main assumption for the derivation of the GB tension mechanism is the reversibility of the process described by eqn. (3.13), i.e., a decrease in GB area provides mechanical work. This need not be the case; Ashby and Verrall (1973), for example, argue that the energy released in passing from the intermediate to the final state of their switching event (see Fig. 2.2(a)) is completely dissipated. However, experimental data which tentatively support the GB tension mechanism suggested above are available for wires with a bamboo structure. Heumann and Wulff (1976) found anelastic contractions of the order of 0.1% for such wires. Since in experiments of this type a significant amount of surface area is involved, however, a conclusive answer on the importance of the GB tension effect cannot yet be given.

3.5. Driving force for anelasticity caused by dislocation line tension

Since a dislocation has a certain amount of energy per unit length, E, associated with it (this energy is here assumed to be positive and independent of the dislocation character), it has also a line tension, i.e., it tends to shorten itself. Consider for example a dislocation segment pinned between two points a distance λ apart. While the segment is bowing out it glides or climbs over an area A_d. For a radius of curvature, r, of the segment one obtains the relations $A_d = \lambda^3/(12r)$ (for $r >> \lambda$) and $\sigma = T/(b\ r)$, where T is the dislocation line tension (Nowick and Berry, 1972, p.359). The reverse driving stress which causes the segment to straighten again is therefore approximately proportional to the area, A_d, over which gliding or climbing occurred. Thus the stress due to line tension and the strain due to the bowing-out of dislocation segments are proportional. If the dislocation motion is impeded by a friction stress anelasticity results. The relaxation strength of such a mechanism was calculated by Friedel, Boulanger and Crussard (1955) as

$$\Delta_r = \beta\ \rho\ \lambda^2 = N_V\ \lambda^3, \qquad (3.21)$$

where β is a numerical constant of the order of unity, ρ is the dislocation density, λ is the length of the bowing dislocation segments and N_V the volume density of these segments. For a homogeneous dislocation distribution $\rho \sim 1/\lambda^2$ and

the relaxation strength is of the order of 1. Friedel, Boulanger and Crussard have pointed out that the average volume density of dislocation segments of length λ may be much larger than $1/\lambda^3$ if the dislocations are polygonized into subgrains of diameter L_s and are spaced a distance h apart at the subgrain walls. Then N_V is approximately $(L_s/h)/(1/\lambda^3)$ and the relaxation strength can become much larger than 1. The geometrical arrangement of the dislocations is therefore crucial in determining the relaxation strength.

Assuming a homogeneous dislocation network, Burton (1977a, p.89) has evaluated the relaxation time expected for viscously climbing dislocations. He obtains:

$$\tau = \frac{2\,k\,T\,\lambda^2}{\pi^2\,G\,D_L\,b^3}\,, \qquad (3.22)$$

for a dislocation link length λ. For small grains λ is of the order of the grain size and $\tau \alpha L^2$.

Burton's model may also be applied to GBs, and then it describes the anelasticity which is expected for two-dimensional Nabarro climb creep (see section 2.3.1), if the components of the GBD Burgers vectors, parallel and vertical to the GBs, are of comparable magnitude. The result, for $b_b \sim b_L$ and a homogeneous dislocation distribution in the GBs (see appendix A3) is:

$$\Delta_r = \lambda/(2L), \qquad (3.23)$$

and

$$\tau = \frac{k\ T\ \lambda^2}{2\ G\ D_B\ b^3} \cdot \qquad (3.24)$$

The appropriate diffusion coefficient is now that for GB self-diffusion. The relaxation strength is expected to be smaller than 1 since the GBD link length is probably not larger than the grain size, L.

Experimental evidence by Friedel, Boulanger and Crussard (1955) supporting the validity of eqn. (3.21) was found from internal friction experiments. This testing method, however, does not distinguish very well between anelastic and plastic contributions to the internal friction. On the other hand, Burton and Reynolds (1974) have found good evidence for the relaxation time given by eqn. (3.22) and the relaxation strength in eqn. (3.21). Burton and Reynolds employed strain relaxation for their investigation of uranium dioxide and disturbing influences from plastic deformation should therefore be negligable.

3.6. Driving force for anelasticity caused by interaction between dislocations

The Ball and Hutchison model for superplastic deformation (eqn. (2.6)) is based on the formation of pile-ups across the grains. Upon unloading, these pile-ups may run back and cause an elastic after-effect. The driving force for the anelasticity is the repulsion between identical dislocations in each pile-up.

Burton (1977b) assumed a constant number of dislocations in each pile-up (no dislocation creation or annihilation). The dislocations in a pile-up are confined between two opposite GBs. Burton calculated a maximum value of the relaxation strength of 0.5. Measurements with a zirconium alloy confirmed the validity of his model.

There is not much evidence for lattice dislocation pile-ups during superplastic deformation at low stresses (Edington, Melton and Cutler, 1976, pp.124-125). Instead of a lattice dislocation mechanism it is therefore preferable to use a GBD model similar to Burton's model. In particular the kinetics of such a model do not yet appear to have been looked at in detail and will be evaluated in an approximate manner below.

Consider n GBDs with Burger's vector b piled up against a triple edge under the action of a shear stress τ_a. The maximum length of such a pile-up is probably of the order of the grain size, L. The number of dislocations in the pile-up is then (Hirth and Lothe, 1968):

$$n = \frac{\pi \quad L \ \tau_a}{G \ b} \ . \tag{3.25}$$

Upon removal of the applied stress, each dislocation will run back by an average distance of ~L/2. If the Burgers vector, b, has a significant component parallel to the considered GB, a GBS displacement of approximately (n b)/2 results. For a polycrystal of grain size L, the anelastic

shear strain, γ_a, is therefore $-(n\ b)/(2L)$. The relaxation strength is now

$$\Delta_r = \frac{\gamma_a}{\gamma_e} = \frac{\pi}{2} , \qquad (3.26)$$

where γ_e is the elastic strain τ_a/G. A more precise calculation (Burton, 1977b) leads to $\Delta_r = 0.5$. It should be noted that the relaxation strength does not depend on the value of b.

In order to calculate the kinetics of the relaxation process, n dislocations piled up against a leading (locked) dislocation will now be described by a superdislocation with Burgers vector, nb, interacting with a single dislocation with Burgers vector b (see also Hirth and Lothe, 1968). In equilibrium with an applied shear stress, τ_a, the distance between the leading dislocation (Burgers vector b) and the superdislocation is:

$$x_o = \frac{G\ b}{2\ \pi\ \tau_a} . \qquad (3.27)$$

The viscous movement of an individual dislocation is described by a mobility M defined by:

$$v = M\ F, \qquad (3.28)$$

where v is the velocity of the dislocation under the action of a force per unit length, F. M is estimated by the Einstein relationship (Friedel, 1964, p.84):

$$M = \frac{D_B \, b}{k \, T} \, . \tag{3.29}$$

If the applied stress, τ_a, is now removed at t = 0, one obtains for the distance, x, between superdislocation and leading dislocation as a function of the time:

$$\frac{dx}{dt} = F \, M = \frac{G \, b \, n \, b}{2 \, \pi \, x} \, M. \tag{3.30}$$

Integration leads to

$$x = x_o \, (1 + \frac{t}{t^*})^{1/2}, \tag{3.31}$$

where t* is defined by:

$$t^* = \frac{\pi \, x_o^2}{G \, n \, b^2 \, M} \, . \tag{3.32}$$

The number of dislocations is assumed to be constant in eqn. (3.31) and source back-stresses have not been taken into account.

For $t > t^*$ (or $x > \sqrt{2} x_o$, after eqn. (3.31)) the elastic after-effect for a polycrystal of grain size L is now approximately:

$$\gamma_a \sim - \frac{n \, b \, x}{x_1 \, L} \, , \tag{3.33}$$

where x_1 is the maximum distance which the superdislocation

can move with respect to the leading dislocation ($x_1 \lesssim L$). Equation (3.33) holds if there are L/x_1 pile-ups along a GB segment. Inserting eqns. (3.31) and (3.32) in eqn. (3.33) leads to:

$$\gamma_a = - \frac{b^2 \, G^{1/2} \, M^{1/2} \, n^{3/2} \, t^{1/2}}{\pi^{1/2} \, x_1 \, L} , \qquad (3.34)$$

for $t > t^*$ (or $x > 2^{1/2} \, x_o$). The length of pile-ups prior to relaxation is x_p. Following eqn. (3.25) the number of dislocations in a pile-up is $(\pi \, x_p \, \tau_a)/(Gb)$. With eqn. (3.29) and after converting into tensile stresses and strains one obtains now for the elastic after-effect:

$$\varepsilon_a = - \frac{\pi \, b \, D_B^{1/2} \, x_p^{3/2} \, \sigma^{3/2} \, t^{1/2}}{4\sqrt{2} \, G \, (k \, T)^{1/2} \, x_1 \, L} , \qquad (3.35)$$

with the additional condition that $\varepsilon_a/\varepsilon_e \leq \pi/2$ (eqn. (3.26)). If the initial length of the pile-ups, x_p, and the maximum dislocation displacement, x_1, do not depend on the stress, the time after unloading, or the grain size, then an inverse grain size dependence of the anelastic strain is obtained. The square root dependence on the diffusion coefficient in eqn. (3.35) should be noted. Comparison of elastic after-effects after identical times after unloading would lead to an activation energy which is smaller than that for GB self-diffusion by a factor of 2. The time-dependence of the elastic after-effect described by eqn. (3.35) is different from that of a Voigt element (eqn. (3.5)) and can therefore not be represented by a single relaxation

time. In addition, the anelasticity is not linear in stress. For a particular applied stress, however, a relaxation spectrum, $X(\ln\tau)$, for the relaxation times, τ, may be evaluated. (Note: the shear stress is called τ_a in this chapter, whereas the relaxation time is called τ). The anelastic compliance can be expressed as (see Nowick and Berry, 1972):

$$J_a(t) = \int_{-\infty}^{+\infty} X(\ln\tau)\ (1-\exp(t/\tau))\ d(\ln\tau), \qquad (3.36)$$

where $X(\ln\tau)$ may be approximated by Alfrey's rule:

$$X(\ln\tau) = \frac{dJ_a(t)}{d(\ln\ t)}\ \Bigg|_{t\ =\ \tau}\ . \qquad (3.37)$$

From eqn. (3.35) it follows immediately that

$$X(\ln\tau)\ \alpha\ \tau^{1/2}\ , \qquad (3.38)$$

for a particular stress σ.

From eqn. (3.35) it follows that $t\ \alpha\ \dot{\varepsilon}_a^{-2}$ and for viscous dislocation movement the maximum variation in $\dot{\varepsilon}_a$ during the relaxation is approximately given by

$$\frac{\dot{\varepsilon}_a(max)}{\dot{\varepsilon}_a(min)} = \frac{x_1}{x_p}\ , \qquad (3.39)$$

since the dislocation velocity is inversely proportional to the distance between repulsive dislocations. This means that the relationships $\dot{\varepsilon}_a\ \alpha\ t^{-1/2}$, $\varepsilon_a\ \alpha\ t^{1/2}$, and $X(\ln\tau)\ \alpha\ \tau^{1/2}$ hold for a range of times defined by:

$$t_{max}/t_{min} = (x_1/x_p)^2 \quad . \tag{3.40}$$

Provided that x_1/x_p is sufficiently large, eqn. (3.38) therefore represents a broad spectrum of relaxation times.

For $x_p < x_1 < L$ the relaxation strength may be much smaller than that given by eqn. (3.26). In a manner similar to the derivation of eqn. (3.26) one obtains:

$$\Delta_r = \frac{\pi\, x_p\, x_1}{L^2} \quad . \tag{3.41}$$

For $x_p = L$ and $x_1 = L/2$ eqn. (3.41) reduces to eqn. (3.26).

The maximum anelastic strain which can be recovered after loading with a stress σ is obtained from eqn. (3.41):

$$\varepsilon_a(max) = \Delta_r\, \varepsilon_e = \Delta_r \frac{\sigma}{E} \sim \Delta_r \frac{3\sigma}{8G} = \frac{3\,\pi\, x_p\, x_1\, \sigma}{8GL^2} \quad . \tag{3.42}$$

From eqns. (3.40) and (3.41) it follows that the relaxation strength of the GBD pile-up mechanism presented here increases if the length of the pile-ups, x_p, and the distance x_1 over which the relaxation occurs, increases. The range of relaxation times, however, becomes wider for increasing values of x_1/x_p.

In order to demonstrate that the modelling of a relaxing pile-up by a super-dislocation is a sufficiently good approximation the result of a numerical calculation

will now be compared with the curve defined by eqn. (3.35). Eight GBDs piled-up against a leading (blocked) GBD were initially assumed to be in equilibrium with an applied shear stress, τ_a. The required locations of the dislocations are given by Mitchell, Heckner and Smialek (1965). Upon removal of the applied stress each dislocation was initially driven by a force $F = -\tau_a b$ and moved with a velocity determined by eqn. (3.29). After all 8 dislocations had been moving with this velocity for a short period of time the forces exerted on each moving GBD by the other 8 GBDs were re-evaluated and the new dislocation velocities determined. The dislocation positions as a function of the time were thus iteratively determined.

The anelastic strain, $\Delta\varepsilon_a$, produced by the displacement, Δx, of a GBD was calculated as:

$$\Delta\varepsilon_a = \frac{\Delta x \; b}{2 \; x_1 \; L} \; . \qquad (3.43)$$

The strain increments produced by the individual GBDs were added after each time increment and led to values of the anelastic strain as a function of the time after unloading of the pile-up. GBDs more than a distance x_1 away from the leading GBD were assumed to be annihilated and thus did not exert any force on the remaining dislocations.

The result of the calculation is represented in Fig. 3.4 (the numerical values employed are found in the caption to this figure). Equation (3.35) was also evaluated within the range in which the approximations employed in

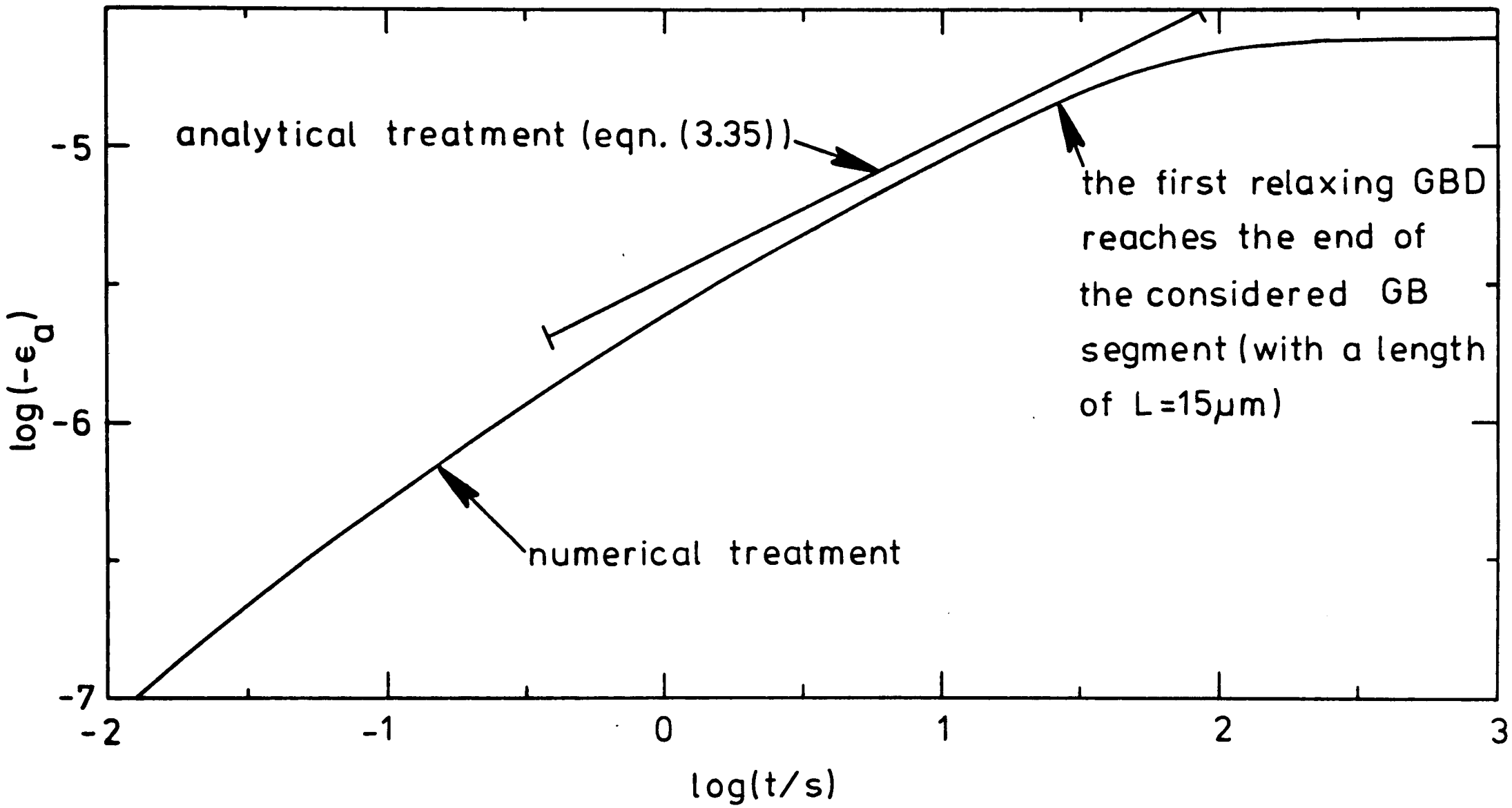

Fig. 3.4. Relaxation of a GBD pile-up calculated analytically employing a super-dislocation (eqn. 3.35) and numerically by considering individual dislocations. Numerical values employed: b = 0.1nm, D_B(Sn, 298K) = $6.2 \cdot 10^{-13} m^2/s$ (Lange and Bergner, 1962), x_p = 1μm, σ = 7.8MPa, τ_a = 3.9MPa, G = 20GPa (Cottrell, 1968, p.308), T = 298K, x_1 = L = 15μm.

its derivation should hold. This range is defined by eqns. (3.40) and (3.42). The agreement between the analytical and the numerical treatment is seen to be satisfactory.

3.7. Summary

Several mechanisms for anelasticity which may be of importance for the deformation of small-grained polycrystals at elevated temperatures have been reviewed or derived.

(1) Mechanisms based on point defects generally have a relaxation strength (= ratio of anelastically to elastically recovered strain) much smaller than 1.

(2) Anelasticity caused by the storage of elastic grain strains has a relaxation strength of the order of 1. Its time-dependence can be described by a relaxation time which is proportional to the grain size.

(3) Relaxation strengths much larger than 1 may be possible for anelasticity caused by the grain boundary tension of elongated grains. The relaxation time depends sensitively on the grain size. For example, a relationship like $\tau \alpha L^4$, where τ is the relaxation time and L the grain size, is possible.

(4) Anelasticity due to dislocation line tension has usually a relaxation strength of the order of 1 or less. Provided that the dislocation link lengths do not vary too much it can be described by a single relaxation time. If the dislocation link lengths are of the order of the grain size,

$\tau \alpha L^2$.

(5) Repulsion between piled-up dislocations is the driving force for non-linear anelasticity which can have a very wide spectrum of relaxation times. The relaxation strengths are of the order of 1 or less.

CHAPTER 4

EXPERIMENTAL PROCEDURES

4.1. Sample preparation

Sn-2w/o Pb and Sn-38.1w/o Pb (eutectic composition) alloys were prepared from Sn and Pb of 99.999% purity by melting in air and casting into a copper chill-mould of dimensions $10 \times 38 \times 95 mm^3$. Prior to the casting, the melts were homogenized for ~300s at ~500K and stirred occasionally.

Some ingots were also melted in an Argon atmosphere. The mechanical behaviour of the samples prepared from them did not show any marked difference from the material melted in air.

The ingots were rolled at room temperature from 10mm to thicknesses between 0.2mm and 1mm, in several passes. From the rolled strips tensile samples with a gauge length of 26mm and a width of 6mm were stamped. Samples which were tested in the as-rolled condition were usually stored in liquid nitrogen prior to the test. Other samples were annealed in silicone fluid for various periods of time at several temperatures in order to produce a wide range of grain sizes. In some cases, annealing was done in water for 2 hours at 373K. Although the sample surfaces discoloured slightly during this treatment no anomalies in the mechanical behaviour were detected. Prolonged annealing (i.e. several days) in silicone fluid at temperatures close to the melting point, at 453K, resulted in a thin dark surface layerwhich was cautiously removed with grade 600 emery paper.

A few examples of the effect of heat treatments on the grain size of Sn-38.1w/o Pb are quotedby Newbury (1972).

After 24 hours at 433K he finds a mean phase boundary intercept length of 5.9μm, after 475 hours at 441K the intercept length is 9.9μm. Characteristic heat treatments for Sn-2w/o Pb were 15 minutes at 393K to obtain a grain size of 50μm and 12 minutes at 453K to obtain 260μm. The range of grain sizes obtained (for the method of measurement see below) was between ~1.5μm and ~20μm for Sn-38.1w/o Pb, and between ~12μm and ~260μm for Sn-2w/o Pb.

4.2. Metallography

Following Newbury (1972), samples were mounted in cold-setting resin and cooled in ice water during the setting process. After initial grinding with emery paper, they were polished with a mixture of alumina powder and liquid soap. Care was taken during this final polish in order to minimize surface deformation which can reduce the quality of the subsequent chemical etching significantly.

The grain boundaries in Sn-2w/o Pb were easily exposed by etching with ~2ml hydrochloric acid in 98ml ethanol. Sn-38.1w/o Pb was also etched with this solution in order to reveal Sn-Sn and Sn-Pb boundaries. Subsequent over-etching with a solution of 10g ammonium molybdate and 25g citric acid in 100ml water in some cases exposed Pb-Pb boundaries.

True grain sizes were determined from metallographic cross-sections perpendicular to the tensile axis of the samples(corresponding to the rolling direction). The average true grain size, L, was calculated as:

$$L = (4/\pi)^{3/2} \ (A_a)^{1/2} \ , \qquad (1.1)$$

(Exner, 1972), where A_a is the average intersect area of the grains (no distinction was made between phase and grain boundaries). In Sn-38.1w/o Pb, grain sizes determined from cross-sections parallel to the tensile axis were found to be larger (by up to 50%) than those obtained from cross-sections perpendicular to the tensile axis, for the same sample. Also, the grains were slightly elongated and the quality of the etching was usually inferior. In order to avoid inconsistencies, only grain sizes determined perpendicular to the tensile axis will be quoted.

4.3. Mechanical testing

4.3.1. Constant stress creep rig

For mechanical tests with strain rates higher than $\sim 10^{-7} s^{-1}$, a tensile creep rig with a constant stress cam was built(*) (Fig. 4.1). The cam was designed such that the load acting on the sample was gradually reduced during the elongation in order to compensate for the decreasing sample cross-section (assuming uniform necking and constant volume of the gauge length of the sample). Garofalo, Richmond and Domis (1962) have given the equation for the shape of the cam.

The loading train consisted of three steel rods with a pull-rod in the center (see also Fig. 4.2(a)). The

(*) The provision of a computer program by Dr. Jakubovics to plot the constant stress cam is gratefully acknowledged.

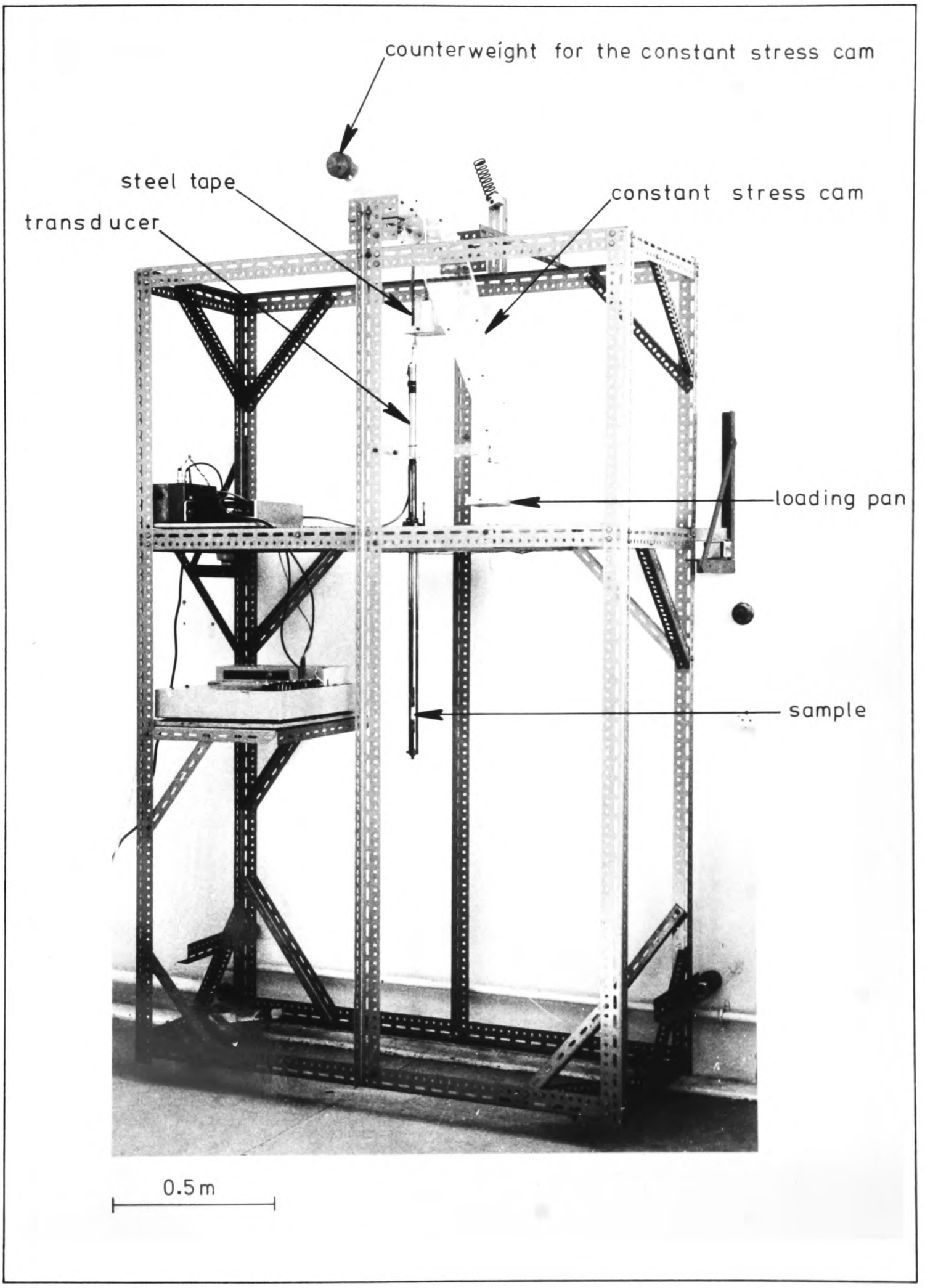

Fig. 4.1. Tensile creep rig with constant stress cam.

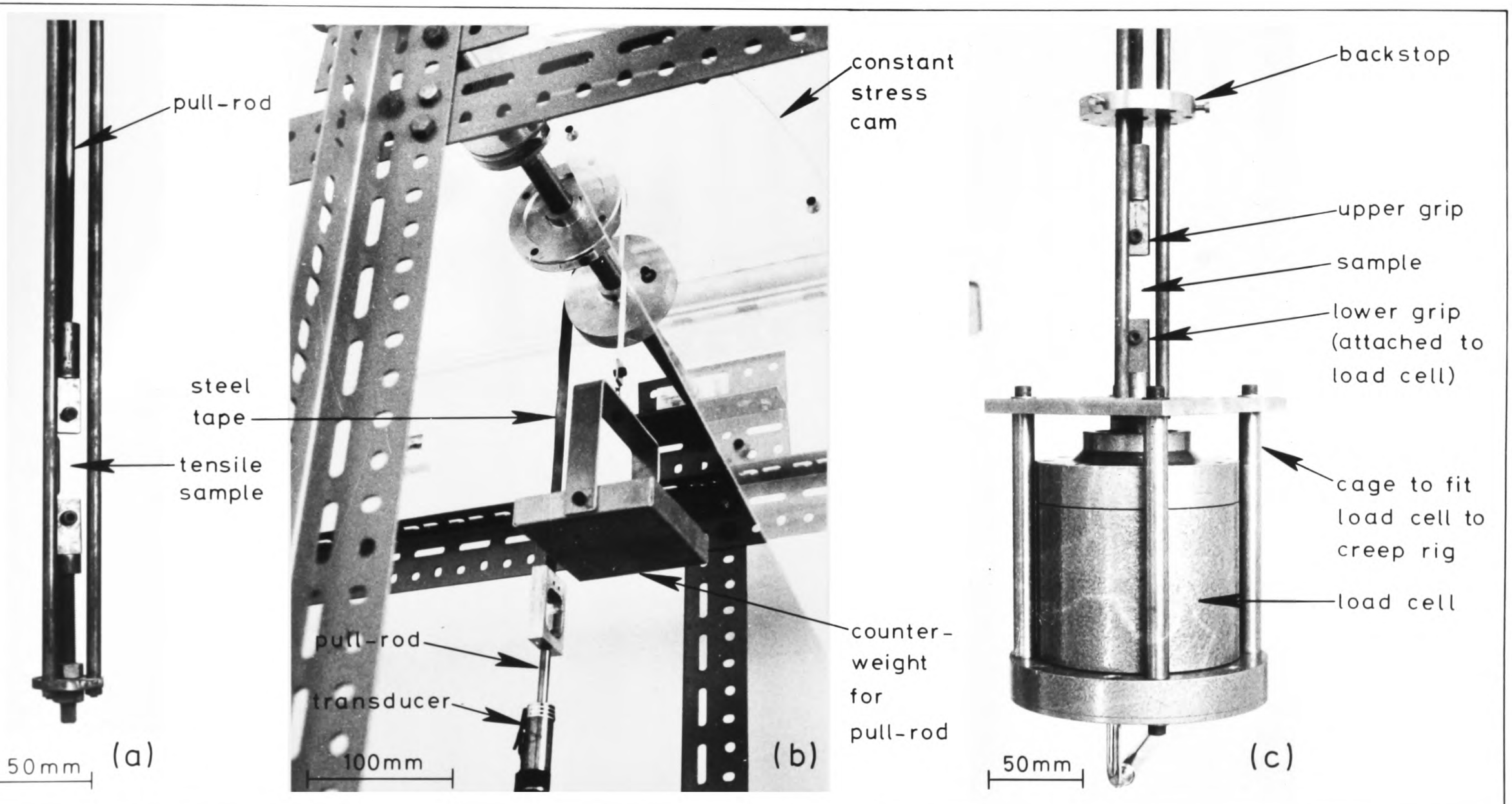

Fig. 4.2. (a) and (b): Magnified sections from Fig 4.1.

(c): Modification of the creep rig shown in Fig 4.1. to allow stress relaxation testing.

pull-rod was attached to a steel tape which was wound onto a wheel on the same axle as the constant stress cam (see Fig. 4.2(b)). The weight of the pull-rod was compensated with a counter-weight.

The sample elongation was monitored with a linear variable differential transducer. Its core connected the top and bottom half of the pull-rod. In order to minimize friction, 3 ball races were arranged around the pull-rod, near the bottom of the transducer. They prevented the transducer core from touching the inner walls of the transducer. The linear range of the transducer was 250mm and sample elongations of up to ~1000% could thus be measured, for an initial sample length of 26mm.

The DC output of the transducer was monitored with a chart-recorder. Discrete stabilized DC voltages were automatically generated(*) to compensate partially the transducer output in order to make full use of the high sensitivity of the chart recorder.

The sample temperature was kept constant by attaching a silicone fluid bath with a depth of 250mm and a temperature accuracy of $\mp$0.5K to the bottom of the loading train. The temperature of the bath was monitored close to the sample.

The friction stress of the rig, after careful alignment, was ~0.01MPa (for a typical sample cross-section of

(*) Mr. Christopher Bartram's efforts in building the corresponding digital equipment are gratefully acknowledged.

5mm). However, due to elastic deflections of the rig (in particular the steel tape attached to the pull-rod), inaccuracies of the actual stress by as much as 5% could result, in particular for stresses above 10MPa. The long-term stability of the displacement measurement (e.g. over several days) was $\sim\bar{+}50\mu m$ as verified with a non-deforming dummy sample. Over short periods of time (e.g. minutes), however, a resolution of $\sim 1\mu m$ could be obtained.

In order to perform stress relaxation tests under carefully controlled conditions, a load cell and a back-stop for the upper sample grip were attached to the rig (see Fig. 4.2(c)). This type of an arrangement has already been described by Blum and Pschenitzka (1976). The input voltage for the load cell (type Instron, maximum load 500N) was 2.7V (2 mercury batteries); the output was monitored on a chart-recorder. The sensitivity of the stress measurement was $\sim\bar{+}0.01$MPa (for a typical sample cross-section of 5mm).

During tests, the whole loading train, including the load cell and the backstop, was enclosed in a thermally insulating polystyrene box. The temperature was controlled with a light bulb and a sensitive contact thermometer. Termperatures with an accuracy better than $\bar{+}0.05$K could be maintained over periods of ~10 hours.

3.2. Constant load creep rig

The loading train of the constant stress creep rig described above has an overall length of ~1.5m. In order

to increase the strain resolution the loading train should be much shorter and as much of it as possible should be kept at a well-controlled, constant temperature. A constant stress cam is not required if the sample deformations employed are small.

A small constant load creep rig was built accordingly in order to measure strain rates as low as $\sim 10^{-10} s^{-1}$ and in order to determine elastic after-effects (see Fig. 4.3). A pull-rod with a square-shaped cross-section was accurately guided by 2 sets of 4 ball races. The load was applied via a cotton tape and a wheel. A sensitive linear variable differential transducer (linear range 0.25mm) was used for the strain measurements. In order to extend the range of the strain measurements the transducer was mounted in a metal block the height of which could be adjusted. The bottom half of the creep rig was immersed in a silicone fluid bath with a temperature accuracy of ∓ 0.2K (at ~300K).

The friction stress of the rig was found to be $\sim 5 \cdot 10^{-3}$MPa (for a typical sample cross-section of 5mm) and at ~300K a long-term strain resolution (over several weeks) of $\sim 10^{-5}$ could be obtained. For temperatures higher than ~300K, the temperature was only as accurate as ∓ 0.5K and the strain resolution decreased to $\sim 3.10^{-5}$.

4.3.3. Constant strain rate testing

An Instron testing machine was employed for the testing with constant strain rates (more accurately: constant extension rates) and for strain rate changes.

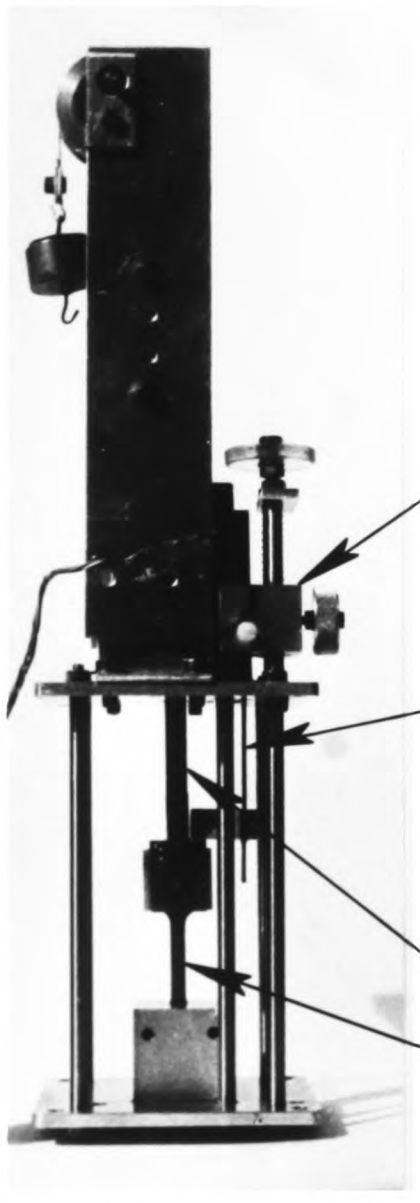

metal block (adjustable height) with transducer

rod attached to upper grip (on this rod the transducer core is mounted)

pull-rod

sample

50mm (a)

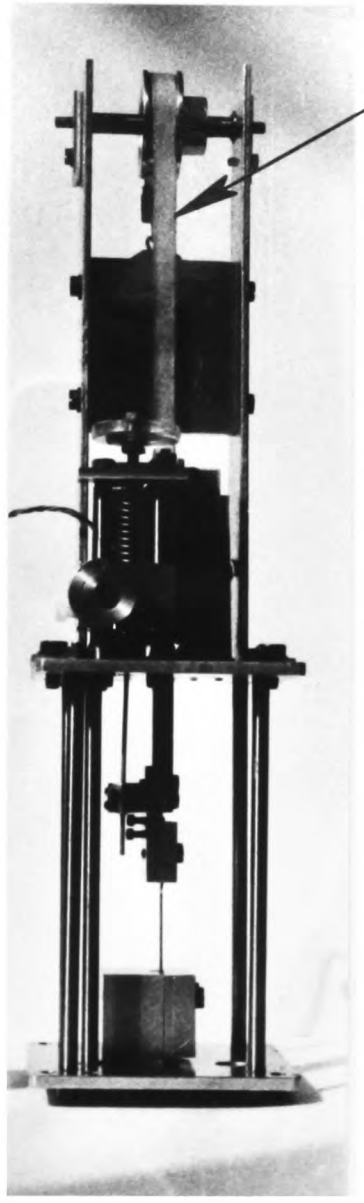

tape attached to pull-rod

50mm (b)

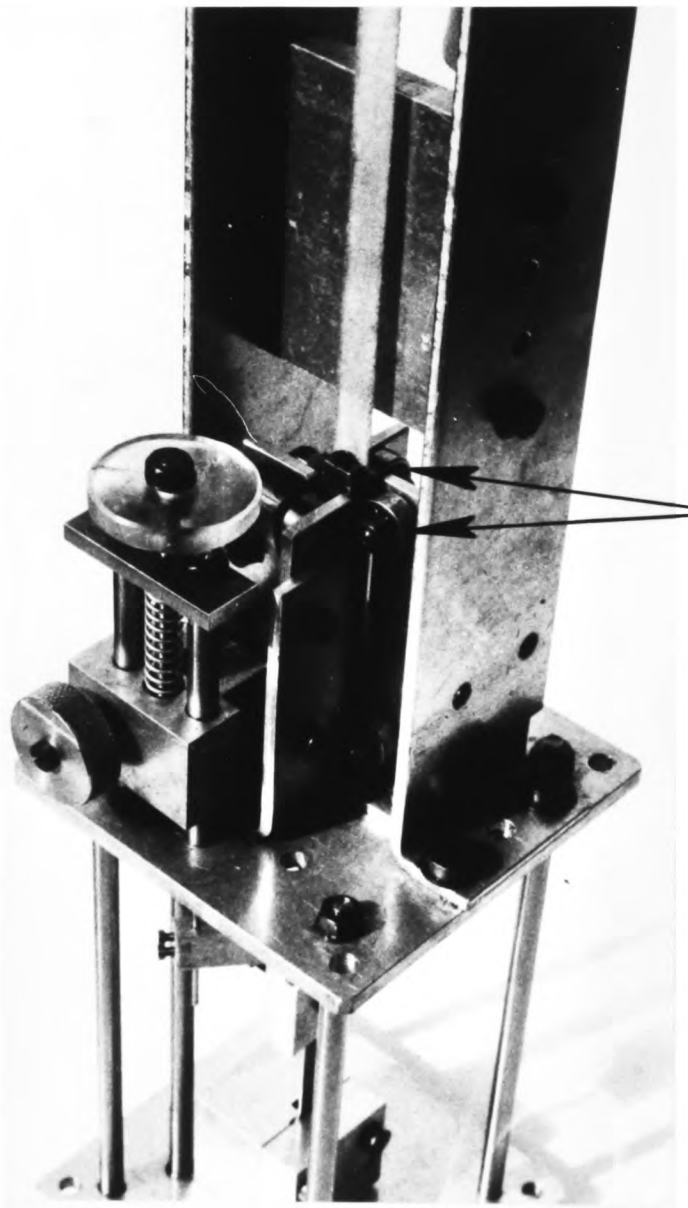

ball races for guiding pull-rod

50mm (c)

Fig 4.3. Three views of constant load creep rig for high strain resolution.

The configuration used is shown schematically in Fig. 4.4. Upon lowering the cross head, the load was applied via the lower sample grip (weight ~0.33N, corresponding to a stress of ~0.07MPa, for a sample cross-section of 5mm). The arrangement shown allows the operator to re-calibrate the zero position of the load between different tests with one sample. The temperature was again controlled with a silicon fluid bath (∓0.5K). A load cell with a maximum range of 500N was employed.

The stiffness of the testing machine (the ratio of the applied force and the elastic deflection), including the load cell, was measured with a stiff dummy sample the elasticity of which could be neglected. Since the testing machine was not found to be strictly linear elastic, different stiffnesses, S, were found depending on the range of loads employed. The following values were obtained:

0 - 200N: S = 2.63N/μm

0 - 10N: S = 2.38N/μm

0 - 2N: S = 1.22N/μm .

The inaccuracy of the stress for a stiff sample under a load of ~1Mpa (this indicates the accuracy of stress relaxation experiments) over a period of ~2ks was ~∓0.08MPa, for a sample cross-section of 5mm.

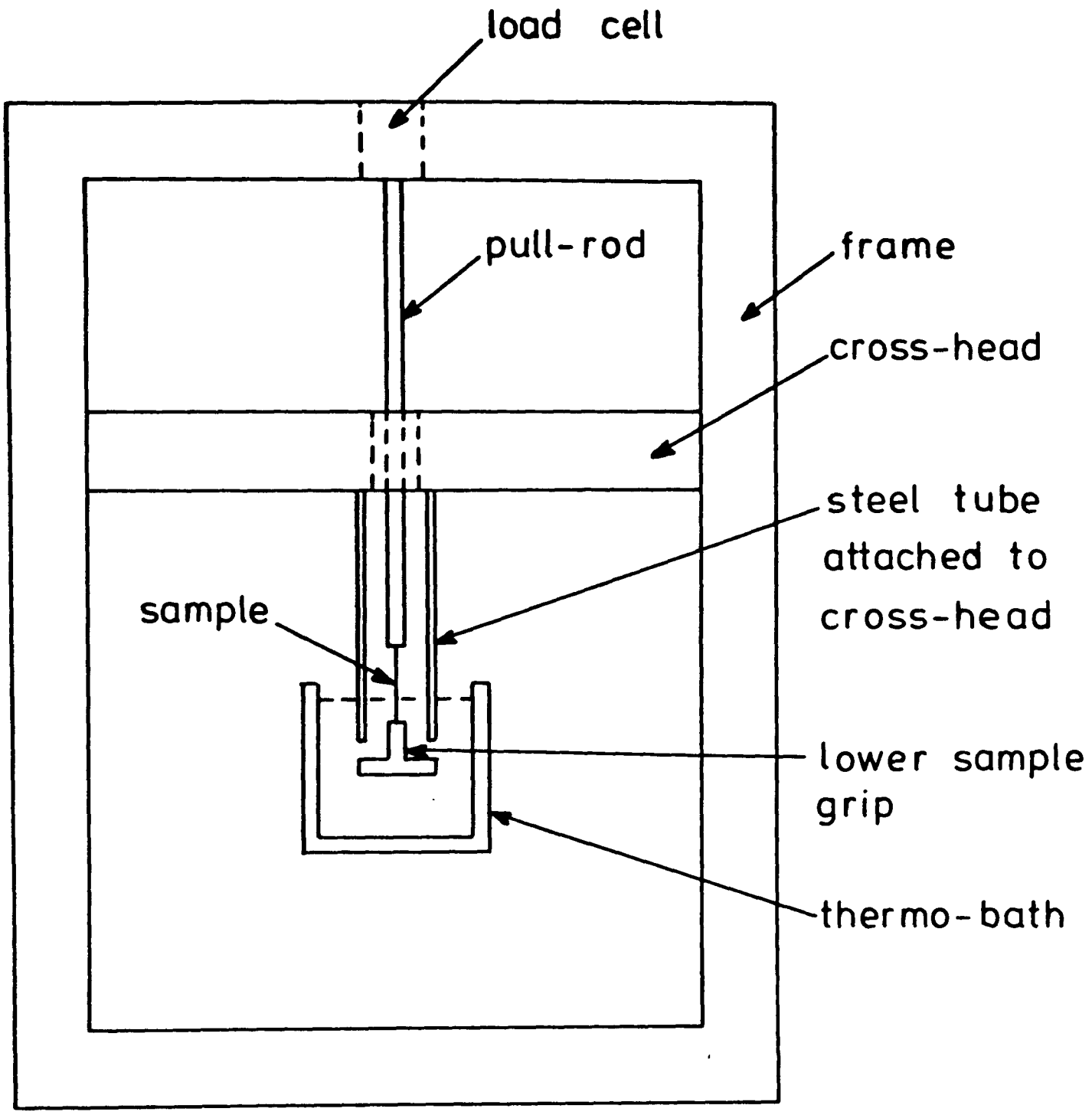

Fig. 4.4. Schematic drawing of the configuration employed for constant strain rate tests and for strain rate change tests.

CHAPTER 5

THE PLASTIC DEFORMATION OF Sn-Pb ALLOYS AND ITS INTERPRETATION

5.1. Introduction

To date no satisfactory description of the role of diffusion creep in superplastic deformation has been obtained, although a theory for superplasticity based on diffusion creep which is inhibited by a threshold stress at low stresses has been advanced (Ashby and Verrall, 1973). Experimental data for Sn-38w/o Pb and Zn-22w/o Al at low strain rates, however (Mohamed and Langdon, 1975a; Mohamed and Langdon, 1975 b), have given evidence neither for diffusion creep nor for a threshold stress. No theoretical mechanism for superplasticity could be identified by Mohamed et. al. The grain sizes investigated in Mohamed and Langdon's and in many other studies (Edington, Melton and Cutler, 1976) are comparatively small. Therefore interface processes which have a grain size dependence of the strain rate like $1/L$ or $1/L^2$ (chapter 2) as compared with $1/L^3$ for Coble creep, may have been rate-determining. One aim of the present research was therefore to identify diffusion creep in a superplastic material by chosing sufficiently large grain sizes. Identification of diffusion creep at large grain sizes and its extrapolation to small grain sizes shows if an interface process is rate-determining at small grain sizes (if the experimental creep rate for small grains is lower than the extrapolated diffusion creep rate). Unequivocal identification of diffusion creep is necessary since diffusion creep rates calculated from independently measured self-diffusion coefficients are too inaccurate

(Edington, Melton and Cutler, 1976, pp.130-131) to allow a decision to be made on the importance or non-importance of interface control. Two-phase alloys with similar fractions of the two phases cannot easily be annealed to produce large equiaxed grains. Therefore a Sn-2w/o Pb alloy was chosen for the verification of diffusion creep. Sn-2w/o Pb is superplastic (Cline and Alden, 1967) and has reasonably stable grain sizes as small as 3μm; much larger grain sizes can however be produced.

In order to investigate eventual interface processes in more detail a two-phase alloy (Sn-38.1w/o Pb) was chosen because its grain size can be smaller and is more stable than that of Sn-2w/o Pb. Fine-grained samples at very low stresses (and strain rates) are thus more easily investigated. Small grains and low stresses often favour rate-controlling interface processes because of the different grain size and stress dependencies of the strain rates for bulk and for interface mechanisms (chapter 2). In particular very low stresses and strain rates were employed in order to check the existence of a threshold stress which has been found by Burton (1971).

The measurement of steady-state plastic strain rates (also called "stationary" or "secondary" creep rates) can be of considerable help in identifying the mechanisms of plastic deformation determining the strain rate. Before presenting the results obtained for Sn-2w/o Pb and Sn-38.1w/o Pb, however, a short discussion of the measurement of steady-state plastic strain rates for these alloys is considered to be necessary.

5.2. The steady-state deformation rate

5.2.1. The importance of the structure

Upon loading of a sample of the investigated alloys with a constant stress (at elevated homologous temperatures) one usually obtains, after a transient period, an approximately constant strain rate. For a given sample, its value depends on the test temperature and on the applied stress. Thus it seems reasonable to assume that an equation of state:

$$\dot{\varepsilon} = \dot{\varepsilon}(\sigma, T, S) \qquad (5.1)$$

for the plastic strain rate, $\dot{\varepsilon}$, holds, where σ is the applied stress, T is the test temperature, and S is a parameter describing the structure of the sample. The structure is defined by all existing lattice defects which are not in thermodynamic equilibrium (Haasen, 1978), for example the grain size, the dislocation density and the dislocation distribution. The constancy of the strain rate for a given stress implies that the structure remains constant (unless changes in the strain rate for an assumed constant structure and changes in the structure during deformation lead to a constant total strain rate).

In many cases a "quasi steady-state" behaviour will be found. This means that the structure term does not stay constant during a test but changes so slowly that a description in terms of equation (5.1) is still meaningful. Examples for a gradual change in S are self-extinguishing

diffusion creep due to grain elongation (see sections 2.2 and 2.7.2(c)), thermal grain growth, and deformation-induced reduction in grain size (Rawal and Murty, 1972).

The structure term S in equation (5.1) is closely related to the grain size. In many theories of superplastic deformation the grain size is the only structural parameter taken into account (see chapter 2) and experimental evidence has suggested that this is a valid approach (Tonejc and Poirier, 1975). However, the results presented in Fig. 5.1 indicate that this view may not be correct. Three as-rolled Sn-38.1w/o Pb samples with an initial approximate grain size of 2.5μm were deformed by $\Delta\varepsilon \sim 0.1$, at a temperature T = 313K and with $\sigma \sim 4.9$MPa. Then the relationships between stress and strain rate were measured, after anneals for various periods of time. For each sample, the measurement was done within a strain interval of $\Delta\varepsilon \sim 0.1$ and a period of time of the order of 10 hours. The deformation schedules were almost identical for the three samples examined. The annealing treatment should increase the grain size and the result in Fig. 5.1 could therefore indicate a weak grain size dependence of the strain rate at low stresses (~1MPa) and a strong grain size dependence at high stresses (~10MPa). On the other hand, experiments employing a wide range of grain sizes (see for example Fig. 5.8) indicate a strong grain size dependence of the strain rate even at low stresses. It is difficult to understand why the grain size dependence should vary with the

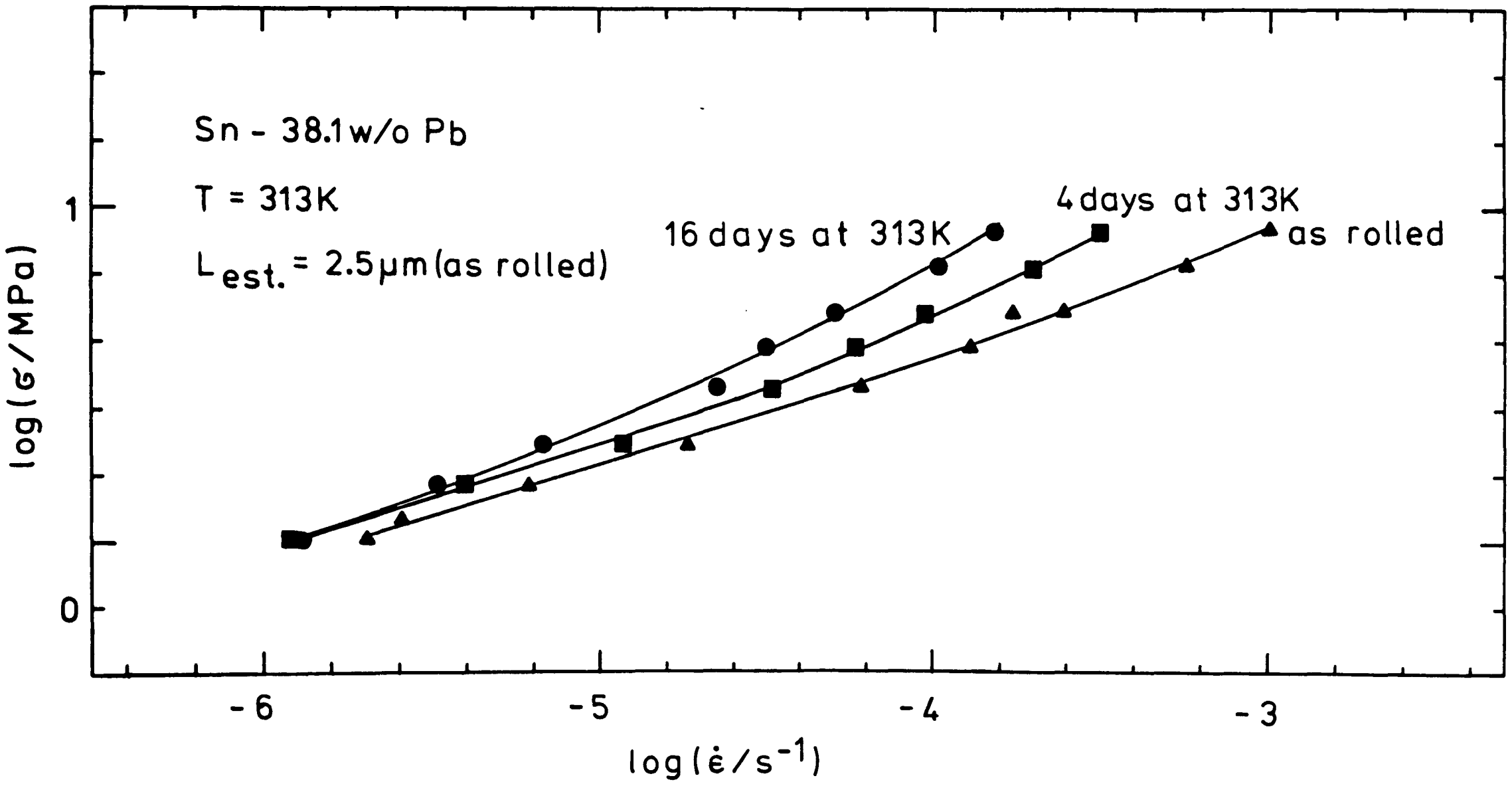

Fig. 5.1. The influence of different annealing treatments on the stress-strain rate relationship of initially as-rolled Sn-38.1w/o Pb.

stress as strongly as Fig. 5.1 suggests. It appears therefore that structural parameters other than the grain size may be involved. For example, during the annealing of the as-rolled material the interface structure and with it the strain rate sensitivity might change. A change in the strain rate sensitivity would cause the grain size dependence of the strain rate to be a function of the stress.

5.2.2. The importance of creep transients

In disagreement with Alden (1969a) transients in superplastic deformation were established in the present work. They are, however, not as pronounced as transients in conventional dislocation creep and are partly anelastic in nature.

Woodford (1969) has discussed the measurement and comparison of strain rates in the presence of transients. One approach suggested by him for determining the dependence of the strain rate on the stress is the comparison of strain rates after identical strains of different samples. The rationalization for this is the development of comparable structures after similar strains rather than similar times. In view of the very low strain rates measured, this technique cannot be applied to the present research. The periods of time needed would be too long and the thermal stability of the grain size could not be guaranteed.

Another approach suggested by Woodford is to measure the strain rates following small stress changes. Strain

rates corresponding to identical structures are probably compared in this case. For low strain rates, this method is again experimentally difficult and the role of anelasticity (see chapter 6) is uncertain.

The difficulties encountered above make it necessary to take the usual approach and to wait long enough after loading of a sample until the strain rate is approximately constant. This strain rate is then identified with the steady-state creep rate. Fig. 5.2 is an example of the variation of the strain rate as a function of the period of loading and demonstrates that an approximately constant strain rate is indeed obtained if sufficient time is allowed to elapse. For example, for a loading stress of 0.36MPa, the strain rate after 10^6s is approximately one half of the strain rate after 10^5s which is a relatively small variation. For stresses smaller than those in Fig. 5.2 the periods of time after which the strain rate is approximately constant become longer; they become shorter for higher stresses. As can be seen from Fig. 5.2, the strains required to establish an approximately constant strain rate decrease significantly for decreasing stresses.

In many cases a sample was tested for many stresses and several temperatures. In particular for fine-grained samples, previously measured data points were occasionally repeated in order to detect whether the sample properties had changed during the test. Usually some scatter in the data resulted. In most cases, however, the testing procedure did not significantly change the plastic properties of the

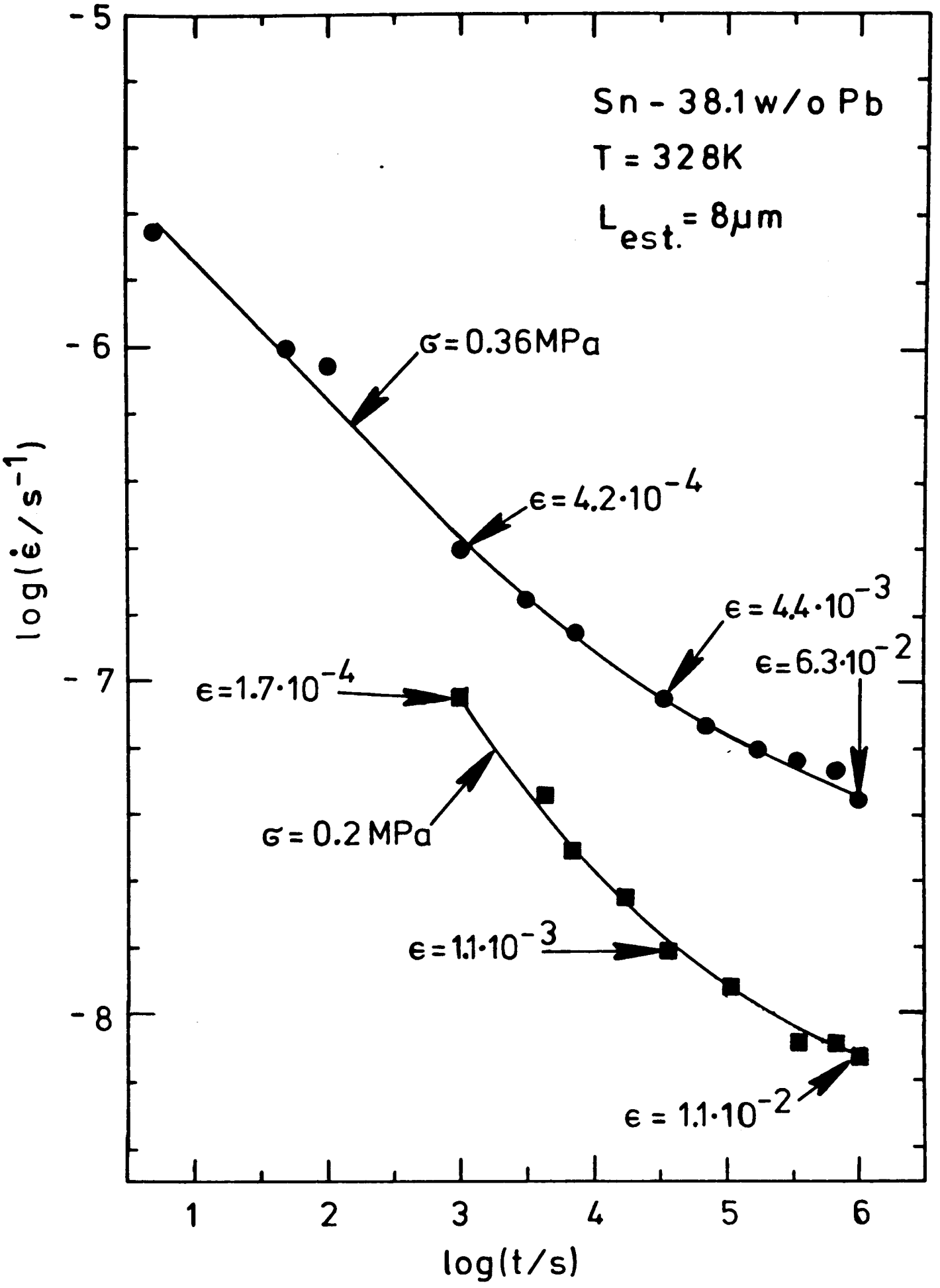

Fig. 5.2. The strain rate, $\dot{\epsilon}$, as a function of the time, t. The samples were loaded with constant stresses at t = 0. The sample strains are indicated.

investigated samples.

For the lowest strain rates measured, the error caused by anelastic strains was estimated in some cases. The procedure employed is depicted schematically in Fig. 5.3. Before loading, samples usually exhibit small negative (anelastic) strain rates caused by their previous deformation history. The plastic strain rate, $\dot{\varepsilon}$, at the time t_1 in Fig. 5.3 may therefore actually be higher than the measured strain rate, $\dot{\varepsilon}_1$, due to the superimposed negative anelastic strain rate, $\dot{\varepsilon}_o$. Since $\dot{\varepsilon}_o$ will progressively decay with increasing time, $\dot{\varepsilon}_1 - \dot{\varepsilon}_o(0)$ is an upper limit for the plastic strain rate (additivity of anelastic and plastic strains is here assumed for simplicity). Similarly, the loading with a stress σ at $t = 0$ causes an anelastic strain rate $\dot{\varepsilon}_a(t)$, for $t \geq 0$. $\dot{\varepsilon}_1 - \dot{\varepsilon}_a(t_1)$ is therefore a lower limit for the plastic strain rate at the time t_1.

In the presence of plastic transients the value of the steady-state creep rate may be even lower than the lower limit for the plastic strain rate derived above. At the small strains involved, however, it would be very difficult to study plastic transients, in particular because anelasticity is involved, and therefore the approach outlined above may suffice. Furthermore, the results of the discussion of the plastic behaviour of the examined alloys will be seen not to change significantly if the experimental results for low stresses and strain rates (e.g. $\sigma \leq$ 1MPa, $\dot{\varepsilon} \leq 10^{-8} s^{-1}$) are shifted to somewhat lower values.

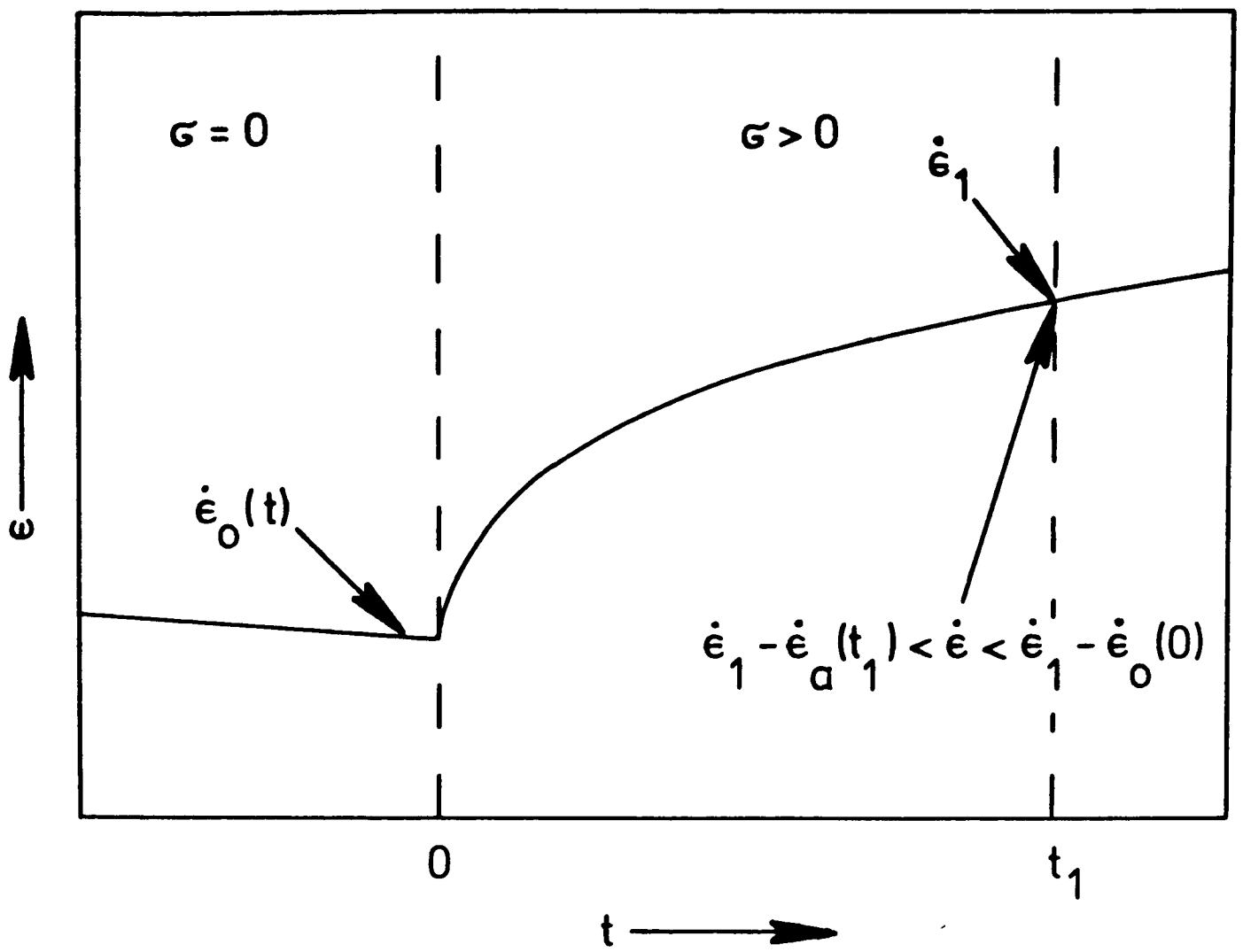

Fig. 5.3. The effect of anelastic deformation on the plastic strain rate, $\dot{\epsilon}$ (schematically).

5.3. The plastic deformation of Sn-38.1w/o Pb and its interpretation

The plastic properties of Sn-38.1w/o Pb for different grain sizes and temperatures are represented in Figs. 5.4 to 5.7. Different symbols for a particular temperature indicate different samples. At low strain rates error bars are plotted (see section 5.2.2). The deformation schedules were similar to those employed for Sn-2w/o Pb (see also Table 5.3). For grain sizes smaller than 10μm the samples were usually pre-deformed to $\varepsilon \sim 0.1$, in the range of maximum superplasticity. This was done in order to reduce the influence of transients which may occur during the initial stages of deformation (Newbury, 1972). Samples with grain sizes larger than 10μm were not pre-deformed, since the grain size of these "large-grained" samples can decrease significantly during deformation (Rawal and Murty, 1972). The total deformation of these samples was always smaller than $\varepsilon \sim 0.05$, whereas samples with grain sizes below 10μm were deformed by up to $\varepsilon \sim 0.3$. Grain sizes were determined from metallographic cross-sections by counting between 200 and 1000 grains for each determination (see chapter 4). In some cases grain sizes were estimated from the measured strain rate and the known relationship between strain rate and grain size (see also Fig. 5.9). These grain sizes are indicated as $L_{est.}$ in the diagrams.

Fig. 5.5 contains also data published by Burton (1971), and Mohamed and Langdon (1975a). Burton's data do not

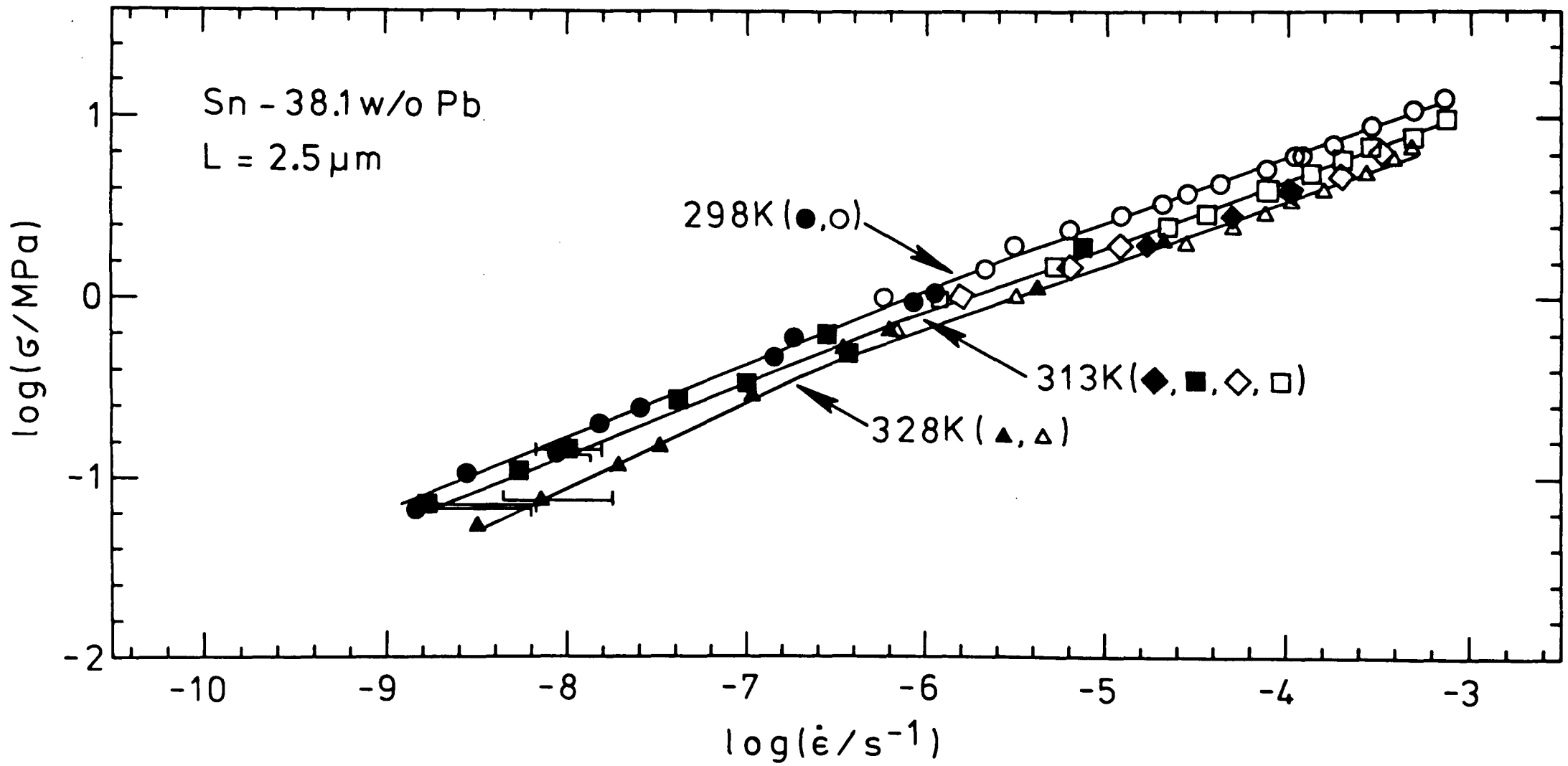

Fig. 5.4. The plastic deformation behaviour of Sn-38.1w/o Pb with a grain size of 2.5μm. Different symbols correspond to different samples.

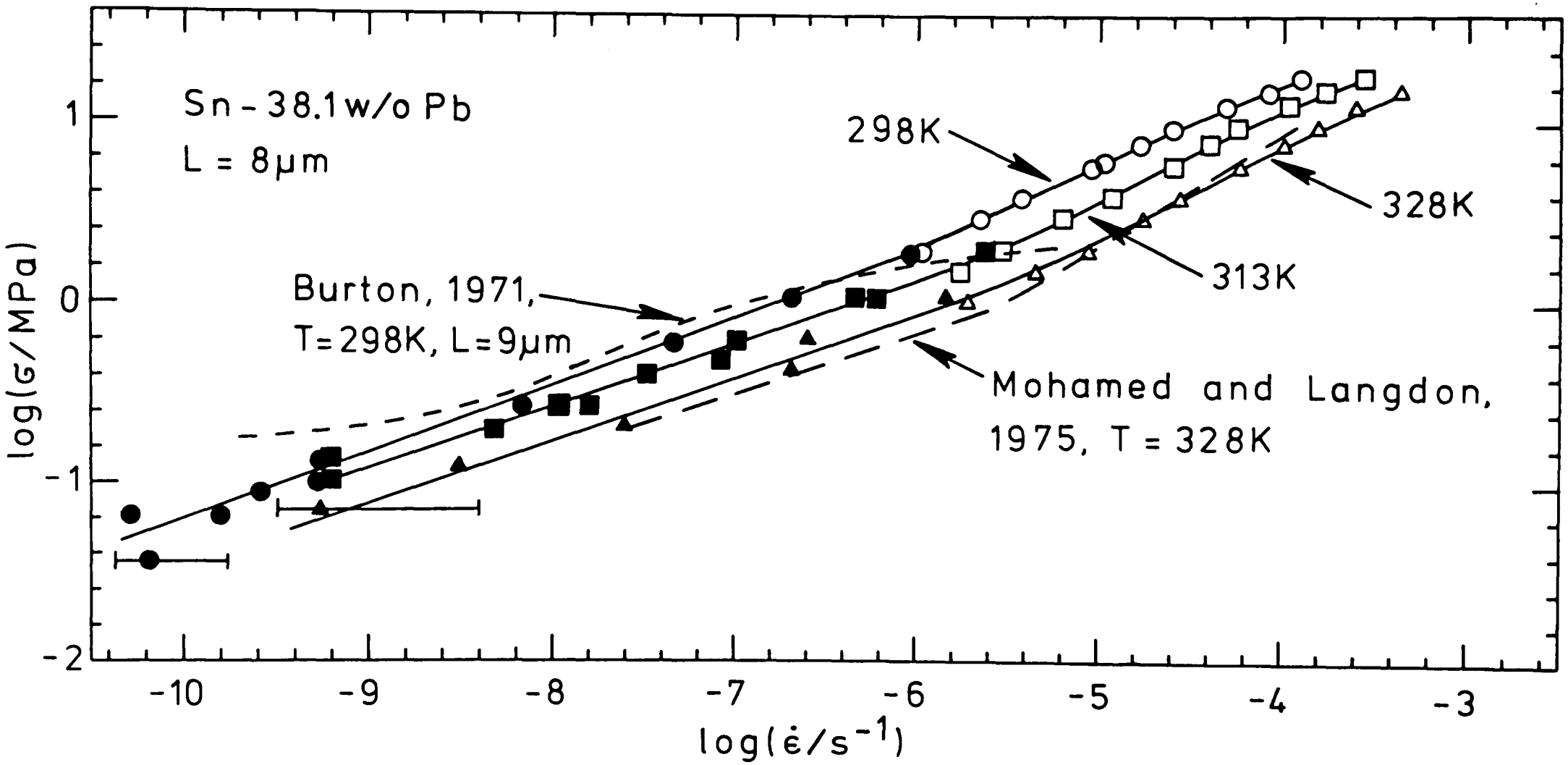

Fig. 5.5. The plastic deformation behaviour of Sn-38.1w/o Pb with a grain size of 8μm.

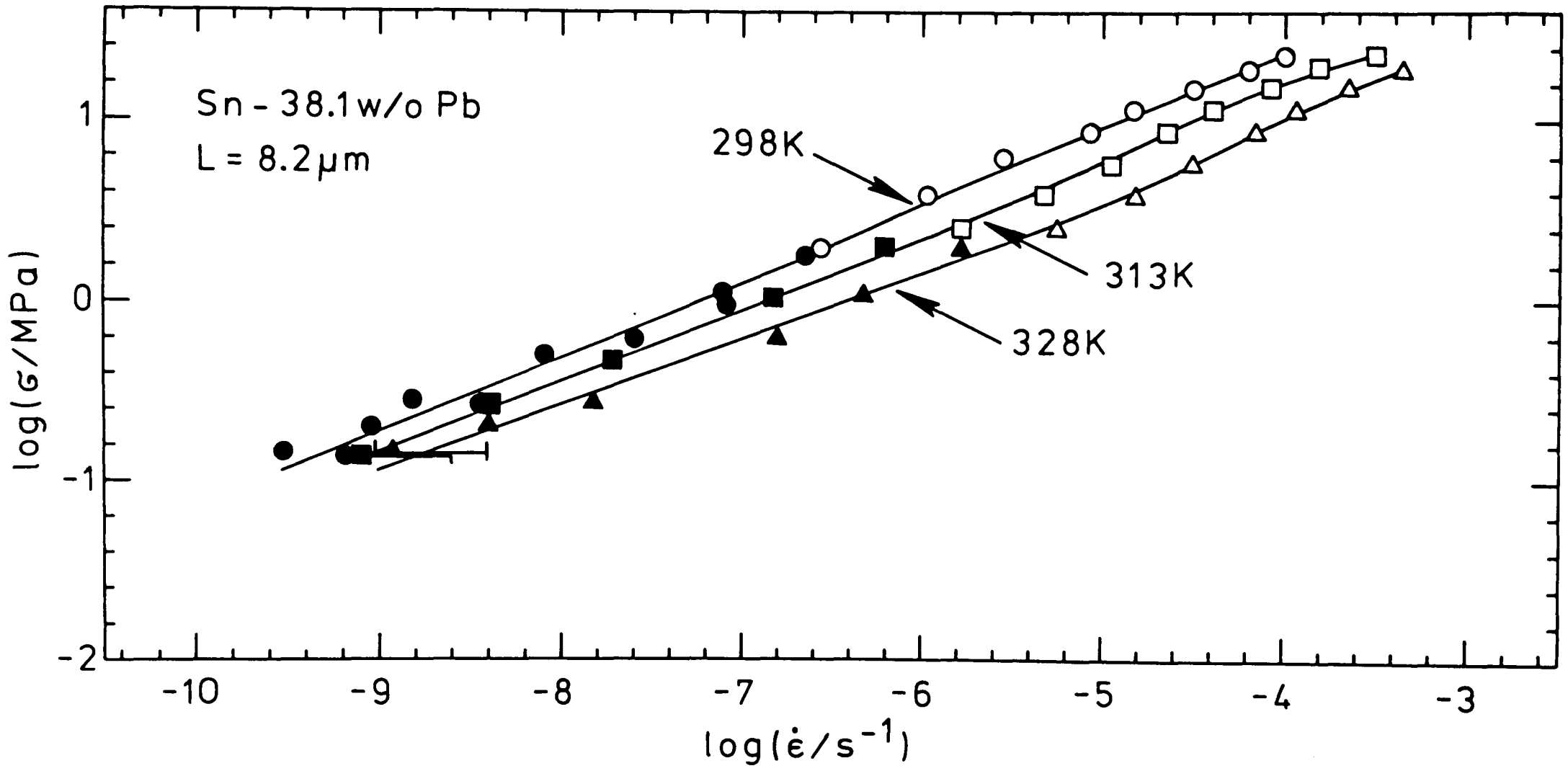

Fig. 5.6. The plastic deformation behaviour of Sn-38.1w/o Pb with a grain size of 8.2μm.

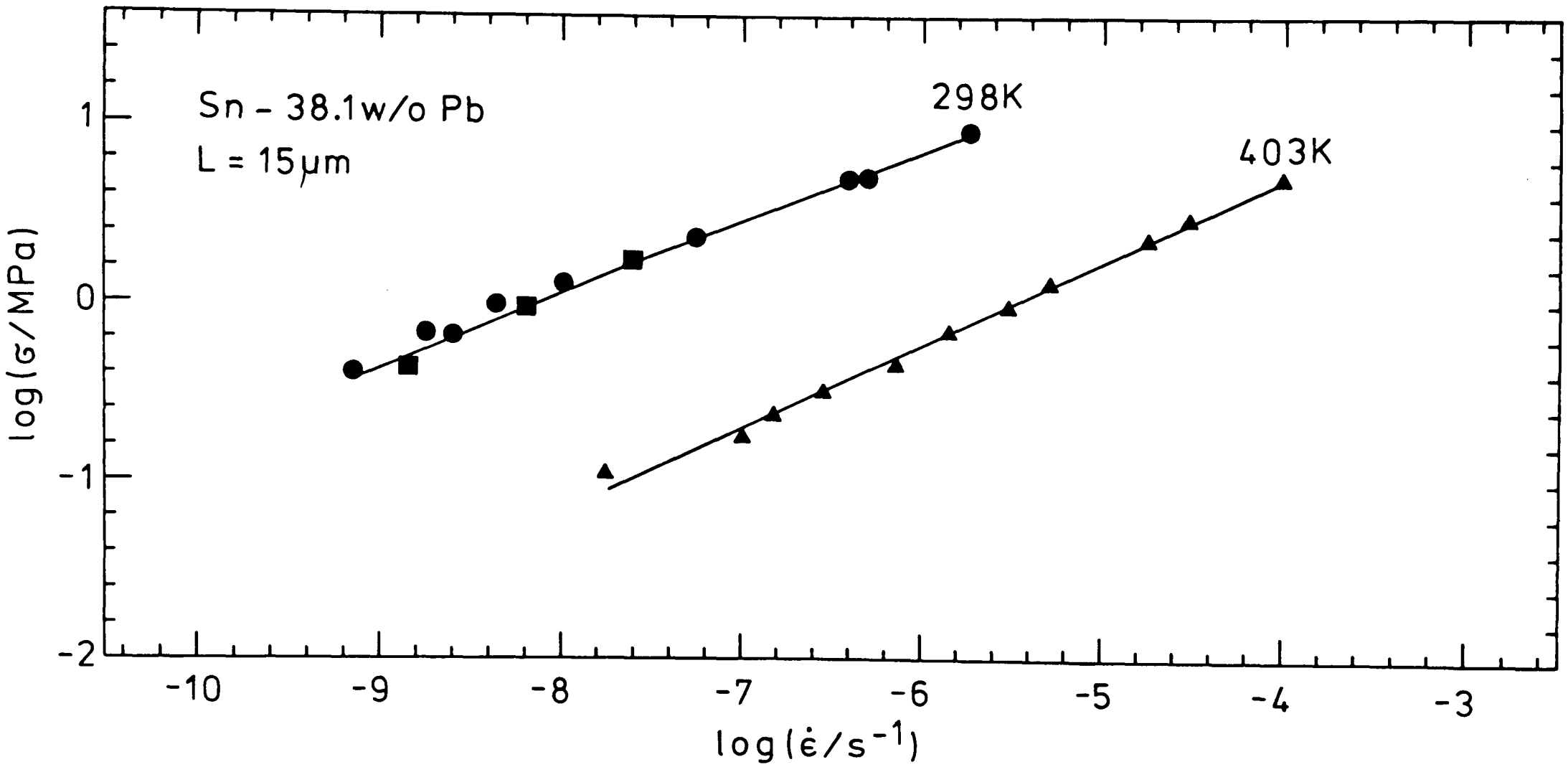

Fig. 5.7. The plastic deformation behaviour of Sn-38.1w/o Pb with a grain size of 15μm.

agree with the present results. Even if his data point for the lowest stress is not accepted (it has been estimated from the limiting sensitivity of the creep rig employed) there is still a severe discrepancey at high stress levels. The reason for this is not known. Mohamed and Langdon's result, however, which has been obtained by interpolation of their data, using their grain size exponent and activation energies, agrees fairly well with the results obtained here.

Geckinli and Barrett (1974) have also published Sn-38.1w/o Pb - data which extend to very low stresses and strain rates. These data have not been plotted in Fig. 5.5 since they have been obtained by stress relaxation. Due to the strong anelasticity in Sn-Pb (see chapter 6) results obtained by stress relaxation are unreliable unless they can be adequately corrected (see chapter 7).

5.3.1. Strain rate sensitivity, grain size dependence and activation energy in Sn-38.1w/o Pb

Strain rate sensitivity

The stress-strain rate dependencies presented in Figs. 5.4 to 5.8 can be tentatively divided in two regions, in accordance with common usage (see Fig. 2.1). Data with $\dot{\varepsilon} \lesssim 10^{-6} s^{-1}$ belong to region I, whereas those with $\dot{\varepsilon} \gtrsim 10^{-6} s^{-1}$ are associated with region II. Table 5.1 represents the strain rate sensitivities found in the two regions. The m-values vary between 0.34 and 0.52. The

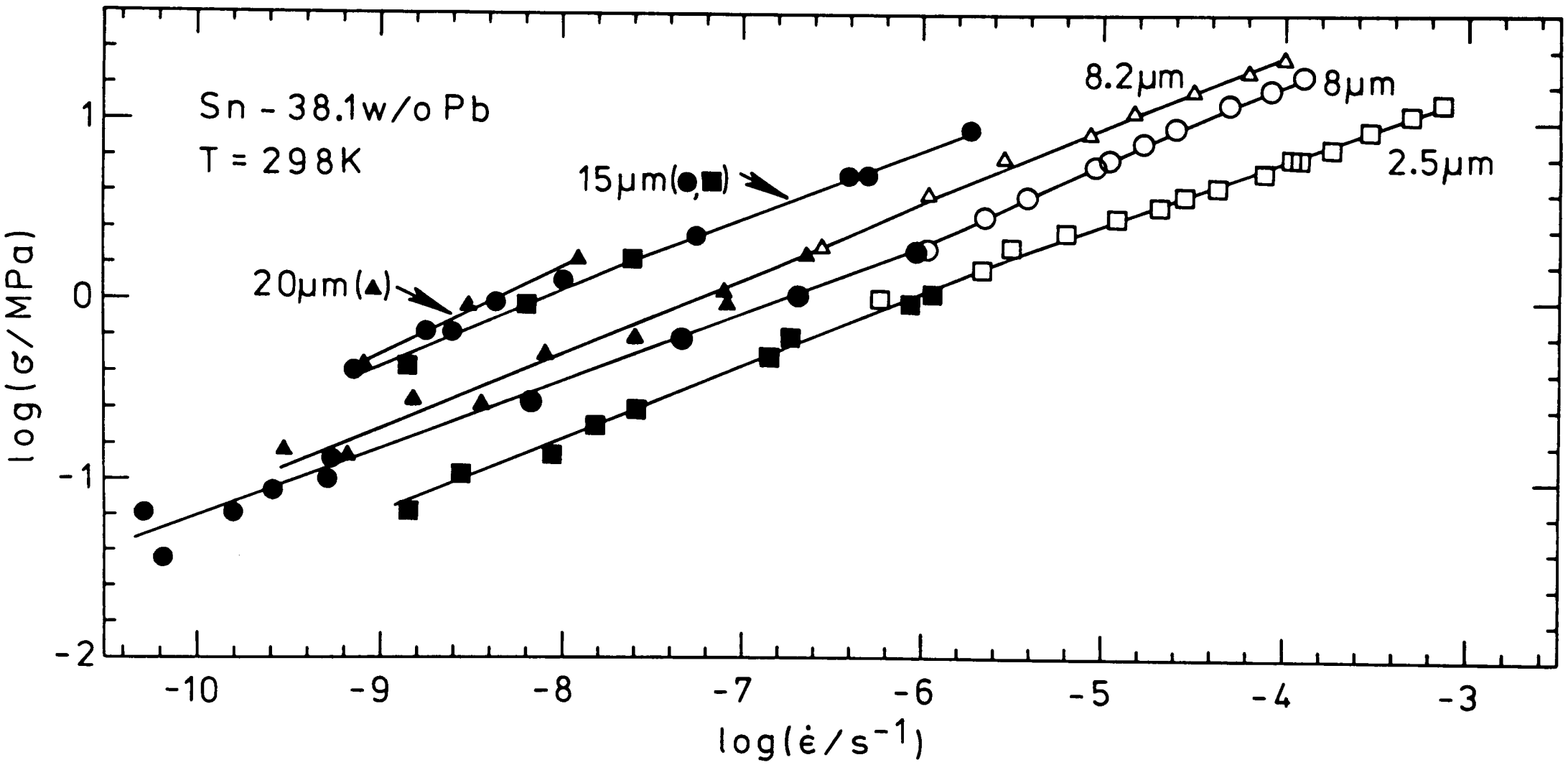

Fig. 5.8. The plastic deformation behaviour of Sn-38.1w/o Pb at a temperature of 298K.

	L/μm	T/K	m	$m_{av.}$
Region II ($\dot{\varepsilon} \geq 10^{-6} s^{-1}$)	2.5	298 313 328	0.35 0.37 0.35	0.36
	8.0	298 313 328	0.45 0.52 0.52	0.50
	8.2	298 313 328	0.4 0.45 0.45	0.43
	15	298 403	0.38 0.46	0.42
Region I ($\dot{\varepsilon} \leq 10^{-6} s^{-1}$)	2.5	298 313 328	0.41 0.41 0.47	0.43
	8.0	298 313 328	0.37 0.34 0.35	0.35
	8.2	298 313 328	0.42 0.40 0.36	0.39
	15	298 403	0.42 0.48	0.45
	20	298	0.49	0.49

Table 5.1. Strain rate sensitivities, m, and $m_{av.}$, for Sn-38.1w/o Pb ($m_{av.}$ is the average value of the strain rate sensitivities at different temperatures, for a particular grain size).

scatter is rather large, in particular for L = 2.5μm; however, there seems to be a tendency for m to increase with increasing grain size. Usually the m-values in region II are slightly higher than those in region I. The difference is not as pronounced as that found by M hamed and Langdon (1975a). These authors obtained m = 0.33 in region I and m = 0.61 in region II. This may be due to different sample treatments. As has been shown in section 5.2.1 samples with similar grain sizes can exhibit markedly different strain rate sensitivities.

Grain size dependence of the strain rate

The grain size dependence of the plastic strain rate of Sn-38.1w/o Pb is demonstrated in Fig. 5.8 which contains data for T = 298K from Figs. 5.4 to 5.7, together with data for an additional grain size. Fig. 5.9 shows the grain size dependence of the strain rate in a double-logarithmic plot. An approximate realationship:

$$\dot{\varepsilon} \alpha L^{-2.3} \qquad (5.2)$$

is found. The scatter of the grain size exponent in equation (5.2) is large. Fig. 5.9 indicates variations between 1.5 and 4. The average value of 2.3, however, is in accordance with Mohamed and Langdon's (1975a) result.

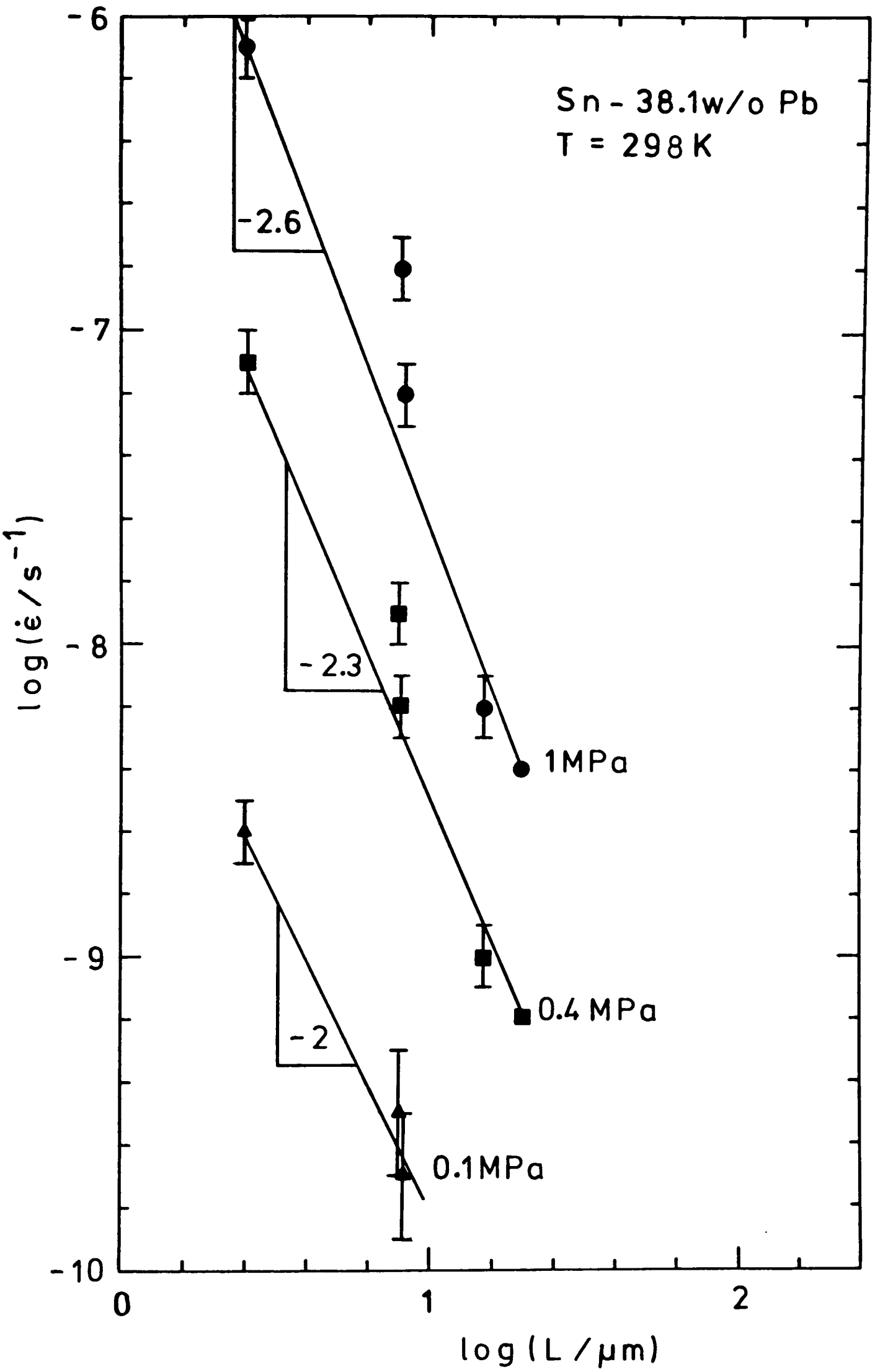

Fig. 5.9. Grain size dependence of the plastic strain rate of Sn-38.1w/o Pb.

Activation energies

The activation energies in regions I and II were determined following the approach by Mohamed and Langdon (1975a). A representation of the strain rate by a semi-empirical relationship of the form

$$\dot{\varepsilon} = A \frac{D_o G b}{k T} \left(\frac{b}{L}\right)^p \left(\frac{\sigma}{G}\right)^{1/m} \exp\left(-\frac{Q}{R T}\right) , \qquad (5.3)$$

where A_o is an adjustable parameter, D_o is the pre-exponential factor of the appropriate diffusion coefficient and p is the grain size exponent, leads immediately to an expression for the activation energy, Q:

$$Q = -R \left(\frac{\delta \ln(\dot{\varepsilon} G^{(1-m)/m} T)}{\delta (1/T)}\right)_{L,\sigma} . \qquad (5.4)$$

An approximate value of the shear modulus, G, was obtained from the experimental value of Young's modulus (21GPa after Subrahmanyam, 1972) and with the relation $G = E/(2(1+\nu))$, where ν is Poisson's ratio. Since $\nu(Pb) = 0.45$ and $\nu(Sn) = 0.36$, a realistic value for G is 7.5GPa. Subrahmanyam's data (1972) show that Young's modulus of Sn-38.1w/o Pb is not very different from that of pure Pb. For this reason the temperature dependence of the shear modulus of Sn-38.1w/o Pb was taken to be that of pure Pb. It is approximately 10MPa/K, as inferred from data compiled by Simmons and Wang (1971) (their reference 270, their approximation R for the average value of G). One obtains:

$$G(\text{Sn-38.1w/o Pb}) = (10.5 - 0.01\ T/K)\,GPa \qquad (5.5)$$

for the shear modulus as a function of the temperature.

With the help of eqns. (5.4) and (5.5), activation energies were determined by plotting $\ln(\dot{\varepsilon}\ G^{(1-m)/m}\ T)$ vs. $1/T$, for various grain sizes and for two stresses corresponding to regions I and II, respectively (see Fig. 5.10 and Table 5.2). No activation energies were determined for the grain size 2.5μm (Fig. 5.4) since the scatter in the data was very large. The temperature dependence of the shear modulus does not have a great influence on the value of the activation energies as may be seen from the broken line in Fig. 5.10 annotated "G = const.". The activation energies in regions I and II, respectively, were found to be 54kJ/mol and 55kJ/mol. The value for region II agrees with Mohamed and Langdon's (1975a) result of 57kJ/mol. Mohamed and Langdon's value for the low-stress region I, 84kJ/mol, however, could not be substantiated. The present results are not compatible with values larger than 72kJ/mol and tend to be much lower than that.

5.3.2. The importance of diffusion creep in Sn-38.1w/o Pb

No proof for diffusion creep in Sn-38.1w/o Pb in the investigated range of grain sizes and temperatures has been found. The strain rate sensitivity is always smaller than ~0.5 and the average grain size exponent is below 3. If diffusion creep is present it is certainly obscured by other

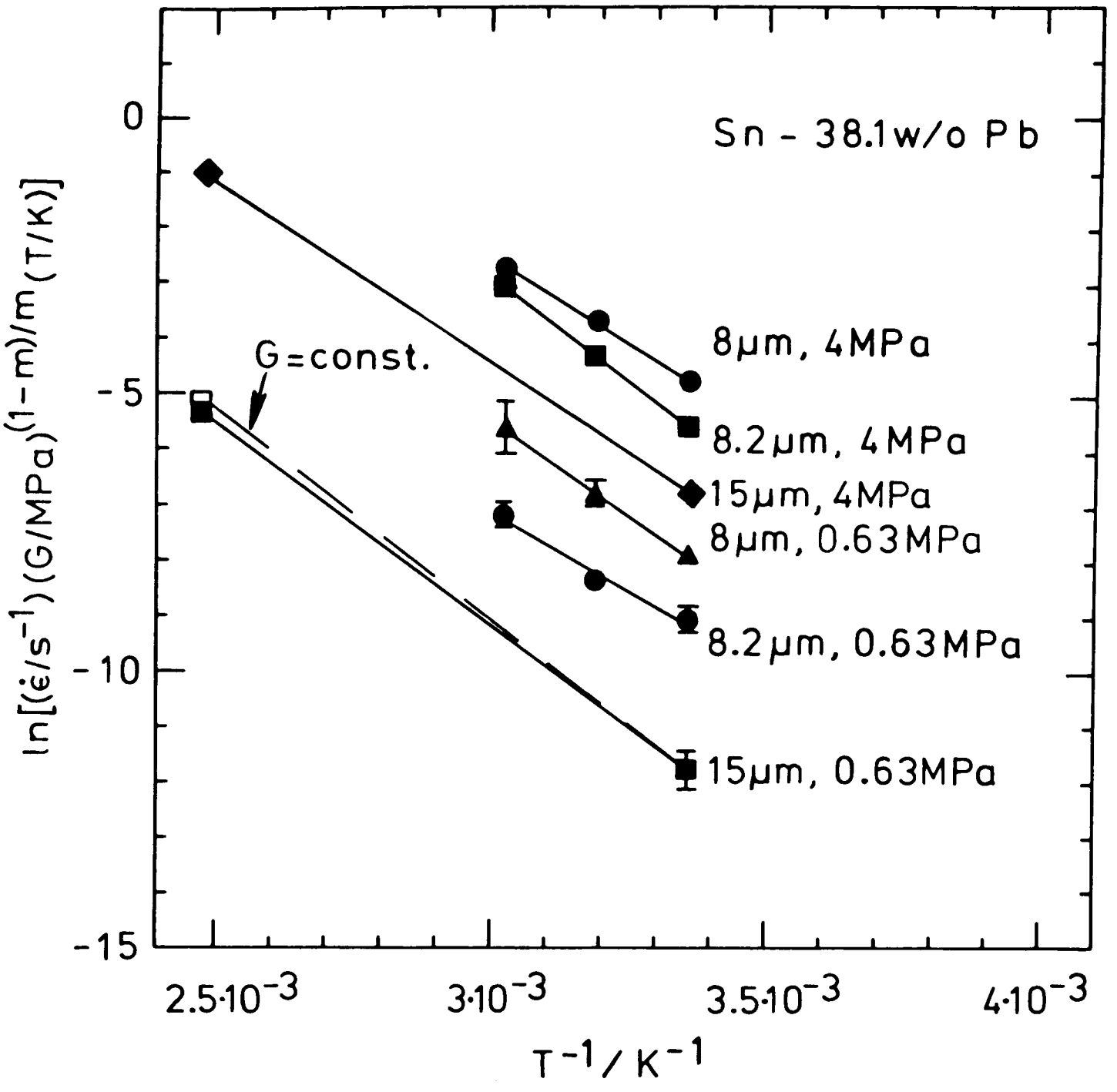

Fig. 5.10. Determination of the activation energy for the plastic deformation of Sn-38.1w/o Pb in Regions I (σ = 0.63MPa) and II (σ = 4MPa). The error bars are derived from the scatter in the plastic strain rates. The activation energies obtained are listed in Table 5.2.

	σ/MPa	L/μm	Q/(kJ mol^{-1})	$Q_{av.}$/(kJ mol^{-1})
Region II	4	8	50	55
		8.2	61.5	
		15	53.5	
Region I	0.63	8	56.5	54
		8.2	46.5	
		15	60	

Table 5.2. Activation energies, Q, for Sn-38.1w/o Pb in region II ("superplastic region") and region I ("low-stress region"). $Q_{av.}$ is the average value of the activation energies for a particular stress and various grain sizes. The evaluation of Q was done according to Fig. 5.19 and equation (5.13).

processes, for example by interface mechanisms.

In order to show that diffusion creep is slower than the mechanism(s) controlling the strain rate at low stresses appropriate diffusion coefficients would have to be inserted in eqn. (2.3) and (2.4). However, it is not clear how to add up the strains caused by the diffusion in Sn-rich and Pb-rich grains and the diffusion-coefficient applicable to Sn-Pb interfaces is not known. The diffusion creep rates in Sn-38.1w/o Pb have therefore been calculated separately for the two phases present in the alloy. Known diffusion coefficients which may be relevant for the deformation of Sn-38.1w/o Pb are:

the atomic GB diffusion coefficient in Sn-2 /o Pb derived from Coble creep in Sn-2w/o Pb (see eqn. (5.17)):

$$D_B(\text{Sn-2w/o Pb}) = 2.4 \cdot 10^{-4} \ \frac{m^2}{s} \ \exp\left(-\frac{42\text{kJ/mol}}{R\,T}\right), \tag{5.6}$$

the atomic GB diffusion coefficient in Pb-0.9w/o Sn which has been measured with a tracer method by Stark and Upthegrove (1966b),

$$D_B(\text{Pb-0.9w/o Sn}) = 1.25 \cdot 10^{-8} \ \frac{m^2}{s} \ \exp\left(-\frac{21\text{kJ/mol}}{R\,T}\right), \tag{5.7}$$

the volume diffusion coefficient in Sn (Lange, Hassner and Berthold, 1961),

$$D_L(\text{Sn}) = 7.8 \cdot 10^{-5} \ \frac{m^2}{s} \ \exp\left(-\frac{95.5\text{kJ/mol}}{R\,T}\right), \tag{5.8}$$

and the volume diffusion coefficient in Pb (Resing and Nachtrieb, 1961),

$$D_L(\text{Pb}) = 1.37 \cdot 10^{-4} \ \frac{m^2}{s} \ \exp\left(-\frac{109\text{kJ/mol}}{R\,T}\right). \qquad (5.9)$$

Earlier data for the GB self-diffusion in Pb (Okkerse, Tudema, Burgers, 1955) which indicate an activation energy of 66kJ/mol have been omitted since they have been criticized by Stark and Upthegrove (1966a). Mixed boundary and volume transport has probably occurred in Okkerse, Tudema and Burgers' measurements.

It is unlikely that lattice diffusion is of any significance under the experimental circumstances employed. The maximum contribution of lattice diffusion is expected for large grains and high temperatures since the activation energies for GB self-diffusion are generally smaller than those for lattice self-diffusion (see also Gleiter and Chalmers, 1972). With $L = 15\mu m$ and $T = 403K$ (Fig. 5.7) one obtains for the tin-rich phase:

$$\frac{\pi\, w}{L} \ \frac{D_B(\text{Sn-2w/o Pb})}{D_L(\text{Sn})} \ \sim 3900 \ , \qquad (5.10)$$

and for the Pb-rich phase:

$$\frac{\pi\, w}{L} \ \frac{D_B(\text{Pb-0.9w/o Sn})}{D_L(\text{Pb})} \ \sim 3500 \ , \qquad (5.11)$$

which suggests GB diffusion control (see eqn. 2.5).

Using eqns. (5.6) and (5.7), Coble creep rates have

been evaluated (eqn. (2.4)) for L = 2.5μm and T = 298K and have been compared with the corresponding experimental result for Sn-38.1w/o Pb (see Fig. 5.11). Coble creep is much faster than the measured strain rates and is therefore not likely to be rate-controlling. Strong evidence will be found later for the inhibition of Coble creep in Sn-2w/o Pb. The similarity in the deformation behaviour of Sn-38.1w/o Pb and Sn-2w/o Pb is therefore additional support for the view adopted above.

5.3.3. The importance of interface control in Sn-38.1w/o Pb

No evidence has been found for a threshold stress in Sn-38.1w/o Pb. If a threshold stress caused by grain switching (section 2.7.2 (c)) exists it should have been observed under the experimental conditions employed. For example, at T = 298K and L = 2.5μm (Fig. 5.4), measurable elongation of a sample occurred for applied stresses below 0.1MPa. This test was done after the sample had been strained by more than 10% and a threshold stress due to grain switching should already have become significant (see Fig. 2.2). For a realistic GB energy of $0.3J/m^2$ (see Murr, 1975, p.131) and a grain size of 2.5μm, one obtains a threshold stress $\sigma_o = 0.72\ \gamma/L \sim 0.09MPa$. It is unlikely that such a threshold stress would not have been noticed. Therefore a threshold stress is not thought to exist or is thought to be significantly smaller than $0.72\ \gamma/L$. A possible reason for this has been discussed in

section 2.7.2(c).

It is likely that interface processes other than threshold mechanisms inhibit Coble creep. Using the diffusion coefficients given by eqns. (5.6) and (5.7), sliding rates have been calculated for GBD creep after Ball and Hutchison (see eqn. (2.15)) and for GBD creep after Nabarro (see eqn. (2.14). The Burgers vector was taken to be 0.35nm. For the shear moduli values of G(Sn, 300K) = 15.4GPa (Simmons and Wang, 1971, p.300, approximation R) and G(Pb, 300K) = 6.6GPa (Simmons and Wang, 1971, their reference 270, approximation R) were employed. The strains rates obtained are plotted in Fig. 5.11. Although the fit for the GBD model after Nabarro is reasonably good, there are objections to the validity of the two models:

(1) The threshold stress Gb_b/L below which interface mechanisms will probably not operate is relatively high. For $b_B = b_L = 0.35$nm, threshold stresses of 2.16MPa and 0.92MPa, respectively, are expected for Sn and for Pb. Significantly smaller threshold stresses can only be obtained if Burgers vectors of GBDs are much smaller than those of lattice dislocations or if GBDs have much smaller self-energies than lattice dislocations. Since GBD Burgers vectors are not much smaller than lattice dislocation Burgers vectors (Ishida and McLean, 1973) the latter hypothesis is preferred.

(2) The activation energies for plastic deformation are noticably higher than those for GB self-diffusion in Sn or Pb (~ 55kJ/mol as opposed to 42kJ/mol and 21kJ/mol).

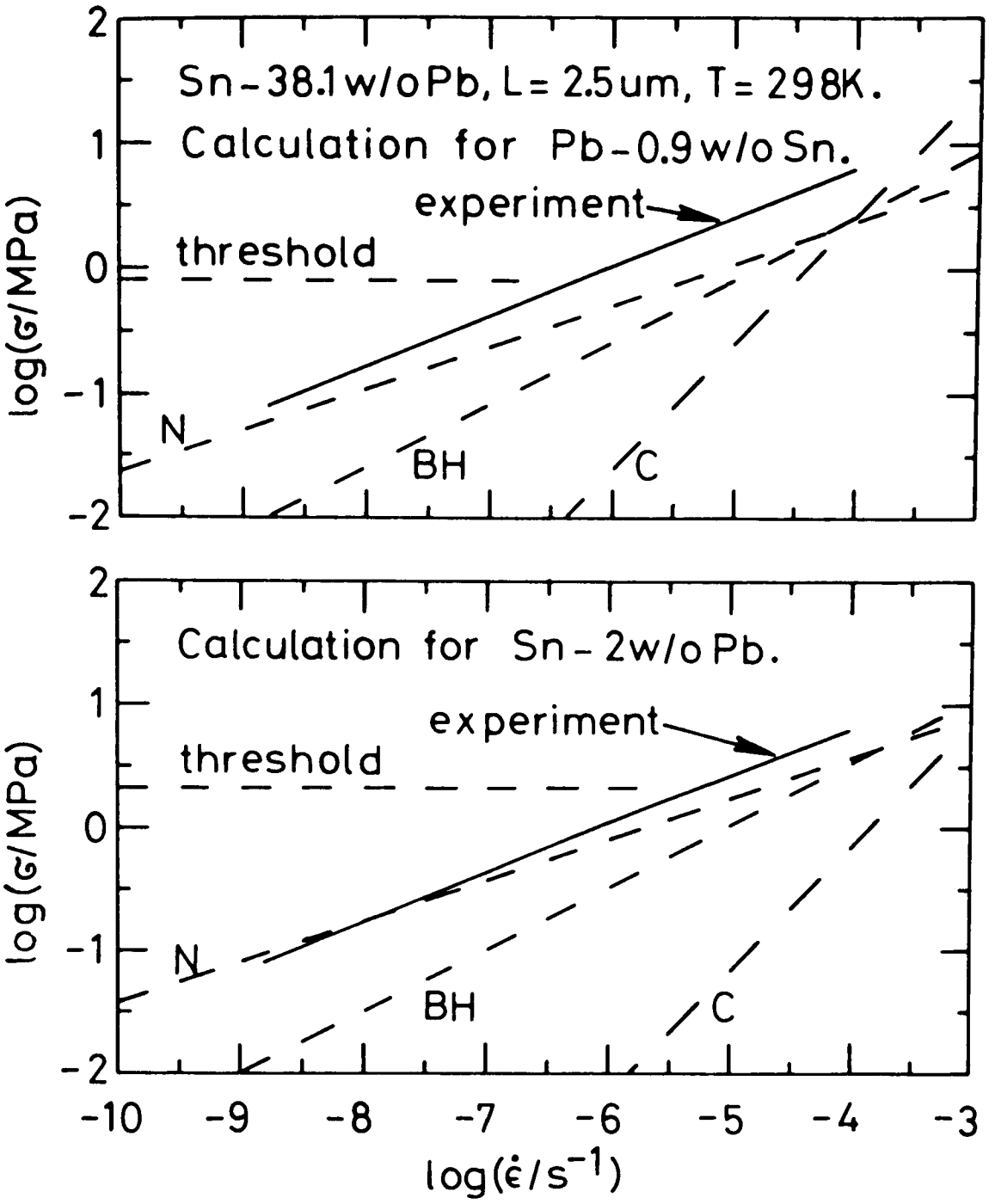

Fig. 5.11. Comparison between experiment and theory for Sn-38.1w/o Pb with a grain size of 2.5μm, at 298K. N = GBD after Nabarro, B = GBD creep after Ball and Hutchison, C = Coble creep.

Since the anelasticity found in Sn-Pb (chapter 6) implies interface control via GBS and since GBS is usually thermally activated with the appropriate activation energy for boundary diffusion (section 2.3), diffusion in the Sn-Pb interface possibly controls interface sliding, with an approximate activation energy of ~55kJ/mol. Alternatively, there might be some contribution from lattice diffusion with its much higher activation energy (see eqns. (5.8) and (5.9)). This is however considered to be unlikely owing to the importance of GB self-diffusion as compared to that of lattice self-diffusion (see eqns. (5.10) and (5.11)).
(3) Neither eqn. (2.14) nor eqn. (2.15) predict the experimentally found dependence of the strain rate on the stress and the grain size, $\dot{\varepsilon} \alpha \sigma^{2.5}/L^{2.3}$, accurately.

In spite of these shortcomings the experiments show clearly that the mechanism controlling the strain rate cannot be ordinary GBS (i.e. $\dot{\varepsilon} \alpha L^{-1}$, see also section 2.3.1(a)): intersecting GBs or the GBDs contained in them interact in such a manner that a grain size dependence stronger than $\dot{\varepsilon} \alpha L^{-1}$ results.

5.4. The plastic deformation of Sn-2w/o Pb and its interpretation

The dependence of the plastic strain rate of Sn-2w/o Pb on the applied stress and the temperature is shown in Figs. 5.12 to 5.16, for various grain sizes. Often one sample was tested at several temperatures. If, at a particular

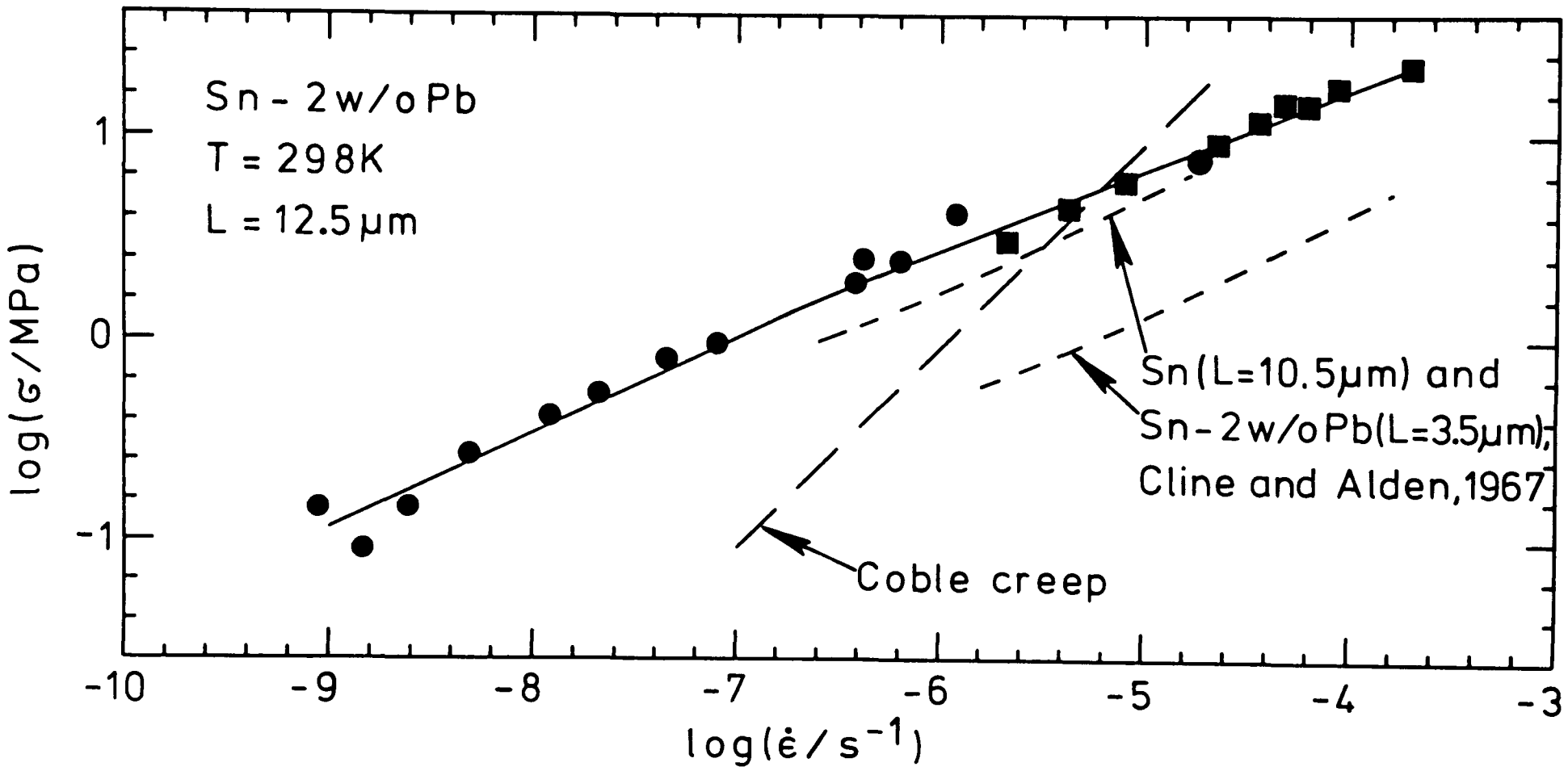

Fig. 5.12. The relationship between the applied stress, σ, and the plastic strain rate, $\dot{\varepsilon}$, for Sn-2w/o Pb with a grain size of 12.5μm.

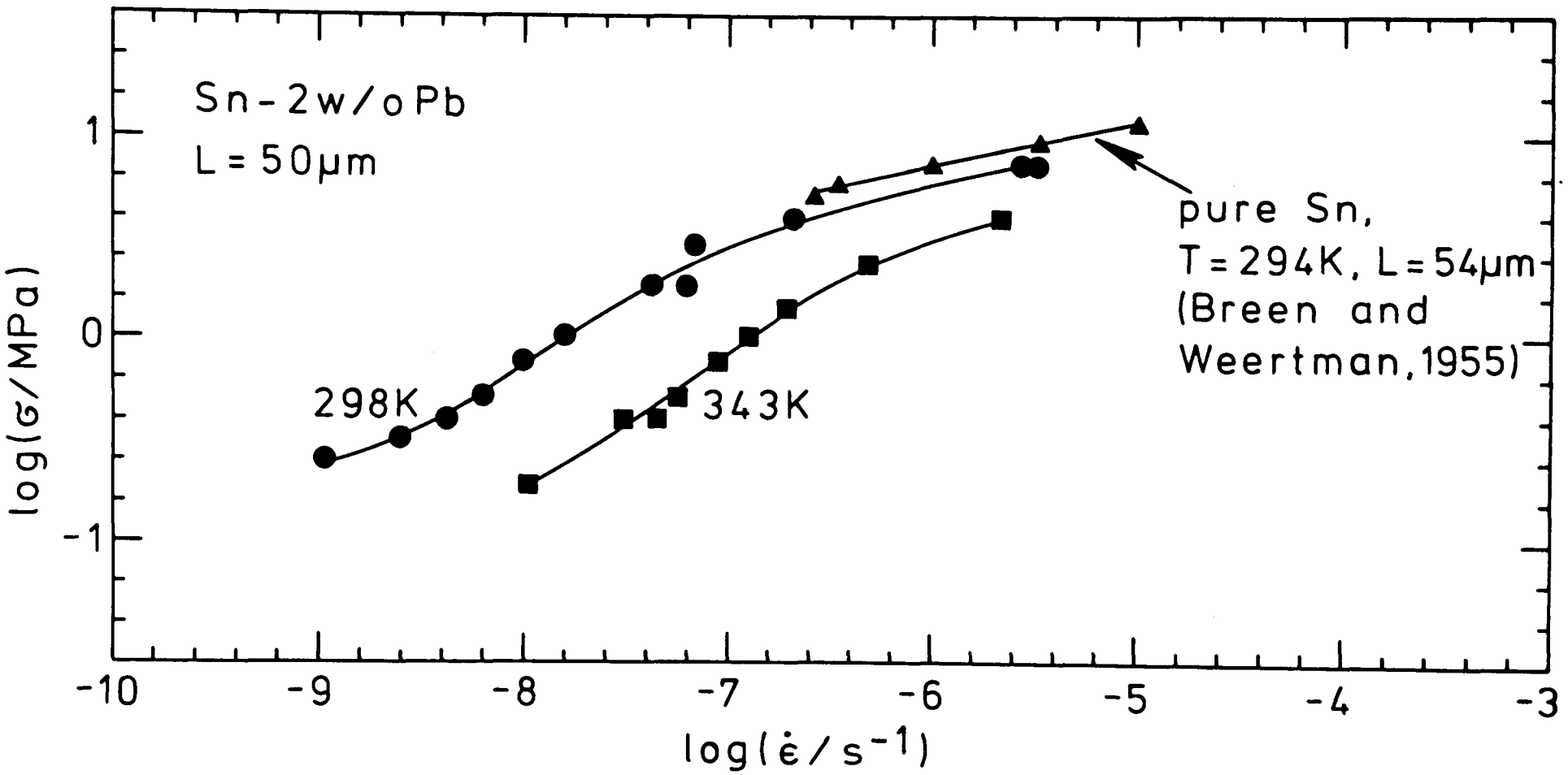

Fig. 5.13. The relationship between the applied stress, σ, and the plastic strain rate, $\dot{\varepsilon}$, for Sn-2w/o Pb with a grain size of 50μm.

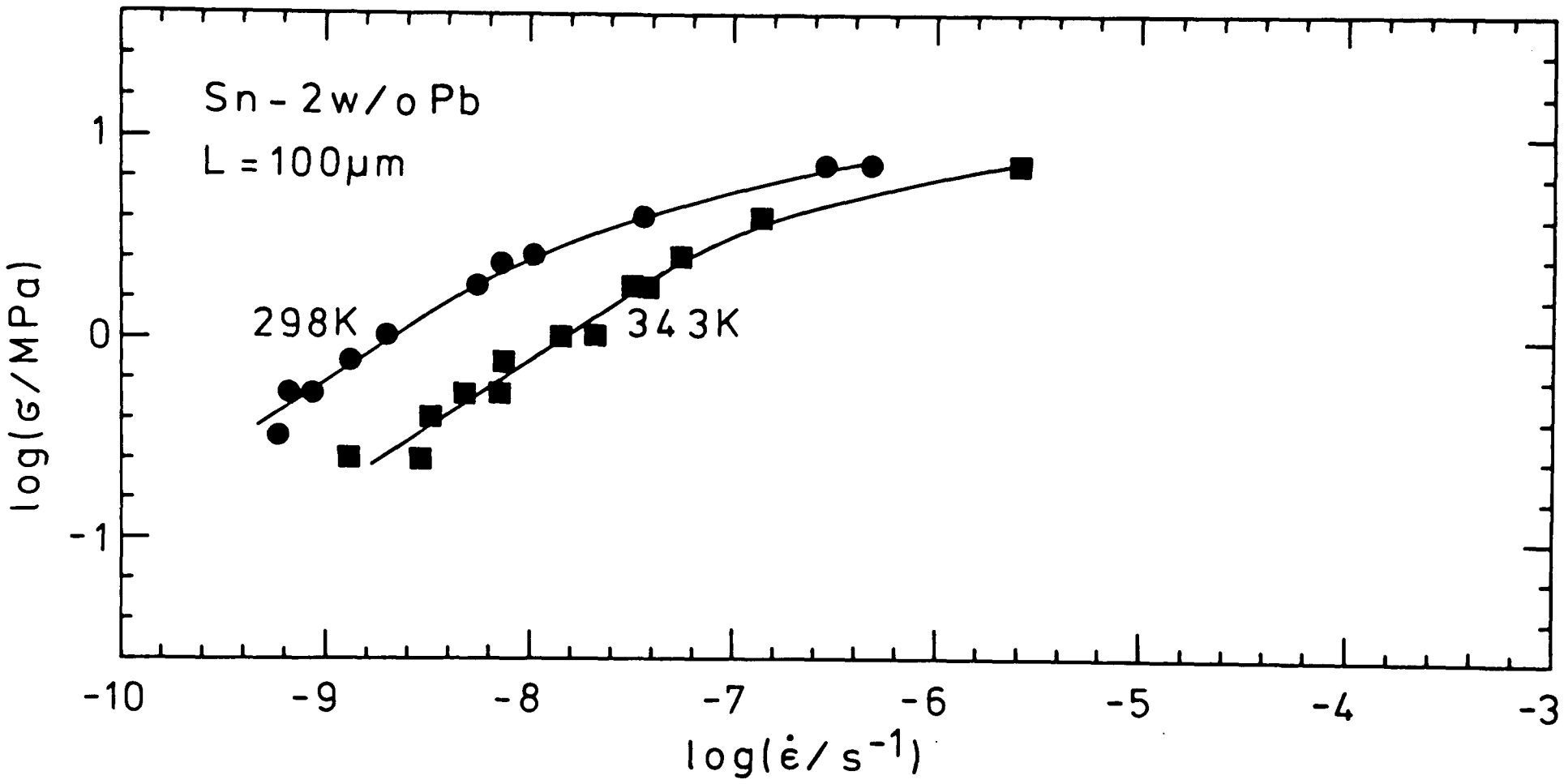

Fig. 5.14. The relationship between the applied stress, σ, and the plastic strain rate, $\dot{\varepsilon}$, for Sn-2w/o Pb with a grain size of 100μm.

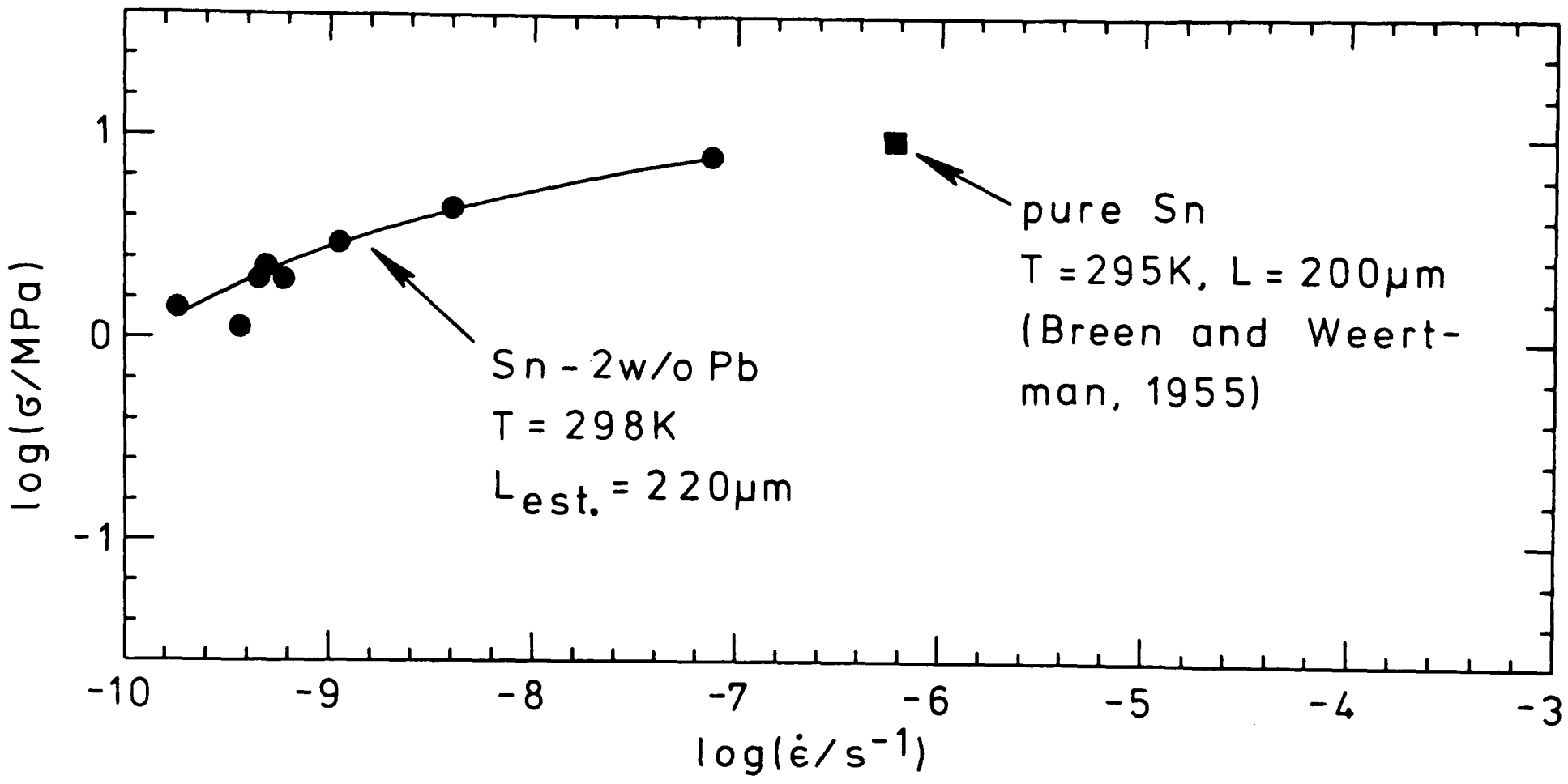

Fig. 5.15. The relationship between the applied stress, σ, and the plastic strain rate, $\dot{\varepsilon}$, for Sn-2w/o Pb with a grain size of ~220μm.

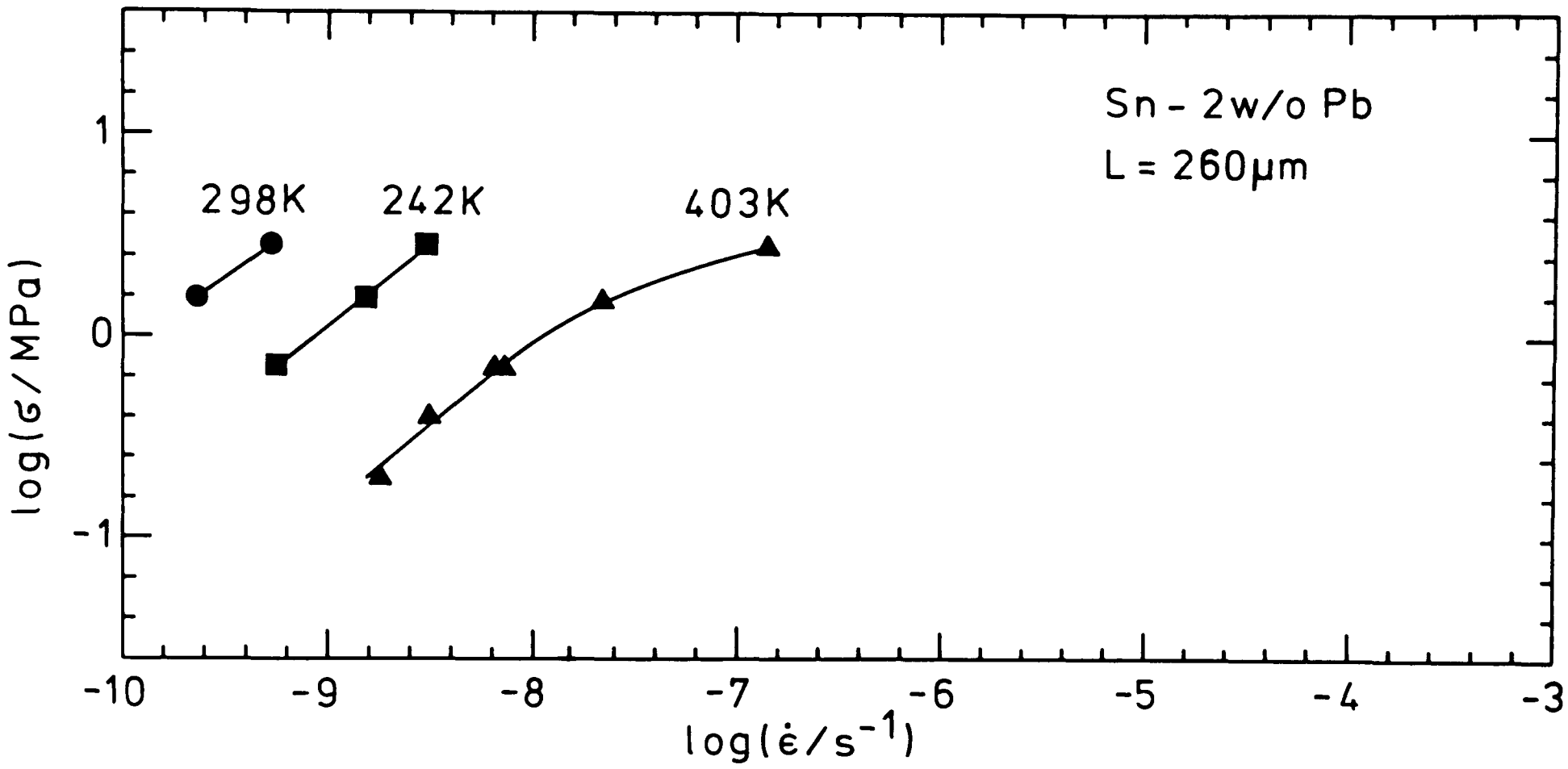

Fig. 5.16. The relationship between the applied stress, σ, and the plastic strain rate, $\dot{\epsilon}$, for Sn-2w/o Pb with a grain size of 260μm.

test temperature, more than one sample had been employed, different symbols for each of these samples have been used in the figures. A typical deformation schedule is described in Table 5.3. Table 5.4 gives a few details of the grain size determinations and also the cross-sections of the corresponding samples investigated for their mechanical behaviour. In some cases the grain size was not much smaller than the sample cross-section so that some influence from surface diffusion is to be expected. This influence is however considered to be small since the mechanical behaviour of the corresponding samples does not show any irregularities as verified in the evaluation of diffusion creep below. In a few instances, grain sizes were estimated from the strain rates measured for a particular sample and the previously determined relationship between strain rate and grain size (see also Fig. 5.18). These grain sizes are indicated as L_{est}.

Fig. 5.17 shows data for a test temperature of 298K (mainly from Figs. 5.3 to 5.7) and demonstrates clearly the strong grain size dependence of the deformation behaviour of Sn-2w/o Pb. A few previously published data for pure Sn and Sn-2w/o Pb are indicated in Figs. 5.12,5.13 and 5.15. They are in substantial agreement with the present results.

The mechanical behaviour of Sn-2w/o Pb, for the smallest grain size employed, is very similar to that of Sn-38.1w/o Pb with similar grain sizes. It is therefore possible that the deformation mechanisms in both alloys are similar or identical.

σ/MPa	T/K	Δt/ks	$\Delta\varepsilon/10^{-5}$	$\dot{\varepsilon}/s^{-1}$
7.20	298	0.8	126.0	$4.8\cdot10^{-7}$
0	"	13.6	-45.4	-
0.32	"	77.7	5.4	$5.8\cdot10^{-10}$
0.52	"	67.7	8.5	$8.5\cdot10^{-10}$
0.75	"	39.4	6.5	$1.3\cdot10^{-9}$
1.02	"	41.7	10.8	$2.0\cdot10^{-9}$
1.81	"	16.4	16.9	$5.5\cdot10^{-9}$
2.56	"	6.8	13.1	$1.0\cdot10^{-8}$
3.98	"	4.7	25.8	$2.9\cdot10^{-8}$
7.20	"	1.1	60.8	$2.8\cdot10^{-7}$
0	"	2.8	-50.0	$-8.4\cdot10^{-9}$
0.52	"	55.6	3.1	$6.6\cdot10^{-10}$
2.33	"	20.1	32.7	$7.2\cdot10^{-9}$
0	343	3.8	-23.1	-
0.25	"	54.1	8.5	$2.9\cdot10^{-9}$
0.52	"	19.0	6.5	$7.1\cdot10^{-9}$
1.02	"	8.3	10.8	$2.1\cdot10^{-8}$
1.81	"	4.6	9.2	$3.8\cdot10^{-8}$
o.4	"	154.5	23.1	$3\cdot10^{-9}$
0.25	"	104.0	6.5	$1.4\cdot10^{-9}$
0.52	"	48.7	11.5	$4.8\cdot10^{-9}$
1.02	"	20.7	18.5	$1.4\cdot10^{-8}$
1.81	"	14.7	26.1	$3.1\cdot10^{-8}$
0.75	"	62.4	20.4	$7.5\cdot10^{-9}$
2.56	"	11.2	33.1	$5.4\cdot10^{-8}$
3.98	"	4.4	35.0	$1.4\cdot10^{-7}$
7.20	"	3.1	858.0	$2.6\cdot10^{-6}$
		t_{tot}=860ks	$\varepsilon_{tot}=1.3\cdot10^{-2}$	

Table 5.3. A typical deformation schedule to produce the data in Fig. 5.14. At the end of a time interval, Δt, during which a stress σ was applied and during which the test temperature was T, the strain increment is $\Delta\varepsilon$ and the strain rate is $\dot{\varepsilon}$. Negative strain increments and strain rates are due to elastic and anelastic contraction.

Number of grains counted	cross section of tested sample	true grain size
1136	5.9 x 0.64 mm^2	12.5 μm
271	5.9 x 0.24 mm^2	50 μm
264	5.9 x 0.24 mm^2	100 μm
159	5.9 x 0.63 mm^2	170 μm
100	5.9 x 0.62 mm^2	260 μm

Table 5.4. Numbers of grains counted for the grain size determinations in Sn-2w/o Pb and the initial cross-sections of the corresponding mechanically tested samples.

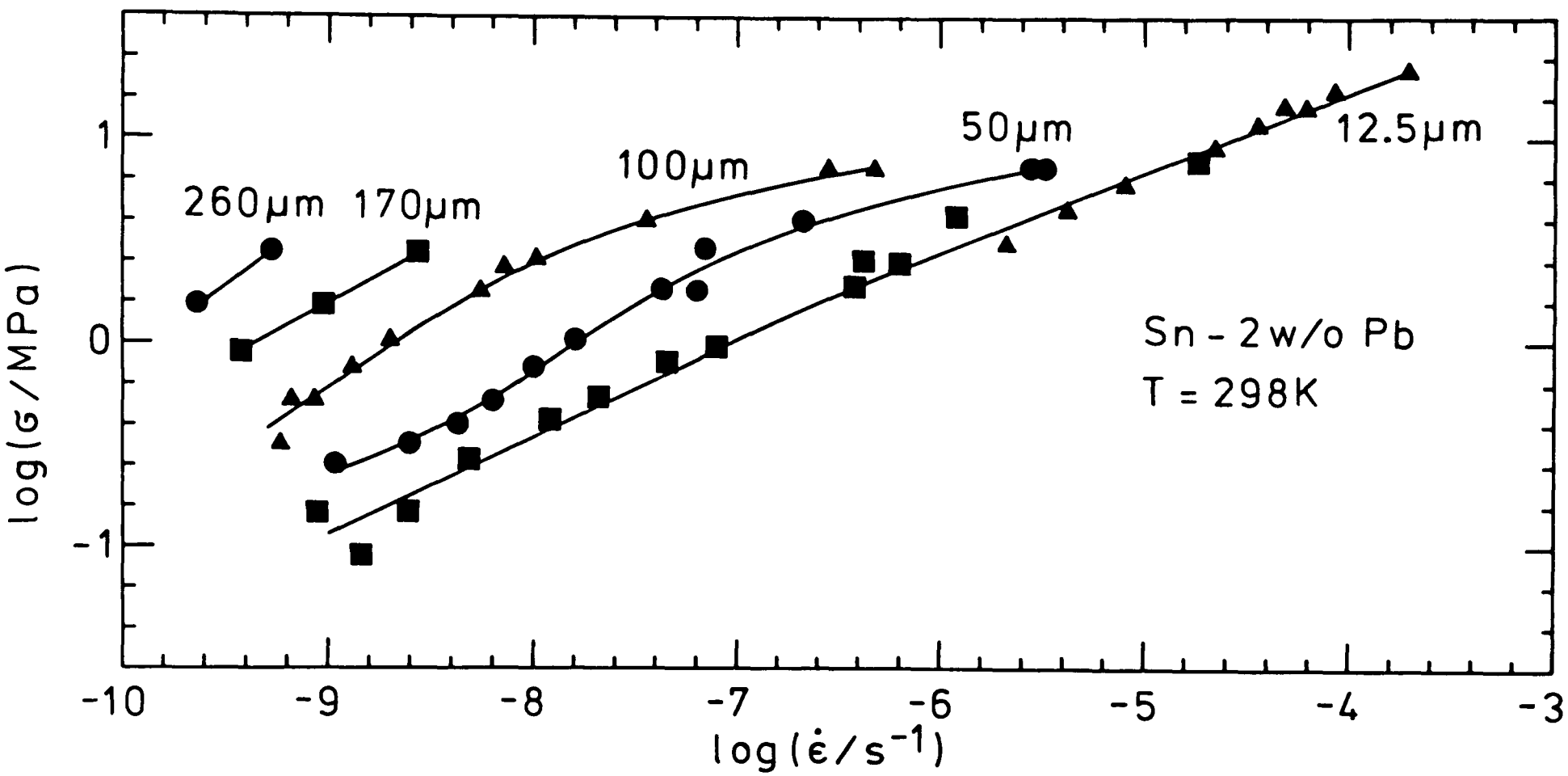

Fig. 5.17. The relationship between the applied stress, σ, and the plastic strain rate, $\dot{\varepsilon}$, at 298K, for various grain sizes.

5.4.1. Grain boundary diffusion creep in Sn-2w/o Pb

Inspection of Figs. 5.12 to 5.17 shows that the stress-strain rate relationships, for grain sizes larger than ~50μm and stresses of the order of 1MPa, exhibit regions with a strain rate sensitivity, m, significantly higher than 0.5. In some cases m is close to 1 (see Table 5.5). In this range of stresses and grain sizes diffusion creep may therefore be operating (it would then be obscured by a faster mechanism for high stresses and a slower mechanism for low stresses).

Grain size dependence of the strain rate

The data in Figs. 5.13 to 5.17 are replotted in Fig. 5.18, for a stress of 1MPa. The strain rate is found to be proportional to $1/L^3$. This dependence is evidence for Coble creep (eqn (2.4)).

Activation energy

Additional evidence for Coble creep is found in the value of the activation energy. With $D_B = D_o \exp(-Q/(RT))$, and using the Coble creep equation (eqn. (2.4)), Q may be written as:

$$Q = -R \frac{\delta \ln(\dot{\varepsilon}\, T)}{\delta (1/T)}, \qquad (5.12)$$

where Q is the activation energy for Coble creep (= activation energy for grain boundary self-diffusion). From the slopes in a plot of ($\dot{\varepsilon}$ T) vs. 1/T, for a stress of 1MPa

L/μm	T/K	m
12.5	298	0.45
50	298	0.68
50	343	0.72
100	298	0.67
100	343	0.68
170	298	0.56
260	298	0.76
260	343	0.82
260	403	0.84

Table 5.5. Strain rate sensitivities, m, for Sn-2 /o Pb, for various grain sizes,L, and temperatures,T, at a stress of 1MPa.

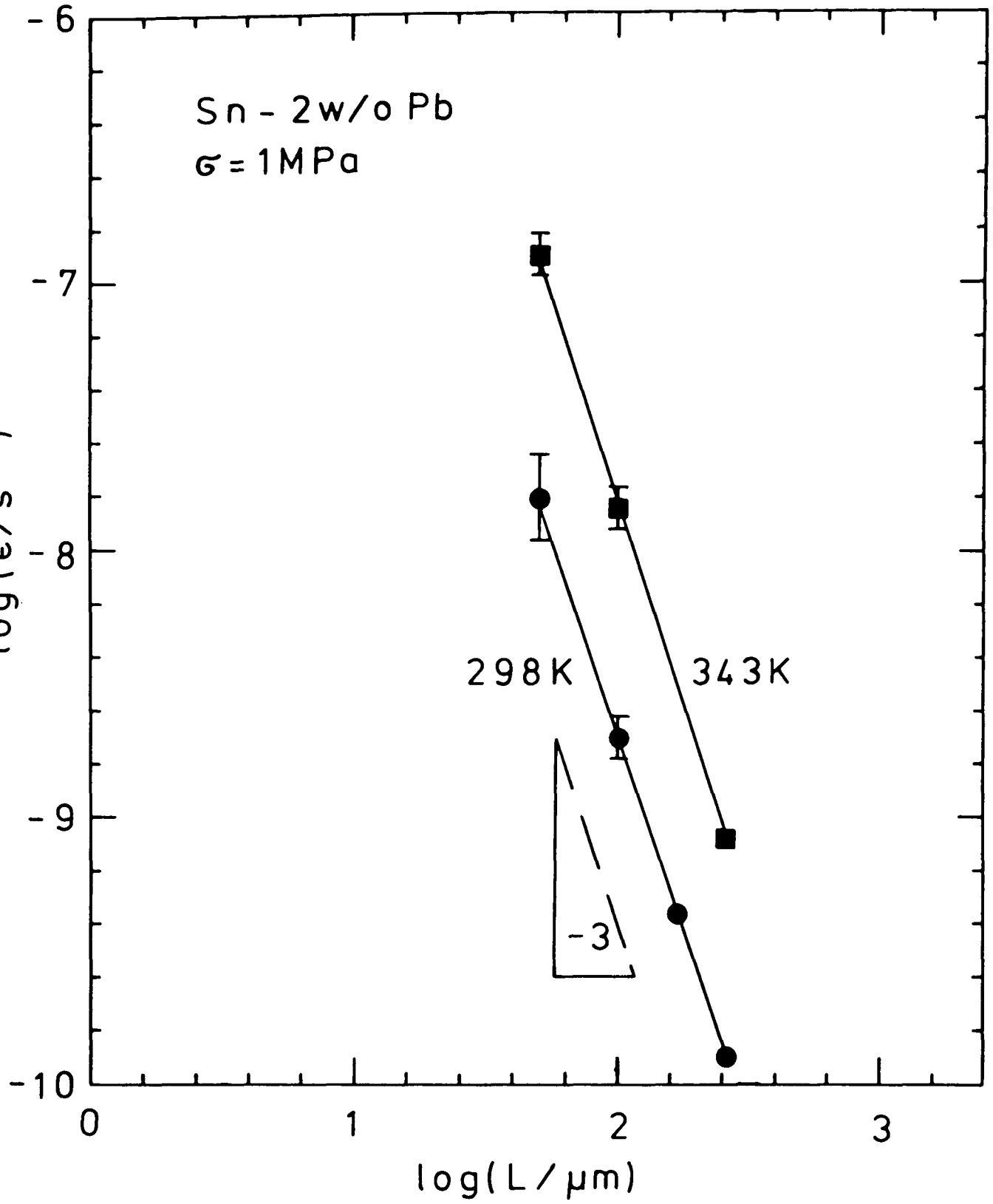

Fig. 5.18. The relationship between the plastic strain rate, $\dot{\varepsilon}$, and the grain size, L, for Sn-2w/o Pb. The data points are from Figs. 5.4 to 5.8. The errors in the strain rates were estimated from the scatter in the plastic strain rates.

(Fig. 5.19), an average activation energy of 42kJ/mol is found for the creep of Sn-2w/o Pb. This value compares very well with the activation energy for the GB self-diffusion in pure Sn, (40 $\mp$ 3)kJ/mol, which has been measured with a radioactive tracer method by Lange and Bergner (1962).

Pre-exponential term of the diffusion coefficient

The pre-exponential term, D_o, in $D_B = D_o \exp(-Q/(RT))$ may be evaluated from the mechanical data, by rearranging eqn. (2.4):

$$D_o = \frac{k\ T\ L^3\ \dot{\varepsilon}}{47\ \Omega\ w\ \sigma} \exp\left(\frac{Q}{RT}\right) . \qquad (5.13)$$

With w = 2b = 0.7nm, T = 298K, Q = 42kJ/mol, $\Omega = 2.7 \cdot 10^{-29} m^3$, for a stress of 1MPa and grain sizes larger than 50µm, the data in Figs. 5.13 to 5.17 result in $D_o = 2.4 \cdot 10^{-4} m^2/s$ (maximum value $3.3 \cdot 10^{-4} m^2/s$, minimum value $2.0 \cdot 10^{-4} m^2/s$). This value is distinctly larger than the value measured by Lange and Bergner (1962), namely $6.4 \cdot 10^{-6} m^2/s$ (maximum value $1.24 \cdot 10^{-5} m^2/s$, minimum value $1.5 \cdot 10^{-6} m^2/s$).

It is preferable to compare the pre-exponential terms for diffusion in Sn and in Sn-2w/o Pb for identical activation energies. Evaluation of eqn. (5.13) for Q = 40kJ/mol results in:

$D_o = 1.1 \cdot 10^{-4} m^2/s$ (minimum value $9.0 \cdot 10^{-5} m^2/s$.
maximum value $1.5 \cdot 10^{-4} m^2/s$).

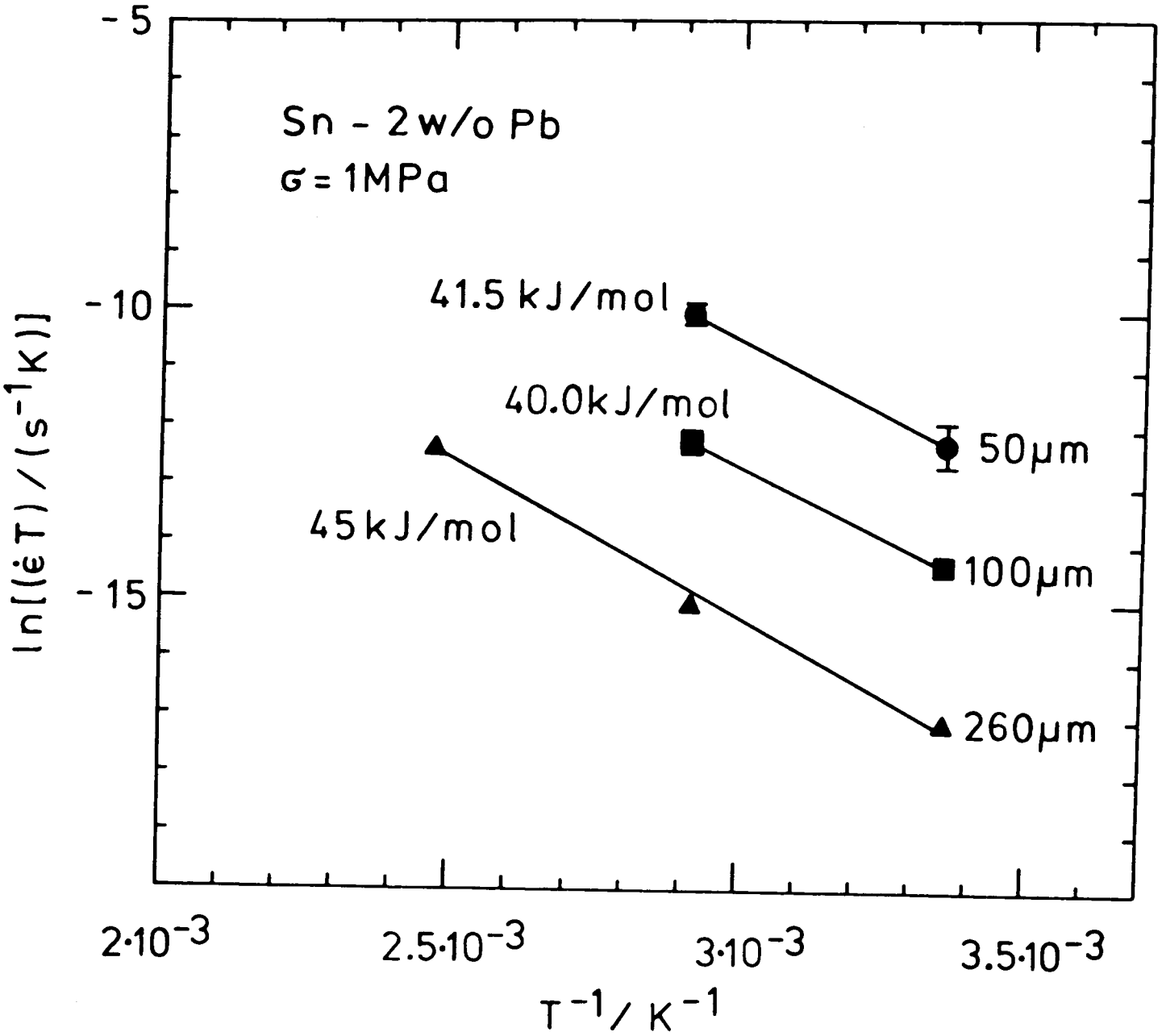

Fig. 5.19. Determination of the activation energy of Sn-2w/o Pb, for a stress of 1MPa, with the data from Figs. 5.4 to 5.8. The error bars were estimated from the scatter in the plastic strain rates.

The agreement with Lange and Bergner's result above is now slightly better. If switching events during deformation of Sn-2w/o Pb occur, the factor 47 in eqn. (5.13) increases (see section (2.2.1)) and the agreement becomes even better. The small degrees of deformation employed for the experiments, (see Table 5.3) however, make a significant contribution from grain switching unlikely.

One might also argue that the actual steady-state strain rates are lower than the measured ones (due to plastic transients) and that the actual value of D_o for Sn-2w/o Pb should therefore be lower than the one found here (compare with eqn. (5.13)). A slowing down of the strain rate, however, would not be caused by diffusion creep itself, since transient strains in diffusion creep are of the order of the elastic deformation corresponding to the particular applied stress (Raj and Ashby, 1971). The strain increments used to determine the strain rate for a particular stress were often only a few times the elastic deformation corresponding to this stress. Such a procedure should be suitable for the correct determination of the Gb diffusion creep rates.

Since the influence of grain switching and transient creep has been ruled out it is concluded that GB self-diffusion in Sn-2w/o Pb is faster than in pure Sn by a factor of ~17. A homogenous distribution of Pb in Sn does not appear to be responsible for the observed acceleration of the GB self-diffusion coefficient. For a homogeneous distribution an average GB diffusion coefficient ,$\tilde{D}$, can be

defined by:

$$\tilde{D} = \nu_{Sn}\, D_B(Sn) + \nu_{Pb}\, D_B(Pb) \quad , \qquad (5.14)$$

where ν_{Sn} and ν_{Pb} are the mole fractions of Sn and Pb, respectively. For Sn-2w/o Pb, $\nu_{Sn} = 0.988$ and $\nu_{Pb} = 0.012$. The GB self-diffusion coefficient for pure Sn at 298K is $D_B(Sn) = 6.4 \cdot 10^{-13} m^2/s$ (Lange and Bergner, 1962). Extrapolation of Stark and Upthegrove's (1966a) GB self-diffusion coefficient for Pb (for a 30^o tilt boundary and using an activation energy of 19kJ/mol) to a temperature of 298K results in $D_B(Pb) = 5.3 \cdot 10^{-12} m^2/s$. Equation (5.14) now leads to $\tilde{D} = 7.0 \cdot 10^{-13} m^2/s$ which is very similar to the GB self-diffusion coefficient for pure Sn quoted above.

A significant acceleration of the GB diffusion in a metal due to the presence of small amounts of impurities, however, is not uncommon as can be seen from the diffusion data collected by Gleiter and Chalmers (1972). An important reason for this acceleration is the segregation at the GBs of a solute with a low solubility in the matrix (Hondros and Seah, 1977). At room temperature, Sn dissolves only ~0.2a/o Pb (Hansen and Anderko, 1958). A GB enrichment ratio higher than ~500 would then be predicted from Hondros and Seah's Fig. 4. (the GB enrichment ratio is defined as the ratio of the interfacial concentration in mole fractions of a monoloyer, and the bulk solute mole fraction). If the Pb is segregated in a narrow region in and around the

GBs (a few atomic layers), a local volume concentration of Pb comparable to that of Sn would be expected at and near the GBs. Since GB self-diffusion is faster in Pb than in Sn, for termperatures below ~400K (see Lange and Bergner (1962) and Stark and Upthegrove (1966a)), Pb is expected to accelerate GB self-diffusion in Sn, according to eqn. (5.14). It is however surprising that the small activation energy for GB self-diffusion in Pb (~19kJ/mol) does not seem to have any bearing on the activation energy for GB self-diffusion in Sn (~40kJ/mol): the activation energy in Sn-2w/o Pb as determined from Coble creep has been found to be very close to 40kJ/mol.

Incidentally, deformation data published by Alden (1967) for Sn-5w/o Bi also imply an acceleration of GB self-diffusion in Sn which this time is caused by Bi. Aldens results for his largest grain size (mean intercept length = 16μm, corresponding to a true grain size of 24μm) demonstrate a strain rate sensitivity of nearly 1 at low stresses. Also, the strain rate is proportional to the inverse cube of the grain size. This evidence indicates diffusion creep. Inserting Alden's data point with σ = 8.7MPa, $\dot{\varepsilon} = 4.2 \cdot 10^{-7} s^{-1}$, L = 24μm, and T = 298K in eqn. (5.13) results in a diffusion coefficient $D_B(\text{Sn-5w/o Bi}) = 3.2 \cdot 10^{-5} \frac{m^2}{s} \exp(-\frac{40kJ/mol}{R\,T})$ which is higher than Lange and Bergner's (1962) diffusion coefficient for pure Sn, $D_B(\text{Sn}) = 6.4 \cdot 10^{-6} \frac{m^2}{s} \exp(-\frac{40kJ/mol}{R\,T})$.

The influence of lattice self-diffusion

The above analysis may have been influenced by lattice self-diffusion. Inspection of the general equation for diffusion creep (eqn. (2.5)) shows that GB diffusion creep is rate-determining as long as:

$$\frac{\pi\ w}{L}\ \frac{D_B(T)}{D_L(T)}\ \gtrsim\ 1\ . \qquad (5.15)$$

The larger L and T become the smaller the expression in eqn. (5.5) becomes. For w = 2b = 0.7nm, L = 260μm, D_B(Sn-2w/o Pb) = $2.4\cdot10^{-4}$ (m^2/s) $\exp(\frac{42kJ/mol}{R\ T})$ (the GB self-diffusion coefficient for Sn-2w/o Pb determined from the Coble creep equation), $D_L(Sn) = 7.8\cdot10^{-5}\ \frac{m^2}{s}\ \exp(-\frac{95.5kJ/mol}{R\ T})$ (Lange, Hassner and Berthold, 1961) and T = 403K one obtains:

$$\frac{\pi\ w\ D_B(T)}{L\ D_L(T)} = 226. \qquad (5.16)$$

The numerical value given by eqn. (5.16) is the minimum value expected for the range of grain sizes and temperatures employed since the lattice self-diffusion coefficient for Sn assumed in eqn. (5.16) is not expected to be increased by the presence of 2w/o Pb. Even at 403K, the solubility of Pb in Sn is low (~1a/o after Hansen and Anderko, 1958) and, in addition, lattice self-diffusion is slower in Pb than in Sn (compare eqns. (5.8) and (5.9)). Therefore it can be concluded from eqn. (5.16) that the influence from lattice diffusion in the diffusion creep regime of Sn-2w/o Pb can be safely ruled out.

Concluding, GB diffusion creep in Sn-2w/o Pb has been verified without any doubt. The GB self-diffusion coefficient governing the deformation rate can be evaluated from the Coble creep equation and is:

$$D_B(\text{Sn-2w/o Pb}) = 2.4 \cdot 10^{-4} \frac{m^2}{s} \exp\left(-\frac{42\text{kJ/mol}}{R\,T}\right) . \qquad (5.17)$$

The value of the diffusion coefficient in eqn. (5.17) is higher than that for pure Sn by a factor of approximately 17. Pb therefore accelerates GB self-diffusion in Sn.

The result above is of particular importance since no direct experimental proof for the existence of Coble creep in superplastic alloys has been available to date (Spingarn and Nix, 1978).

5.4.2. Interface control in Sn-2w/o Pb

Using the GB diffusion coefficient in eqn. (5.17), the Coble creep equation was evaluated for a grain size of 12.5μm (with w = 0.7nm, $\Omega = 2.7 \cdot 10^{-29} m^3$, and T = 298K The result is plotted as a broken line in Fig. 5.12. The experimental strain rates below ~5MPa are much lower than the theoretical Coble creep rate and therefore one of the interface mechanisms discussed in chapter 2 is presumably operating (either GBS or a vacancy-interface mechanism). Diffusion creep is most certainly inhibited: even if the GB self-diffusion coefficient for pure Sn would be employed (Lange and Bergner, 1962) which is much smaller than the

coefficient in eqn. (5.17), the theoretical Coble creep line in Fig. 5.12 would be shifted to strain rates about one order of magnitude lower and GB diffusion creep would still be seen to be inhibited.

The inhibition of diffusion creep in the case of Sn-2w/o Pb is not thought to be caused by a threshold stress below which no deformation takes place. A threshold stress causes a reduction of the strain rate sensitivity for diffusion creep, $m = 1$, to $m \sim 0$, within an interval of two decades of the strain rate and one decade of the stress (compare Fig. 12 in Ashby and Verall, 1973). The data in Fig. 5.12, however, form an approximately straight line over 3 decades of the strain rate and 1.5 decades of the stress. If there is a threshold stress at all, its value will be below 0.1MPa (at 298K). The situation may of course be different after elongations $\gtrsim 0.3$ since threshold stresses due to grain switching may then become effective (Ashby and Verrall, 1973).

Diffusion creep-inhibiting mechanisms with suitable strain rate sensitivities could be GBD creep after Ball and Hutchison (eqn. (2.15)) and after Nabarro (eqn. (2.14)). These mechanisms, GB diffusion creep and a lattice dislocation mechanism were used in order to predict the mechanical behaviour of Sn-2w/o Pb over a wide range of stresses and strain rates. GBS as suggested by Langdon (see eqn. (2.18)) can easily be seen to be unrealistically slow, since it is lattice diffusion controlled (lattice diffusion coefficient:

see section 5.3.2) and has therefore been omitted. For the same reason the vacancy-interface control mechanism suggested by Burton (1972) has been omitted (see section 2.6).

The input data for the calculation were:

$T = 298K$,

$D_B = 1.03 \cdot 10^{-11} m^2/s$ (after eqn. (5.17)),

$G = 15.4GPa$ (shear modulus for Sn at 298K, after Simmons and Wang (1971), p.300, their approximation R),

$b = b_B = b_L = 0.35nm$,

$w = 0.7nm$,

$\Omega = 2.7 \cdot 10^{-29} m^3$.

Equations (2.15), (2.14), (2.4) and (2.22) (eqn. (2.22) was fitted) can now be written as:

$$\dot{\varepsilon} = 1.08 \cdot 10^{11} s^{-1} \, (b/L)^2 \, (\sigma/G)^2 \qquad (5.18)$$

(GBD creep after Ball and Hutchison, see section 2.3.1(b)),

$$\dot{\varepsilon} = 5.4 \cdot 10^{10} s^{-1} \, (b/L) \, (\sigma/G)^3 \qquad (5.19)$$

(GBD Creep after Nabarro, see section 2.3.1(a)),

$$\dot{\varepsilon} = 3.43 \cdot 10^{-17} s^{-1} \, (1/L)^3 \, (\sigma/G) \qquad (5.20)$$

(Coble creep), and

$$\dot{\varepsilon} = 3.57 s^{-1} \, (1/L)^2 \, (\sigma/G)^{4.5} \qquad (5.21)$$

(lattice dislocation creep after Gifkins (1973), fitted to the experimental data).

The above equations were combined according to the rheological models shown in Figs. 5.20 and 5.21. The dashpots representing GBS were placed in parallel with the dashpot representing Coble creep since Coble creep requires a substantial amount of GBS in order to operate continuously (see section 2.2.1). On the other hand, the dashpot representing Gifkin's mechanism was connected in series with the Coble creep and GBS mechanisms. At sufficiently high stresses, the ratio of GBS and grain strain is small in Gifkin's model and the presence of many lattice dislocations should provide some accommodated GBS such that a GBS mechanism based on GBDs should not be rate-controlling any more.

For both interface mechanisms, the agreement between theory and experiment is surprisingly good (see Figs. 5.20 and 5.21). Below a stress of $Gb/L \sim 5.4 \cdot 10^{-6}$ MPam/L, however, the GBD mechanisms in their present form are unlikely to operate because the GBDs cannot multiply (see section 2.7.2(b)). Below this (grain size dependent) stress the theoretical lines have therefore not been fully drawn in Figs. 5.20 and 5.21. Threshold stresses may be smaller than $5.4 \cdot 10^{-6}$ MPam/L for GBDs with Burgers vectors smaller than those of lattice dislocations. The difference is however expected to be small, for example a factor of 2 (compare for example the GBD Burgers vectors for coincidence boundaries summarized by Ishida and McLean (1972)). Threshold stresses smaller than Gb/L would also result if the line tension of GBDs would be significantly smaller than the line tension of lattice dislocations with the same Burgers vector. In

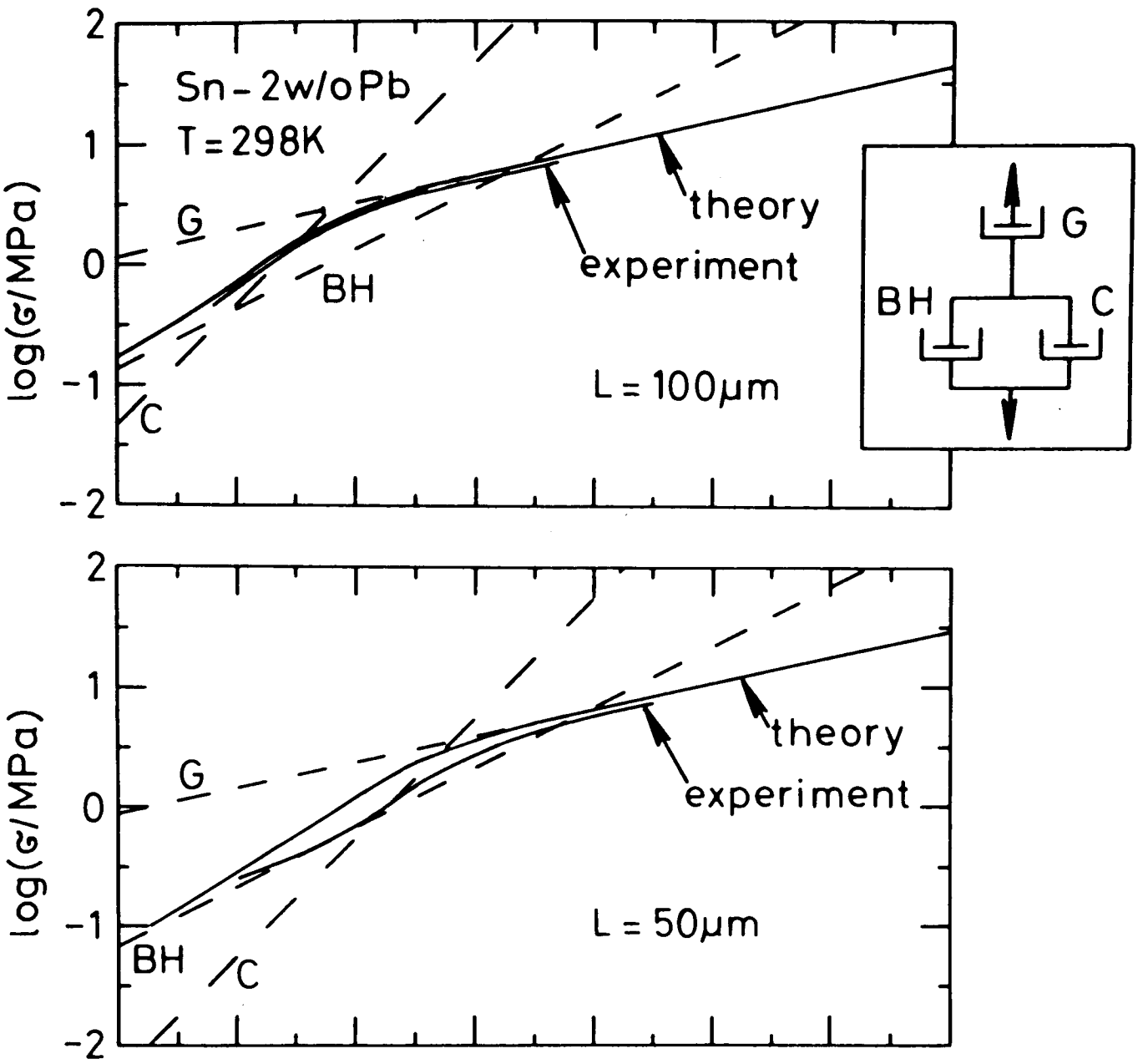

Fig. 5.20. Calculation of stress-strain rate relationships for Sn-2w/o Pb (T = 298K) employing GBD creep after Ball and Hutchison (BH), Coble creep (C) and Gifkins creep (G). The stress-strain rate relationships for the different mechanisms are plotted as broken lines. The total strain rate was calculated according to the rheological model shown and is annotated as "theory". The experimental data are from Fig. 5.8.

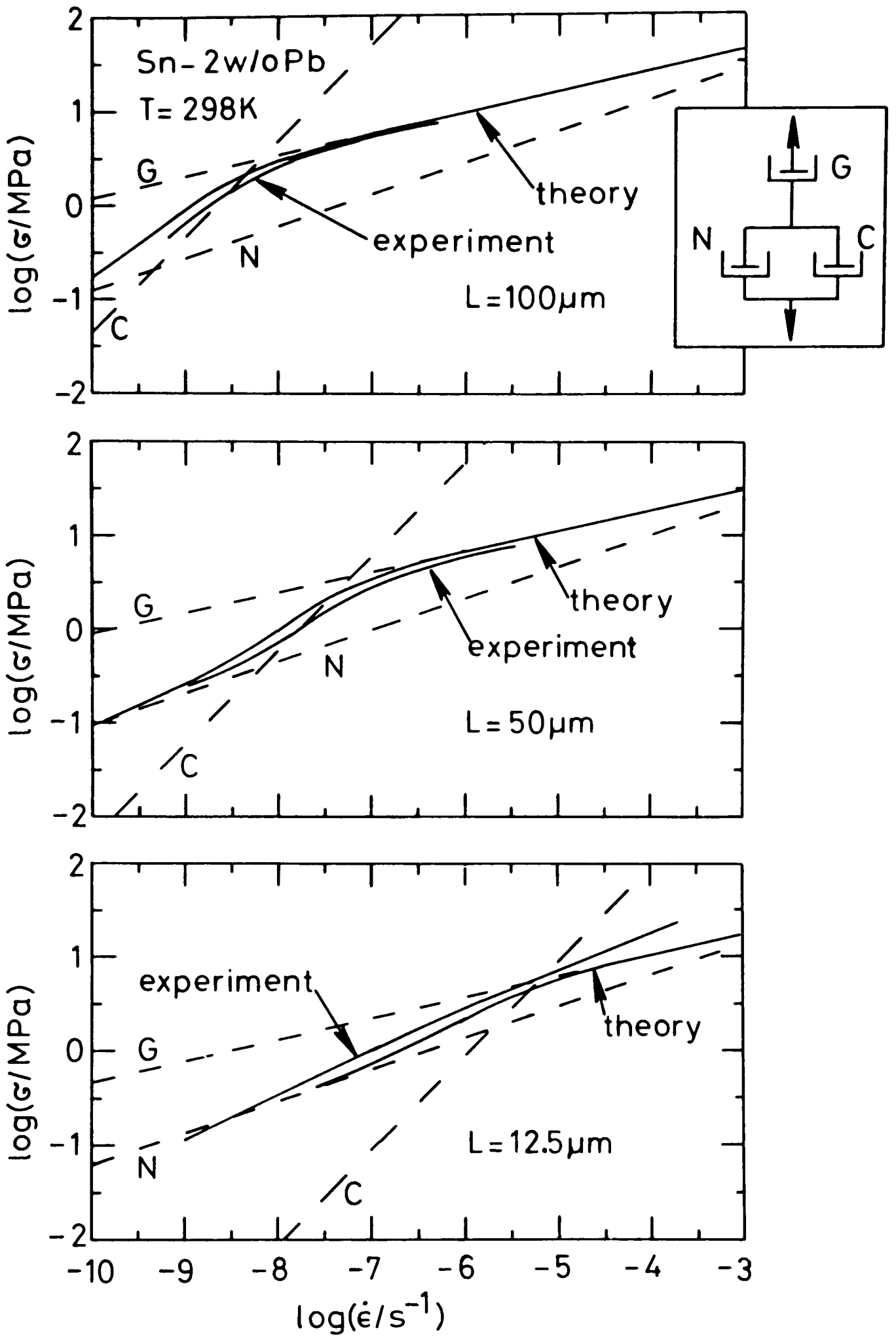

Fig. 5.21. Calculation of stress-strain rate relationships for Sn-2w/o Pb (T = 298K) employing GBD creep after Nabarro (N), Coble creep (C), and Gifkins creep (G). The stress-strain rate relationships for the different mechanisms are plotted as broken lines. The total strain rate was calculated according to the rheological model shown and is annotated as "theory". The experimental data are from Fig. 5.8.

a later chapter it will be seen that the anelastic behaviour of fine-grained Sn-Pb alloys also implies a comparatively low GBD line tension.

Equation (5.18) is identical to the equation predicted by the Ball and Hutchison (BH) model for lattice dislocations (eqn. (2.6)), for the data employed above. If the Ball and Hutchison model in its original form would operate it is not clear why there should be any evidence for Coble creep. One would have to assume that below the stress for which Coble creep is faster than BH creep, BH creep is rate-determining. In the region where BH creep is faster than Coble creep, Coble creep would have to be rate-controlling (compare for example the broken lines for Coble and BH creep in Fig. 5.20). This is rather unlikely and therefore the GBD mechanism is preferred. In addition, one has to remember the sparseness of evidence for lattice dislocations in superplastic alloys at small stresses (Edington, Melton and Cutler, 1976). It may definitely be concluded that some interface-controlled mechanism operates in Sn-2w/o Pb to prevent Coble creep from occurring. The mechanical data for Sn-2w/o Pb are not sufficient to define the interface mechanism in detail. Any relationship of the form $\dot{\varepsilon} \propto \sigma^n/L^p$ with $0.3 \leq n \leq 0.5$ and $1 \leq p \leq 2$ is realistic, as, for example, the GBS mechanism suggested by Ashby and Verrall (1973) (see eqn. 2.13). Greenwood's vacancy-interface reaction control (see section 2.7.2), with $\dot{\varepsilon} \propto f(\sigma)/L$, would also be able to give qualitative agreement with the experimental data at low stresses. The measured grain size

dependence of the plastic strain rates of Sn-38.1w/o Pb, however, tentatively supports a GBD mechanism involving interaction between the GBDs in intersecting GBs, i.e., a grain size dependence of the strain rate approximately like L^{-2}. The GBD pile-ups assumed in such a model are also in qualitative agreement with the anelasticity found in Sn-Pb alloys (see chapter 6).

5.5. Summary and conclusions

(1) The plastic properties of superplastic Sn-Pb eutectic (Sn-38.1w/o Pb) and Sn-2w/o Pb have been measured at temperatures between 298K and 403K and at strain rates as low as $10^{-10}s^{-1}$, using a high-resolution creep rig. No threshold stress for plastic deformation was found although stresses as low as 0.1MPa were employed. The deformation properties of the two investigated alloys are similar for comparable grain sizes. This implies that the underlying deformation mechanisms are similar.

(2) In Sn-38.1w/o Pb Coble creep is probably inhibited by interface control. The measured dependence of the strain rate on the grain size (approximately $1/L^2$) implies that the interface process is not conventional GBS (i.e. $\dot{\varepsilon} \propto 1/L$) but rather that intersecting GBs or the defects contained in them interact. The experimental activation energy is tentatively explained by assuming that the Sn-Pb interfaces, rather than the Sn-Sn and Pb-Pb boundaries, are rate-controlling. The relatively high threshold stresses which

are predicted by GBS mechanisms based on GBDs suggest that GBDs have a significantly lower line tension than lattice dislocations with comparable Burgers vectors.

(3) GB diffusion creep (Coble creep) has been experimentally verified in Sn-2w/o Pb without any doubt. The diffusion creep data imply that the addition of 2w/o Pb to pure Sn enhances the GB self-diffusion coefficient by a factor of approximately 17.

(4) In Sn-2w/o Pb clear evidence has been found that Coble creep is inhibited for small grain sizes and at low stresses. The interface control takes the form $\dot{\varepsilon} \alpha \sigma^n/L^p$, where n is between 2 and 3, and p between 1 and 2. The Sn-38.1w/o Pb data, however, imply a value of $p \sim 2$. The experimental stress-strain rate relationships found for Sn-2w/o Pb are in reasonable agreement with predicted relationships based on GBS (caused by GBDs), Coble creep and lattice dislocation creep.

CHAPTER 6

THE ANELASTIC DEFORMATION OF Sn-Pb ALLOYS AND ITS INTERPRETATION

6.1. Introduction

In the past fine-grained superplastic materials have been investigated mainly with respect to their plastic properties. However, pronounced anelastic behaviour of fine-grained alloys was found as early as 1920: Rosenhain, Haughton and Bingham (1920) compared the behaviour of heavily rolled Zn-7%Al-4%Cu to that of pitch.

Whereas Rosenhain, Haughton and Bingham studied elastic after-effects, more recently internal friction experiments have usually been employed to study anelasticity of superplastic alloys. Nuttall (1971) found a strong damping peak for superplastic Zn-Al eutectoid at ~470K which he attributed to reversible GBS. Sn-Pb eutectic exhibits similar damping properties (Homer and Baudelet, 1977). Strong internal friction has also been found in fine-grained Cu-12%Al and Al-11%Si (Zolotukhin and Tikhonov, 1976).

Newbury (1972) found a anomalously low value for the Young's modulus of Sn-Pb eutectic, using a stress relaxation technique. This result is probably explained, at least partly, by anelastic effects. Anelasticity in Sn-Pb eutectic can give rise to apparent internal stresses (Geckinli and Barrett, 1974). The anelasticity has also been studied by measuring elastic after-effects and has indeed been shown to make stress relaxation tests difficult to interpret (Schneibel and Hazzledine, 1977). Pronounced elastic after-effects have also been observed in superplastic Zn-Al eutectoid (Eastgate, 1978). Anelastic strains of the order of 0.1% were recovered in this case.

The results which will be reported in this chapter (some of these results have already been published by Schneibel and Hazzledine, 1979) show some special features which indicate a distinctive mechanism which may be applicable to other small-grained materials. In particular the relaxation strength reaches values as high as 100 and the relaxation spectrum governing the time-dependence of the elastic after-effect extends over several decades in time.

6.2. The elastic after-effect in Sn-38.1w/o Pb and Sn-2w/o Pb

6.2.1. Experimental procedure

The elastic after-effect (anelastic strain after unloading of a previously loaded sample) was measured for samples identical or similar to the ones employed for the measurement of the plastic behaviour (chapter 5). Usually many tests were done with one sample. Before each loading sufficient time was allowed to elapse so that the anelastic strain rate caused by previous tests had decayed to a very small value. Thus the measured elastic after-effects originated solely from the immediately previous loading period. The grain sizes were measured or estimated as described in chapter 5.

6.2.2. Influence of the loading period on the elastic after-effect

A Sn-38.1w/o Pb sample was successively loaded for different periods of time after which the anelastic strain upon unloading, ε_a, was measured as a function of the time after unloading, t. ε_a was arbitrarily set to 0 at the moment of unloading, t = 0. Experimental results are shown in Fig. 6.1 and they demonstrate that the length of the loading period influences the elastic after-effect. This implies that long relaxation times (e.g. $\gtrsim$ 30s in Fig. 6.1) have some influence on the short term relaxation behaviour (t $\lesssim$ 30s in Fig. 6.1). For long loading periods, however, the recovered strain seems to approach a limiting curve which is independent of the length of the loading period. This view finds additional support in Fig. 6.2, where elastic after-effects after relatively long loading periods (3.6ks and 25ks) are compared. In Fig. 6.2 the anelastic compliance, J_a ($J_a = -\varepsilon_a/\sigma$, where σ is the loading stress) has been plotted instead of the anelastic strain, since slightly different loading stresses have been employed for the two tests depicted. It is reasonable to define such an anelastic compliance as will be shown in section 6.2.3.

In the present work, elastic after-effects were usually evaluated for times up to one half of the period of time during which loading occurred. For short loading periods (e.g. 60s) this procedure can lead to substantial errors in the anelastic strains. Fig. 6.1 indicates errors up to ~40%. For long loading periods, the influence of the load-

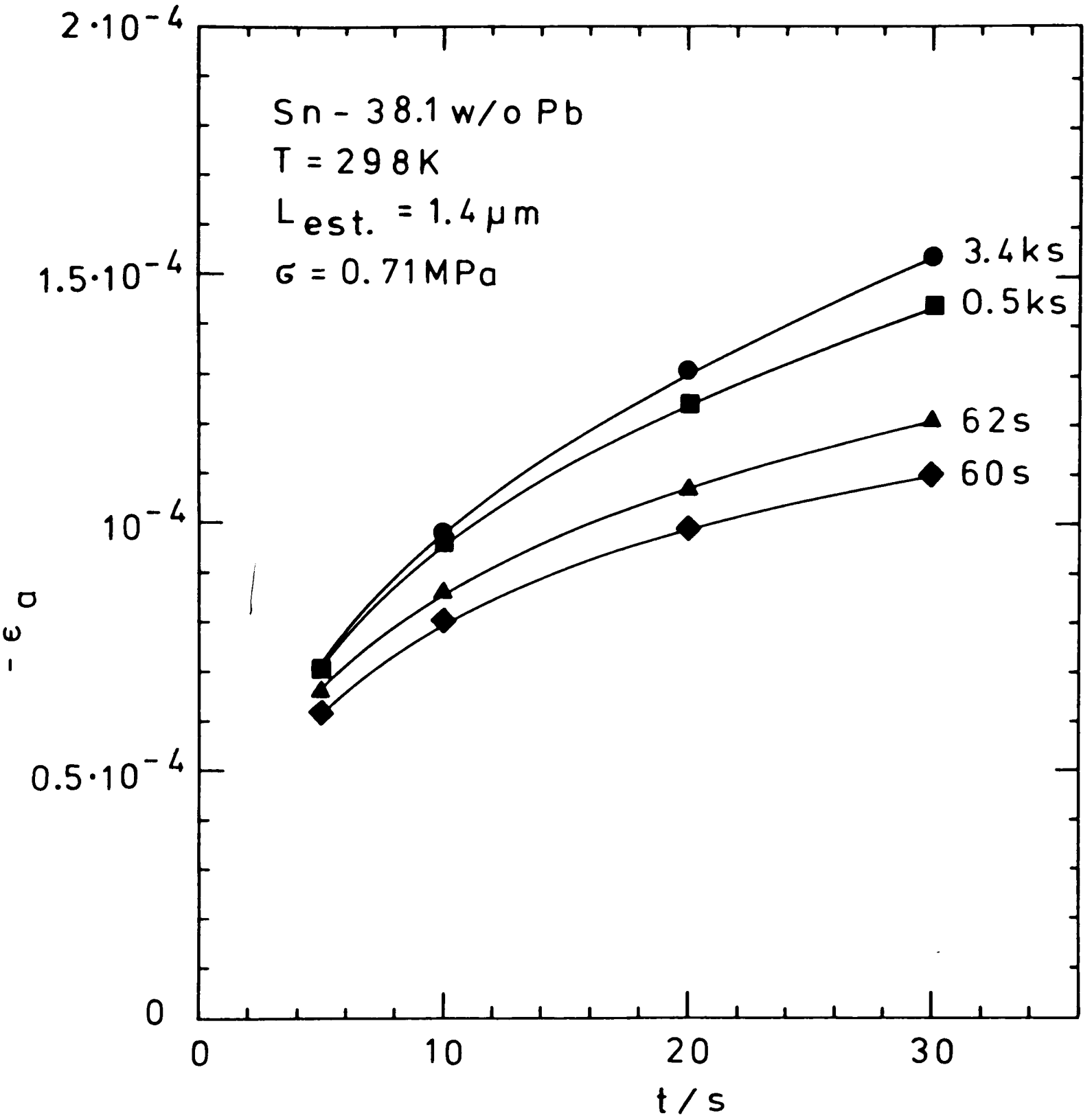

Fig. 6.1. Anelastic strain, ε_a, as a function of the time after unloading, t, after various loading periods as indicated.

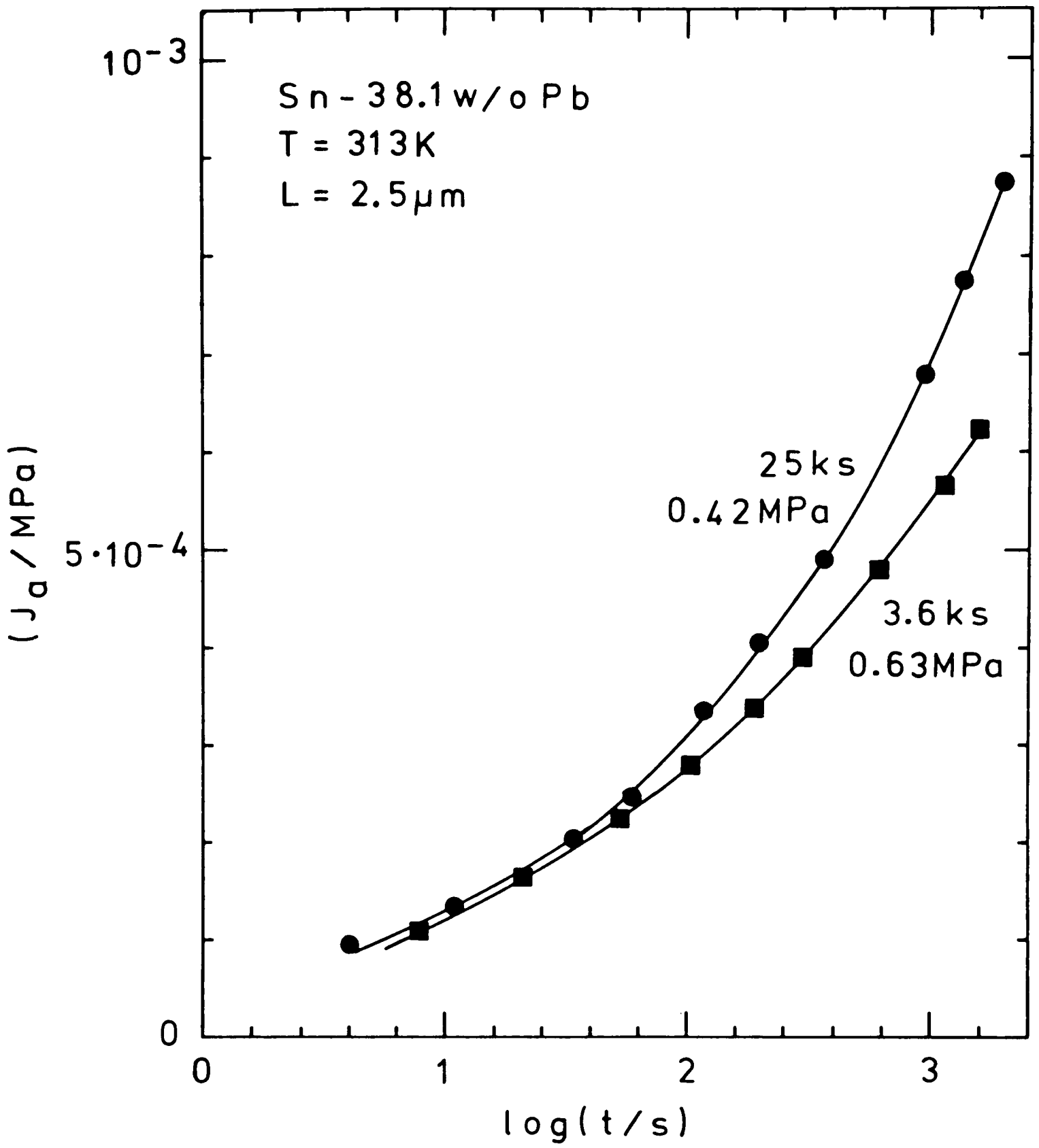

Fig. 6.2. Anelastic compliance, J_a, as a function of the time after unloading, t, after two different loading periods (and for slightly different stresses) as indicated.

ing period should become relatively small since the anelastic strain stored during the loading comes close to or reaches its saturation value. In order to reduce errors caused by different lengths of the loading period it was attempted to compare elastic after-effects after similar loading periods. This introduces usually a systematic error (under-estimation of the anelasticity). The dependence of the anelasticity on experimental parameters such as temperature and grain size is however not thought to change significantly due to this systematic error.

6.2.3. Linearity of the elastic after-effect

A sample was successively loaded with different stresses and the elastic after-effects upon unloading were determined. The relationship between loading stress and anelastically recovered strain, for various times after unloading, is shown in Fig. 6.3. The loading periods varied between 60s and 9ks. This large variation was inevitable since at the highest stresses employed the samples strained rapidly during loading and could therefore not be stressed as long as desired.

For a constant time after unloading, one obtains from Fig. 6.3:

$$\varepsilon_a\big|_{t=\text{const.}} \alpha\ \sigma^{+1.2} \qquad (6.1)$$

Anelastic strain and the stress are approximately linearly

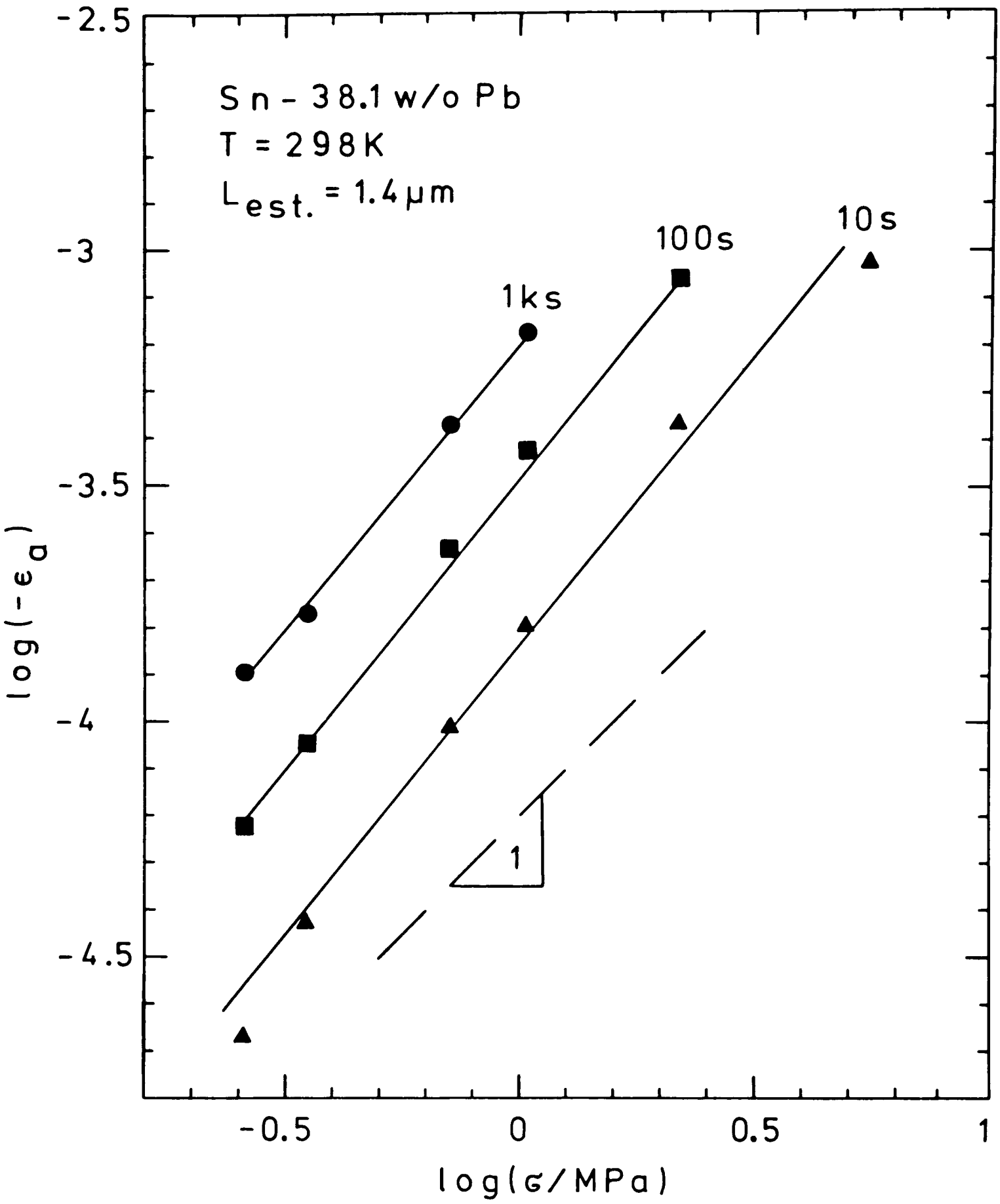

Fig. 6.3. Anelastic strain, ε_a, as a function of the loading stress, σ, for various times after unloading as indicated.

related. In order to facilitate the evaluation of the experimental data, strict linearity isassumed and a (stress-independent) anelastic compliance, J_a, is defined by:

$$J_a(t) = - \frac{\varepsilon_a(t)}{\sigma} \qquad (6.2)$$

6.2.4. Magnitude of the elastic after-effect

The tests discussed so far do not indicate the maximum value of the anelastically recovered strain. From Fig. 6.2, however, one anticipates very large anelastic compliances for long periods of recovery. Samples were therefore loaded for long periods of time (~13 days) in order to store as much anelastic strain in them as possible and to study the elastic after-effect for long periods of time. The experimental results in Fig. 6.4 show that the slopes of the elastic after-effect curves decrease after $\sim 10^5$s and that the anelastic compliance seems to reach a maximum value after longer times. It is concluded that maximum anelasticity has been stored during the loading period of 13 days. It seems unlikely that longer loading would change the results presented in Fig. 6.4.

It should be noted that the relaxation strengths characterizing the anelasticity are extraordinarily large. The elastic compliance for Sn-38.1w/o Pb is $5.76 \cdot 10^{-5} MPa^{-1}$ (Subrahmanyam, 1972). With eqn. (3.3), the relaxation strength for a Sn-38.1w/o Pb sample with a grain size of 8μm (see Fig. 6.4) is found to be 130. For a grain size

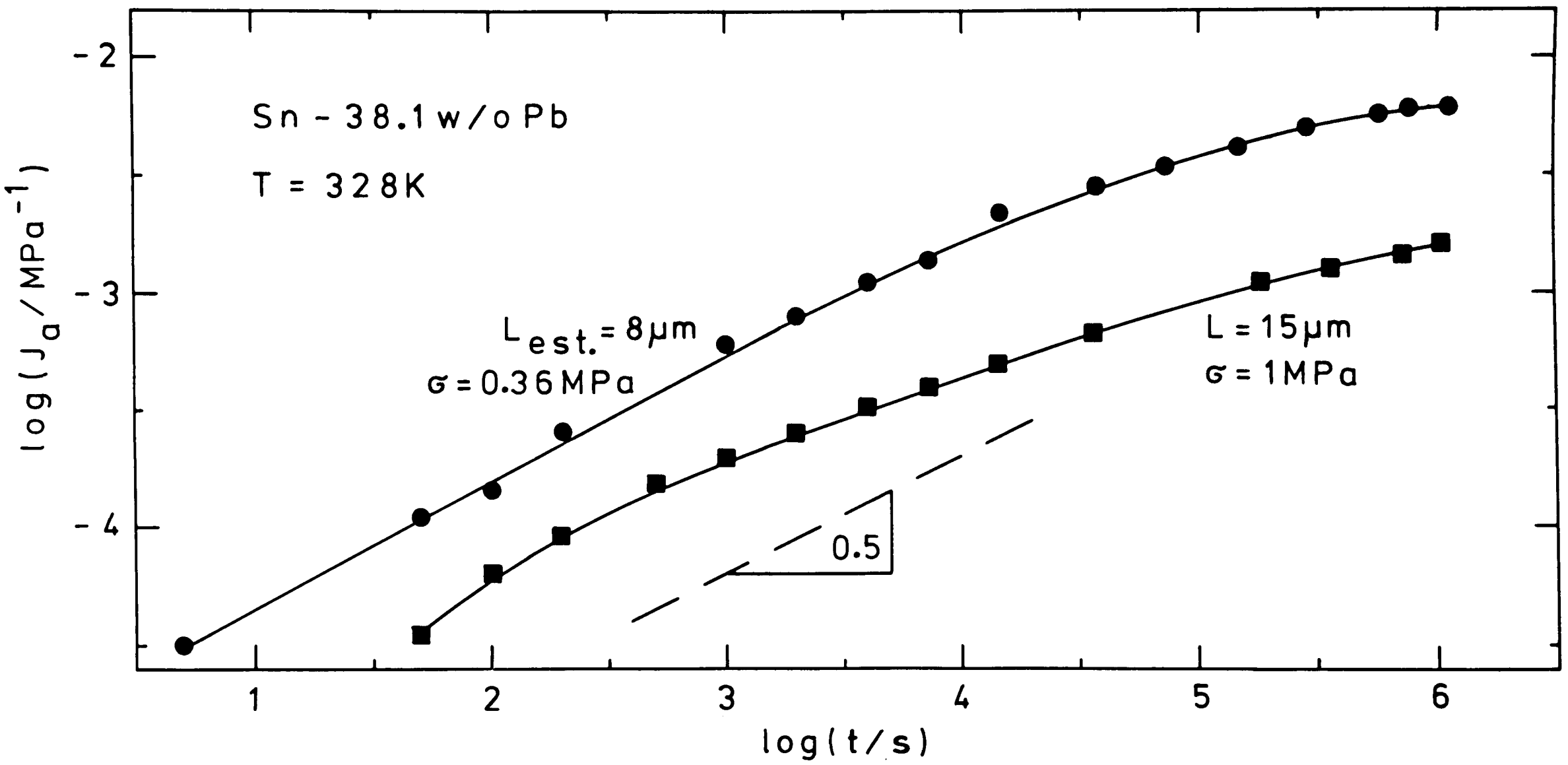

Fig. 6.4. Anelastic compliance, J_a, as a function of the time after unloading, t. The grain sizes and loading stresses are indicated. The loading period prior to the relaxations was 13 days ($10^{6.05}$s).

of 15μm the relaxation strength is smaller ($\Delta_r = 33$).

The strains recovered during the elastic after-effects are large. For a grain size of 8μm (Fig. 6.4) a strain of 0.23% is recovered. The stress and the strain during the loading in this case were only 0.36MPa and 6.5%, respectively. Since superplastic materials reach very high elongations, the loading stress could be increased without inducing premature fracture and much higher strains than 0.23% could probably be recovered.

After short times (e.g. t ~ 1s) the elastic after-effects are only of the order of the elastic strains corresponding to the particular stress employed (compare Fig. 6.2 and remember the value of $4.76 \cdot 10^{-5} MPa^{-1}$ for the elastic compliance). This means that dynamical tests with frequencies of the order of $1s^{-1}$ which are frequently employed to measure anelasticity will not usually detect the high relaxation strengths found here but rather apparent relaxation strengths of the order of 1.

6.2.5. Relaxation spectrum of the elastic after-effect

The time-dependence of the elastic after-effect cannot be accurately described by a single relaxation time. Alfrey's rule was used to determine an experimental relaxation spectrum (see eqns. (3.36) and (3.37)). Fig. 6.5 shows that the range of relaxation times is very wide for Sn-38.1w/o Pb, it is approximately 6 orders of magnitude. Since the spectrum varies only gradually with time the use of Alfrey's rule is not thought to introduce serious errors

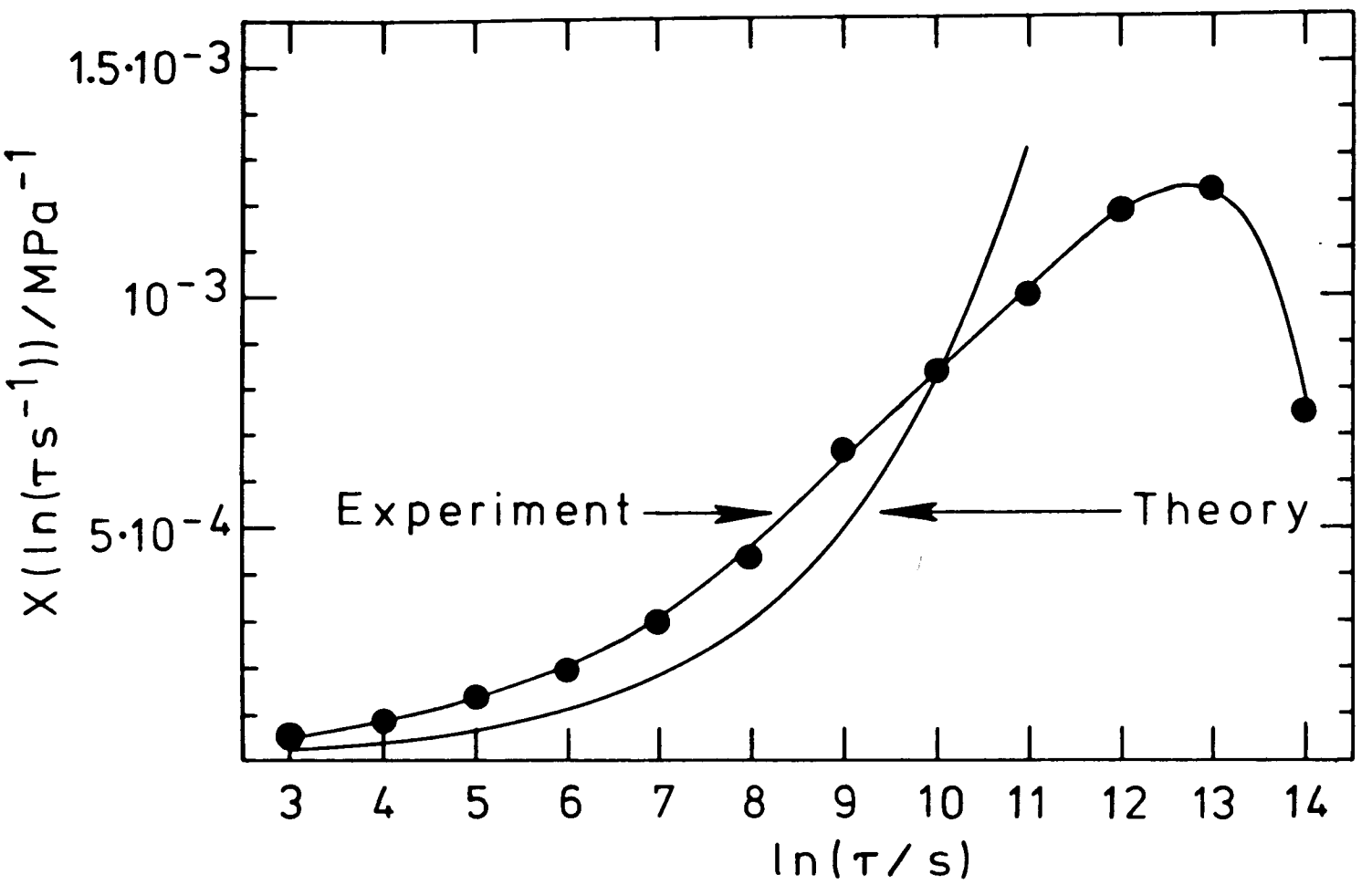

Fig. 6.5. An experimental relaxation spectrum, $x(\ln \tau)$ (derived from the result for a grain size of 8μm in Fig. 6.4). A theoretical spectrum is plotted in arbitrary units.

(Nowick and Berry, 1972,p.84).

6.2.6. Grain size dependence of the elastic after-effect

Elastic after-effects were studied for various grain sizes, L, and temperatures, T (Fig. 6.6). The data for T = 298K is replotted in Fig. 6.7 and shows the distinct grain size dependence of the elastic after-effect. For values of t between 10s and 1ks a relationship:

$$J_a \Big|_{\substack{t=\text{const.} \\ T=298K}} \alpha\ L^{-0.9} \qquad (6.3)$$

is obtained. The anelastic compliance depends therefore approximately inversely on the grain size.

It is not clear how well eqn. (6.3) holds for the maximum anelastic strains which may be achieved ($t \rightarrow \infty$). Inspection of Fig. 6.4 (see also section 6.2.4) suggests a relationship close to $J_a \alpha L^{-2}$. Equation (6.3) therefore probably holds only for a limited range of grain sizes and times.

6.2.7. Temperature dependence of the elastic after-effect

Data from Fig. 6.6 are replotted in Fig. 6.8 in order to determine an apparent activation energy, Q, for the elastic after-effect. An approximate relationship

$$J_a \Big|_{\substack{t=\text{const.} \\ L=\text{const.}}} \alpha\ \exp(-Q/RT)) \qquad (6.4)$$

is obtained from Fig. 6.8, where Q varies between 12kJ/mol

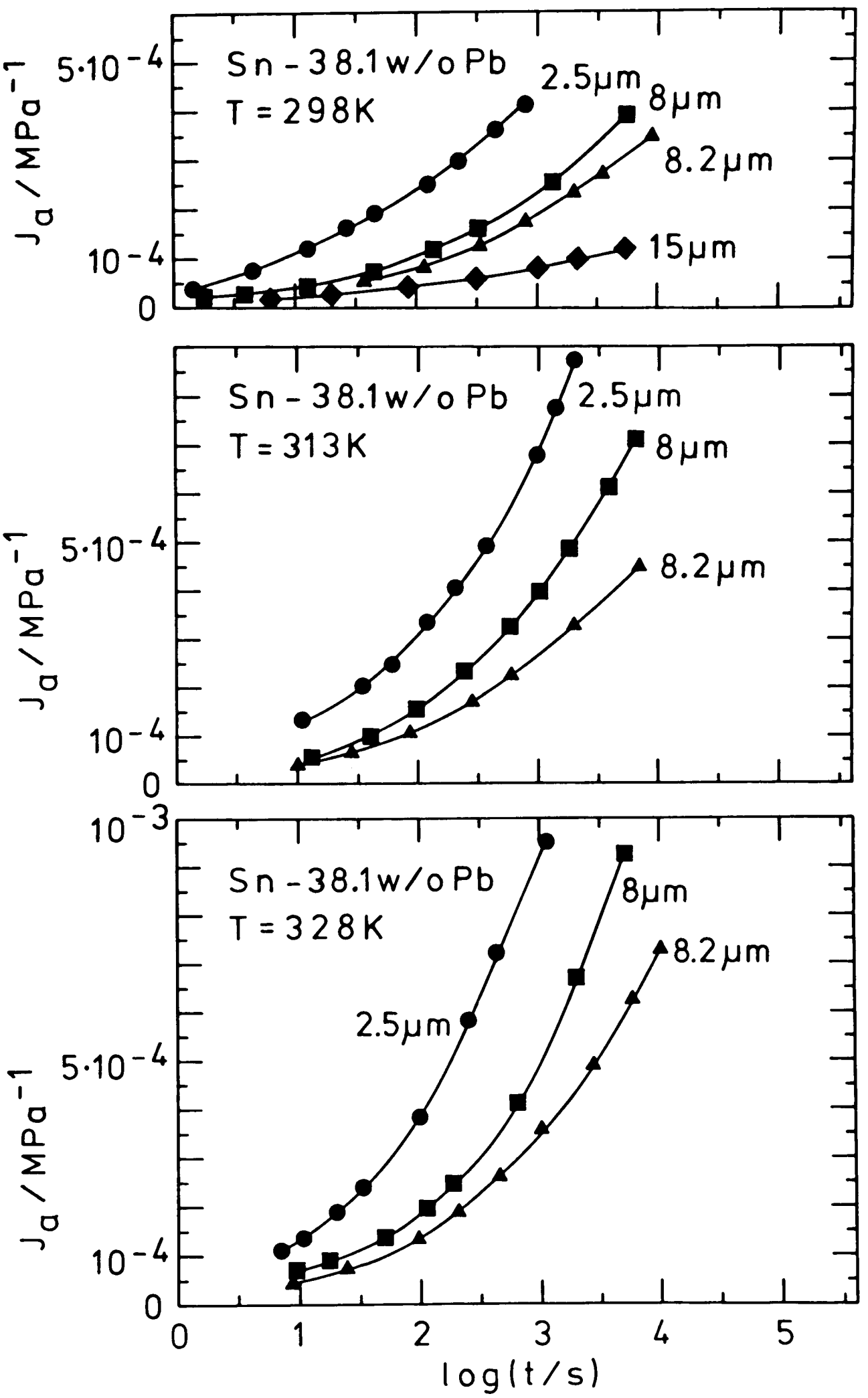

Fig. 6.6. Anelastic compliance, J_a, as a function of the time after unloading, t, for various test temperatures, T, and grain sizes as indicated. Loading periods between 1.7ks and 25ks, loading stresses between 0.4MPa and 2MPa

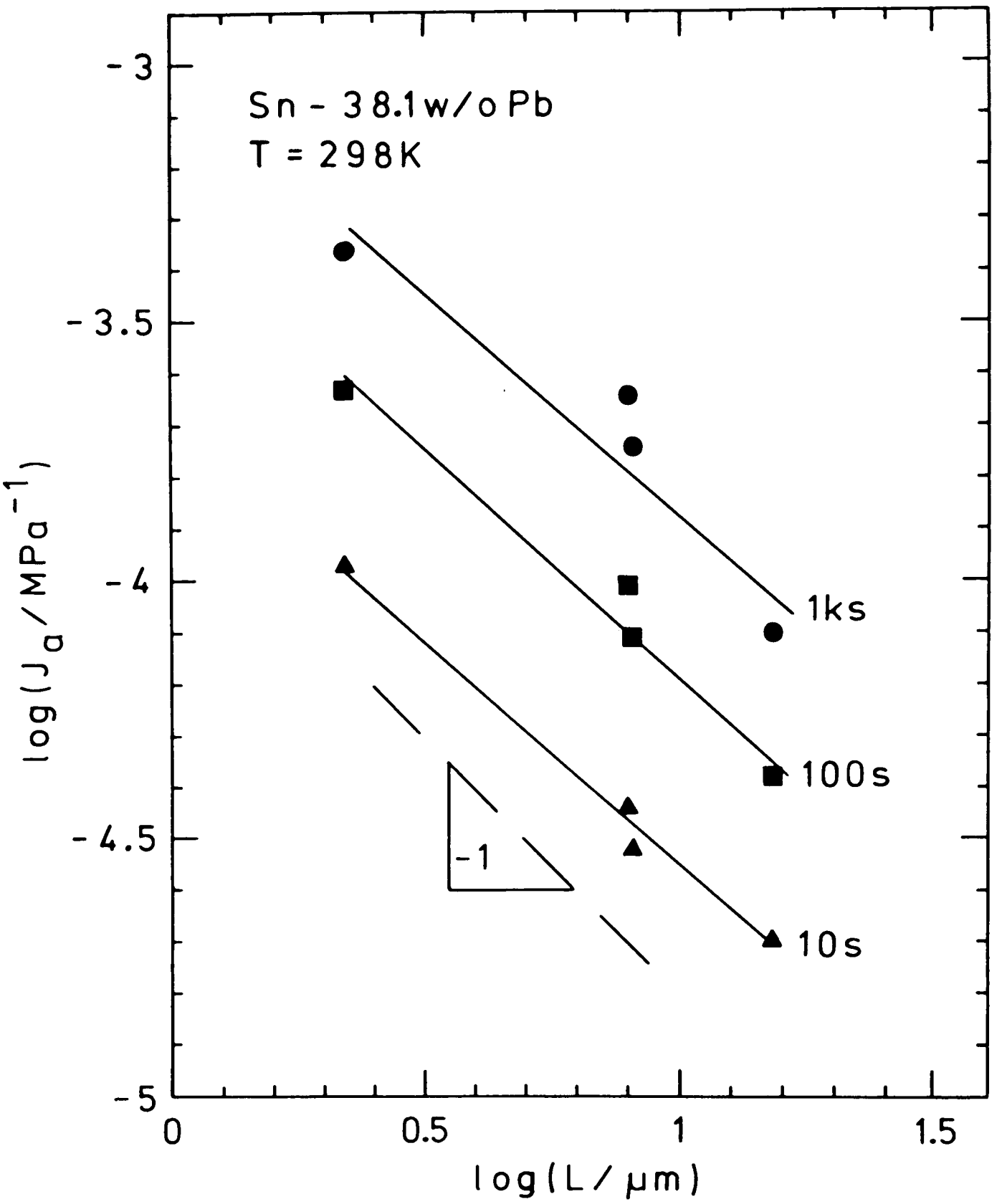

Fig. 6.7. Anelastic compliance, J_a, as a function of the grain size, L, for various times after unloading as indicated.

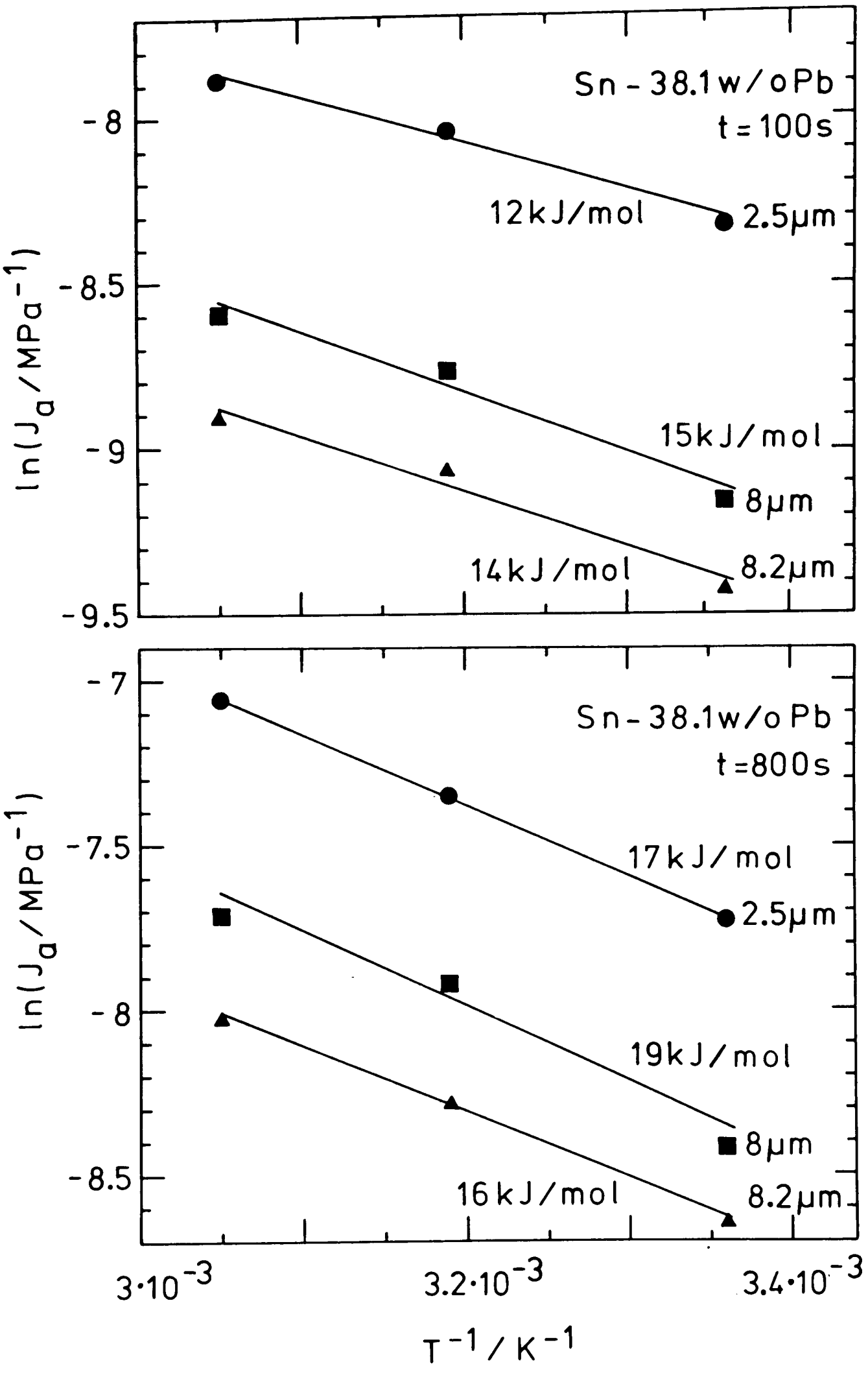

Fig. 6.8. Anelastic compliance, J_a, as a function of the test temperature, T, for various grain sizes, and times after unloading, t, as indicated. The activation energies determined from the slope of the various curves are indicated.

and 19kJ/mol with an average value of ~ 15kJ/mol. The evaluation was done for relatively short times (100s and 800s) for which the anelastic reco ery is far from being terminated. For longer relaxation periods (which require also longer previous loading periods) the temperature dependence of the anelastic compliance has not been determined. However, if the relaxation strength is temperature independent as most of the mechanisms in chapter 3 suggest, then eqn. (6.4) would be expected to break down after long loading/relaxation periods.

6.2.8. Dependence of the elastic after-effect on the alloy composition

Fig. 6.9 shows the anelastic compliance of a superplastic Sn-2w/o Pb alloy (see also chapter 5). Comparison with a Sn-38.1w/o Pb alloy with a similar grain size (broken line in Fig. 6.9) demonstrates the similarity in the behaviour of the two alloys. The elastic after-effect does not depend very much on the alloy composition.

6.3. Discussion of the anelasticity of Sn-38.1w/o Pb and Sn-2w/o Pb

The main purpose of the discussion will be to show that currently available mechnisms of anelasticity cannot explain the anelasticity observed here. However, a theory based on relaxing GBD pile-ups can explain qualitatively several features of the anelasticity. In particular, it predicts a wide relaxation spectrum with a realistic shape.

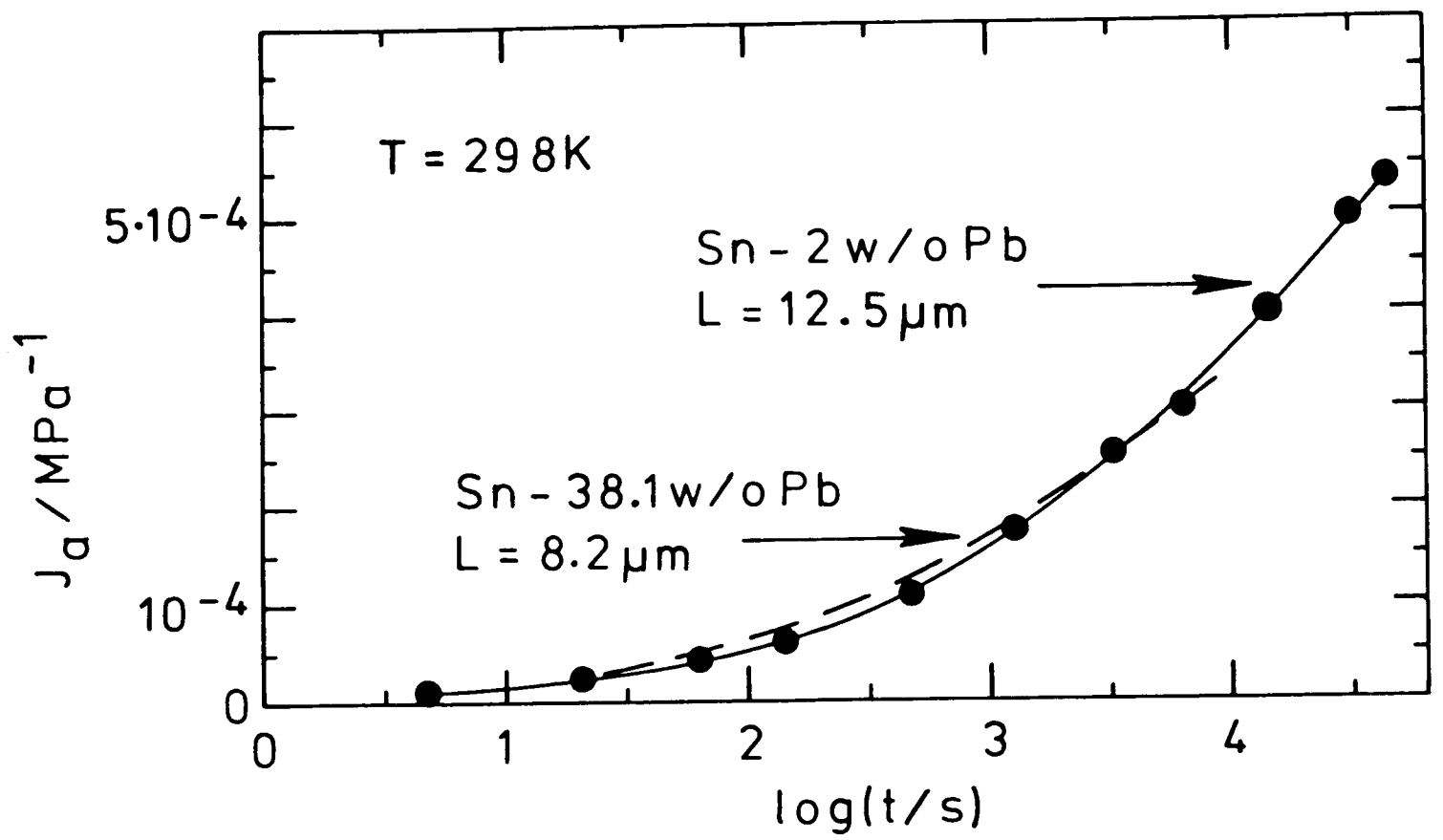

Fig. 6.9. Anelastic compliances, J_a, of Sn-2w/o Pb and Sn-38.1w/o Pb with similar grain sizes as a function of the time after unloading, t.

6.3.1. Importance of point defects

Anelastic relaxation by stress-induced site change (eqn (3.6)) is ruled out not only because of the small relaxation strengths (<<1) which it predicts but also because it is a bulk effect and should therefore not be grain size dependent.

Sn-2w/o Pb has only a small proportion of Pb-rich recipitates, with diameters much smaller than the grain size (no "big" Pb-rich particles could be identified by optical microscopy). The Pb-rich precipitates in Sn-38.1w/o Pb, however, have a volume fraction and diameters similar to the Sn-rich grains. Krivoglaz's mechnism (eqn. (3.7)) thus suggests a pronounced difference in the relaxation times for Sn-2w/o Pb and Sn-38.1w/o Pb ($\tau \alpha L_p^2$, where L_p is the precipitate diameter) which has not been observed. In addition, his mechanism should be important only near the phase transformation temperature of the considered system. For Sn-Pb this temperature is 456K (Hansen and Anderko, 1958) and thus well above the testing temperature ($\leq$ 328K). Krivoglaz's mechanism is therefore not applicable to the present experiments.

One might also argue that applied stresses cause a solute redistribution within each grain and that this redistribution is responsible for anelastic strains. For example, in stressed Sn-2w/o Pb the dissolved Pb (~0.2/o at 293K after Hansen and Anderko, 1958) might diffuse from compressed regions in the grains to dilatated regions and

thus cause elongation of the grains.

The pressure dependence of the concentration of Pb in the Sn-rich phase (α-phase) of a Sn-2w/o Pb alloy was estimated following the treatment of Hilliard and Cahn (1960). From their eqn. 6 it follows (see also Fig. 6.10):

$$\left(\frac{\delta \nu^{\alpha}}{\delta P}\right)_T = \frac{\nu^{\alpha} \left(\bar{V}_{Pb}^{\alpha+\beta} - \bar{V}_{Pb}^{\alpha}\right)}{R\ T}\ , \qquad (6.5)$$

where

ν^{α} = atomic fraction of Pb in Sn,

P = applied pressure,

$\bar{V}_{Pb}^{\alpha+\beta}$ = gram atomic volume of a mixture of the α- and β-phase, extrapolated to the Pb-side of a diagram of the atomic volume vs. the composition,

$\bar{V}_{Pb}^{\alpha}$ = gram atomic volume of a dilute solution of Pb in Sn, extrapolated to the Pb-side of a diagram of the atomic volume vs.the composition.

From lattice parameter measurements in the Sn-Pb system (Pearson, 1958) the atomic volumes of pure Sn, Sn-0.2a/o Pb (= α-phase at 293K), and Pb-1.9a/o Sn (= β-phase at 293K) at 293K can be calculated: $\bar{V}_{Sn}^{\alpha} = 1.6194 \cdot 10^{-4} mm^3/mol$, $\bar{V}_{Sn-0.2a/oPb}^{\alpha} = 1.6201 \cdot 10^{4} mm^3/mol$ and $\bar{V}_{Pb-1.9a/oSn}^{\beta} = 1.8116 \cdot 10^{4} mm^3/mol$. Using the construction shown schematically in Fig. 6.10 one obtains now $\bar{V}_{Pb}^{\alpha+\beta} = 1.8153 \cdot 10^{4} mm^3/mol$ and $\bar{V}_{Pb}^{\alpha} = 1.9694 mm^3/mol$.

Using the values above, eqn. (6.5) now leads to $(\delta \nu^{\alpha}/\delta P)_T = -1.26 \cdot 10^{-6} MPa^{-1}$. For a typical compressive

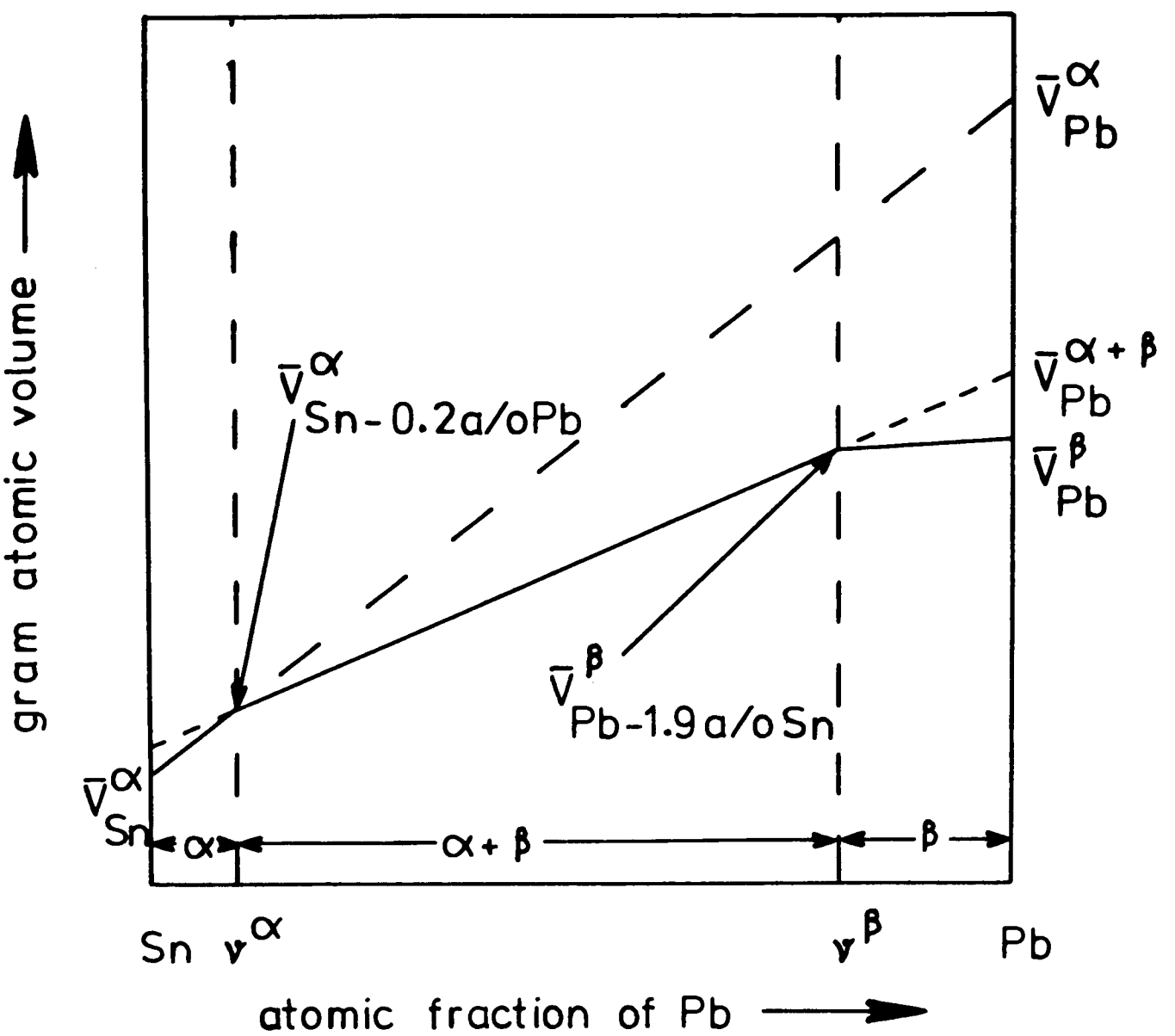

Fig. 6.10. Schematic diagram to determine the effect of pressure on the phase boundaries of a binary system (after Hilliard and Cahn, 1960).

stress of 1MPa one obtains $\Delta\nu^{\alpha} = -1.26\cdot10^{-6}$ or $\Delta c^{\alpha}_{Pb} = -1.26\cdot10^{-4}$a/o, respectively, for the change in the equilibrium Pb-content of the Sn-rich phase. A diffusive flow of Pb from compressed to dilatated GB regions results. However, even if all the Pb needed to establish the concentration difference between compressed and dilatated GB regions is employed in elongating individual grains, maximum anelastic strains which are only of the order of 10^{-4}% would result. Such strains are much smaller than the measured strains ($\gtrsim$0.1% for Sn-2w/o Pb). Anelasticity due to solute redistribution is therefore of no importance.

6.3.2. Importance of elastic grain deformation

Zener's viscous GBS mechanism (see section 3.3) is not capable of explaining the present results. It predicts a grain size-independent relaxation strength smaller than 1. This is incompatible with the experimental results presented in section 6.2. In addition the data discussed in chapter 5 may be interpreted as GBS control of the plastic deformation. An important requirement for Zener's mechanism, namely, that GBs are relaxed in shear, may therefore not be fulfilled.

The relaxation time of the Zener mechanism is proportional to the length of GB segments and the GB viscosity. In a real polycrystal there is a distribution of grain sizes which is probably similar to the distribution in the length of GB segments. In Sn-2w/o Pb this distri-

bution is too narrow to explain the observed spread in the relaxation times of more than 4 decades (compare Figs. 6.9 and 6.11). On the other hand, GB viscosities may vary considerably from boundary to boundary. The sliding rates of GBs with different misorientations have been found to vary substantially (Gleiter and Chalmers, 1972, chapter 7). Nevertheless, the evidence presented above is thought to rule out the Zener mechanism.

6.3.3. Importance of GB tension

Anelasticity caused by GB tension, if it exists, can produce very large relaxation strengths as shown in section 3.4 and it is linear in the stress. Although these two features make it an attractive model, there are severe objections to its validity for the anelasticity of small-grained alloys. Depending on the plastic properties of the grains or GBs during relaxation three cases may be considered:

(1) The viscosity of the plastic process (i.e. the viscous dashpot of a Voigt element) during relaxation is only weakly grain size-dependent: Consider for example viscous GBS with $\tau \alpha L^2$ (eqn. (3.20)). Since the relaxation strength is proportional to the grain size, L (eqn. (3.17)), the elastic after-effect strain is proportional to $L(1-\exp(-t/\tau)) \sim t/L$, for $t \ll \tau$. This result agrees with the inverse grain size dependence of the anelastic compliance in Fig. 6.7. However, consideration of a measured grain size distribution for Sn-2w/o Pb (Fig.

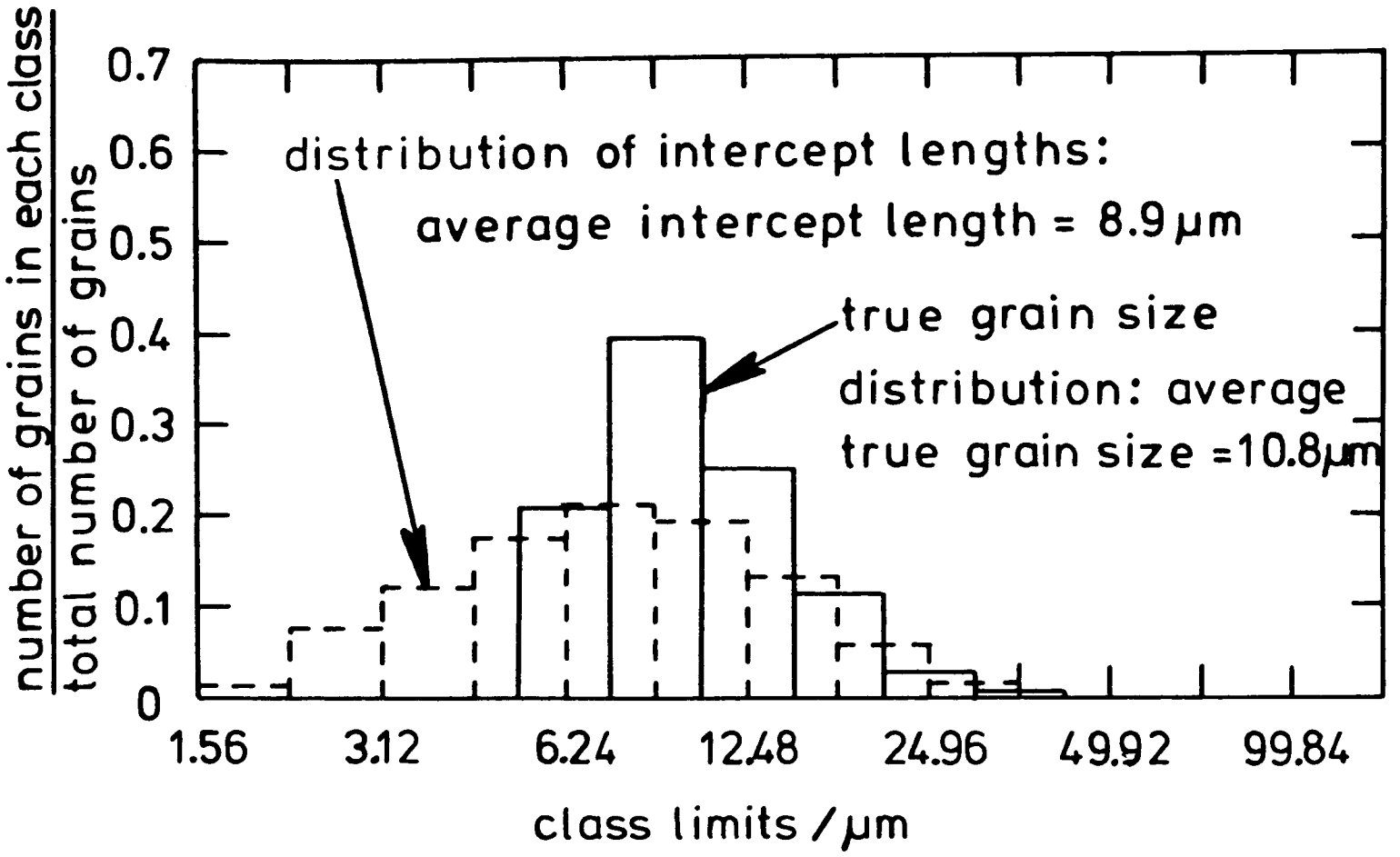

Fig. 6.11. Distribution of the linear intercept lengths and the true grain sizes for the Sn-2w/o Pb sample employed in Fig. 6.9.

The true grain size distribution was evaluated from the relationship:

$$r(s) = \frac{\pi}{2} s \int_{L=s}^{L_{max}} n(L)\, dL,$$

(Exner, 1972), where:

$r(s)\,\Delta s$ = number of intercepts per unit length with lengths between $s-\Delta s$ and s,

$n(L)$ = number of grains per unit volume with grain sizes between $L-\Delta L$ and L,

L_{max} = maximum true grain size.

For discrete classes, a recursive formula for the true grain size distribution, $n(s_{i_o})$, is obtained:

$$n(s_{i_o}) = [r(s_{i_o}) - \frac{\pi}{2} s_{i_o} \sum_{i=i_o+1}^{i_{max}} n(s_i)\Delta s_i]/(\frac{\pi}{2} s_{i_o} \Delta s_{i_o}),$$

where s_{i_o} is the middle of the true grain size class i_o (= upper limit of the intercept class i_o), $s_i = 1.56\mu m \cdot 2^{i/2}$ is the upper limit of the intercept class i, $\Delta s_i = 0.384\, s_i$ is the class interval, and $2^{1/4} s_i$ is the class middle. $n(s_{1_o})$ to $n(s_{3_o})$ where found to be negative and set to 0 in the example considered.

6.11) for $\tau \alpha L^2$ leads to a maximum ratio between possible relaxation times of ~ 25 (if individual grains deform independently from each other). This is much smaller than the relaxation spectrum observed for Sn-2w/o Pb which indicates ratios between different relaxation times of the order of $\sim 10^4$ or larger (see Fig. 6.9). The grain size distribution in Sn-2w/o Pb can therefore not explain the wide range of the experimentally observed relaxation times.

(2) The viscosity of the plastic process during relaxation is strongly grain size-dependent: If Coble creep governs the time-dependence of the elastic after-effect, $\tau \alpha L^4$ (eqn. (3.18)). A relatively wide relaxation spectrum is expected. The true grain size distribution in Fig. 6.11 indicates a ratio of maximum to minimum relaxation time of the order of $6^4 \sim 1300$. Even such a large spread in the relaxation times does not explain the time-dependence of the elastic after-effect in Sn-2w/o Pb (Fig. 6.9)).

$\tau \alpha L^4$ leads to an initial grain size dependence of the after-effect proportional to $L\ (1-\exp(-t/\tau)) \sim 1/L^3$. This result is incompatible with the inverse grain size-dependence of the anelastic compliance in Fig. (6.7). Similarly, $\tau \alpha L^3$ (eqn. (3.19)) cannot explain the observed elastic after-effect.

(3) The plastic process during anelastic relaxation is non-linear, e.g. $\sigma \alpha \dot{\varepsilon}^{0.45}$ (Fig. 5.12): According to eqn. (3.11) the anelastic strain rate and the recovered strain during the elastic after-effect should depend strongly on

the anelastic strain stored during the previous loading period. This has not been observed (see Fig. (6.1)).

Finally, the GB tension mechanism predicts an increase in the relaxation strength for increasing grain sizes (eqn. (3.17)), in disagreement with the findings in section 6.2.4. It is concluded that a mechanism based on GB tension cannot explain the observed anelasticity.

6.3.4. Importance of lattice dislocations

In sections 3.5 and 3.6 it has been said that the relaxation strengths expected for anelastic lattice dislocation mechanisms are usually only of the order of 1. Only for highly inhomogeneous dislocation structures like for example cell walls are higher relaxation strengths anticipated (Friedel, Boulanger and Crussard, 1955) and have indeed been found for heavily deformed Al (see Ke and Zener, 1950). However, superplastic alloys at small stresses, e.g. of the order of 1MPa, do not seem to establish such structures. In superplastic Zn-Al eutectoid which exhibits an anelastic behaviour similar to that of Sn-Pb alloys (Eastgate, 1978) only few lattice dislocations or dislocation pile-ups are found at low stresses (Mukherjee, 1974; Kaibyschev, Rodionov, Valiev, 1978). In the Sn-Pb alloys only few lattice dislocations are expected because of the relatively high stresses which are probably needed to operate sources. In pure Pb and Sn with grain sizes of $1.4\mu m$ the critical stress for lattice dislocation generation, $\sigma_o = (Gb)/L$, is approximately 1.6MPa and 3.8MPa, respectively.

Anelasticity can however easily be demonstrated for a stress of 0.25MPa (see Fig. 6.3). Therefore it seems very unlikely that a lattice dislocation mechanism causes the observed anelasticity.

6.3.5. Importance of grain boundary dislocations

(a) Anelasticity caused by GBD line-tension

The elastic after-effect due to the straightening of bowed GBDs is characterized by a relaxation strength of the order of 1 or smaller (eqn. (3.23)). The relaxation time is proportional to the square of the length of bowed-out GBD segments (eqn. (3.24)). The theoretical relaxation strength is not in accord with experimentally found values > 100. An explanation of an experimental relaxation spectrum (Fig. 6.4) would require a very wide distribution of dislocation link lengths ($\gamma_{max}/\gamma_{min} \sim 10^3$) which is unlikely in view of the small grains employed (which impose probably an upper limit on the dislocation link length).

In order to obtain high theoretical relaxation strengths one could assume that the line tensions of GBDs are much lower than the line tensions of lattice dislocations with similar Burgers vectors. There is limited evidence for this assumption which will be given at the end of this chapter.

(b) Anelasticity caused by repulsion between grain boundary dislocations

Several features of the theory based on GBD pile-ups

developed in section 3.6 are in qualitative agreement with the measured elastic after-effect data. A wide range of relaxation times is predicted without the necessity of assuming a wide distribution of dislocation link lengths as for the GBD line tension model discussed above. A plot of the theoretical relaxation spectrum in arbitrary units (eqn. (3.38)) is indeed in qualitative agreement with an experimental relaxation spectrum (Fig. (6.5)) if one considers that neither the initial nor the final stages of the elastic after-effect have been treated accurately. Also the time dependence of the elastic after-effect, $\varepsilon_a \alpha t^{1/2}$ (eqn. (3.35)), is approximately valid. This is verified in Fig. 6.4. Moreover, the inverse grain size dependence of the anelastic strain in eqn. (3.35) is in substantial agreement with the measured dependence (see Fig. 6.7 and eqn. (6.3)). With the assumptions leading to an inverse grain size dependence a relaxation strength proportional to $1/L^2$ is derived (eqn. (3.41)). As discussed in section 6.2.6, such a relationship is realistic.

Another attractive feature of the theory is the value of the apparent activation energy obtained by comparing anelastic strains at different temperatures after identical times. After eqn. (3.35), this activation energy has half the value of the activation energy for GB self-diffusion. The experiments have indeed shown a very low value, between 12 and 19kJ/mol, of the apparent activation energy for anelastic deformation of Sn-38.1w/o Pb. The value of the

average activation energy for GB self-diffusion in Sn-38.1w/o Pb is not certain (see section 5.3.2). It seems however reasonable to take the value of the activation energy for plastic deformation of Sn-38.1w/o Pb, 54kJ/mol (section 5.3.1). Half this value, 27kJ/mol, points at least in the right direction (it should be remembered that the scatter in the experimental activation energies for plastic and anelastic deformation is substantial).

The anelastic strain predicted by eqn. (3.35) is not linear in the stress: $\varepsilon_a \alpha \sigma^{3/2}$. Although, with a reasonable degree of accuracy, linearity was assumed for the evaluation of the experiments the experimental relationship between strain and stress is more like $\varepsilon_a \alpha \sigma^{1.2}$ (eqn. (6.1)). Thus the agreement between the experimental and the theoretical stress-dependence is considered to be reasonable.

A numerical example which shows also the limitations of the theory, is presented in Fig. 6.12 and compared with data for Sn-2w/o Pb. Equation (3.35) was evaluated using the GB diffusion coefficient for Sn-2w/o Pb determined from the Coble creep rate (eqn. 5.17). The range of the validity of eqn. (3.35) was found from eqns (3.40) and (3.42). Although approximate agreement between theory and experiment is found over a small range of times the main difficulty with the suggested pile-up theory is obvious: the high observed relaxation strengths (in the example $\Delta_r \sim 23$) are not predicted.

It is difficult, however, to imagine a theory which

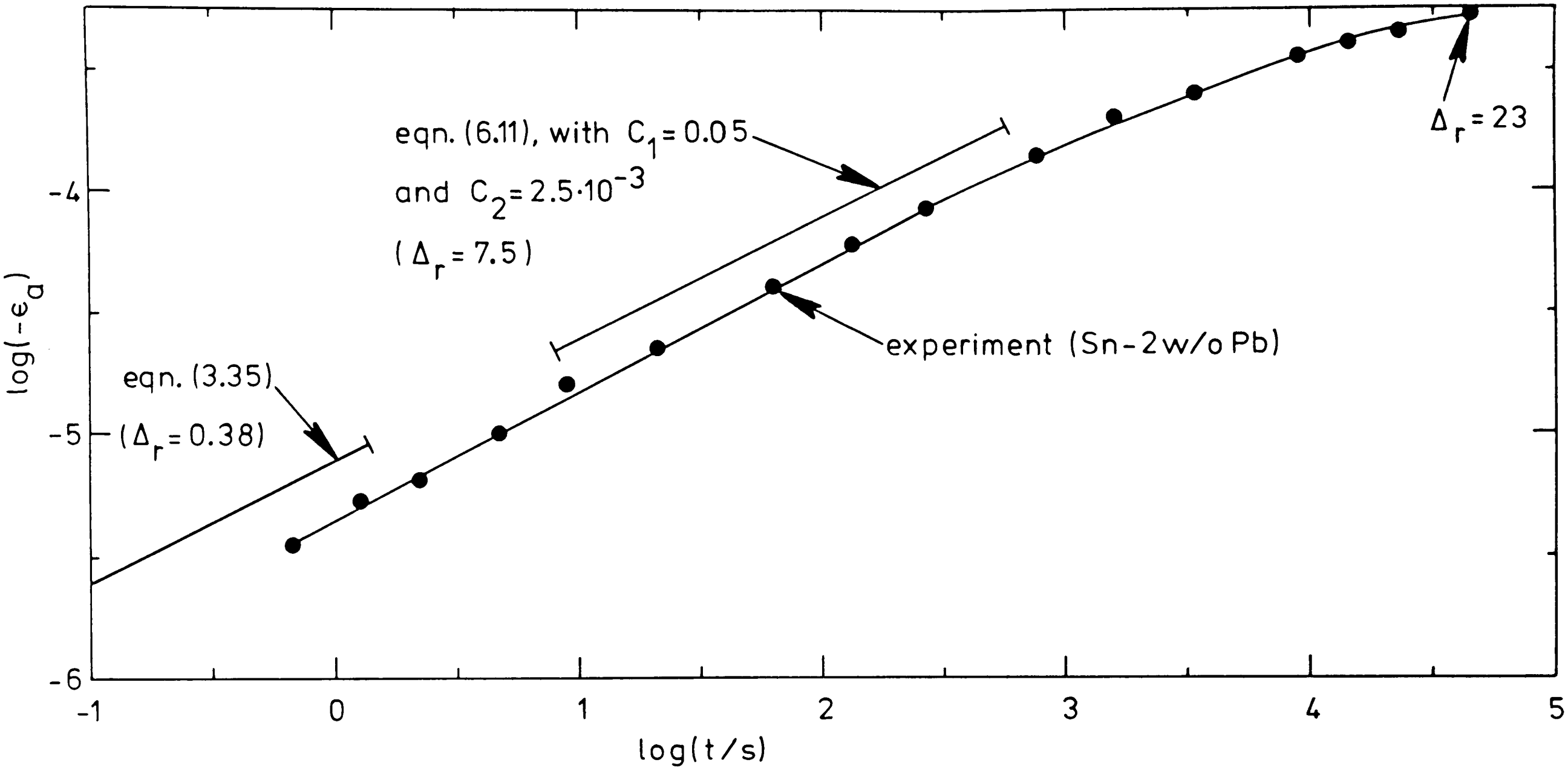

Fig. 6.12. Comparison between measured and calculated elastic after-effects. The experimental data for Sn-2w/o Pb are from Fig. 6.9. The following values were employed in eqns. (3.35) and (6.11):
σ = 1MPa, T = 298K, D_B(Sn-2w/o Pb, 298K) = $1.03 \cdot 10^{-11} m^2/s$ (eqn. 5.17),
G(Sn) = 15.4MPa, b = 0.35nm, $x_1 = L = 12.5\mu m$,
$x_p = 1.5\mu m$, $C_1 = 0.05$, $C_2 = 2.5 \cdot 10^{-3}$.

is not based on GBs and, in particular, on GB line defects. Bulk mechanisms of anelasticity have been seen to predict usually relaxation strengths less than 1. If only point-defects are involved, the theoretical relaxation strengths are much smaller than 1. The only mechanisms which predict relaxation strengths much larger than 1 are those based on GB tension and on highly inhomogeneous lattice dislocation distributions. Both mechanisms have been ruled out. Also, experiments indicate very rarely relaxation strengths of bulk mechanisms much higher than 1 (see Nowick and Berry, 1972). One exception is the high relaxation strength (≥ 8) which has been found in Al by Kê and Zener (1950) (see also Nowick and Berry, 1972, p.457). The sample employed, however, had been heavily cold-rolled and contained therefore a highly inhomogeneous lattice dislocation arrangement (Schuh, 1974). Since superplastic materials contain only few lattice dislocations a highly inhomogeneous dislocation structure can be ruled out in the present experimental situation. It is concluded that for theoretical and experimental reasons anelastic bulk mechanisms cannot explain the observed anelasticity.

The strong anelasticity has therefore to be ascribed to the GBs. Anelasticity caused by GB tension has been ruled out and therefore anelastic GBS is thought to be responsible (relative grain displacements perpendicular to the GBs are of no importance because they are easily relaxed by diffusion). Anelastic GBS is also in keeping

with the suggested GBS control of the plastic strain rate at low stress levels: since the GBs are not relaxed they can store the strain which is gradually being released during anelastic recovery.

The amount of anelastic GBS of a GB segment of length L, u_a, is approximately:

$$u_a = L\,\varepsilon_a. \qquad (6.6)$$

For a recovered strain of $2.3 \cdot 10^{-3}$ and a grain size, L, of 8μm (see section 6.2.4), eqn. (6.6) predicts maximum anelastic displacements of adjacent grains, parallel to the GB separating them, of the order of 20nm. Point defects in the GBs could explain displacements at the most of the order of b ~0.3nm. Only linear defects in the GBs are thought to account for the large displacements found from eqn. (6.6).

It might be thought that the elastic interaction between adjacent pile-ups reduces the elastic energy required for a certain amount of GBS. As an example, individual GB segments could be modelled by freely sliding cracks (which could in principle be represented by a distribution of dislocations with infinitesimal Burgers vectors). The cracks are joined and form a corrugated piece of GB. The sliding displacement of such a boundary has been calculated by Raj and Ashby (1971) and is:

$$u = \frac{4\ (1-\nu^2)}{\pi^3}\ \frac{\lambda^3}{h^2}\ \frac{\tau_a}{E} \quad , \tag{6.7}$$

where the GB is approximated by a sine function with an amplitude h/2 and a periodicity λ. Since for a polycrystal $\lambda \sim 2L$ it is easily realised that the relaxation strength which might be provided by the displacement given by eqn. (6.7) is significantly larger than 1 only if $h \ll L$. For an equiaxed polycrystal, however, $h \sim L$. It is therefore thought unlikely that the large magnitude of the observed anelasticity is due to the elastic interaction between pile-ups.

The question may now be asked: what should the static and dynamic properties of GBDs be like in order to explain the measured anelasticity? For reasons which will be discussed later one could assume that the interaction between GBDs is weaker than that between lattice dislocations with the same Burgers vector. To this end the lattice shear modulus, G, is replaced by an effective shear modulus, G*:

$$G^* = C_1\ G, \tag{6.8}$$

where $C_1 \leq 1$ is an adjustable parameter. The force acting between two identical screw dislocations a distance x apart can then be written as:

$$F = C_1\ \frac{G\ b^2}{2\ \pi\ x}\ . \tag{6.9}$$

It will also be assumed that the GBD mobility is lower than that given by the Einstein relationship and eqn. (3.29) is replaced by:

$$M = C_2 \frac{D_B\, b}{k\, T} \quad , \tag{6.10}$$

where C_2 is an adjustable constant.

Analogous to eqn. (3.35) one obtains now for the anelastic strain:

$$\varepsilon_a = - \frac{C_2^{1/2}}{C_1} \frac{\pi\, b\, D_B^{1/2}\, x_p^{3/2}\, \sigma^{3/2}\, t^{1/2}}{4\sqrt{2}\, G\, (k\, T)^{1/2}\, x_1\, L} \quad . \tag{6.11}$$

Similarly, the relaxation strength is seen to be:

$$\Delta_r = \frac{\pi\, x_1\, x_p}{C_1\, L^2} \quad . \tag{6.12}$$

The range of times for which the approximation leading to eqn. (6.11) is valid is again given by eqn. (3.40). Reasonable agreement with the experimental data in Fig. 6.12 is obtained for $C_1 \sim 0.05$ and $C_2 = 2.5 \cdot 10^{-3}$. However, much lower values of C_1 would have to be employed in order to account for relaxation strengths as high as 100.

Weak GBD interactions and low mobilities have been seen to be necessary in order to obtain reasonable agreement between the theory (eqn. 6.11) and the experiment. The following discussion is therefore concerned with the question whether GBDs have properties very different from those of

lattice dislocations. Ashby (1972) argued that the GB volume around a GBD is much smaller than the volume of crystal surrounding it. The presence of a GB does therefore not change the stress field around a dislocation significantly. Only for dislocations spaced a few Burgers vectors apart can the line energy (and presumably the interaction force) decrease significantly. On the other hand, Pond and Smith (1974) suggested that the interaction between GBDs does not closely resemble that of lattice dislocations. Recent atomistic relaxation calculations for GBs with different misorientation angles have shown that the shear modulus in GBs may be smaller, by up to a factor of 5, than the corresponding lattice shear modulus (Provan and Bamiro, 1977). In particular if the GBDs are closely spaced the low shear modulus might lead to a reduction in their interaction forces. In qualitative agreement with this is that the density of GBDs found by Kegg, Horton and Silcock (1973) in deformed Al bicrystals is relatively high. For example, for an applied stress τ_a = 1.2MPa, for L = 2μm, G_{Al} = 28GPa and b = 0.1nm, eqn. (3.25) predicts a maximum number of 3 dislocations in a pile-up. Silcock et. al.'s Fig. 2, however, shows approximately 60 dislocations in a similar experimental situation. Therefore relaxation strengths much larger than 1 may be possible.

In order to explain the high relaxation strengths observed, however, the GB shear modulus would have to be unrealistically small. In the example above, it would have

to be smaller than the lattice shear modulus by at least a factor of 20: even larger factors would be required to explain the highest relaxation strengths observed. It is therefore likely that not only a reduced shear modulus but also the special structure of GBDs, as compared to that of lattice dislocations, is responsible for the small interaction forces. If GBDs sit in low-energy sites in the GBs the elastic energy associated with them would be relatively low and interactions between neighbouring GBDs would be weak. Similarly, the mobility of GBDs could be reduced with respect to that of lattice dislocations if they are on energetically favoured sites in the GBs. Such sites exist probably for structural GBDs. In order to move, a GBD would then have to go through high energy sites and its mobility would therefore presumably be reduced.

It is concluded that the observed anelasticity is indeed an intrinsic GB phenomenon, i.e., it is caused by GBS within the thickness of the GBs. If lattice dislocation movement can be ruled out (e.g. by selecting low stresses and small grain sizes) and if intrinsic GBS and not diffusion creep controls the deformation, the measurement of the anelastic properties of small-grained polycrystals is thought to be suitable for studying intrinsic GB properties.

6.4. Summary and conclusions

Sn-38.1w/o Pb samples with grain sizes between 1.4μm and 15μm were loaded for periods of time up to 13 days at temperatures between 298K and 328K and stresses between

0.25 and 2MPa. The anelastic contraction upon subsequent unloading was studied.

The relaxation strength, defined as the ratio of the anelastically recovered to the elastically recovered strain, exceeds values of 100 (i.e. the relaxed modulus is only 1% of the unrelaxed modulus). Anelastic strains larger than 0.2% can be recovered. For a particular time after unloading the anelastic strains are approximately proportional to the stress and to the inverse grain size. The underlying mechanism is thermally activated with an apparent activation energy below that for GB self-diffusion. The time-dependence of the elastic after-effect is described by a relaxation spectrum extending over 6 decades in time. The approximate relationship $\varepsilon_a \alpha t^{1/2}$, where ε_a is the strain recovered anelastically after a period of time, t, holds for a major part of the relaxation. Data for a Sn-2w/o Pb alloy demonstrate the close resemblance between the anelasticity in Sn-2w/o Pb and Sn-38.1w/o Pb.

Known mechanisms of anelasticity cannot fully explain the experimental results. In particular the following mechanisms have to be excluded: point defect relaxation, reversible viscous GBS due to grain elasticity, anelasticity due to GB tension, and lattice dislocation anelasticity. Anelasticity due to relaxation of GBD pile-ups approximately explains the measured dependence on stress, grain size, time and temperature. It fails however in explaining the high relaxation strengths found. The possibility that GBD interaction is weaker than lattice dislocation

interaction, which would result in an increase in the relaxation strength, is discussed.

It seems likely that a study of small-grained polycrystals at low stresses can be useful in determining the intrinsic mechanical properties of GBs, without complicating influences in particular from lattice dislocations.

CHAPTER 7

THE TRANSIENT BEHAVIOUR OF SUPERPLASTIC Sn-38.1w/o Pb

7.1. Introduction

During a mechanical transient, stress and strain rate acting on a material are not held simultaneously constant over a finite strain interval. Transient behaviour may, for example, be caused by work hardening or anelasticity. In these cases it is generally impossible to keep the stress and the strain rate constant at the same time and transient behaviour will be found regardless of the testing method. In simpler situations, the strain rate of a material depends uniquely on the applied stress. Then no transient will be found upon application of a constant stress (more precisely: the transient is infinitely fast). Loading with a constant total strain rate (i.e. the sum of the elastic and the plastic strain rate of the material is constant), however, results in a transient: the stress increases gradually until it reaches a constant value corresponding to the applied strain rate.

An important application of transient behaviour is the stress relaxation test (Feltham, 1960/61; Gibbs, 1966). The stress-strain rate behaviour of a material can be easily predicted from such a test provided that only plastic and elastic deformation occurs and that in the strain interval needed for the test the strain rate depends uniquely on the stress. In a relatively short period of time (e.g. 1 to 100Ks) a wide range of stress-strain rate data can be generated. Because of the small time and strain

intervals usually needed, the sample structure may be thought to be approximately constant during the test, which would facilitate the interpretation of the mechanical properties (Edington, Melton and Cutler, 1976, p.79).

The stress relaxation behaviour is more complicated if strain and/or time have to be taken into account to describe the deformation of a sample. Hammamy, Dubofsky and Stüwe (1977) have investigated the situation in which the strain rate of a material depends on some power of the time or of the strain, for a constant applied stress. They obtained good agreement for a number of metals and alloys (e.g. Cu, Mg, Al-Cu) by taking strain hardening during the relaxation into account. The influence of linear anelasticity on stress relaxation tests has been approximately evaluated by Lubahn and Felgar (1961, pp.363-404). Lloyd and McElroy (1975) stressed the importance of anelastic deformation on transient testing and in particular on the outcome of stress transient dip tests (after deformation for a certain period of time the stress is instantaneously reduced and, immediately afterwards, the total strain is kept constant).

In chapter 6, the pronounced anelasticity in Sn-38.1w/o Pb was demonstrated. Following Lubahn and Felgar, and Lloyd and McElroy, the anelasticity is expected to influence the transient behaviour of this alloy and a close examination seems therefore appropriate. Since Lubahn and Felgar's method may be difficult in practice because it requires solving an integral equation and since

Lloyd and McElroy's approach is not capable of predicting in detail the mechanical transients of a material displaying elastic, plastic and anelastic deformation at the same time, a sufficiently accurate analysis in terms of differential equations is presented in this chapter. Transients can thus be predicted with a reasonable degree of accuracy.

7.2. Mathematical description of simultaneous elastic, plastic and anelastic deformation

7.2.1. Anelasticity described by one relaxation time

A simple rheological model describing simultaneous elastic, plastic, and anelastic deformation will now be presented. It is not accurate enough for a detailed comparison with experimentally found transients (in particular the anelasticity is represented by only one Voigt element). However, it is discussed here because of its simplicity and because it demonstrates the pronounced influence which anelastic strains may have on the transient behaviour.

The model is shown in Fig. 7.1. It consists of a spring, a Voigt element representing the anelasticity, and a non-linear viscous dashpot representing the plastic deformation. Important assumptions inherent in the model are:

(1) the elastic, plastic and anelastic strains are linear additive.

(2) the anelastic strain is represented by only one Voigt element (one relaxation time).

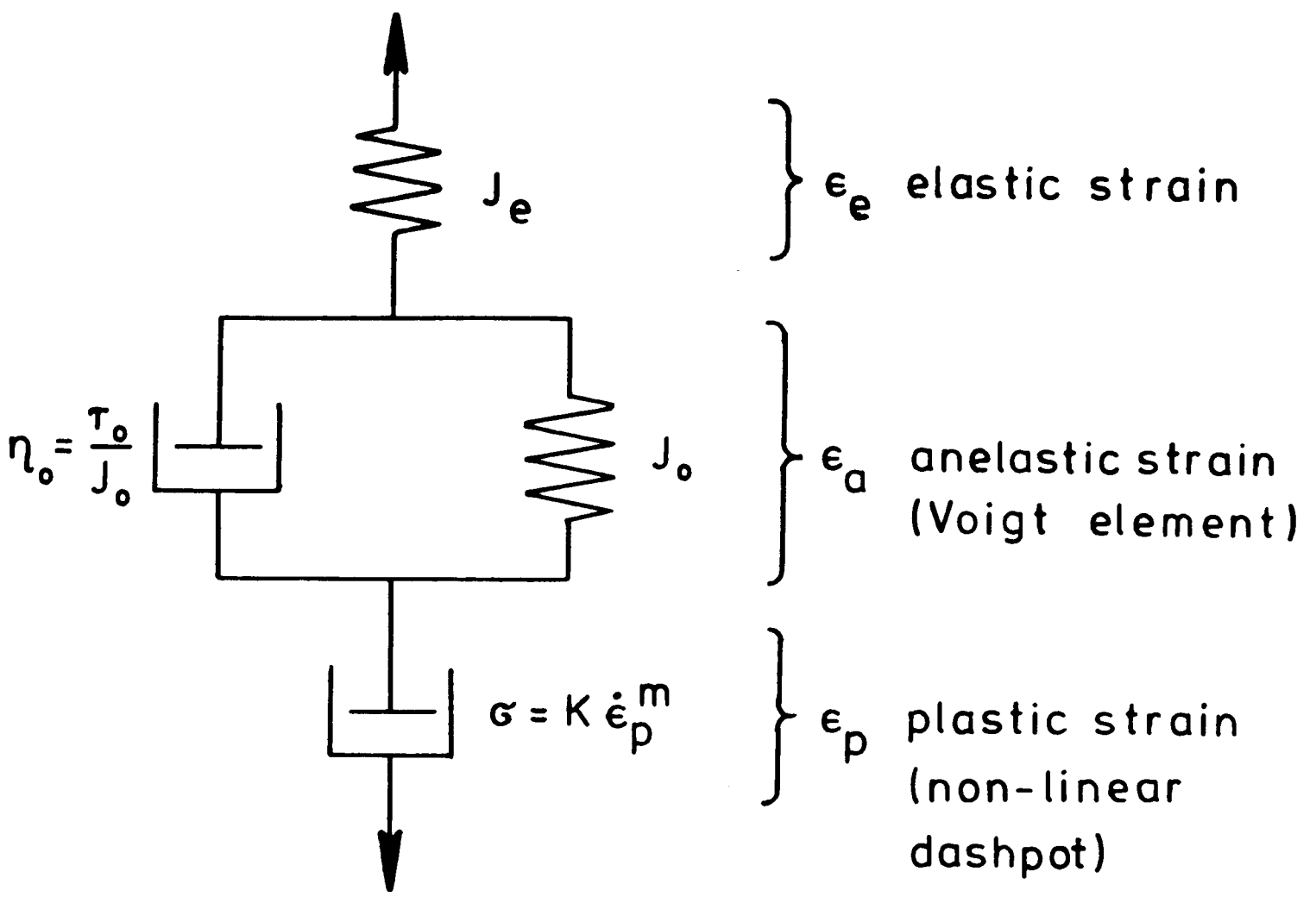

Fig. 7.1. Rheological model combining elasticity, anelasticity (1 relaxation time) and plasticity (non-linear dashpot).

(3) the plastic strain rate depends uniquely on the stress via a power-law.

Differential equation

The following equations for the elastic, anelastic and plastic components of the model hold:

$$J_e \sigma = \varepsilon_e , \tag{7.1}$$

$$J_o \sigma = \varepsilon_a + \tau_o \dot{\varepsilon}_a , \tag{7.2}$$

$$\sigma = K \dot{\varepsilon}_p^m , \tag{7.3}$$

$$\varepsilon = \varepsilon_e + \varepsilon_a + \varepsilon_p , \tag{7.4}$$

where:

σ = stress,

J_e = elastic compliance,

ε_e = elastic deformation,

J_o = compliance of the Voigt element,

τ_o = relaxation time of the Voigt element,

ε_a = anelastic strain,

K = proportionality constant in the equation describing the plastic deformation,

m = strain rate sensitivity,

ε_p = plastic deformation,

ε = total deformation.

Equations (7.1) and (7.2) define the differential equation for a standard anelastic solid (see for example Nowick and Berry, 1972, p.47). Adding to this equation $\dot{\varepsilon}_p$ and $\ddot{\varepsilon}_p$ (see eqn. (7.3); $\dddot{\varepsilon}_p$ is found by differentiating eqn. (7.3)), with appropriate weighting factors, leads to the differential equation for the model in Fig. 7.1:

$$a_o \sigma^n + (J_e + J_o)\,\dot{\sigma} + n\,a_o\,\tau_o\,\sigma^{n-1}\,\dot{\sigma} + J_e\,\tau_o\,\ddot{\sigma} = \dot{\varepsilon} + \tau_o\,\ddot{\varepsilon}\,, \qquad (7.5)$$

where

$$n = 1/m \qquad (7.6)$$

and

$$a_o = K^{-1/m}\,. \qquad (7.7)$$

Initial values

Tests in which the stress varies like a step function need not be considered here since in such a case ε and its derivatives are immediately found from eqns. (7.1) to (7.4) without employing eqn. (7.5). On the other hand, if the strain rate varies like a step function, eqn. (7.5) has to be solved numerically using suitable initial values of σ, $\dot{\sigma}$, $\dot{\varepsilon}$, and $\ddot{\varepsilon}$. $\dot{\varepsilon}$ in an actual test is usually determined by the testing machine employed ($\dot{\varepsilon}\,(t_o \leq t \leq t_1) = \dot{\varepsilon}_o$) and $\ddot{\varepsilon} = 0$, for $\dot{\varepsilon}_o$ = constant. The initial value of σ, σ_o, is defined by the previous test history.

From eqns. (7.1) and (7.4) one obtains now:

$$\dot{\varepsilon}_o = J_e \dot{\sigma} + \dot{\varepsilon}_p + \dot{\varepsilon}_a \quad . \tag{7.8}$$

With eqns. (7.2) and (7.3) the initial value of $\dot{\sigma}$ is now found to be:

$$\dot{\sigma}_o = (\tau_o \dot{\varepsilon}_o + \varepsilon_a - a_o \tau_o \sigma_o^n - J_o \sigma_o)/(J_e \tau_o). \tag{7.9}$$

Starting at $t = t_o$, eqn. (7.5) may therefore be integrated over a time interval $[t_o, t_1]$ if $\sigma(t = t_o) = \sigma_o$, $\dot{\varepsilon}(t_o \leq t \leq t_1) = \dot{\varepsilon}_o$ and $\varepsilon_a(t = t_o)$ are known. In the simplest case (after relaxation for $\Delta t >> \tau_o$ with $\sigma = 0$) the initial anelastic strain is $\varepsilon_a(t = t_o) = 0$.

The integration of eqn. (7.5) between t_o and t_1 now results in values for $\sigma(t_1) = \sigma_1$, $\dot{\sigma}(t_1) = \dot{\sigma}_1$, and $\ddot{\sigma}(t_1) = \ddot{\sigma}_1$. A strain rate change at $t = t_1$ to $\dot{\varepsilon}(t_1 \leq t \leq t_2) = \dot{\varepsilon}_1$ usually changes these values. For example, stress relaxation testing starting at $t = t_1$ ($\dot{\varepsilon}_1 = 0$) may reverse the sign of $\dot{\sigma}$. The value of σ, however, remains unchanged at $t = t_1$ in such a case: ε_a and ε_p cannot change instantaneously for finite values of σ and therefore ε_e and, after eqn. (7.1), σ, will not change instantaneously.

From eqn. (7.2) follows for $t = t_1$:

$$\varepsilon_a = J_o \sigma_1 - \tau_o \dot{\varepsilon}_a \tag{7.10}$$

and

$$\dot{\varepsilon}_a = J_o \dot{\sigma}_1 - \tau_o \ddot{\varepsilon}_a \,, \tag{7.11}$$

and eqn. (7.4) can be written as:

$$\ddot{\varepsilon}_e + \ddot{\varepsilon}_a + \ddot{\varepsilon}_p = 0. \tag{7.12}$$

Together with eqn. (7.3), ε_a can now be expressed as a function of the (known) values of $\sigma(t_1) = \sigma_1$, $\dot{\sigma}(t_1) = \dot{\sigma}_1$ and $\ddot{\sigma}(t_1) = \ddot{\sigma}_1$ immediately prior to the strain rate change:

$$\varepsilon_a = J_o \sigma_1 - \tau_o J_o \dot{\sigma}_1 - \tau_o^2 J_e \ddot{\sigma}_1 - a_o \tau_o^2 n \sigma_1^{n-1} \dot{\sigma}_1 \,. \tag{7.13}$$

The stress at $t = t_1$, the strain rate for $t_1 \leq t \leq t_2$, and the anelastic strain at $t = t_1$ (eqn. (7.13)) now define the new stress rate $\dot{\sigma}(t = t_1)$ immediately after the strain rate change at $t = t_1$, according to eqn. (7.9), (replace σ_o by σ_1 and $\dot{\varepsilon}_o$ by $\dot{\varepsilon}_1$). Equation (7.5) may now be integrated in the interval $[t_1, t_2]$. The flow stress σ can thus be calculated successively from eqn. (7.5) for any series of strain rate changes.

7.2.2. A few examples to illustrate simultaneous elastic, plastic and anelastic deformation

Using a computer program, eqn. (7.5) has been evaluated for a few realistic examples. The constants for the non-linear plastic dashpot in the model in Fig. 7.1 have been determined from the data for Sn-38.1w/o Pb shown in

Fig. 7.2. For material with the same grain size and at the same temperature, the anelastic compliance rates were determined from the elastic after-effect (Fig. 7.3). Depending on the desired relaxation time, two estimates of J_o and τ_o have been chosen. Both underestimate the measured anelastic strain rates.

The elastic compliance in Fig. 7.1, J_e, is

$$J_e = J_m + J_s = A/(S\ L_s) + J_S\ , \qquad (7.14)$$

where:

J_m = elastic compliance of the testing machine employed,

J_s = elastic compliance of the sample,

S = stiffness of the testing machine (applied force/ elastic deflection),

A = sample cross-section,

L = sample gauge length.

The following realistic parameters have been used for the calculations in this section (7.2.2):

S = 2.33 N/μm (see chapter 4),

$A = 5mm^2$,

L_s = 30mm,

$J_s = 4.76 \cdot 10^{-5} MPa^{-1}$ (Subrahmanyam, 1972).

With these values one obtains from eqn. (7.14):

$J_e = 1.19 \cdot 10^{-4} MPa^{-1}$.

Strain rate increase

A sample behaving according to the model in Fig. 7.1

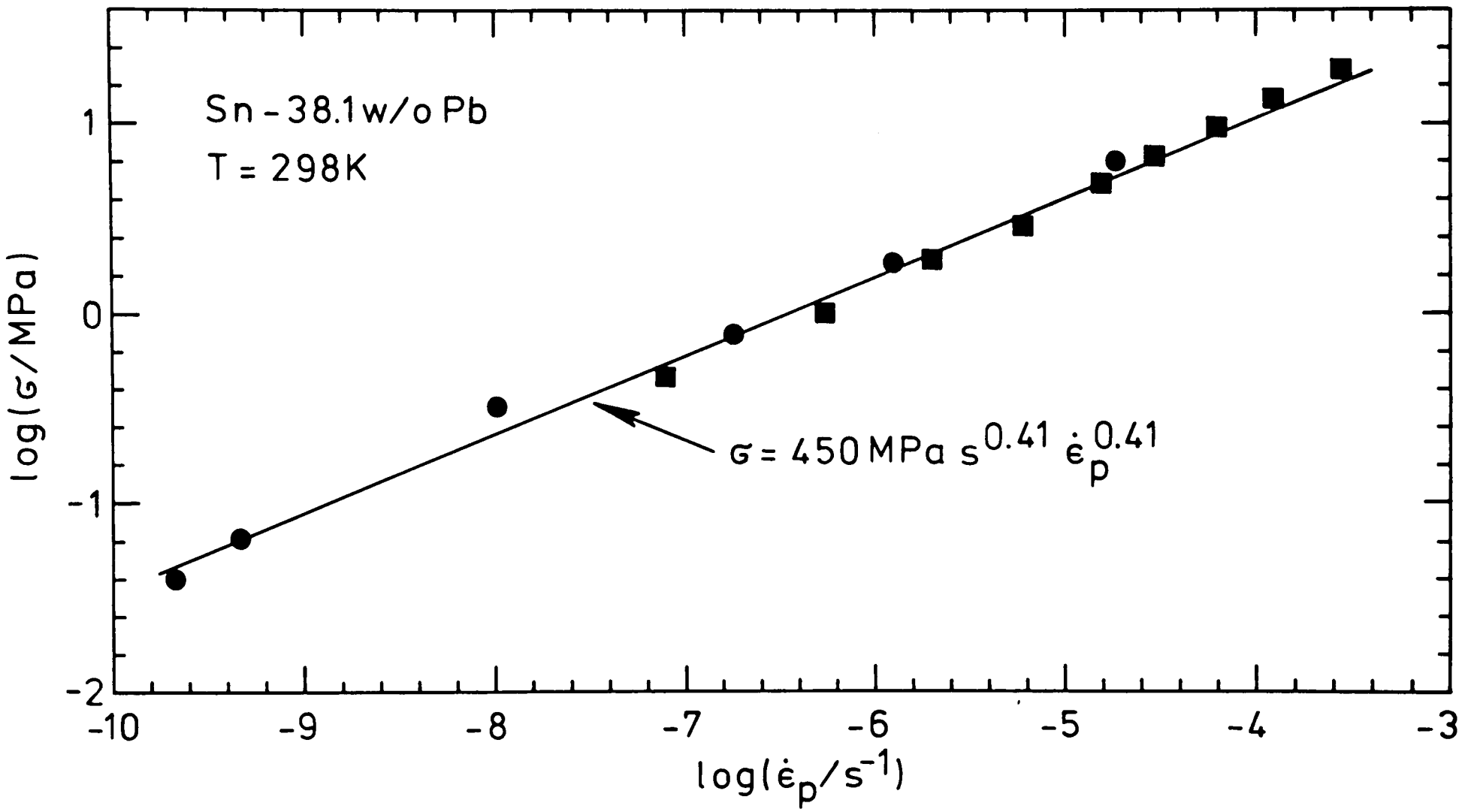

Fig. 7.2. The flow-stress, σ , as a function of the plastic strain rate, $\dot{\epsilon}_p$, for a Sn-38.1w/o Pb sample (grain size estimated after Fig. 5.9: L ~ 4μm). The plasticity can be characterized by K = 450MPas$^{0.41}$ and m = 0.41 (see also Fig. 7.1).

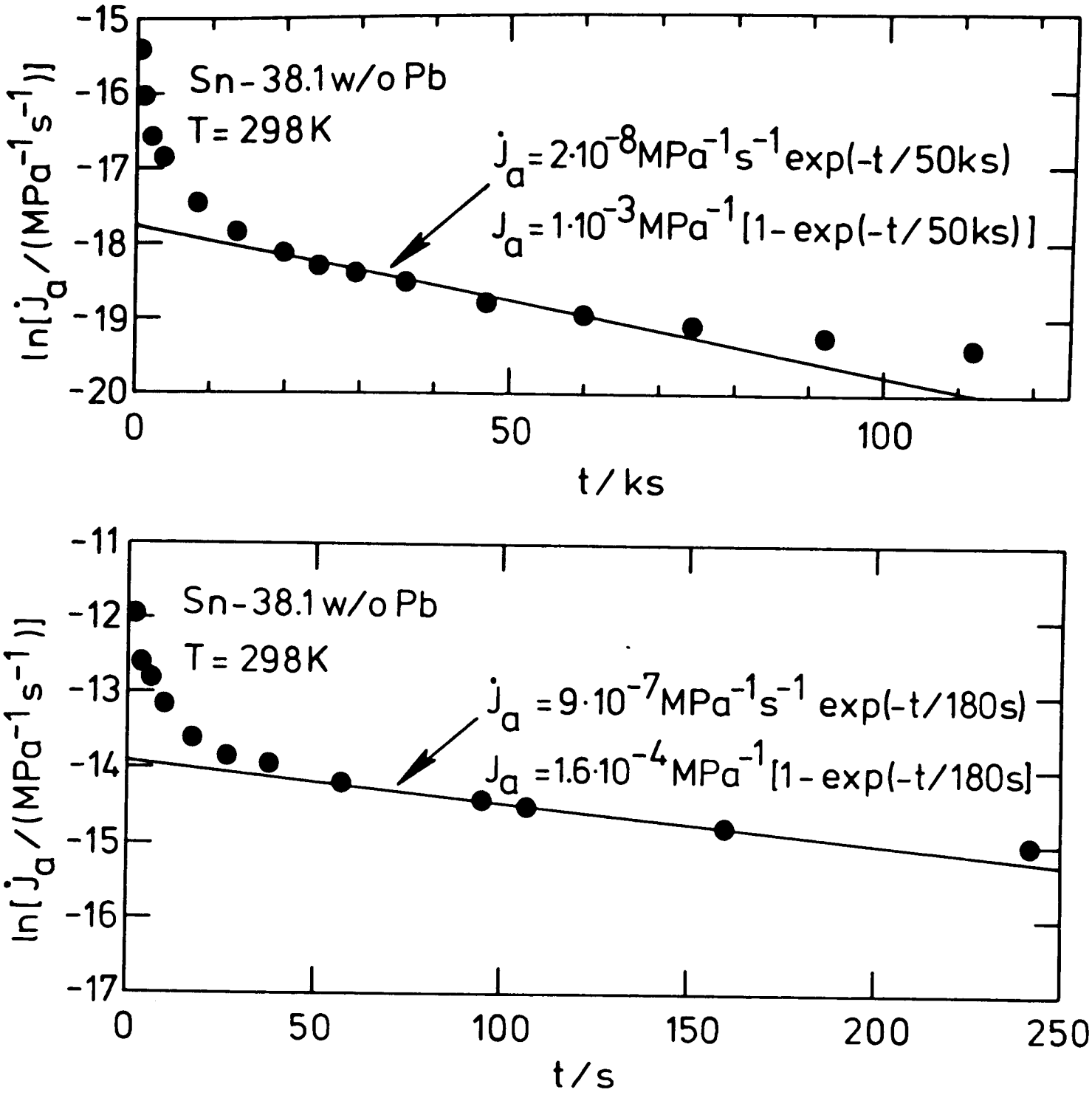

Fig. 7.3. The anelastic compliance rate, $\dot{J}_a$, for a Sn-38.1w/o Pb sample with a grain size of ~4μm, determined from an elastic after-effect curve (unloading at t = 0). Depending on the time scale, the experimental results can be approximated by Voigt elements with different relaxation times, τ_o, and compliances, J_o. In the examples shown here (τ_o, J_o) = (50ks, 10^{-3} MPa^{-1}) or (180s, $1.6 \cdot 10^{-4}$ MPa^{-1}), respectively.

is considered to have been strained at a constant strain rate for a period of time $\Delta t >> \tau_o$. At t = 0 the strain rate is instantaneously increased to another constant value. A stress vs. time curve for such a strain rate change has been obtained by solving eqn. (7.5) and is depicted in Fig. 7.4 (annotated "with anelasticity"). The constants and initial values employed for the calculation are listed in the caption to Fig. 7.4. The influence of anelasticity is negligable for very small values of J_o and τ_o or it can be eliminated completely by setting $J_o = \tau_o = 0$ in eqn. (7.5). The corresponding transient curve (annotated "no anelasticity") is also plotted in Fig. 7.4. Comparison of the two curves for deformation with and without anelasticity shows the pronounced influence which anelasticity can have. Qualitatively, after a strain rate increase, the anelastic strain introduces a lag in the stress increase and thus reduces the rate of the stress increase.

Stress relaxation

Using a relatively long relaxation time of 50ks (Fig. 7.3), the influence of anelasticity on a stress relaxation test has been determined, using the model in Fig. 7.1 (see also Schneibel and Hazzledine, 1977). Two curves calculated with eqn. (7.5) are represented in Fig. 7.5 by full lines. The stress during the relaxation can be plotted as a function of the stress rate, $\dot{\sigma}$, or of $(\dot{\varepsilon}_p + \dot{\varepsilon}_a)$ since after eqns. (7.4) and (7.1):

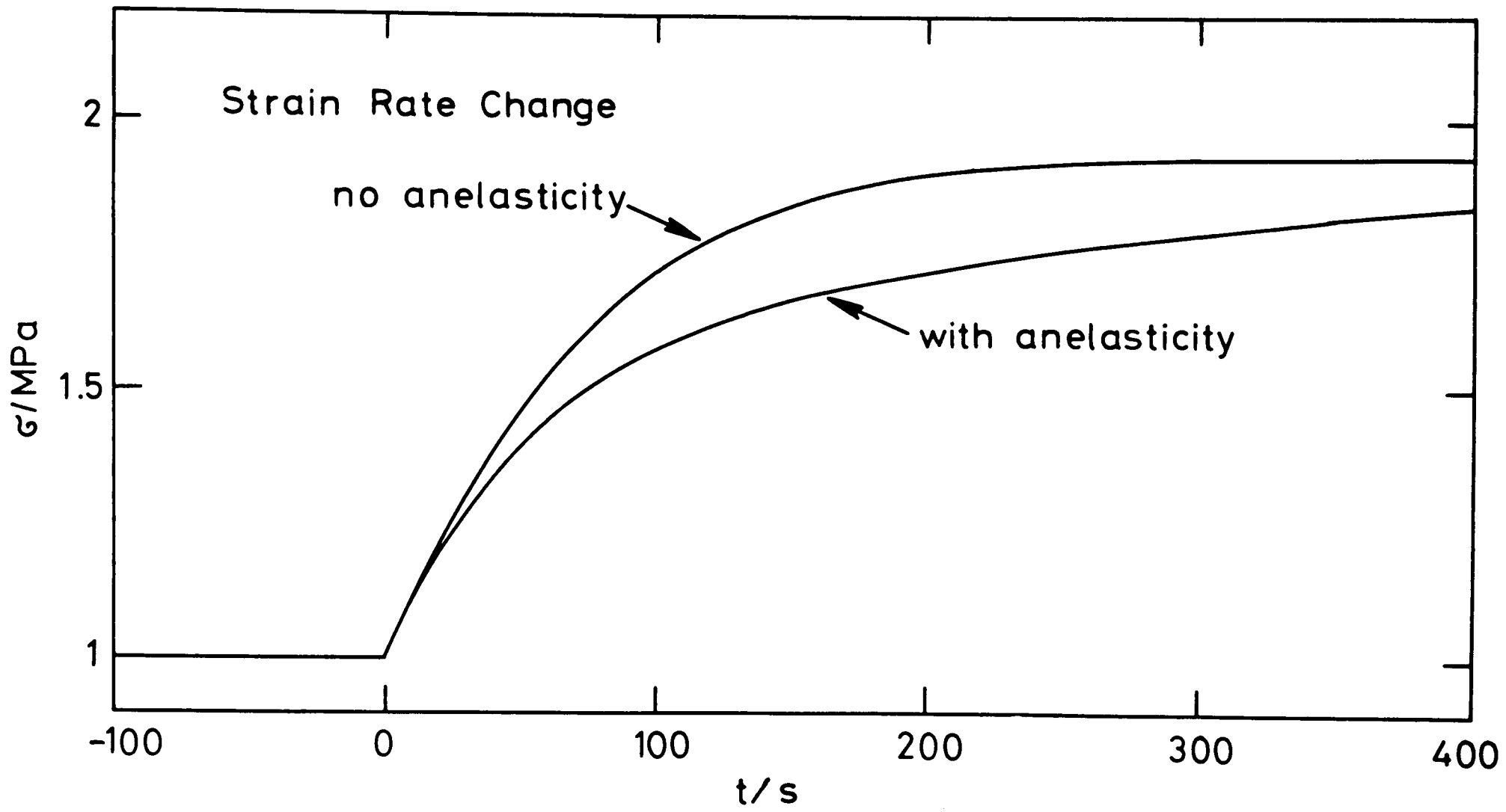

Fig. 7.4. Stress transient after a strain rate increase by a factor of 5 at $t = 0$, calculated with the model shown in Fig. 7.1. For $t \leq 0$ straining occurred with $\dot{\varepsilon} = 3.38 \cdot 10^{-7} s^{-1}$ for a long period of time ($\Delta t >> \tau_o$). At $t = 0$ the strain rate was increased to $1.69 \cdot 10^{-6} s^{-1}$. The values employed to solve eqn. (7.5) were: $J_e = 1.19 \cdot 10^{-4} MPa^{-1}$, $K = 450 MPas^{0.41}$ and $m = 0.41$ (see Fig. 7.2), $J_o = 1.6 \cdot 10^{-4} MPa^{-1}$, $\tau_o = 180s$ (see Fig. 7.3), $\sigma(t = 0) = 1MPa$, and $\varepsilon_a(t = 0) = J_o \, \sigma(t = 0) = 1.6 \cdot 10^{-4}$. To calculate the curve annotated "no anelasticity", values of $\tau_o = 10^4 s$ and $J_o = 10^{-6} MPa^{-1}$ were used.

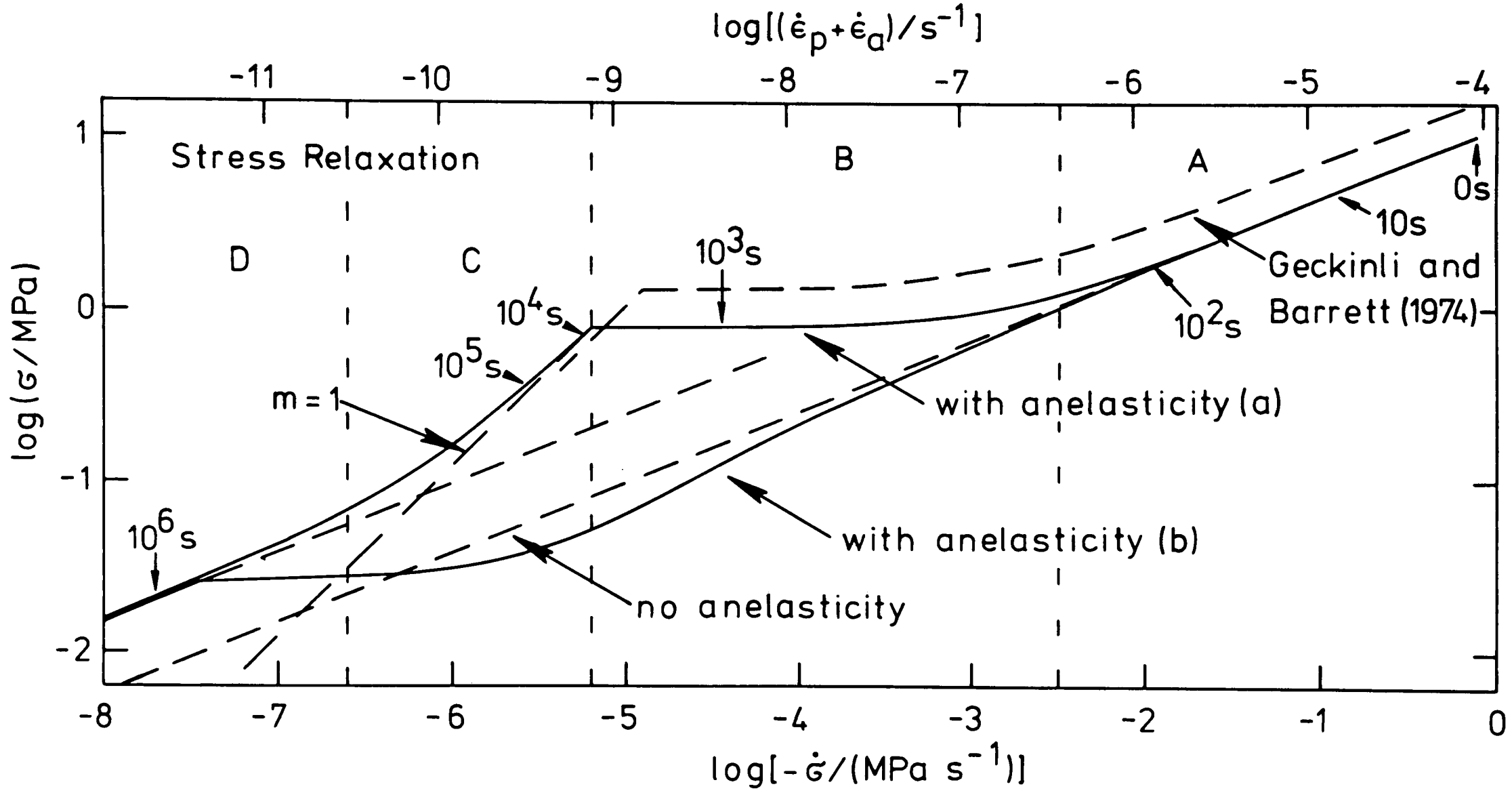

Fig. 7.5. Stress relaxation behaviour calculated with the model shown in Fig. 7.1. Curve (a) has been calculated for relaxation after long loading ($\Delta t >> \tau_o$) with $\sigma(t \leq 0) = 10MPa$ ($\varepsilon_a(t = 0) = 10^{-2}$), curve (b) for relaxation after instantaneous loading to $\sigma(t = 0) = 10MPa$ ($\varepsilon_a(t = 0) = 0$). The times elapsed after relaxation to different stresses are indicated for curve (a). The data employed for the integration of eqn. (7.5) are (see also Figs. 7.2 and 7.3): $J_e = 1.19 \cdot 10^{-4} MPa^{-1}$, $K = 450 MPa s^{0.41}$ $m = 0.41$, $J_o = 10^{-3} MPa^{-1}$ and $\tau_o = 50ks$.

$$\dot{\varepsilon}_p + \dot{\varepsilon}_a = -J_e \dot{\sigma} \quad . \tag{7.15}$$

In one case (curve (a)) the loading previous to the relaxation at t = 0 was for a period of time $\Delta t >> \tau_o$ with a constant strain rate, $\dot{\varepsilon}_o$, or a constant stress, σ_o. At t = 0 the strain rate was set equal to 0. The anelastic strain immediately at the start of the relaxation is then given by $\varepsilon_a = J_o \sigma_o$ since the Voigt element incorporated in the model is initially in equilibrium with the applied stress, σ_o. In another case, a previously unstrained sample ($\sigma = 0$ for $\Delta t >> \tau_o$) was loaded instantaneously to σ_o prior to the relaxation (curve (b) in Fig. 7.5). Therefore, at the beginning of the relaxation, $\varepsilon_a = 0$, since the strain of the Voigt element lags behind the applied stress.

The relaxation with ε_a (t = 0) = $J_o \sigma_o$ (curve (a) in Fig. 7.5) will now be qualitatively discussed in some detail. Initially, the anelastic element can be considered to be static since the stress is σ_o. The anelasticity is therefore not taken into account. Setting $J_o = \tau_o = 0$ in eqn. (7.5) thus leads to an equation for the initial part of the stress relaxation:

$$\log \sigma = m \log(-\dot{\sigma}) + \log(K J_e^m) . \tag{7.16}$$

A broken line corresponding to eqn. (7.16) is plotted in Fig. 7.5 and is annotated by "no anelasticity". It

represents the stress relaxation behaviour of a spring (elasticity) and a non-linear dashpot (plasticity) in series ("power-law relaxation").

One requirement for the validity of eqn. (7.16) during the initial stage of the relaxation is that the relaxation time for power-law relaxation, τ_p, is smaller than that of the anelastic element, τ_o. τ_p is obtained by integrating eqn. (7.16):

$$\int_{\sigma_o}^{\sigma} \frac{d\sigma'}{\sigma'^{1/m}} = -\frac{1}{J_e K^{1/m}} \int_0^t dt' \,, \qquad (7.17)$$

where σ_o is the stress at the beginning of the relaxation ($t = 0$) and σ the stress at some time $t \geq 0$. Evaluation of eqn. (7.17) leads to:

$$(\sigma/\sigma_o)^{(m-1)/m} - 1 = t/\tau_p, \qquad (7.18)$$

where

$$\tau_p = \frac{J_e K^{1/m}}{(1-m)\ \sigma_o^{(1-m)/m}} = \frac{\varepsilon_{e(\text{before the test})}}{(1-m)\ \dot{\varepsilon}_{p(\text{before the test})}} \,. \qquad (7.19)$$

In the example shown in Fig. 7.5, τ_o is 50ks, whereas τ_p is only ~22s. This confirms the applicability of eqn. (7.16) for the present case (region A in Fig. 7.5).

At a later stage in the relaxation (region B in Fig. 7.5) a plateau is reached with an approximately constant stress.

In region A, the stress decreased rapidly due to the power-law relaxation and therefore the anelastic element, the strain of which is still $\sim J_o \sigma_o$, contracts. Over a period of time $\Delta t < \tau_o$ it contracts almost as rapidly as the plastic element extends. Therefore the stress remains approximately constant during this stage of the relaxation.

Following the relaxation from region B into region C, the rate of contraction of the anelastic element decreases. However, due to its high compliance and time lag it still has much more strain stored than the elastic spring in the model. This anelastic strain is now gradually reduced. In a first approximation, the Voigt element can be considered to be strain relaxing (i.e. $\sigma = 0$) and at the same time driving the non-linear dashpot with hardly any expenditure of energy ($\sigma \gtrsim 0$). Neglecting the elastic strain (which is relatively small due to the small value of J_e), eqns. (7.4) and (7.3) can be written as:

$$\dot{\varepsilon}_a + \dot{\varepsilon}_p = \dot{\varepsilon}_a + (\sigma/K)^{1/m} = 0. \qquad (7.20)$$

Since the stress acting on the Voigt element was assumed to be approximately 0 eqn. (7.2) reduces to:

$$0 = \dot{\varepsilon}_a + \tau_o \ddot{\varepsilon}_a \quad . \qquad (7.21)$$

Substitution of $\dot{\varepsilon}_a$ and $\ddot{\varepsilon}_a$ by σ and $\dot{\sigma}$ (see eqn. (7.20) results in:

$$\log(-\dot{\sigma}) = \log(m/\tau_o) + \log\sigma \quad . \qquad (7.22)$$

Correspondingly, a straight broken line with a slope of m = 1 has been plotted in region C in Fig. 7.5.

Finally, for $t >> \tau_o$, the deformation ε_a of the anelastic element corresponds to the actual stress. The relaxation is now so slow that the Voigt element is in phase with the actual stress. Its compliance now corresponds to that of an elastic spring and power-law relaxation results with an elastic compliance $J_e + J_o$ instead of J_e. In analogy to eqn. (7.16) one obtains $\log \sigma = m \log(-\dot{\sigma}) + \log[K(J_o + J_e)^m]$. A broken line corresponding to this equation is plotted in region D in Fig. 7.5.

The equation above will eventually be obeyed also if the anelastic strain prior to the relaxation is 0. The shape of curve (b) in Fig. 7.5 is thus understandable: although the initial rate of relaxation is faster than for curve (a) since the Voigt element is extending intially, curves (a) and (b) finally have to come together in a later stage of the relaxation.

An experimental result published by Geckinli and Barrett (1974) (their grain size 5μm) has been plotted in Fig. 7.5. It agrees reasonably well with the calculated relaxation behaviour after long previous loading (curve (a)). The agreement will later be seen to be fortuitous. The calculated example nevertheless demonstrates that Geckinli and Barrett's data cannot be interpreted in a simple manner to evaluate the plastic strain rate as a function of the applied stress: $\dot{\sigma}$ is not generally proportional to $\dot{\varepsilon}_p$.

Incorporation of anelasticity into a stress relaxation test using simple but realistic assumptions can change the relaxation behaviour markedly. In particular (see curve (a) in Fig. 7.5)), a plateau region cannot be interpreted as a threshold stress for plastic deformation and a region with a slope of 1 does not necessarily indicate a plastic deformation mechanism with a strain rate sensitivity of 1.

Stress transient dip test

An experimental test method which can be considerably influenced by anelasticity is the stress transient dip test (Gibbs, 1966). After straining with a positive strain rate the stress is abruptly reduced by applying a high negative strain rate for a short time and, immediately afterwards, the total strain is kept constant. For example, if the stress is reduced to 0, after a loading period, reloading will be observed. During the loading period, the anelastic element has been storing strain. It contracts upon unloading and thus strains the plastic element. This causes the observed stress increase.

The calculated dependence of the stress on the time after different partial unloadings at t = 0 is shown in Fig. 7.6. In the examples shown, straining with a stress σ_o prior to the stress reduction occurred over a period of time $\Delta t >> \sigma_o$. Therefore $\varepsilon_a(t = 0) = J_o \sigma_o$. If the stress is not reduced at t = 0, the previously discussed stress relaxation behaviour results.

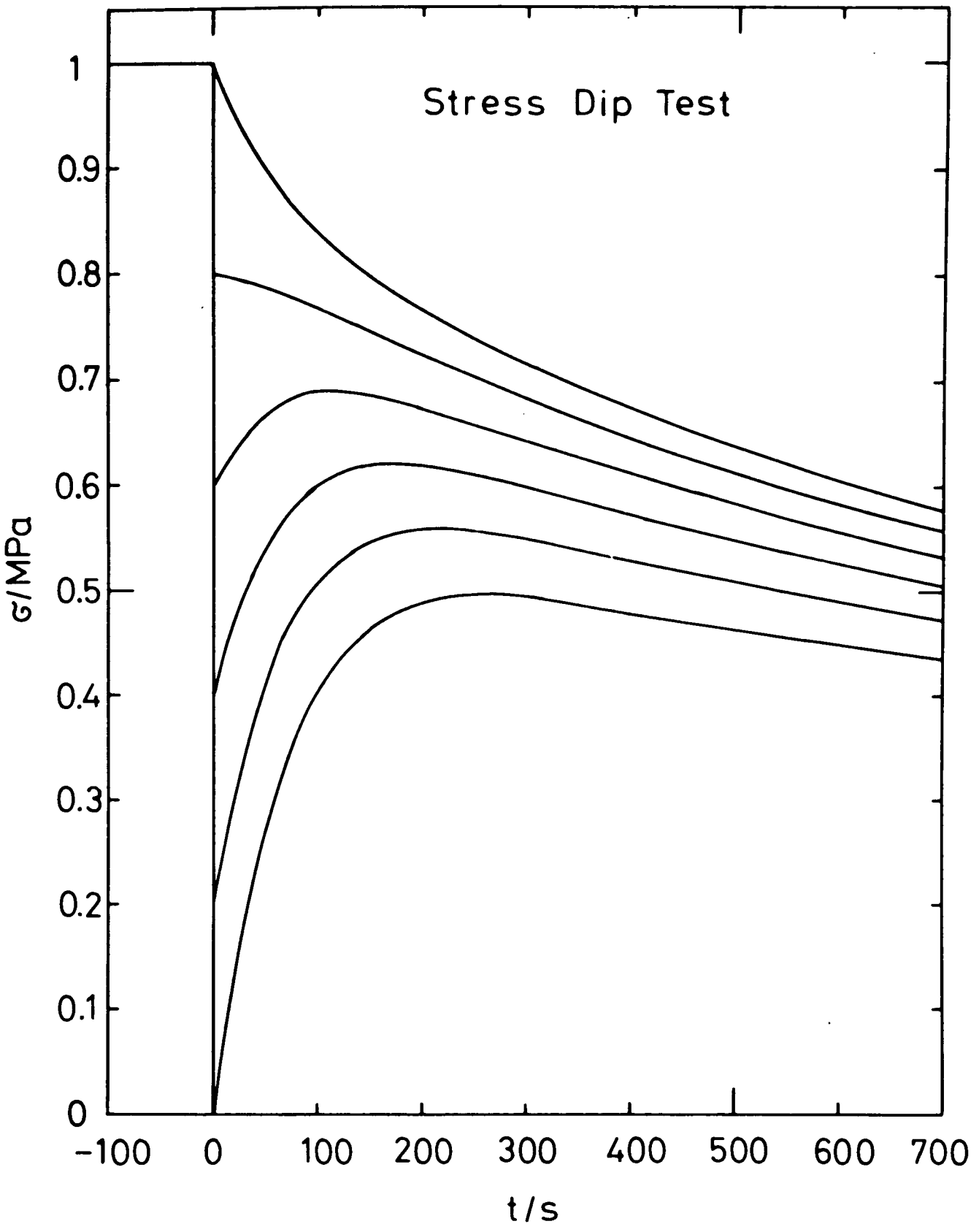

Fig. 7.6. Calculated stress transient dip tests. The loading period ($\sigma(t \leq 0) = 1$MPa) prior to the instantaneous stress reduction at $t = 0$ was $>>\tau_o$. The data employed for the integration of eqn. (7.5) were (see also Figs. 7.2 and 7.3): $J_e = 1.19 \cdot 10^{-4}$MPa^{-1}; $K = 450$MPas$^{0.41}$; $m = 0.41$; $J_o = 1.6 \cdot 10^{-4}$MPa^{-1}; $\tau_o = 180$s; $\varepsilon_a(t = 0) = J_o \cdot 1\text{MPa} = 1.6 \cdot 10^{-4}$; and $\sigma(t = 0) = 1$MPa, 0.8MPa, 0.6MPa, 0.4MPa, 0.2MPa or 0.

In order to solve eqn. (7.5) it is not necessary to consider in detail the short period of straining with a high negative strain rate needed for the stress reduction since the anelastic strain does not change abruptly after the stress change. It is merely required to know the stress immediately after the unloading.

The anelasticity can cause an apparent internal stress σ_i. Straining with a stress σ_o for a long time and unloading to σ_i (and keeping the total strain constant immediately afterwards) results in $\dot{\sigma}(t = 0) = 0$, i.e. the anelastic element contracts at the same rate with which the plastic element extends. Since the anelastic strain prior to the stress reduction is $J_o \sigma_o$, eqn. (7.2) can be written, at t = 0, as:

$$J_o \sigma_i = J_o \sigma_o + \tau_o \dot{\varepsilon}_a \quad . \tag{7.23}$$

Since for $\sigma = \sigma_i$:

$$\dot{\varepsilon}_a = -\dot{\varepsilon}_p \quad , \tag{7.24}$$

one obtains from eqns. (7.23), (7.24) and and (7.2) an eqn. for the apparent internal stress, σ_i:

$$\tau_o (\sigma_i/K)^{1/m} + J_o \sigma_i = J_o \sigma_o \quad . \tag{7.25}$$

The dependence of σ_i/σ_o on the stress prior to the dip test, σ_o, is shown in Fig. 7.7, for realistic values of the

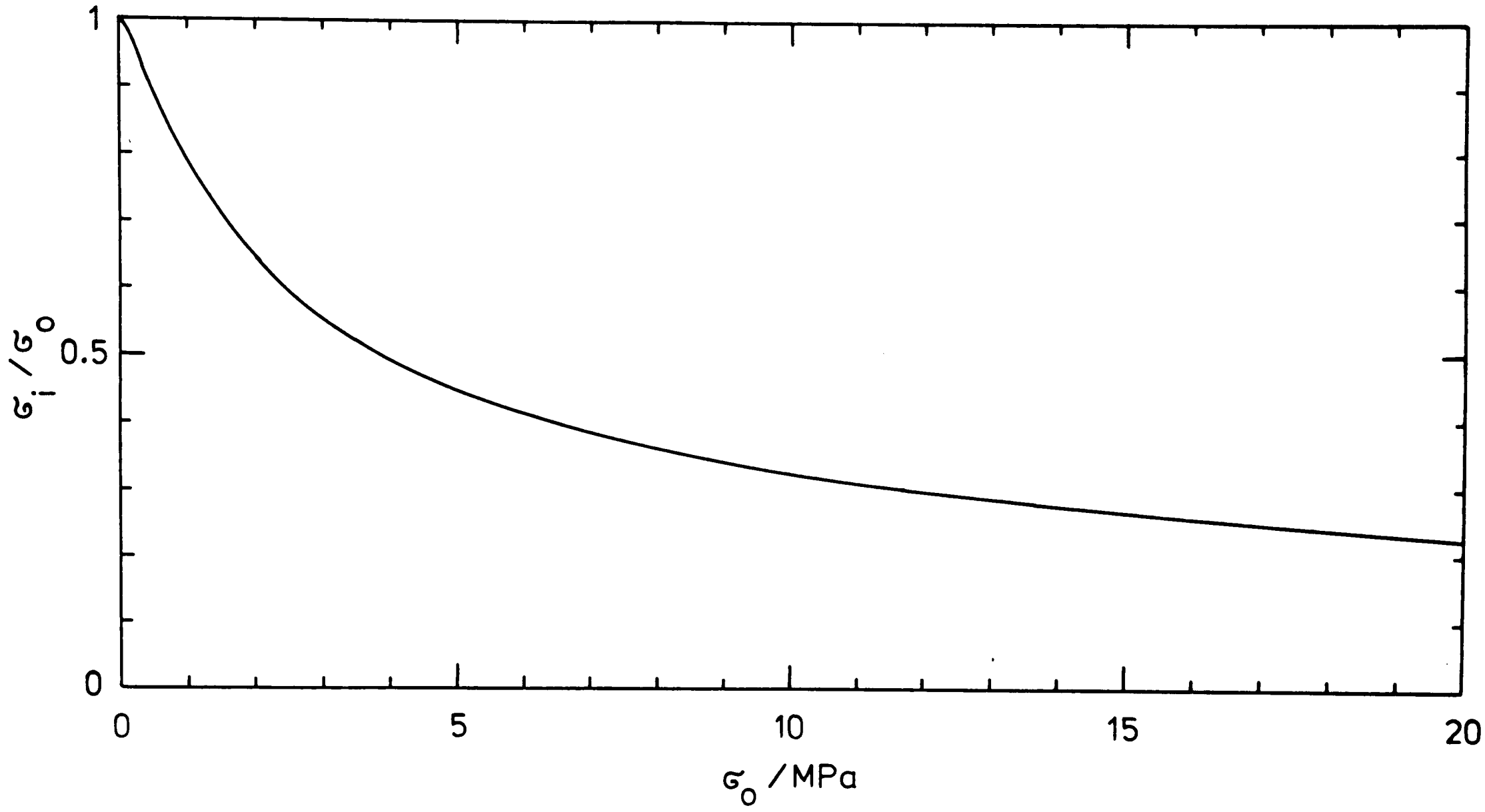

Fig. 7.7. Apparent internal stress, σ_i, as a function of the applied stress, σ_o. The parameters employed in eqn. (7.25) are those employed in Fig. 7.6.

parameters in eqn. (7.25). Not surprisingly, σ_i/σ_o decreases with increasing σ_o. Only for m = 1 is σ_i proportional to σ_o (σ_i/σ_o = const.) as has already been derived by Geckinli and Barrett (1974).

The examples presented using the model in Fig 7.1 with realistic parameters show convincingly the pronounced influence which anelasticity may have on mechanical transients. However, as demonstrated in Fig. 7.3, the approximation of the anelastic behaviour of Sn-38.1w/o Pb by only one Voigt element is poor. An accurate comparison between calculated and experimentally determined transients is therefore not possible with this model. Consequently, two additional Voigt elements will now be incorporated in a more realistic model.

7.2.3. Anelasticity described by three relaxation times

The model shown in Fig. 7.8 incorporates 3 Voigt elements to describe the anelasticity, one linear elastic spring and one non-linear dashpot (plasticity).

Differential equation

The equations for the individual elements of the model are:

$$J_e \sigma = \varepsilon_e \quad , \tag{7.26}$$

$$J_{oi} \sigma = \varepsilon_{ai} + \tau_i \dot{\varepsilon}_{ai} \quad , \; i=1,2,3, \tag{7.27}$$

$$\sigma = K \dot{\varepsilon}_p^m \quad , \tag{7.28}$$

$$\varepsilon = \varepsilon_e + \sum_{i=1}^{3} \varepsilon_{ai} + \varepsilon_p \quad , \tag{7.29}$$

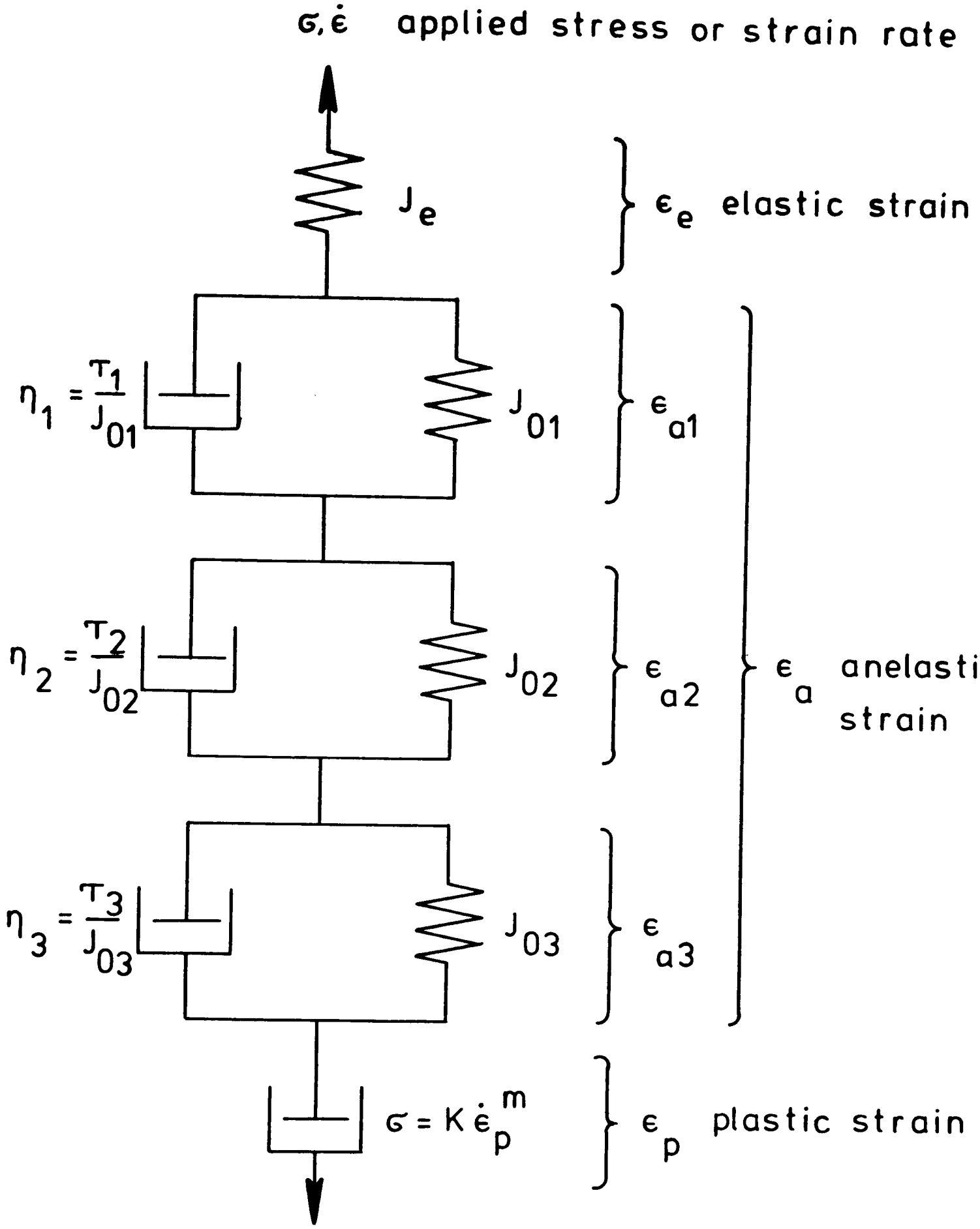

Fig. 7.8. Rheological model combining elasticity, anelasticity (3 relaxation times) and plasticity (non-linear dashpot).

where:

J_{oi} = compliance of the i-th Voigt element,

τ_i = relaxation time of the i-th Voigt element,

ε_{ai} = strain of the i-th Voigt element,

and the other notations are as in section 7.2.1.

Equations (7.26) and (7.27) define the differential equation for an anelastic solid with three discrete relaxation times (see for example Nowick and Berry, 1972, p.64):

$$a_1 \sigma + a_2 \dot{\sigma} + a_3 \ddot{\sigma} + a_4 \dddot{\sigma} = \varepsilon_{ae} + b_1 \dot{\varepsilon}_{ae} + b_2 \ddot{\varepsilon}_{ae} + b_3 \dddot{\varepsilon}_{ae} \quad , \tag{7.30}$$

where:

$$\varepsilon_{ae} = \varepsilon_e + \varepsilon_{a1} + \varepsilon_{a2} + \varepsilon_{a3} \quad , \tag{7.31}$$

$$a_1 = J_e + J_{o1} + J_{o2} + J_{o3} \quad , \tag{7.32}$$

$$a_2 = \tau_3 (J_e + J_{o1} + J_{o2}) + \tau_2 (J_e + J_{o1}) + \tau_1 (J_e + J_{o2}) + (\tau_1 + \tau_2) J_{o3} \quad , \tag{7.33}$$

$$a_3 = \tau_1 \tau_3 (J_e + J_{o2}) + \tau_2 \tau_3 (J_e + J_{o1}) + \tau_1 \tau_2 (J_e + J_{o3}) \quad , \tag{7.34}$$

$$a_4 = \tau_1 \tau_2 \tau_3 J_e \quad , \tag{7.35}$$

$$b_1 = \tau_1 + \tau_2 + \tau_3 \quad , \tag{7.36}$$

$$b_2 = \tau_1 \tau_3 + \tau_2 \tau_3 + \tau_1 \tau_2 \quad , \tag{7.37}$$

$$b_3 = \tau_1 \tau_2 \tau_3 \quad . \tag{7.38}$$

Evaluation of $\dot{\varepsilon}_p$ and its higher derivatives from eqn. (7.28) and adding the resulting expressions to eqn. (7.36), with suitable weighting factors, results in the differential equation describing the model in Fig. 7.8:

$$a_o \sigma^n + a_1 \dot{\sigma} + a_2 \ddot{\sigma} + a_3 \dddot{\sigma} + a_4 \ddddot{\sigma} + a_5 \sigma^{n-1} \dot{\sigma} +$$

$$a_6 \sigma^{n-2} \dot{\sigma}^2 + a_7 \sigma^{n-3} \dot{\sigma}^3 + a_8 \sigma^{n-1} \ddot{\sigma} + a_9 \sigma^{n-2} \dot{\sigma} \ddot{\sigma} +$$

$$a_{10} \sigma^{n-1} \dddot{\sigma} =$$

$$\dot{\varepsilon} + b_1 \ddot{\varepsilon} + b_2 \dddot{\varepsilon} + b_3 \ddddot{\varepsilon} \quad , \tag{7.39}$$

where:

$$a_o = K^{-1/m} \quad , \tag{7.40}$$

$$n = 1/m \quad , \tag{7.41}$$

$$a_5 = a_o b_1 n \quad , \tag{7.42}$$

$$a_6 = a_o b_2 n (n-1) \quad , \tag{7.43}$$

$$a_7 = a_o b_3 n (n-1) (n-2) \quad , \tag{7.44}$$

$$a_8 = a_o b_2 n \quad , \tag{7.45}$$

$$a_9 = 3 a_o b_3 n (n-1) \quad , \tag{7.46}$$

$$a_{10} = a_o \, b_3 \, n \quad . \tag{7.47}$$

Initial values

From eqn. (7.27) follows:

$$\dot{\varepsilon}_{ai} = (J_{oi} \, \sigma - \varepsilon_{ai})/\tau_i \quad , \; i=1,2,3. \tag{7.48}$$

From eqns. (7.29), (7.26), and (7.28) one obtains for a constant applied strain rate $\dot{\varepsilon}\ (t_o \leq t \leq t_1) = \dot{\varepsilon}_o$ and an initial stress $\sigma(t_o) = \sigma_o$:

$$\dot{\sigma}_o = (\dot{\varepsilon}_o - \sum_{i=1}^{3} \dot{\varepsilon}_{ai} - a_o \, \sigma_o^n)/J_e \quad . \tag{7.49}$$

Since $\ddot{\varepsilon}_o = \dddot{\varepsilon}_o = 0$, differentiating of eqns. (7.48) and (7.49) leads to:

$$\ddot{\varepsilon}_{ai} = (J_{oi} \, \dot{\sigma}_o - \dot{\varepsilon}_{ai})/\tau_i \quad , \; i=1,2,3, \tag{7.50}$$

$$\ddot{\sigma}_o = - (\sum_{i=1}^{3} \ddot{\varepsilon}_{ai} + a_o \, n \, \sigma_o^{n-1} \, \dot{\sigma}_o)/J_e \quad , \tag{7.51}$$

$$\dddot{\varepsilon}_{ai} = (J_{oi} \, \ddot{\sigma}_o - \ddot{\varepsilon}_{ai})/\tau_i \quad , \; i=1,2,3, \tag{7.52}$$

$$\dddot{\sigma}_o = - \sum_{i=1}^{3} \dddot{\varepsilon}_{ai} + a_o \, n \, [\, (n-1)\sigma_o^{n-2} \, \dot{\sigma}_o +$$

$$\sigma_o^{n-1} \, \ddot{\sigma}_o \,] \, /J_e \quad , \; i=1,2,3. \tag{7.53}$$

Equations (7.48) to (7.53) define the initial values of $\dot{\sigma}(t_o) = \dot{\sigma}_o$, $\ddot{\sigma}(t_o) = \ddot{\sigma}_o$ and $\dddot{\sigma}(t_o) = \dddot{\sigma}_o$ if initial values

of $\sigma(t_o) = \sigma_o$, $\dot{\varepsilon}(t_o \leq t \leq t_1) = \dot{\varepsilon}_o$ and $\varepsilon_{ai}(t = 0)$ (i=1,2,3) are provided. With these initial values eqn. (7.39) can now be integrated between $t = t_o$ and $t = t_1$. Similar to the reasoning in section 7.2.1, a strain rate change at $t = t_1$ usually changes the values of $\sigma^{(i)} = d^i\sigma/dt^i$ (i=1 to 4). From the values of $\sigma^{(i)}(t_1) = \sigma_1^{(i)}$ (i=0 to 3) immediately prior to the strain rate change the values of ε_{ai} (i=1,2,3) at this moment can be found by solving a system of linear equations in $\dot{\varepsilon}_{ai}$ as will now be shown.

The first equation is obtained by rewriting eqn. (7.49):

$$\sum_{i=1}^{3} \dot{\varepsilon}_{ai} = \dot{\varepsilon}_o - J_e \dot{\sigma}_1 = a_o \sigma_1^n \quad . \tag{7.54}$$

In the relation obtained from eqn. (7.27):

$$\sum_{i=1}^{3} \ddot{\varepsilon}_{ai} = \sum_{i=1}^{3} (J_{oi} \dot{\sigma}_1 - \dot{\varepsilon}_{ai})/\tau_i \tag{7.55}$$

one replaces (with eqns. (7.26), (7.28) and (7.29)) $\sum_{i=1}^{3} \ddot{\varepsilon}_{ai}$ by:

$$\sum_{i=1}^{3} \ddot{\varepsilon}_{ai} = -J_e \ddot{\sigma}_1 - a_o n \sigma_1^{n-1} \dot{\sigma} \tag{7.56}$$

and obtains:

$$\sum_{i=1}^{3} \dot{\varepsilon}_{ai}/\tau_i = (\sum_{i=1}^{3} J_{oi}/\tau_i)\, \dot{\sigma}_1 + J_e \ddot{\sigma}_1 + a_o n \sigma_1^{n-1} \dot{\sigma}_1 \,. \tag{7.57}$$

Similarly, differentiating eqns. (7.55) and (7.56) and elimination of $\sum_{i=1}^{3} \dddot{\varepsilon}_{ai}$ results in the third equation for

$\dot{\varepsilon}_{ai}$:

$$\sum_{i=1}^{3} \dot{\varepsilon}_{ai}/\tau_i^2 = \left(\sum_{i=1}^{3} J_{oi}/\tau_i^2\right) \dot{\sigma}_1 - \left(\sum_{i=1}^{3} J_{oi}/\tau_i\right) \ddot{\sigma}_1 -$$

$$J_e \dddot{\sigma}_1 - a_o n \left[(n-1)\, \sigma_1^{n-2} \dot{\sigma}_1^2 + \sigma_1^{n-1} \ddot{\sigma}_1\right] . \qquad (7.58)$$

From the system of linear equations defined by eqns. (7.54), (7.57) and (7.58) one calculates $\dot{\varepsilon}_{ai}(t = t_1)$ (i=1,2,3) and obtains, with eqn. (7.27):

$$\varepsilon_{ai} = J_{oi}\, \sigma_1 - \tau_i\, \dot{\varepsilon}_{ai} , \quad i=1,2,3. \qquad (7.59)$$

The anelastic strains ε_{ai} (i=1,3) thus found define, via eqns. (7.48) to (7.53), the new initial values of $\sigma^{(i)}$ (i=1,2,3) for the integration of eqn. (7.39), after a strain rate change at $t = t_1$. The flow stress σ can thus be calculated successively from eqn. (7.39) for any series of strain rate changes.

7.3. Experimentally determined transients for Sn-38.1w/o Pb and comparison with calculated transients

7.3.1. The influence of anelasticity on the strain rate after discontinuous stress changes

Loading behaviour

A sample was stressed for ~13 days with 0.36MPa

(see Fig. 5.2) and subsequently unloaded in order to measure its elastic after-effect (Fig. 6.4). In Fig. 7.9 the anelastic strain thus obtained has been subtracted from the combined plastic and anelastic strain obtained upon loading, in order to find the plastic component of the strain during loading. In this example additivity of plastic and anelastic strains (and strain rates) has been assumed. If this assumption is correct then there exists a plastic transient upon loading; the plastic strain rate decreases with increasing plastic strain or time and is not a unique function of the stress. Alternatively, anelastic and plastic strains may have to be added in a non-linear way and in this case there might be no plastic transient at all. In general, neither additivity nor transient-free plasticity can be inferred from the experiment shown in Fig. 7.9. Moreover, the anelasticity is not strictly linear (see eqn. (6.1)) and can therefore not be accurately represented by Voigt elements as in the model shown in Fig. 7.8.

However, the subtraction of the anelasticity in Fig. 7.9 reduces the magnitude of the transient behaviour considerably. Therefore, the assumptions made in section 7.2.3 (eqns. (7.28) and (7.29)) should at least constitute a significant improvement over the assumption of no anelasticity at all.

Partial unloading and loading

The anelastic behaviour of a Sn-38.1w/o Pb sample

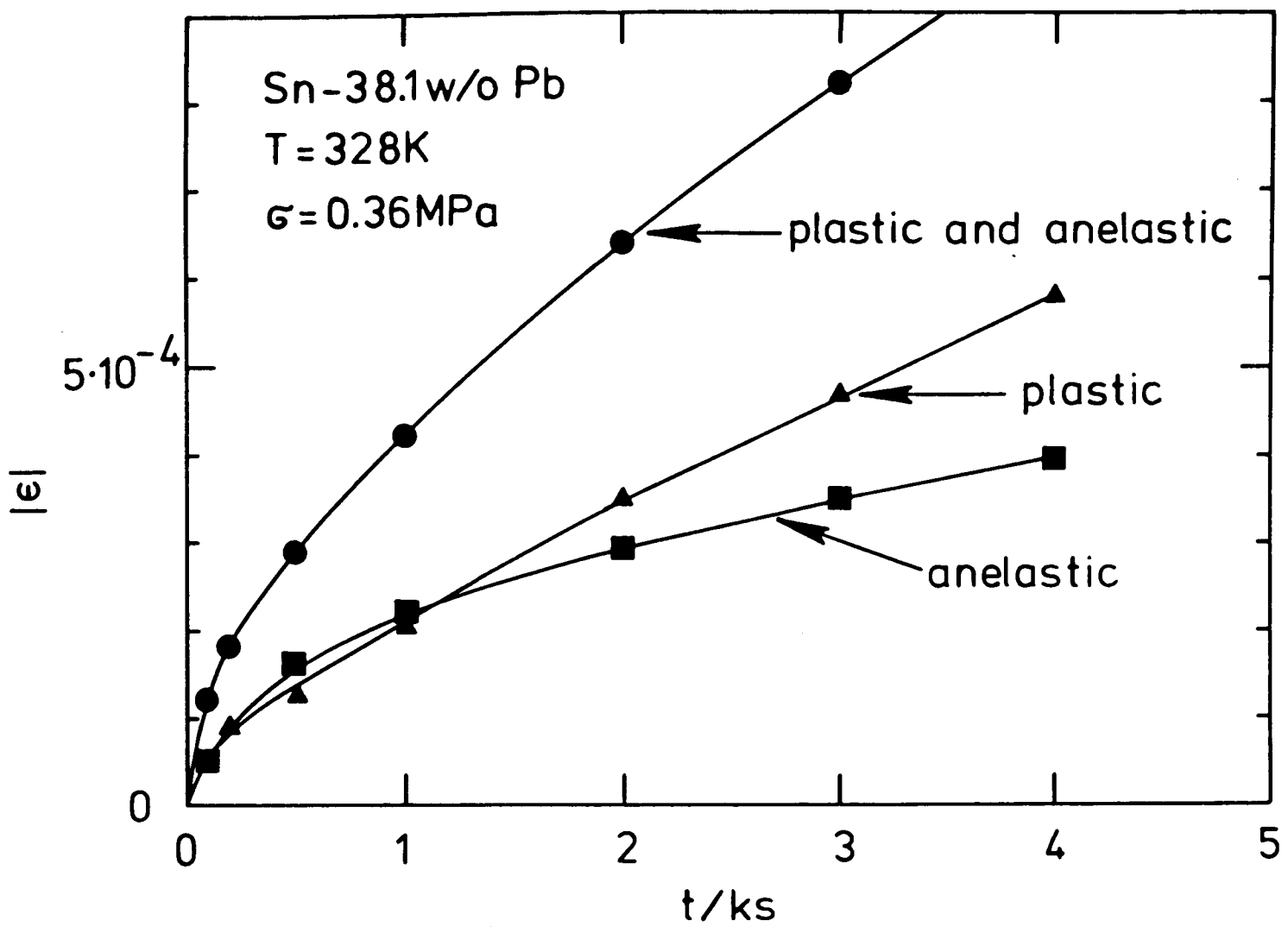

Fig. 7.9. Loading of a Sn-38.1w/o Pb sample with a constant stress, σ , at t = 0, and the influence of anelasticity on the observed transient. The anelastic strain as a function of the time has been obtained from the elastic after-effect after previous loading with 0.36MPa for ~13 days and has been subtracted from the combined plastic and anelastic strain in order to obtain an estimate for the plastic strain.

was determined from the elastic after-effect (Fig. 7.10) and stress change experiments were performed with this sample (Fig. 7.11). After a stress drop from 1.1MPa to 0.54MPa, the combined plastic and anelastic strain rate is initially negative and gradually takes on a new, approximately constant value. A subsequent stress increase results in an initially high strain rate which gradually settles down to an approximately constant value.

The anelastic strain rate at any moment during the deformation in Fig. 7.11 was subtracted using Fig. 7.10. Additivity of plastic and anelastic strain rates, as well as Boltzmann's superposition principle for the anelastic compliances and compliance rates (see Nowick and Berry, 1972, chapter 2) were assumed. For example, for $t \geq 501s$, the anelastic strain rate in Fig. 7.11 is:

$$\dot{\varepsilon}_a(t) = 1.1\text{MPa}\cdot\dot{J}_a(t) - 0.56\text{MPa}\cdot\dot{J}_a(t-330s) + 0.56\text{MPa}\cdot\dot{J}_a(t-501s), \qquad (7.60)$$

where $\dot{J}_a(t)$ is the compliance rate in Fig. 7.10.

The plastic strain rate evaluated in Fig. 7.11 indicates anomalous transients. After a stress reduction, the plastic strain rate decreases gradually to a lower and finally almost constant value. Similar behaviour, although less pronounced, is encountered after a stress increase.

The strain rate found after subtraction of the anelastic strain rates from the combined plastic and anelastic ones is thus not a unique function of the applied stress.

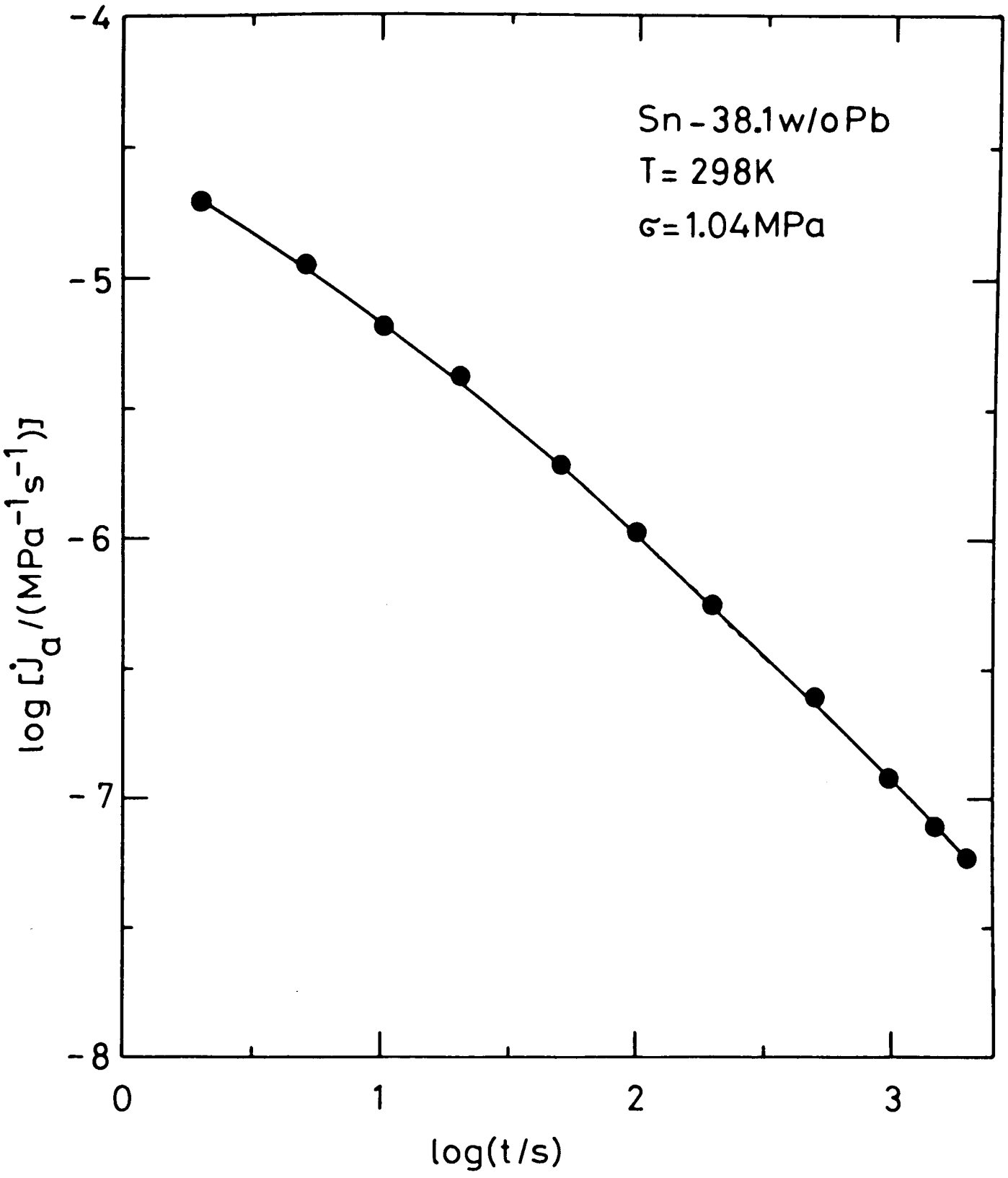

Fig. 7.10. Anelastic compliance rate of a Sn-38.1w/o Pb sample, determined from the elastic after-effect. Loading period prior to unloading: 3.6ks.

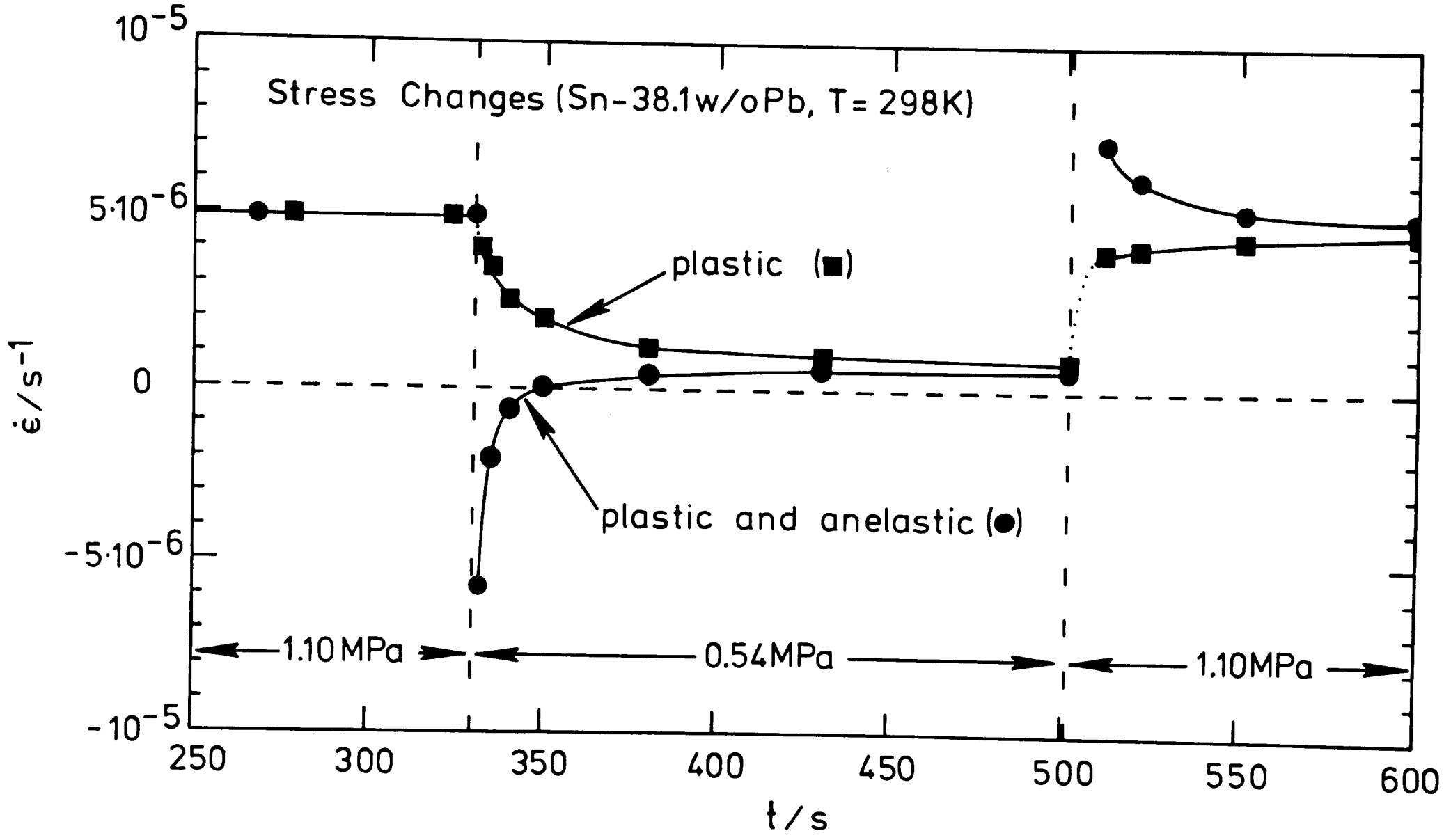

Fig. 7.11. Stress change experiments with a Sn-38.1w/o Pb sample. The initial loading started at t = 0 with σ = 1.1MPa. At t = 330s the stress was reduced by 0.56MPa and at t = 501s it was increased to 1.1MPa. The anelastic strain rate (see Fig. 7.10) was subtracted from the combined plastic and anelastic strain rate in order to obtain an estimate of the plastic strain rate.

However, subtracting of the anelasticity reduces the magnitude of the transient behaviour and in particular it removes the contradiction which would be found in Fig. 7.11 if anelasticity were neglected, namely, negative plastic strain rates in response to positive applied stresses.

7.3.2. The influence of anelasticity on the stress after discontinuous strain rate changes

In section 7.3.1 it has been demonstrated that the assumptions made in the mathematical treatment of transients in section 7.2.3 do not hold strictly. These assumptions nevertheless have been seen to provide a more realistic description of the mechanical behaviour of Sn-38.1w/o Pb then a description omitting anelasticity completely. It seems therefore reasonable to compare measured transients and those calculated with equation (7.39), by inserting in eqn. (7.39) independently measured parameters characterizing the plastic and anelastic properties.

Anelastic and plastic parameters employed for the calculation

The anelastic behaviour characterizing the tests described in this section [7.3.2] is represented in Fig. 7.12. The anelastic compliance rate, $\dot{J}_a$, may be approximated by sums of exponentials, using the "subtraction of tails"-method (Gibela and Wert, 1966). Three different approximations ((a), (b), and (c)) for $\dot{J}_a$ have been calculated from which sets of parameters τ_i, J_{oi} (i=1,2,3) describing $J_a(t)$ can be found by integration (see Fig. 7.12).

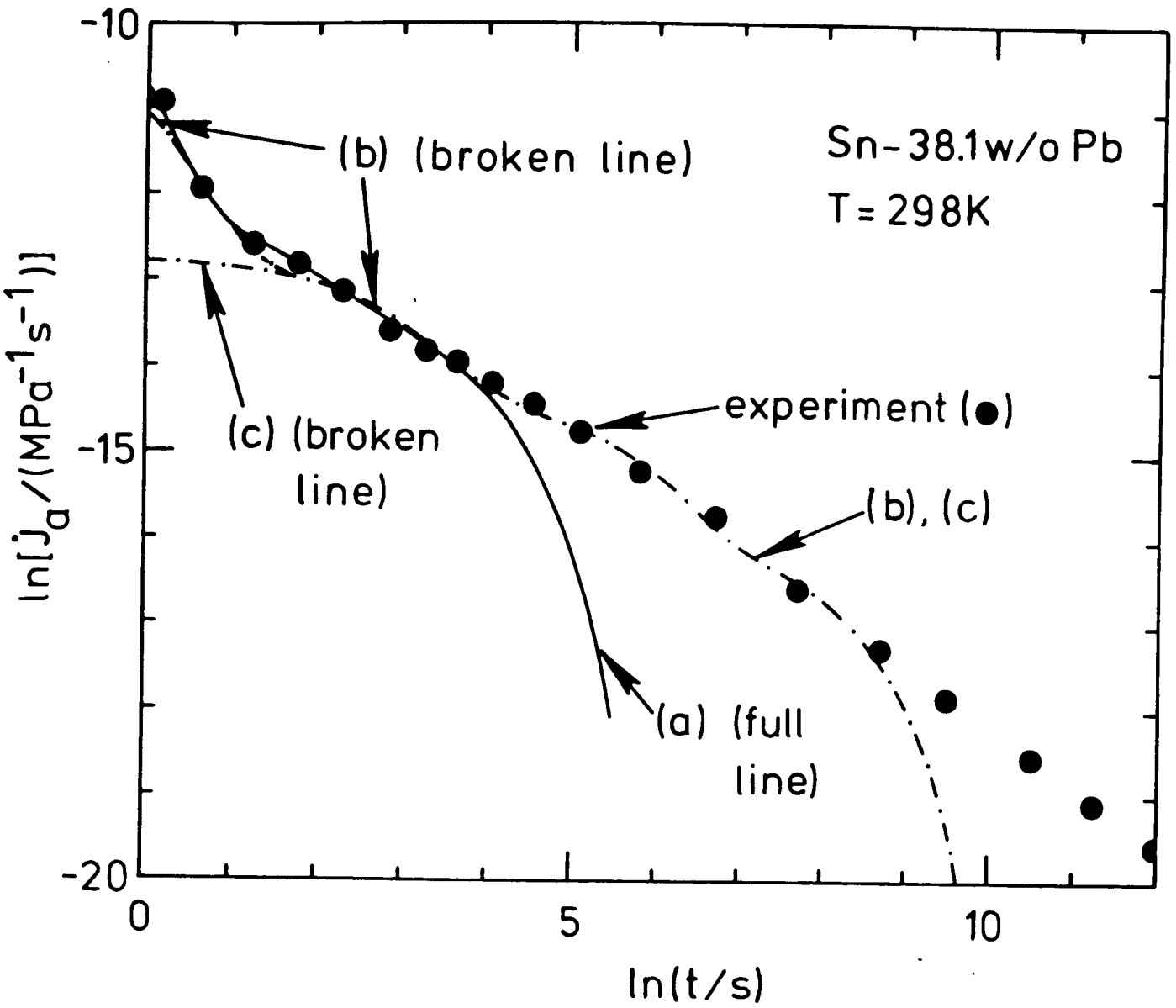

Fig. 7.12. Anelastic compliance rate of a Sn-38.1w/o Pb sample, determined from the elastic after-effect (the data corresponds to that in Fig. 7.2). The loading period prior to unloading was 345ks. The data points are approximated by 3 different sums of exponentials:

(a) $\dot{J}_a(t) = [1.2\cdot10^{-4}\ \exp(-t/0.5s) + 3.7\cdot10^{-6}\ \exp(-t/5s) + 1.8\cdot10^{-6}\ \exp(-t/50s)]MPa^{-1}s^{-1}$, therefore:
$J_{o1} = 6\cdot10^{-5}MPa^{-1}$; $\tau_1 = 0.5s$; $J_{02} = 1.85\cdot10^{-5}MPa^{-1}$; $\tau_2 = 5s$;
$J_{o3} = 9\cdot10^{-5}MPa^{-1}$; $\tau_3 = 50s$.

(b) $\dot{J}_a(t) = [5.8\cdot19^{-5}\ \exp(-t/0.8s) + 2.3\cdot10^{-6}\ \exp(-t/18s) + 5\cdot10^{-7}\ \exp(-t/300s) + 1.2\cdot10^{-7}\ \exp(-t/400s)]MPa^{-1}s^{-1}$, therefore: $J_{oo} = 4.64\cdot10^{-5}MPa^{-1}$; $\tau_o = 0.8s \sim 0$ (i.e. the Voigt element corresponding to J_{oo} and τ_o has been approximated by an elastic spring); $J_{o1} = 4.14\cdot10^{-5}MPa^{-1}$; $\tau_1 = 18s$; $J_{o2} = 1.5\cdot10^{-4}MPa^{-1}$; $\tau_2 = 300s$; $J_{o3} = 4.8\cdot10^{-4}MPa^{-1}$; $\tau_3 = 4000s$.

(c) approximation like (b), only the exponential with $\tau_o = 0.8s$ has been omitted (i.e. $J_{oo} = 0$).

The plastic properties are given by the parameters determined in Fig. 7.2. In the examples below, these parameters have been adjusted in order to take account of the relatively high strain rate sensitivity at high stresses (i.e. at 10MPa) or of local changes in the value of the proportionality constant, K (e.g. due to temperature fluctuations).

Loading with a constant strain rate

Fig. 7.13 shows the experimentally determined transient behaviour of a previously relaxed Sn-38.1w/o Pb sample (the applied stress was ~0 for a period of time much longer than the period of time used for the subsequent test) upon straining with a constant strain rate. In the actual experiment the extension rate was held constant. The strain rate is nevertheless approximately constant since the elongations employed in this and other tests discussed below are small. Using a stiffness of 2.38N/μm for the testing machine employed (type "Instron", see also chapter 4) the machine compliance, J_m, was calculated from eqn. (7.14).

In one approximation used for J_a (approximation (b) in Fig. 7.12) the smallest relaxation time, $\tau_o = 0.8s$, has been set to 0 and the compliance $J_{oo} = 4.64 \cdot 10^{-5} MPa^{-1}$ of the corresponding Voigt element has then to be added to the elastic compliances of the testing machine and the sample such that:

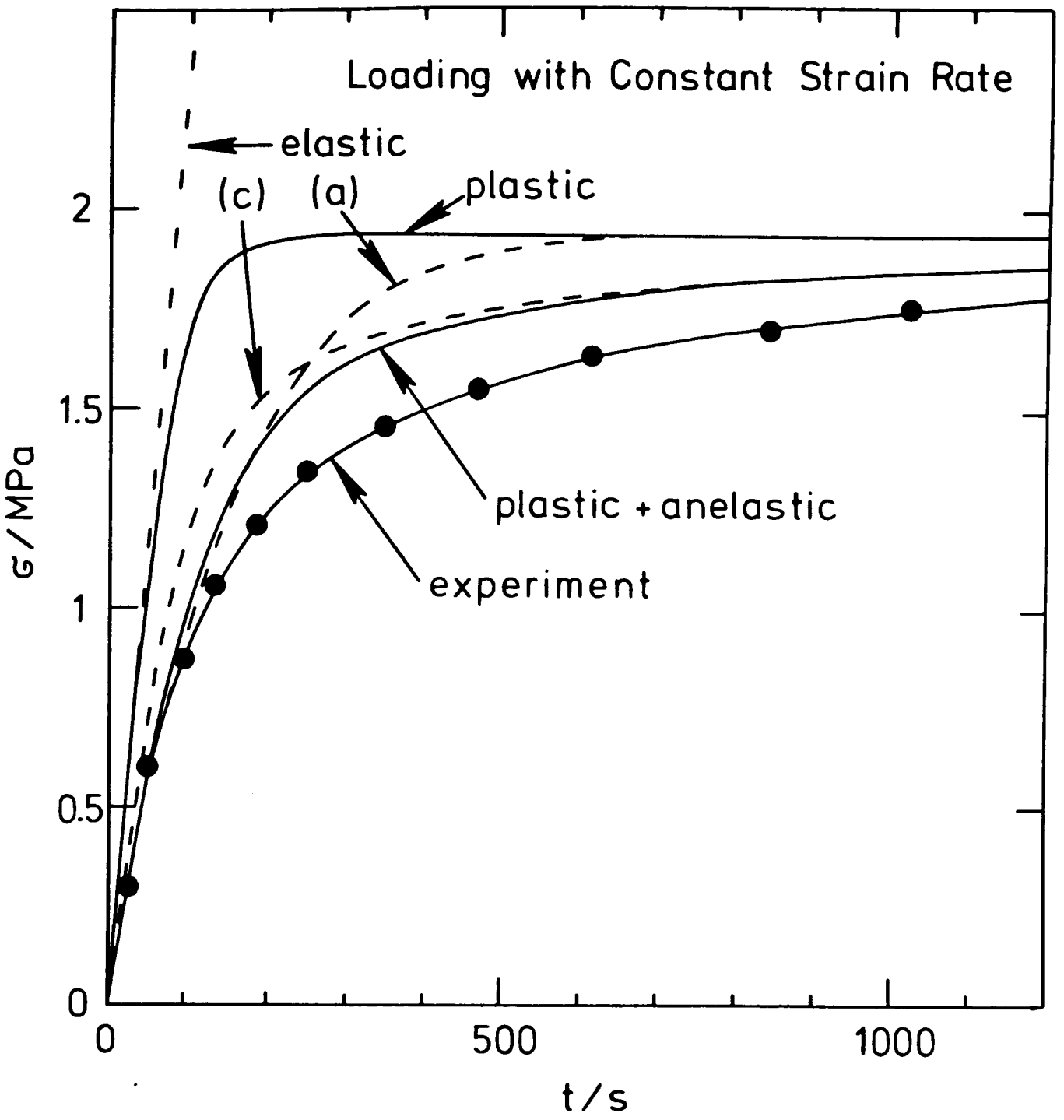

Fig. 7.13. Calculated and experimental transients for Sn-38.1w/o Pb upon loading with a constant strain rate. The data employed were: $\dot{\varepsilon}(t \geq 0) = 2.05 \cdot 10^{-5} s^{-1}$; $\sigma(t = 0) = 0$; $\varepsilon_{ai}(t = 0) = 0$ $(i = 1,2,3)$; $J_m = 3.91 \cdot 10^{-5} MPa^{-1}$; $J_s = 4.76 \cdot 10^{-5} MPa^{-1}$ (Subrahmanyam, 1972); $K = 480 MPas^{0.41}$; $m = 0.41$. In the curve termed "plastic + anelastic" the anelasticity is represented by approximation (b) in Fig. 7.12.
Curve (a): anelasticity represented by approximation (a) in Fig. 7.12.
Curve (c): anelasticity represented by approximation (c) in Fig. 7.12.
Curve termed "plastic": anelasticity omitted in the calculation of the transient.

$$J_e = J_m + J_s + J_{oo} \,. \qquad (7.61)$$

All the numerical values employed for the calculation of the transients are listed in the caption to Fig. 7.13.

Reasonable agreement between the calculated transient (annotated "plastic + anelastic in Fig. 7.13) and the experimental transient is obtained. The approximation of the shortest relaxation time (0.8s) by 0 should not introduce a serious error in the calculation since the lag of the strain behind the stress for the corresponding Voigt element is only of the order of a second and the transient extends over a relatively long period of time (~1000s). A perfect agreement cannot be expected since a plastic transient is present (if additivity between plasticity and anelasticity holds, see also Figs. 7.9 and 7.11). The initial plastic strain rate in the experiment is higher than the steady-state strain rate employed for the calculation. This explains why the measured stresses are lower than the calculated ones. It should be noted, however, that the "plastic + anelastic" curve in Fig. 7.13 agrees much better with the experiment than the "plastic" curve (obtained by straining a spring and a non-linear dashpot in series with a constant strain rate: use for example eqn. (7.5) with $\tau_o = J_o = 0$.

In order to demonstrate the influence of various degrees of anelasticity two additional transients have been calculated with different approximations of the

anelasticity. They are plotted as broken lines in Fig. 7.13. For the calculation of curve (c), the previously employed Voigt element with a relaxation time of 0.8s ~ 0s has been omitted and J_{oo} in eqn. (7.61) is therefore 0. Thus the total elastic compliance, J_e, is reduced. The stress increase during the transient is therefore faster than for the "plastic + anelastic" curve in Fig. 7.13.

In another example, relaxation times $\lesssim$50s have been used to represent the anelasticity. For $t \lesssim 50s$ the agreement between the calculated curve (approximation (a) in Fig. 7.13) and the experimental one is good. After longer times the calculated stress increases rapidly since the influence of Voigt elements with relaxation times larger than 50s is missing.

Strain rate cycling

The strain rate cycling behaviour of Sn-38.1w/o Pb is also significantly influenced by anelasticity. A typical experimental stress vs. time relationship is shown in Fig. 7.14 and compared with the transient calculated with eqn. (7.39). For the strain rate increase, the calculation results in stresses smaller than the measured ones. Probably the strain rate sensitivity has been underestimated. However, the general shape of the calculated curve (i.e. the values of $\dot{\sigma}(t)$) is in much better agreement with the experiment than the shape of the calculated plastic transient. This can be seen in particular from the calcu-

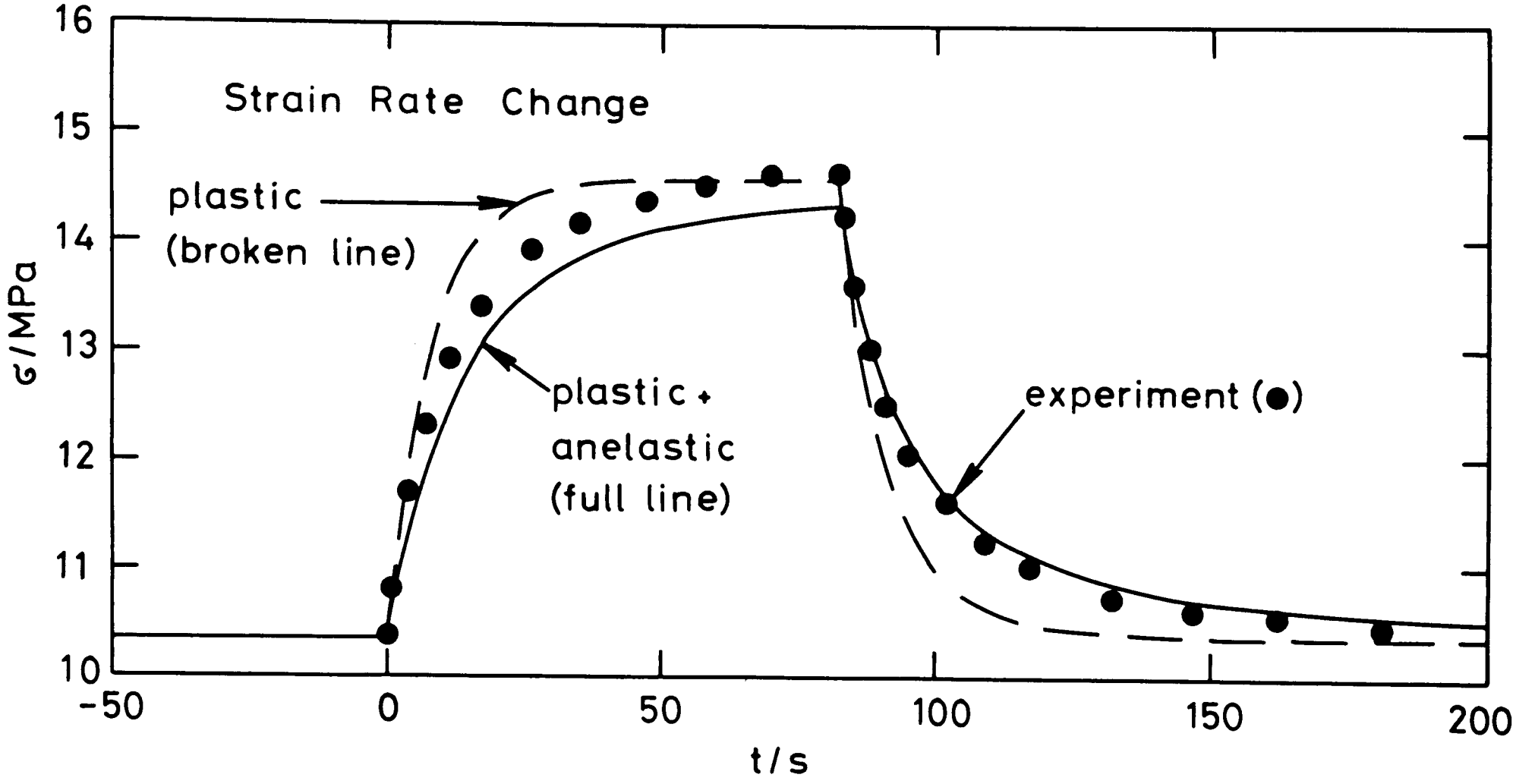

Fig. 7.14. Experimental and calculated transients after strain rate changes for Sn-38.1w/o Pb. Prior to the first strain rate change shown the sample was deformed with a stress of ~10.4MPa for ~150s. The data employed were:
$\dot{\varepsilon}(-150s \leq t \leq 0) = 4.62 \cdot 10^{-5} s^{-1}$; $\dot{\varepsilon}(0 \leq t \leq 82s) = 9.23 \cdot 10^{-5} s^{-1}$;
$\dot{\varepsilon}(t \geq 82s) = 4.62 \cdot 10^{-5} s^{-1}$;
$J_m = 4.5 \cdot 10^{-5} MPa^{-1}$; $K = 1380 MPa s^{0.49}$; $m = 0.49$; $J_e = 4.76 \cdot 10^{-5} MPa^{-1}$ (Subrahmanyam, 1972); τ_i, J_{oi} (i=1,2,3): approximation (a) in Fig. 7.12; $\varepsilon_{ai}(t = 0) = 6.22 \cdot 10^{-4}$; $\varepsilon_{a2}(t = 0) = 1.92 \cdot 10^{-4}$; $\varepsilon_{a3}(t = 0) = 8.87 \cdot 10^{-4}$.

lation following the strain rate reduction at t = 82s in Fig. 7.14.

Hedworth and Stowell (1971) suggested that after a strain rate change in a typical test there is an initially linear increase in the stress ($\dot{\sigma}$ = const.). They evaluated strain rate sensitivities using the difference between the stress immediately prior to a strain rate change and the stress for which the transient after the strain rate change deviates from linearity. Since Fig. 7.14 suggests that the shape of the transient is significantly influenced by anelasticity, the deviation of the initial transient from linearity should not be used to measure a parameter characterizing plastic deformation, namely, the strain rate sensitivity, unless proper account is taken of the anelasticity.

Stress relaxation

A Sn-38.1w/o Pb sample was tested in stress relaxation, after previous straining for various lengths of time. Two experimental results are depicted in Fig. 7.15. For the calculation according to eqn. (7.39), approximation (b) of the anelasticity shown in Fig. 7.12 has been used. Since the shortest relaxation time (0.8s) has been set to 0 in this approximation and the corresponding Voigt element has been approximated by an elastic spring the effective elastic compliance, J_e, has been increased. This explains why the calculated relaxations in Fig. 7.15 start with

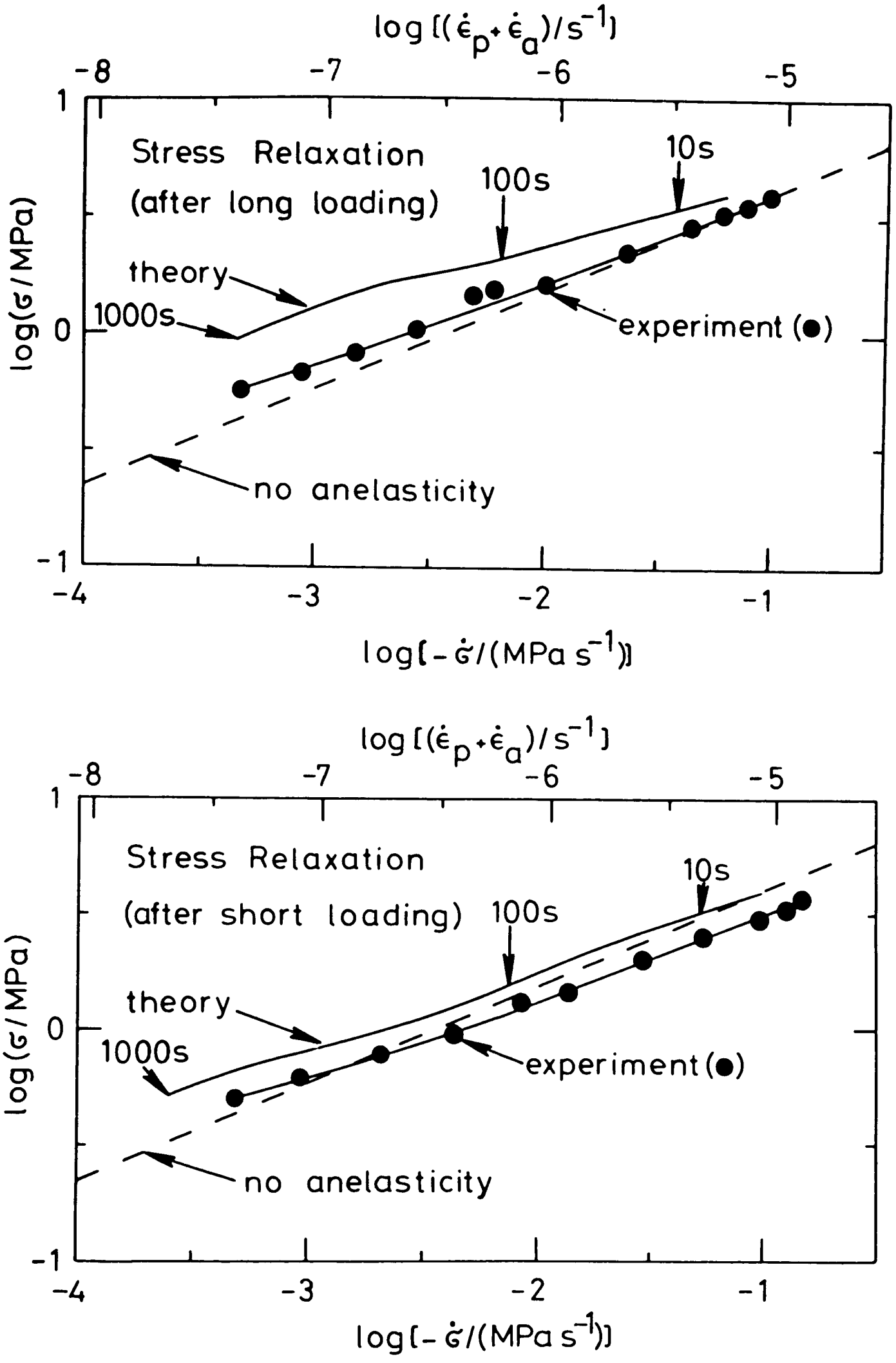

Fig. 7.15. Stress relaxation of Sn-38.1w/o Pb at 298K after long loading ($\dot{\varepsilon} = 8.19 \cdot 10^{-6} s^{-1}$ for 1330s) and after short loading ($\dot{\varepsilon} = 2.05 \cdot 10^{-5} s^{-1}$ for 38s) to a stress of ~3.9 MPa. The data employed were:
$J_m = 3.91 \cdot 10^{-5} MPa^{-1}$; $J_s = 4.76 \cdot 10^{-5} MPa^{-1}$ (Subrahmanyam, 1972); $K = 480 MPas^{0.41}$; $m = 0.41$; J_{oo}, τ_i, J_{oi} (i=1,2,3): approximation (b) in Fig. 7.12. Prior to the loading: $\varepsilon_{a1} = \varepsilon_{a2} = \varepsilon_{a3} = 0$, $\sigma = 0$.

noticeably smaller values of $|\dot{\sigma}|$ then the experimental ones. For times longer than 0.8s after the beginning of the relaxation, the approximation should not influence the result of the calculation significantly. Due to the slowing down of the relaxation, the strain of the Voigt element with τ = 0.8s should then approximately be in phase with the stress during the relaxation. The oscillations in the calculated curves are due to the approximation of the anelasticity by a sum of exponentials (compare also the effect of anelasticity on the stress relaxation if the anelasticity is represented by only one exponential (see Fig. 7.5)).

The experimental relaxation rates, $|\dot{\sigma}|$, for a given stress, are generally higher than the calculated ones which is in agreement with the presence of a transient for plastic deformation (see Figs. 7.9 and 7.11).

The effect of the anelasticity on the measured relaxations is not as strong as predicted. Whereas the average slope of the calculated curves in Fig. 7.15 is quite different for different lengths of the previous straining (i.e. m = 0.29 and m = 0.35), the duration of the previous straining does not seem to have much influence on the slope of the measured curves. This is also evident from more accurately controlled stress relaxation tests (Fig. 7.16). These tests have been performed with a modified creep rig (see also chapter 4) in which the whole loading train including the load cell was kept at

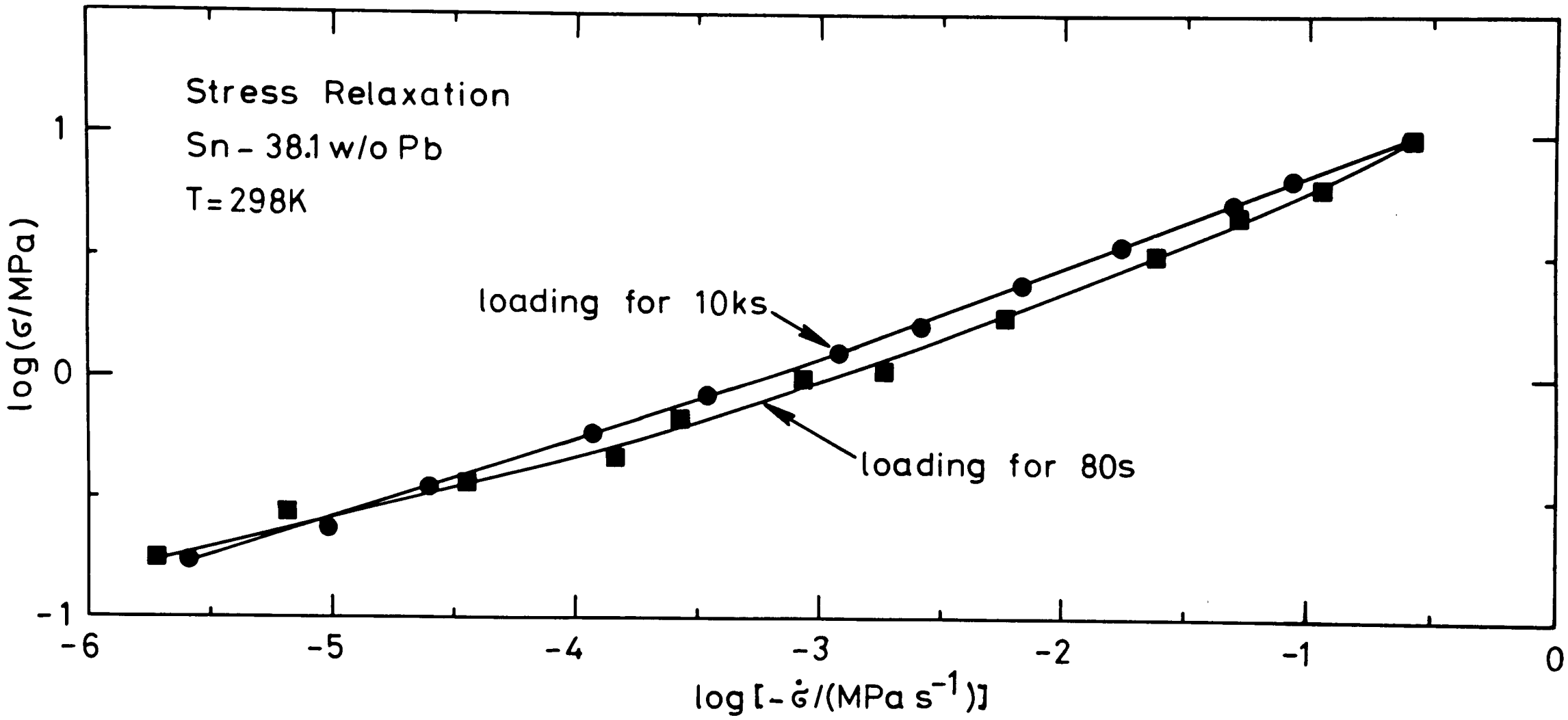

Fig. 7.16. Measured stress relaxation behaviour of Sn-38.1w/o Pb under carefully controlled conditions. The influence of anelastic strains has been varied by varying the length of the loading with 9.5MPa previous to the relaxation. The elastic compliance of the modified creep rig used for the measurement (see chapter 4) was estimated from the initial relaxation rate and is $\sim 2 \cdot 10^{-4} \mathrm{MPa}^{-1}$.

(298 ± 0.05)K during the relaxation in order to prevent inaccurate results owing to temperature fluctuations. The two curves shown are very similar, with the exception of the beginning of the relaxation where their slopes differ markedly.

In spite of the limitations of the theory, one main feature predicted is born out by the experiments, namely, that anelasticity reduces the slope of the relaxation curves in a $\log\sigma$ vs. $\log\dot{\sigma}$ plot. It can therefore certainly not be neglected during a stress relaxation test as has already been pointed out in section 7.2.2. This view is opposed to Murty's (1973) results. He did not find an appreciable difference between data found from stress relaxation tests with Sn-Pb by conventional evaluation (neglecting anelasticity), and data generated by strain rate cycling. However, he compared his data only over ~ 1 decade in the strain rate. The influence of anelasticity on stress relaxation tests may therefore have been overlooked.

The agreement between Geckinli and Barrett's (1974) result and the calculated curve (a) in Fig. 7.5 is now seen to be purely coincidental. Neither the stress relaxation experiments performed in the present work nor the calculated curves using the model in Fig. 7.8 substantiate their result. The reason for this discrepancy is not known.

Stress transient dip tests

A series of stress transient dip tests (Gibbs, 1966) was performed with a Sn-38.1w/o Pb sample. In the first example a previously strained sample was unloaded as rapidly as possible by applying a negative strain rate for a short period of time and, immediately afterwards, the strain rate was set equal to 0 (Fig. 7.17). Reloading is observed, caused by the anelastic strain stored during the previous straining. The reloading in turn causes plastic deformation. Later on, ordinary stress relaxation (i.e. a decrease in the load) is observed.

Equation (7.39) was successively solved starting with unloading at t = 0 and with appropriate values of the anelastic strains of the three Voigt elements ("realistic unloading" in Fig. 7.17). As would be expected from the plastic transient found in Fig. 7.11 the predicted stresses increase to higher values than the measured ones. However, the stress rates immediately after the stress drop are similar.

Another calculated curve presented in Fig. 7.17 ("instantaneous unloading") demonstrates that the rate with which the unloading occurs is important. For instantaneous unloading, much higher reloading-stresses are predicted than for realistic unloading. In terms of the model in Fig. 7.8, the fastest Voigt element employed (τ_1 = 0.5s) does not contract during instantaneous unloading and thus can cause very high reloading. For realistic unloading rates (in the calculated case ~ 7s

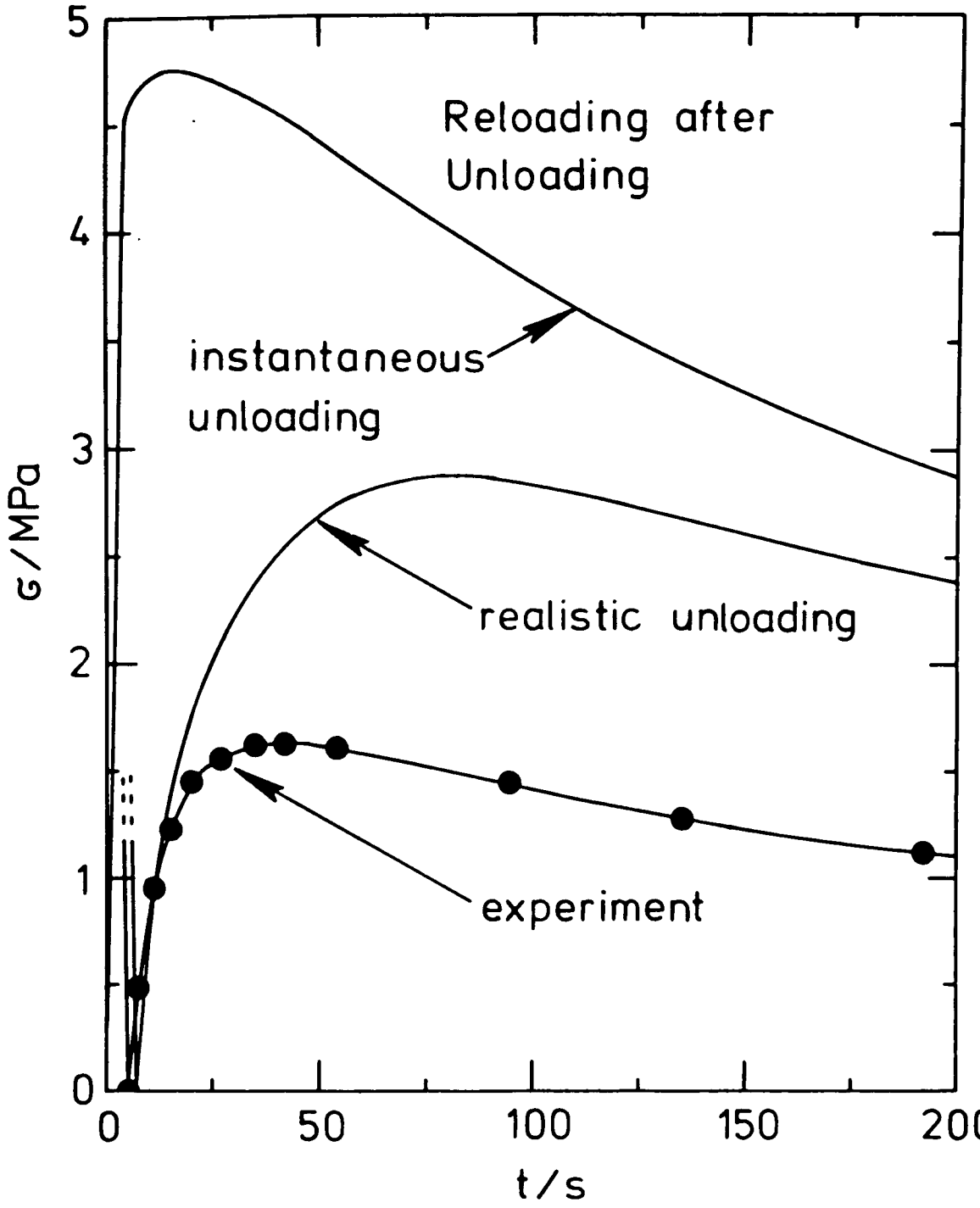

Fig. 7.17. Experimental and calculated mechanical behaviour of Sn-38.1w/o Pb at 298K after reducing the stress quickly to 0 and immediately afterwards, keeping the total strain (of testing machine + sample) constant. Previously to the unloading at t = 0, the sample was loaded for ~300s with 10MPa. The initial anelastic strains were $\varepsilon_{ai}(t = 0) = 6 \cdot 10^{-4}$, $\varepsilon_{a2}(t = 0) = 1.85 \cdot 10^{-4}$ and $\varepsilon_{a3}(t = 0) = 8.98 \cdot 10^{-4}$. The strain rate employed for the unloading was $\dot{\varepsilon} = -2.24 \cdot 10^{-4} s^{-1}$. The time needed for unloading was 5s (in the calculation 7s). Other values employed for the calculation: $J_e = 9.45 \cdot 10^{-5} MPa^{-1}$; $K = 600 MPas^{0.41}$; $m = 0.41$, τ_i, J_{oi} (i=1,2,3): approximation (a) in Fig. 7.12.

were needed for complete unloading), however, the strain of the fastest Voigt element is nearly in phase with the actual stress and does therefore not contribute much to the reloading. In this case, the Voigt element with $\tau_1 = 0.5s$ only introduces an additional, approximately elastic compliance and causes therefore the reloading due to the Voigt elements with $\tau_2 = 5s$ and $\tau_3 = 50s$ to be less pronounced.

In Fig. 7.18 the measured stress vs. time behaviour after partial unlaodings is shown, together with computed curves. The calculated stress increments, during the first second after the completion of the partial unloadings, may have been caused by an overestimate of the anelastic strain rates for short times (approximation (a) in Fig. 7.12). After the initial stress increase the predicted curves are in reasonable agreement with the experimental ones, for unloadings by less than ~50% of the previously applied stress. This demonstrates that the influence of anelastic strains on dip tests can certainly not be neglected.

7.4. Summary and conclusions

The influence of anelasticity on the transient behaviour of Sn-38.1w/o Pb has been investigated. A model in which the anelasticity is described by a single relaxation time (one Voigt element) and the plasticity by a non-linear viscous dashpot is discussed using realistic

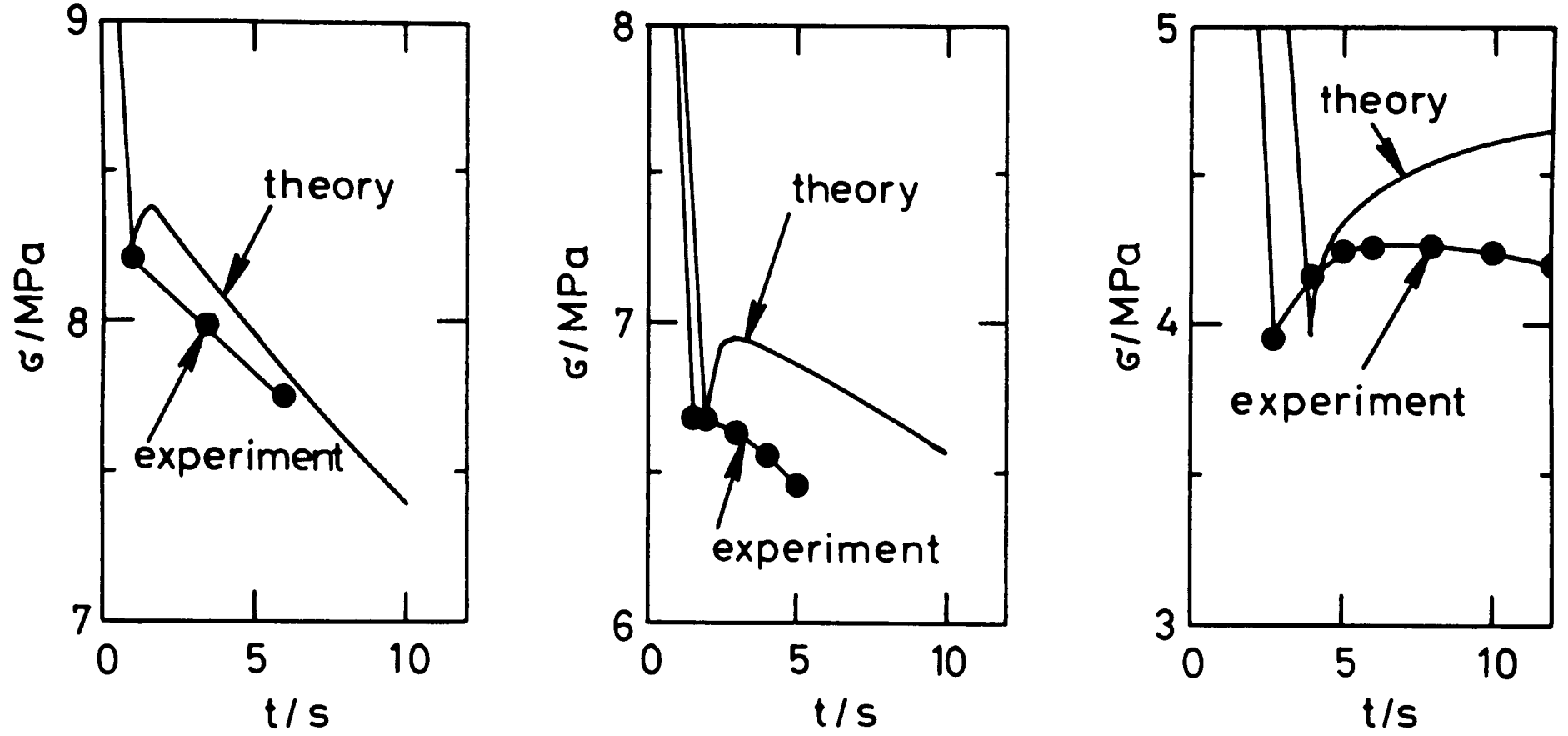

Fig. 7.18. Experimental and calculated mechanical behaviour of Sn-38.1w/o Pb at 298K during relaxation after partial unloading. The data employed were:
$J_e = 9.45 \cdot 10^{-5} MPa^{-1}$; $K = 600 MPas^{0.41}$, $m = 0.41$, τ_i, J_{oi} (i=1,2,3): approximation (a) in Fig. 7.12. Strain rate used for the unloading starting at t = 0: $\dot{\varepsilon} = -2.24 \cdot 10^{-4} s^{-1}$. The anelastic strains prior to the unloading were evaluated from the stress history prior to the unloading. Immediately prior to the unloading they were, in all three examples shown: $\varepsilon_{a1} = 6 \cdot 10^{-4}$, $\varepsilon_{a2} = 1.85 \cdot 10^{-4}$, $\varepsilon_{a3} = 8.55 \cdot 10^{-4}$.

data for Sn-38.1w/o Pb. In particular the stress relaxation behaviour can be markedly influenced by anelasticity. As opposed to stress relaxation tests without anelasticity, the stress rate, $\dot{\sigma}$ (t), as a function of the time, t, at which the relaxation starts, is not generally proportional to the plastic strain rate. In particular, a plateau region in a plot of log σ vs. log($-\dot{\sigma}$) cannot be readily identified with a threshold stress for plastic deformation. Similarly, a region with a slope of 1 in such a plot does not necessarily indicate a plastic deformation mechanism with a strain rate sensitivity of 1. The model with one relaxation time also demonstrates the way in which anelasticity creates an apparent internal stress. After rapid unloading to the apparent internal stress and, immediately afterwards, keeping the total strain constant, $\dot{\sigma}$ is initially 0. For a strain rate sensitivity $m < 1$, the ratio of the apparent internal stress to the previously applied stress decreases with increasing applied stress.

The calculated examples show that transient tests can only be used to measure plastic properties if proper account is taken of the anelasticity. Otherwise, combined plastic and anelastic strain rates are measured and it becomes difficult to disentangle the separate effects.

In a rheological model more accurate than that mentioned above the anelasticity is represented by three relaxation times (three Voigt elements). The applicability of the model to transients in Sn-38.1w/o Pb is critically ex-

amined by estimating the influence of anelasticity on stress change tests. Two assumptions of the model, namely, linear additivity of plastic and anelastic strains, and a unique relationship between the applied stress and the plastic strain rate, do not hold rigorously. A better model would require more than three relaxation times for the anelasticity. In addition, the strain dependence of the plastic strain rate as well as the way according to which anelastic and plastic strains should be combined would need further investigation and the model would have to be improved accordingly.

However, the incorporation of anelasticity using the simple assumptions above constitutes a considerable improvement over a treatment neglecting anelasticity completely. The results of strain rate change tests, stress relaxation tests and stress transient dip tests (stress relaxation after partial unloading) are compared with the predictions of the model with three relaxation times. The transient behaviour of Sn-38.1w/o Pb upon straining with a constant strain rate or after a more general strain rate change can be reasonably well predicted. The strain rate sensitivity found from stress relaxation tests with Sn-38.1w/o Pb by conventional evaluation (i.e. neglecting anelasticity) is shown to be smaller than that characterizing the plastic properties of this material. Stress transient dip tests are also significantly influenced by anelasticity. The rate with which the partial unloading required for these tests occur can be important, due to the presence of short relaxation times characterizing the anelasticity.

CHAPTER 8

CONCLUSIONS AND SUGGESTIONS FOR FURTHER WORK

Conclusions

(1) The mechanisms which may account for superplastic deformation have been outlined. Bulk mechanisms (which cause grain strains) predict strain rates which depend on the stress, σ, and the grain size, L, as σ/L^2, σ/L^3, σ^2/L or σ^2/L^2. Two known lattice dislocation mechanisms have been applied to grain boundary dislocations (GBDs). If grain boundary sliding (GBS) controls the strain rate, dependencies like σ/L, σ^2/L, σ^3/L or σ^2/L^2 are possible. Grain size dependencies different form 1/L arise because of the interaction of the GBDs in the intersecting grain boundaries (GBs). The influence of simultaneous grain strain and grain deformation on the superplastic strain rate as well as processes which inhibit superplasticity have been discussed.

(2) Known mechanisms which may be of importance for the anelasticity observed in superplastic materials have been reviewed. Two mechanisms based on grain boundary tension and on the viscous relaxation of GBD pile-ups, respectively, have been suggested and the equations describing the models quantitatively have been derived and discussed. Only the GB tension mechanism explains relaxation strengths (= ratio of anelastically recovered to elastically recovered strain) significantly higher than 1. The GBD mechanism, on the other hand, is capable of predicting a wide range of relaxation times characterizing the anelasticity.

(3) The plastic properties of superplastic Sn-Pb eutectic (Sn-38.1w/o Pb) and Sn-2w/o Pb have been measured at temperatures between 298K and 403K at strain rates as low as $10^{-10}s^{-1}$, using a high-resolution creep rig. No threshold stress for plastic deformation was found although stresses as low as 0.1MPa were employed. The dependencies of the strain rate on the stress are qualitatively similar in both alloys investigated. This implies that the underlying deformation mechanisms are similar.

GB diffusion creep (Coble creep) has been established in Sn-2w/o Pb for grain sizes larger than ~50μm The measured Coble creep rates are in approximate agreement with the creep rates calculated with the tracer GB self-diffusion coefficient for pure Sn. At low stress levels the measured strain rates are lower than the calculated Coble creep rates and for grain sizes of the order of 10μm Coble creep in Sn-2w/o Pb is completely inhibited by an interface process. Calculated stress-strain rate relationships using GBS mechanisms, Coble creep and lattice dislocation creep predict the measured Sn-2w/o Pb data well. The measured dependence of the strain rate on the grain size in Sn-38.1w/o Pb (approximately $\dot{\varepsilon} \alpha L^{-2}$) implies that the interface process is not conventional GBS (i.e. $\dot{\varepsilon} \alpha L^{-1}$) but rather that intersecting GBs or the defects contained in them interact.

In fine-grained Sn-38.1w/o Pb relatively high threshold stresses, caused by the GBD line tension, are predicted. The experimental results can therefore be interpreted as

indicating that GBD line tensions are lower than those of lattice dislocations with comparable Burgers vectors.
(4) The anelastic contraction following the unloading of previously loaded samples (elastic after-effect) has been studied. At the temperatures employed (298K to 328K) anelastic contractions can be detected as long as ~2 weeks after unloading. The relationship $\varepsilon_a \propto t^{1/2}$, where ε_a is the strain recovered after a time, t, after unloading, holds for a major part of the relaxations. The relationship above corresponds to a relaxation spectrum extending over up to 6 decades in time. For a particular time after unloading, the anelastically recovered strains are approximately proportional to the stress and the inverse grain size. The underlying mechanism is thermally activated with an activation energy lower than that for GB self-diffusion.

An extraordinary feature of the observed anelasticity is the high relaxation strength: it exceeds values of 100. Anelastic strains as high as 0.2% are recovered.

None of the known mechanisms of anelasticity can fully explain the measured anelastic strains. A mechanism based on the viscous relaxation of GBD pile-ups, however, explains approximately the dependence of the anelastic strains on the stress, the grain size, the time after unloading and the temperature. It fails in explaining the high relaxation strengths found. The possibility that GBD interaction is weaker than lattice dislocation interaction which would result in an increase in the theoretical relaxation strength

is discussed. The interaction of GBDs might be relatively weak owing to their special structure (as compared to lattice dislocations) and would probably be associated with relatively low GBD self-energies and line tensions. Therefore, both plastic and anelastic properties are in agreement with the hypothesis that GBDs interact much more weakly than lattice dislocations with similar Burgers vectors. Such a hypothesis would also be in qualitative agreement with the extremely small spacings which GBDs may have, e.g. structural dislocations (Smith and Pond, 1976) or experimentally observed, piled-up GBDs (Kegg, Horton and Silcock, 1973).

(5) The influence of anelasticity on the deformation behaviour of Sn-38.1w/o Pb has been investigated. A rheological model consisting of a Voigt element (anelasticity), a non-linear viscous dashpot (plasticity) and a spring (elasticity) has been described mathematically with a differential equation. Using realistic plastic and anelastic data for Sn-38.1 w/o Pb, transient tests (stress change tests, stress relaxation tests, stress transient dip test) involving anelasticity have been discussed. In particular, stress relaxation tests are markedly influenced by anelasticity. The relaxation rate, $\dot{\sigma}$, is not in general proportional to the plastic strain rate. A plateau region in a plot of log σ vs. log$(-\dot{\sigma})$ cannot be readily identified with a threshold stress for plastic deformation. Similarly a region with a slope of 1 in such a plot does not necessarily indicate a plastic deformation mechanism with a strain rate sensitivity of 1. The calculated examples show that

transient tests can only be used to measure plastic properties if proper account is taken of the anelasticity. Otherwise combined plastic and anelastic strain rates are measured and it becomes difficult to disentangle the separate effects.

In a rheological model more accurate than that above the anelasticity has been represented by three Voigt elements. The applicability of this model to the deformation of Sn-38.1 w/o Pb has been critically examined. Transients calculated by solving numerically the 4th order differtial equation describing the model have been compared with measured transients and in a number of cases reasonable agreement is obtained. All transients are much more accurately described by the present model than by a model neglecting anelasticity completely.

Suggestions for further work

Further work is needed in order to find out whether the mechanical properties in fine-grained materials are indeed related to GBDs and what the interaction between these dislocations is like. A few ideas about the kind of work which should be done in order to try to answer these and some other questions will now be outlined:
(1) Apart from the Sn-Pb alloys examined here, Zn-22w/o Al also exhibits strong anelasticity (Eastgate, 1978). By investigating a range of different superplastic alloys it should be confirmed that the anelasticity observed

here is indeed a general phenomenon associated with small grains or a large portion of GBs, respectively. Superplastic alloys amenable to transmission electron microscopy (TEM), e.g. Al-4w/oCu-0.5w/oZr (Watts, Stowell, Baikie and Owen, 1976) and with anelastic properties similar to those of Sn-Pb should be critically examined for the presence of GBDs. If anelasticity is caused by GBDs it should not be difficult to preserve their structure for TEM examination since anelasticity and therefore the structural changes associated with it have been seen to be relatively slow processes. Since the anelastic strains are thermally activated it should be possible to preserve the structures associated with them effectively by employing materials which deform anelastically only at high absolute temperatures. Then the diffusion rates at room temperature, even in the thin foils required for TEM investigations, should be low enough to guarantee a stable structure. The preservation of the deformation-induced structure after cooling under load may also be verified by checking whether the anelasticity can be frozen in, i.e. whether subsequent annealing of a deformed and cooled (under load) sample leads to anelastic deformation. If the microscopic results are encoura ing, GBD structures might be studied at different stages of the elastic after-effect in order to obtain information on the kinetics and interaction of GBDs. Similar studies should also be done to find out whether the plastic properties at low stresses are indeed related to GBDs.

(2) Sn-2w/o Pb, with equiaxed grains, should be investigated in more detail, for lower stresses, lower strain rates, and a wide range of grain sizes. This alloy is preferable to Sn-38.1w/o Pb because the diffusion along its GBs is described by only one diffusion coefficient which is well known and because Coble creep as well as its inhibition can be verified. Sn-2w/o Pb is considered to have a sufficiently stable grain size to enable such tests to be performed and it is also very well suited for optical metallography. Relatively big samples may be needed for the measurements with the large grain sizes (e.g. 250μm). Experiments in torsion or with spiral-shaped samples may be considered in order to improve the strain resolution.

The aim of these measurements would be to determine the grain size dependence of the interface control mechanism found in Sn-2w/o Pb,i.e., to determine whether intersecting GBs or the defects associated with them interact. For large grains the influence of the interaction is expected to be relatively weak (the ratio of the GB area to the length of the intersections is high) and an inverse grain size dependence of the plastic strain rate is expected. For small grain sizes, however, a realationship more like $\dot{\varepsilon} \alpha 1/L^2$ is predicted. Also of interest would be the determination of the activation energy for plastic deformation in this region. The maximum relaxation strengths and their dependence on the grain size should be studied since this could give additional information on the properties of GBDs.

(3) Valuable information might also be found by measuring the anelasticity of a superplastic material with a range of grain sizes extending from amorphous over fine-grained to coarse-grained. Even if the GBD line tension is very small, threshold stresses should be detected if the grain sizes are sufficiently small. Since a GBDdescription of anelasticity is not likely to hold for amorphous materials the increase in the relaxation strength for decreasing grain sizes observed for Sn-Pb should be followed by a decrease of the relaxation strength for very small grain sizes or for the amorphous state.

(4) Atomistic calculations of the properties and kinetics of GBDs in GBs are needed. The predictions of such calculations would provide the ultimate test for the validity of the hypothesis advanced above that GBDs interact more weakly than lattice dislocations.

(5) A better knowledge of the plastic and anelastic properties of fine-grained materials and in particular of the creation and annihilation of GBDs would assist in a better uderstanding of the influence of anelasticity on transients. If both plasticity and anelasticity are caused by GBDs neither the assumption of transient-free plasticity nor the additivity of plastic and anelastic strains are likely to hold and the theory of transient deformation advanced above would have to be modified correspondingly.

References

Alden, T. H. (1967). Acta Metall., 15, 469-480.

Alden, T. H. (1969a). Acta Metall., 17, 1435-1440.

Alden, T. H. (1969b). J. Aust. Inst. Met., 14, 207-216.

Aldrich, J. W., and D. H. Avery (1970). Alternating Strain Behaviour of a Superplastic Metal. In J. J. Burke and V. Weiss (Eds.), Ultrafine-Grain Metals. Proc. 16th Sagamore Army Materials Research Conference, Syracuse University Press, pp.397-413.

Ashby, M. F. (1969). Scr. Metall., 3, 837-842.

Ashby, M. F. (1972). Surf. Sci., 31, 498-542.

Ashby, M. F. and R. A. Verrall, (1973). Acta Metall., 21, 149-163.

Ashby, M. F., G. H. Edward, J. Davenport and R. A. Verrall (1978). Acta Metall., 26,1379-1388.

Avery, D. H. and J. M. Stuart (1968). The Role of Surfaces in Superplasticity. In J. J. Burke, N. L. Reed, V. Weiss (Eds.), Proc. 14th Sagamore Army Materials Research Conference, Syracuse University Press, pp.371-390.

Ball, A. and M. M. Hutchison (1969). Met. Sci., 3, 1-7.

Balliett, R. W., J. A. Forster and J. L. Duncan (1977). Metall. Trans., 9A, 1259-1264.

Bardeen, J. and C. Herring (1952). In W. Schockley (Ed.), Imperfections in Nearly Perfect Crystals. John Wiley & Sons, New York, pp. 261-288.

Baudelet, B. and M. Suery (1972). J. Mater. Sci., 7,512-516.

Blum, W. and F. Pschenitzka (1976). Z. Metallkd., 67, 62-65.

Burton, B. (1971). Scr. Metall., 5, 669-672.

Burton, B. (1972). Mater. Sci. Eng., 10, 9-14.

Burton, B. (1977a). Diffusional Creep of Polycrystalline Materials. In Y. Adda, A. D. Le Claire, L. M. Slifkin and F. H. Wöhlbier (Eds.), Diffusion and Defect Monograph Series, No. 5, TRANS TECH S. A., Aedermannsdorf, Switzerland.

Burton, B. (1977b). Met. Sci., 11, 245-248.

Burton, B. and G. L. Reynolds (1974). Philos. Mag., 29, 1359-1370.

Cannon, W. R. (1971). Philos. Mag., 23, 1489-1497.

Cannon, W. R. and W. D. Nix (1973). Philos. Mag., 27, 9-16.

Cline, H. E. and T. H. Alden (1967). Trans. Metall. Soc. AIME, 239, 710-714.

Coble, R. L. (1963). J. Appl. Phys., 34, 1679-1682.

Coiley, J. A. (1974). Physics in Technology, 5, 86-90.

Cottrell, A. H. (1964). The Mechanical Properties of Matter. John Wiley & Sons, New York.

Cottrell, A. H. (1968). An Introduction to Metallurgy. William Clowes&Sons, London and Beccles.

Crossland, I. G. and B. D. Clay (1977). Acta Metall., 25, 929-937.

Crossman, F. W. and M. F. Ashby (1975). Acta Metall., 23, 425-440.

Cutler, C. P. and J. W. Edington (1971). Met. Sci. J., 5, 201-205.

Dawson, T. H. (1972). Metall. Trans., 3, 3201-3204.

Dingley, D. J. (1970). 3rd S. E. M. Symposium I.I.T.R.I., Chicago, pp. 329-337.

Eastgate, D. J. (1978). Viscoelastic Properties of Aluminium Alloys at High Temperatures. Part-II-Thesis, Oxford.

Edington, J. W., K. N. Melton and C. P. Cutler (1976). Prog. Mater. Sci., 21, 61-170.

Exner, H. E. (1972). Int. Metall. Rev., 17, 25-42.

Feltham, P. (1960-61). J. Inst. Met., 89, 210-214.

Friedel, J. (1964). Dislocations. Pergamon Press, Oxford.

Friedel, J., C. Boulanger and C. Crussard (1955). Acta Metall., 3, 380-391.

Garofalo, F., O. Richmond and W. F. Domis (1962). J. Basic Eng., 84, 287-293.

Gates, R. S. (1973). Acta Metall., 21, 855-864.

Geckinli, A. E. and C. R. Barrett (1974). Scr. Metall., 8, 115-120.

Geckinli, A. E. and C. R. Barrett (1976). J. Mater. Sci., 11, 510-521.

Gibbs, G. B. (1966). Philos. Mag., 13, 317-329.

Gibela, R. and C. A. Wert (1966). Acta Metall., 14, 1095-1103.

Gifkins, R. C. (1973). J. Aust. Inst. Met., 18, 137-145.

Gifkins, R. C. (1976). Metall. Trans., 7A, 1225-1232.

Gleiter, H. and B. Chalmers (1972). Prog. Mater. Sci., 16, 1-272.

Green II, H. W. (1970). J. Appl. Phys., 41, 3899-3902.

Greenwood. G. W. (1970). Scr. Metall., 4, 171-174.

Haasen, P. (1978). Physical Metallurgy. Cambridge University Press, Cambridge.

Hammamy, A. K., W. Dubofsky and H. P. Stüwe (1977). Z. Metallkd., 68, 417-420.

Hansen, M. and K. Anderko (1958). Constitution in Binary Alloys. McGraw-Hill, New York, Toronto and London.

Harper, J. and J. E. Dorn (1957). Acta Metall., 5, 61-170.

Hayden, H. W., R. C. Gibson , H. F. Merrick and J. H. Brophy (1967). A. S. M. Trans. Q., 60, 3-14.

Hazzledine, P. M. and D. E. Newbury (1976). In G. A. Chadwick and D. A. Smith (Eds.), Grain Boundary Structure and Properties. Academic Press, London. pp. 235-264.

Hedworth, J. and M. J. Stowell (1971). J. Mater. Sci., 6, 1061-1069.

Herring, C. (1950). J. Appl. Phys., 21, 437-445.

Hestbech, J., E. W. Langer and A. Rosen (1971). J. Inst. Met., 99, 306-309.

Heumann, Th. and H. Wulff (1976). Scr. Metall., 10, 1001-1002.

Hilliard, J. E. and J. W. Cahn (1960). The Effect of High Pressures on Transformation Rates. In F. P. Bundy, W. R. Hibbard, Jr., and H. M. Strong (Eds.), Progress in Very High Pressure Research, John Wiley & Sons, New York and London, pp. 109-125.

Hirth, J. P. and J. Lothe (1968). Theory of Dislocations. McGraw-Hill, New York.

Holt, D. A. and W. A. Backofen (1966). ASM Trans. Q., 59, 755-768.

Homer, C. and B. Baudelet (1977). Scr. Metall., 11, 185-189.

Hondros, E. D. and M. P. Seah (1977). Int. Metall. Rev., 22, 262-301.

Horiuchi, R., A. B. El-Sebai and M. Otsuka (1974). Phys. Status Solidi A, 21, K89.

Humphries, C. W. and N. Ridley (1977). J. Mater. Sci., 12, 851-853.

Ishida, Y. and M. McLean (1973). Philos. Mag., 27, 1125-1134.

Jones, R. B. and R. H. Johnson (1966). ASM Trans. Q., 59, 356-359.

Kaibyschev, O. A., B. V. Rodionov and R. Z. Valiev (1978). Acta Metall., 26, 1877-1886.

Kê, T. S. and C. Zener (1950). In Symposium on the Plastic Deformation of Crystalline Solids. Mellon Institute, Pittsburgh. ONR Document Navexos-P-834. p. 185.

Kegg, G. R., C. A. P. Horton and J. M. Silcock (1973). Philos. Mag., 27, 1041-1055.

Krivoglaz, M. A. (1960). Phys. Met. Metallogr., 10, No. 4, 1-19.

Kutschej, R. and H. P. Stüwe (1977). Z. Metallkd., 68, 779-782.

Langdon, T. G. (1970). Philos. Mag., 22, 689-700.

Lange, W., A. Hassner and I. Berthold (1961). Phys. Status Solidi, 1, 50-61.

Lange, W. and D. Bergner (1962). Phys. Status Solidi, 2, 1410-1414.

Lee, D. (1969). Acta Metall., 17, 1057-1069.

Lifshitz, I. M. (1963). Sov. Phys. J. E. T. P. (Engl. Transl.), 17, 909-920.

Lloyd, G. J. and R. J. McElroy (1975). Philos. Mag., 32, 231-244.

Lubahn, J. D. and R. P. Felgar (1961). Plasticity and Creep of Metals. J. Wiley & Sons, Inc., New York and London.

Martin, P. J. and W. A. Backofen (1967). ASM Trans. Q., 60, 352-359.

Melton, K. N., C. P. Cutler and J. W. Edington (1975). Scr. Metall. 9, 515-520.

Misro, S. C. and A. K. Mukherjee (1975). In J. C. M. Li, A. K. Mukherjee (Eds.), Rate Processes in Plastic Deformation. John E. Dorn Memorial Symposium, Cleveland, Ohio, American Society for Metals. pp. 434-458.

Mitchel, T. E., S. S. Heckner and R. L. Smialek (1965). Phys. Status Solidi, 11, 585-594.

Mohamed, F. A. and T. G. Langdon (1973). Philos. Mag., 27, 1125-1134.

Mohamed, F. A. and T. G. Langdon (1974). Metall. Trans., 5, 2339-2345.

Mohamed, F. A. and T. G. Langdon (1975a). Philos. Mag., 32, 697-709.

Mohamed, F. A. and T. G. Langdon (1975b). Acta Metall., 23, 117-124.

Mohamed, F. A., M. M. I. Ahmed and T. G. Langdon (1977). Metall. Trans., 8A, 833-938.

Mukherjee, A. K. (1971). Mater Sci Eng., 8, 83-89.

Mukherjee, A. K. (1974). In J. H. Westbrook, D. A. Woodford (Eds.), Proc. 4th Bolton Landing Conference. pp. 93-104.

Murr, L. E. (1975). Interfacial Phenomena in Metals and Alloys. Addison-Wesley Publishing Company, Reading, Massachusetts.

Murty, G. S. (1972). Scr. Metall., 6, 1075-1078.

Murty, G. S. (1973). J. Mater. Sci., 8, 611-614.

Nabarro, F. R. N. (1967). Philos. Mag., 16, 231-237.

Nachtrieb, N. H. and G. S. Handler (1955). J. Chem. Phys., 23, 1569-1570.

Newbury, D. E. (1972). An Investigation into Mechanisms of Superplasticity. D. Phil. Thesis, Oxford.

Newbury, D. E. (1973). J. Mater. Sci., 8, 145-146.

Newbury, D. E. and D. C. Joy (1970). Scr. Metall., 4, 825-829.

Nowick, A. S. and B. S. Berry (1972). Anelastic Relaxation in Crystalline Solids. Academic Press, New York and London.

Nuttall, K. (1971). J. Inst. Met., 99, 266-270.

Okkerse, B., T. J. Tiedema and W. G. Burgers (1955). Acta Metall., 3, 300-302.

Packer, C. M. and O. D. Sherby (1967). ASM Trans. Q., 60, 21-28.

Pearce, R. and D. Ganguli (1972). J. Inst. Met., 100, 289-295.

Pearson, C. E. (1934). J. Inst. Met., 54 (No. 1), 111-124.

Pearson, W. B. (1958). A Handbook of Lattice Spacings and Structures of Metals and Alloys (Vol. 1). Pergamon Press, London.

Pond, R. C. and D. A. Smith (1974). In J. H. Westbrook, D. A. Woodford (Eds.), Proc. 4th Bolton Landing Conference. pp. 309-318.

Provan, J. W. and O. A. Bamiro (1977). Acta Metall., 25, 309-319.

Rachinger, W. (1952-53). J. Inst. Met., 81, 33-41.

Raj, R. and M. F. Ashby (1971). Trans. Metall. Soc. AIME, 2, 1113-1127.

Rawal, S. P. and G. S. Murty (1972). Trans. Jpn. Inst. Met., 13, 57-58.

Resing, H. A. and N. H. Nachtrieb (1961). J. Phys. Chem. Solids, 21, 40-56.

Rosenhain, W., J. Haughton and K. E. Bingham (1920). J. Inst. Met., 23 (No. 1), 261-317.

Saller, R. A. and J. L. Duncan (1971). J. Inst. Met., 99, 173-177.

Schneibel, J. H. and P. M. Hazzledine (1977). Scr. Metall., 11, 953-956.

Schneibel, J. H. and P. M. Hazzledine (1979). 5th Int. Conf. on the Strength of Metals and Alloys (Aachen, W.- Germany). Pergamon Press, Oxford. To be published.

Schuh, F. (1974). Z. Metallkd., 65, 346-352.

Simmons, G. and H. Wang (1971). Single Crystal Elastic Constants and Calculated Aggregate Properties: A Hand-book. The M.I.T. Press, Cambridge.

Smith, D. A. and R. C. Pond (1976). Int. Metall. Rev., 21, 61-74.

Smithells, C. J. (1955). Metals Reference Book. Butterworths, London.

Spingarn, J. R. and W. D. Nix (1978). Acta Metall., 26, 1389-1398.

Spingarn J. R. and W. D. Nix (1979). Acta Metall., 27, 171-177.

Stark, J. P. and W. R. Upthegrove (1966a). ASM Trans. Q., 59, 479-485.

Stark, J. P. and W. R. Upthegrove (1966b). ASM Trans. Q., 59, 486-490.

Stevens, R. N. (1971). Philos. Mag., 23, 265-283.

Subrahmanyam, B. (1972). Trans. Jpn. Inst. Met., 13, 89-92.

Takeuchi, S. and A. S. Argon (1976). J. Mater. Sci., 11, 1542-1566.

Tonejc, A. and J. P. Poirier (1975). Scr. Metall., 9, 555-558.

Watts, B. M., M. J. Stowell, B. L. Baikie and D. G. E. Owen (1976). Met. Sci., 10, 189-197.

Weertman, J. (1968). ASM Trans. Q., 61, 681-694

Woodford, D. A. (1969). Mater. Sci. Eng., 4, 146-154.

Wray, P. J. (1973). Metall. Trans., 4, 2475-2476.

Zehr, S. W. and W. A. Backofen (1968). ASM Trans. Q., 61, 300-313.

Zener, C. (1941). Phys. Rev., 60, 906-908.

Zener, C. (1948). Elasticity and Anelasticity of Metals. The University of Chicago Press, Chicago, Illinois.

Zolotukhin, I. V. and A. S. Tikhonov (1976). Sov. Phys. Dokl. (Engl. Transl.), 21, 280-281.

Appendix A1

Two-dimensional Nabarro climb creep for GBDs

Assume a square mesh of GBDs where λ is the distance between individual dislocations. The dislocation density is given by $\rho = 1/\lambda$. The driving force for annihilation is the attractive force per unit length between opposite dislocations, $G\, b_B^2/(2\pi\lambda)$, where b_B is the GBD Burgers vector. The dislocations have a mobility, M, which is given by:

$$v = \frac{G\, b_B^2}{2\ \pi\ \lambda}\, M\ , \qquad \text{(A1.1)}$$

where v is the dislocation velocity.

The time Δt needed for annihilation is λ/v. The annihilation rate is therefore approximately given by:

$$\left(\frac{\Delta\rho}{\Delta t}\right)_{ann.} = -\frac{M\ G\ b_B^2}{2\ \pi\ \lambda^3}\ , \qquad \text{(A2.1)}$$

since all dislocations present are annihilated in the time interval Δt.

On the other hand, dislocations are created by an effective stress, σ_e, which is found from the applied stress, σ, and the stress necessary to bow out dislocations sufficiently to enable annihilation to occur:

$$\sigma_e = \sigma - \frac{G\, b_B}{\lambda}\ . \qquad \text{(A1.3)}$$

In order to operate a Bardeen-Herring type dislocation source (Bardeen and Herring, 1952) a dislocation segment

moves a distance of approximately λ, thereby creating a dislocation length of about 4λ. The time needed to operate such a source is $\lambda/v = \lambda/(M\ \sigma_e\ b_B)$. The rate of creation, for a source density of $1/\lambda^2$, is now given by:

$$\left(\frac{\Delta\rho}{\Delta t}\right)_{cre.} = \frac{1}{\lambda^2}\ 4\lambda\ \frac{M\ \sigma_e\ b_B}{\lambda} = \frac{4\ M\ b_B}{\lambda^2}\ \left(\sigma - \frac{G\ b_B}{\lambda}\right) . \qquad (A1.4)$$

A comparison of the annihilation and the creation rate leads to an approximate relationship between the link length λ and the applied stress:

$$\sigma = \frac{G\ b_B}{\lambda} . \qquad (A1.5)$$

Now the rate of climb of a GB edge dislocation with the Burgers vector vertical to the boundary plane will be calculated. Using the geometry in Fig. A1.1, the vacancy volume transported in the GB by the vacancy flux, j_v, in the time intervall Δt, is given by:

$$j_v\ \Delta t\ 2b_L\ 2\lambda\ \Omega = \lambda\ \Delta x\ b_B , \qquad (A1.6)$$

where the GB width was taken to be twice the value of the lattice Burgers vector, b_L, and b_B is the Burgers vector of the GBD. Δx is the distance by which the GBD climbs in the time interval Δt.

With $j_v = D_v\ dc_v/dx$ where D_v is the vacancy diffusion coefficient and c_v the vacancy concentration, and with equation (A1.6) the climb velocity, $v = dx/dt$, is:

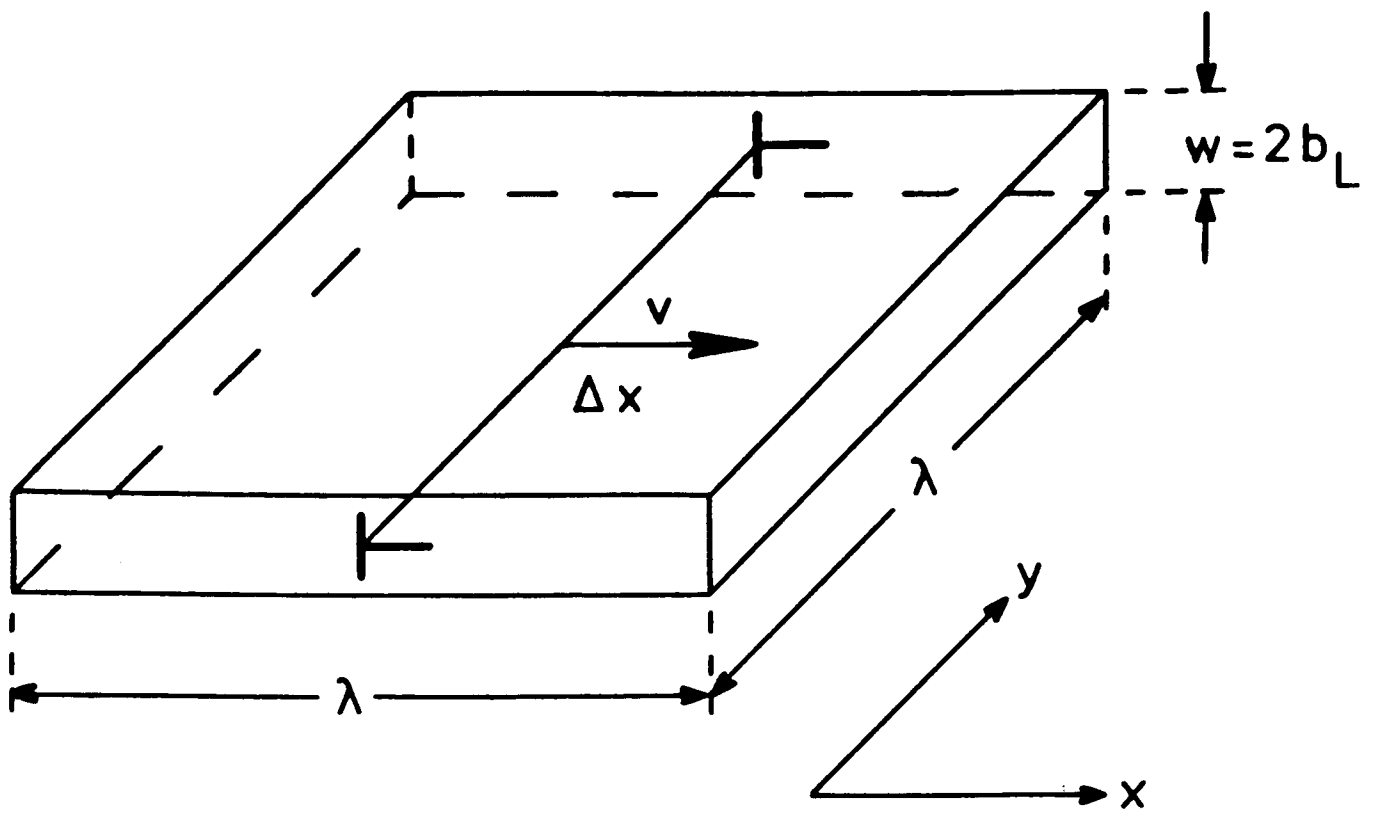

Fig. A1.1. Grain boundary dislocation in a grain boundary segment.

$$v = \frac{4\ b_L\ \Omega}{b_B} D_v \frac{dc_v}{dx} \ . \qquad \text{(A1.7)}$$

Rearranging and integrating from b to λ over the variable x and from c_1 to c_2 over the variable c_v, where $c_2-c_1 = c_o \frac{\Omega\ \sigma}{k\ T}$ and c_o is the equilibrium vacancy concentration in the stress free state results for $b_L << \lambda$ in:

$$v = \frac{4\ \Omega\ D_B\ b_L\ \sigma}{\lambda\ b_B\ k\ T} \ , \qquad \text{(A1.8)}$$

where D_B is the GB self-diffusion coefficient, $D_B = D_v\ c_o\ \Omega$.

Finally, the strain rate for a polycrystal with a grain size L is approximately given by:

$$\dot{\varepsilon} = \frac{\rho\ b_B\ v}{L} = \frac{4\ G\ \Omega\ D_B\ b_L}{L\ b_B^2\ k\ T} \left(\frac{\sigma}{G}\right)^3 \ , \qquad \text{(A1.9)}$$

if the climbing dislocations have a component of the Burgers vector parallel to the sliding GB, with a magnitude of approximately $|b_B|$.

Appendix A2

Ball-Hutchison model for grain boundary dislocations

Assume that GBDs glide along a GB. Their Burgers vectors have no or only a small climb component. The GBDs pile up against a triple edge and have now to climb along a boundary approximately perpendicular to the plane in which the pile-up lies. They have to climb a distance of approximately half the grain size L until they are annihilated. The climb velocity is assumed to be the rate determining process. After Friedel (1964), the climb velocity for GBDs will be given by:

$$v = \frac{b_L\ D_B}{b_B (L/2)} \left(\frac{c-c_o}{c_o}\right) = \frac{2\ b_L\ D_B}{b_B\ L} \frac{\Omega\ \sigma_h}{k\ T}\ , \qquad \text{(A2.1)}$$

where D_B is the GB self-diffusion coefficient, c_o the equilibrium vacancy concentration and c the vacancy concentration under the action of the stress, σ_h, at the head of the pile-up. Now, after Friedel (1964):

$$\sigma_h = \frac{2\ L\ \sigma^2}{G\ b_B}\ . \qquad \text{(A2.2)}$$

The time interval, Δt, after which annihilation of an individual dislocation occurs is $\Delta t \sim (L/2)/v$.

With equations (A2.1) and (A2.2) one obtains immediately for the strain rate:

$$\dot{\varepsilon} = \frac{b_B}{\Delta t\ L} = \frac{8\ G\ \Omega\ D_B\ b_L}{k\ T\ b_B\ L^2} \left(\frac{\sigma}{G}\right)^2\ . \qquad \text{(A2.3)}$$

Appendix A3

The anelastic mechanism considered here is based on the reverse stress exerted by bowed-out GBD segments in the GBs. Its derivation is very similar to the corresponding derivation for 3-dimensional dislocation arrangements (Burton, 1977a).

Consider a GBD segment which is pinned at two points a distance λ apart. The Burgers vector of the GBD is b. Bowing-out to a semi-circle creates a back-stress, σ_s:

$$\sigma_s = \frac{G\ b}{\lambda} \ , \qquad \text{(A3.1)}$$

and a reversible GBS displacement, u:

$$u = b/2. \qquad \text{(A3.2)}$$

With the Einstein relationship (Friedel, 1964, p.84) the friction force per unit length, F, acting on the dislocation segment is now:

$$F = \frac{k\ T}{D_B\ b}\ v = \sigma_s\ b \ , \qquad \text{(A3.3)}$$

where v is the dislocation velocity.

With eqns. (A3.1) and (A3.3) the relaxation time, τ, is:

$$\tau = \frac{\lambda/2}{v} = \frac{k\ T\ \lambda^2}{2\ D_B\ G\ b^3} \ , \qquad \text{(A3.4)}$$

which is very similar to Burton's result, apart from the

choice of the grain boundary self-diffusion coefficient instead of the lattice self-diffusion coefficient. The relaxation strength is easily evaluated for a homogeneous GBD distribution (e.g. square grid of mesh width λ). For a polycrystal of grain size L, one obtains for the maximum anelastic after-effect:

$$\gamma_a = \frac{b/2}{L} \quad . \tag{A3.5}$$

The relaxation strength is therefore given by:

$$\Delta_r = \frac{\gamma_a}{\gamma_e} = \frac{\gamma_a G}{\sigma_s} = \frac{\lambda}{2 L} \quad . \tag{A3.6}$$

Since usually $\lambda \lesssim L$, the relaxation strength will at the most be of the order of 1.

J.H. Schneibel

Oxford, 15 October 1979

Errata

p. 42: eqn. (3.4) should read: $\tau = \eta/E_o$.

Fig. 5.16: replace 242K by 342K.

p. 94: eqn. (5.14) for the average GB diffusion coefficient should be replaced by the more appropriate equation:

$$\tilde{D} = \frac{D_B(Sn)\ D_B(Pb)}{\nu_{Sn}\ D_B(Pb) + \nu_{Pb}\ D_B(Sn)}$$

(Burton, B. and B.D. Bastow (1973). Acta Metall., 21, 13-20). The use of the above equation alters the numerical values employed in the subsequent discussion only slightly and does therefore not change the discussion.

pp. 109-110: the relaxation strengths quoted should be considered as a lower limit for the true relaxation strengths since it has not been clearly established that the anelastic recovery shown in Fig. 6.4 is exhausted after 10^6s.